NEAR-INFRARED EMITTING LANTHANIDE METAL-ORGANIC FRAMEWORKS WITH TUNABLE PHOTOPHYSICAL PROPERTIES

by

Kiley A. White

BA, Barnard College, Columbia University, 2004

Submitted to the Graduate Faculty of

Arts and Sciences in partial fulfillment

of the requirements for the degree of

Doctor of Philosophy

University of Pittsburgh

2010

UNIVERSITY OF PITTSBURGH

SCHOOL OF ARTS AND SCIENCES

This dissertation was presented

by

Kiley A. White

It was defended on

December 3, 2010

and approved by

Tara Meyer, Associate Professor, University of Pittsburgh

Alexander Star, Assistant Professor, University of Pittsburgh

Stéphane Petoud, Professor, Centre de Biophysique Moléculaire, CNRS UPR 4301

Dissertation Advisor: Nathaniel Rosi, Assistant Professor, University of Pittsburgh

NEAR-INFRARED EMITTING LANTHANIDE METAL-ORGANIC FRAMEWORKS WITH TUNABLE PHOTOPHYSICAL PROPERTIES

Kiley A. White, PhD

University of Pittsburgh, 2010

NEAR-INFRARED EMITTING LANTHANIDE METAL-ORGANIC FRAMEWORKS WITH TUNABLE PHOTOPHYSICAL PROPERTIES

Kiley A. White, PhD

University of Pittsburgh, 2010

In this thesis, we present a MOF-based method for modulating the photophysical properties of near-infrared (NIR) emitting lanthanide cations, specifically their excitation and emission properties. We designed and synthesized a ligand, **H_2-PVDC**, that is capable of sensitizing four NIR lanthanide cations: neodymium, holmium, erbium, and ytterbium. Reacting **H_2-PVDC** with $Yb(NO_3)_3$ produced an Yb^{3+}-MOF, **Yb-PVDC-1**, that demonstrated NIR lanthanide luminescence via the antenna effect. We tuned the synthesis of **Yb-PVDC-1** to prevent coordination of water molecules to Yb^{3+}, as seen in **Yb-PVDC-1,** and yielded a material, **Yb-PVDC-2**, with higher quantum yields. The removal of water molecules allowed for coordination of more PVDC ligands and a subsequent increase in their $\pi-\pi$ interactions, resulting in a lower excitation energy for **Yb-PVDC-2**.

The first example of a barcoded MOF was synthesized by incorporating Er^{3+} cations into the synthesis of **Yb-PVDC-1**, generating materials **Er_xYb_{1-x}-PVDC-1**. We demonstrate the controlled preparation of a luminescent barcoded MOF whereby Yb^{3+} and Er^{3+} emission intensities vary linearly with the lanthanide composition of **Er_xYb_{1-x}-PVDC-1**. These materials display luminescence while dispersed in a polymer coating. We further elaborate on the potential applications of bi-metallic MOFs by demonstrating an improvement of the Er^{3+} emission upon tuning the dopant amount of Yb^{3+} within **Er_xYb_{1-x}-PVDC-1**.

A series of water-stable MOFs, **Ho-PVDC-3**, **Tb-PVDC-3**, **Nd-PVDC-3**, **Er-PVDC-3**, **Yb-PVDC-3**, and barcoded MOFs, **Er_xYb_{1-x}-PVDC-3**, **Nd_xYb_{1-x}-PVDC-3**, **$Er_xNd_YYb_z$-PVDC-3** were also synthesized. These MOFs appear stable in water for at least a one month duration, rendering these materials potentially more suitable for biomedical applications. **Nd-PVDC-3** and **Yb-PVDC-3** exhibit Nd^{3+} and Yb^{3+} luminescence while suspended under water, respectively. The barcoded MOFs are synthesized in a controlled fashion, including the potential 3-component tag, **$Er_xNd_YYb_z$-PVDC-3**. To further modulate these materials for potential biomedical applications, we utilized a synthesis to make the nanocomposite materials, **Nd-PVDC-3 nMOF**, **Yb-PVDC-3 nMOF**, and barcoded **Nd_xYb_{1-x}-PVDC-3 nMOFs**. These exhibit luminescence and barcoded emission intensities while suspended under water.

Finally, we present a strategy for assembling macrocycles into permanently porous 3-D crystalline structures that relies on strong inter-macrocycle π-π interactions. We created a highly stable mesoporous macrocycle by utilizing another chromophore, **H-TPY**. To our knowledge, this is the first mesoporous macrocycle-based crystalline material.

TABLE OF CONTENTS

LIST OF TABLES

LIST OF FIGURES

LIST OF SCHEMES

ACKNOWLEDGMENTS

First I would like to thank everyone who made this research possible.

I would like to express my gratitude to my research advisor, Prof. Nathaniel Rosi, for allowing me to be one of the first graduate students to join his research group and for his guidance, support, and general enthusiasm for chemistry throughout the years.
I would also like to thank my thesis committee, Prof. Tara Meyer, Prof. Alex Star, and Prof. Stéphane Petoud, for all of their time and helpful suggestions.
Thank you to my collaborators, Demetra Chengelis and Kristy Gogick, for all of your hard work.

I am very grateful for having so many caring and patient people in my life. The completion of my PhD would not have been possible without them.

I need to thank my loving boyfriend, Ted Dell'Abate, for his never-ending encouragement. Thank you for never complaining about all of our canceled plans, my daily mood swings, or that most of our vacations revolved around my running a marathon. Thank you for being supportive of my endeavor, even though that meant being in the same city not often enough. Thank you for having complete confidence in my abilities and reminding me of them when I had forgotten. Most of all, thank you for making me your Bolognese sauce so I always had something delicious to eat when I had no time to cook.
Thank you to my parents, Sandra and Edward White, for your love and support through this process. Thank you for your willingness to do anything to make my life less stressful, including quickly learning to stop asking when I would be graduating. Thank you for always reminding me of how proud you are of me.
Thank you to my Aunt Barbara, Barbara Barkley, for your loving support and your generosity that made taking a vacation feasible even on a grad student salary.
Thank you to my brothers, Ted White and Brad White, and their significant others, Natalie White and Marissa Tuohy for always changing your schedules to see me when I took last minute trips to NYC.
I also need to thank Kristy Gogick, who in addition to being my collaborator, is a great friend.
Thank you to my oldest friends, Melissa Gallo and Chase Polan, for being my cheerleaders and always being there for me.

I cannot express my gratitude enough to you all.

1.0 INTRODUCTION

1.1 METAL-ORGANIC FRAMEWORKS

Metal-organic frameworks (MOFs) are porous materials in which metal ions or clusters are linked together by organic ligands into 2-D or 3-D periodic, crystalline networks.[1,2] A variety of structures can be synthesized by altering the ligand, metal, or synthetic parameters (Scheme 1). Their crystallinity allows for characterization by single crystal X-ray diffraction, which gives the precise locations of atoms in the crystal structure. Knowing the exact structure provides extraordinary amounts of information about the material, such as the ligand arrangement, the distance(s) between metal ions, and the coordination environment about the metal center. This information can be correlated to the synthetic conditions in some case, which can then be modified to give structures with varying properties. Structure and properties of materials are intimately linked, and in order to control properties, one must have exact knowledge of structure; therefore, preparing materials in single crystalline form is advantageous and allows one to expressly precisely structure and properties. Importantly, common building blocks that form *in situ*, known as secondary building units (SBUs), can be synthetically targeted. These SBUs have well-defined structures and can be used to synthesize MOFs in a logical fashion.[3]

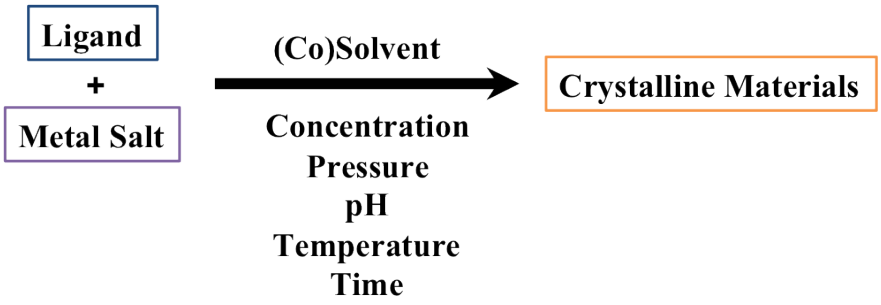

Scheme 1.1. General MOF synthesis.

1.1.1 Secondary building units (SBUs)

Secondary building units (SBUs) are rigid entities that form *in situ* and are composed of metal clusters and the binding portion of the ligand.[3] SBUs can be discrete metal clusters or they can be infinite 1-D chains. General reaction conditions can be determined so that either specific discrete SBUs or infinite SBUs can be targeted. Two common discrete SBUs are known as the copper paddle-wheel and zinc octahedral cluster (Figure 1.1). When frameworks contain the same SBU, but differ only in their respective linkers, they are known as isoreticular MOFs.[4] For example, various aromatic carboxylates have been reacted with zinc salts, to yield 3-D cubic networks consisting of the zinc octahedron clusters, $Zn_4O(COO)_6$, linked by the aromatic ligands (Figure 1.2). The ability to target specific structures is highly advantageous, because it allows one to systematically tune the properties of a structure by simply varying the linker.

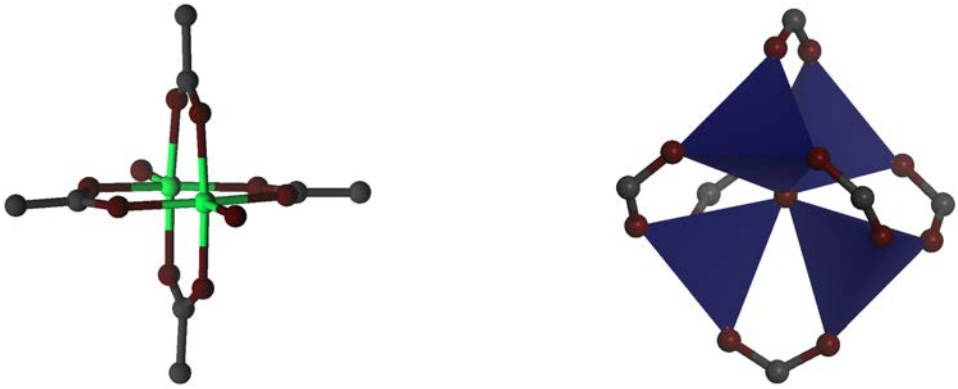

Figure 1.1. Copper paddle-wheel cluster (left; C, grey; O, red; Cu, green) and $Zn_4O(COO)_6$ cluster with Zn^{2+} shown as polyhedra (right; C, grey; O, red; Zn^{2+}, blue)

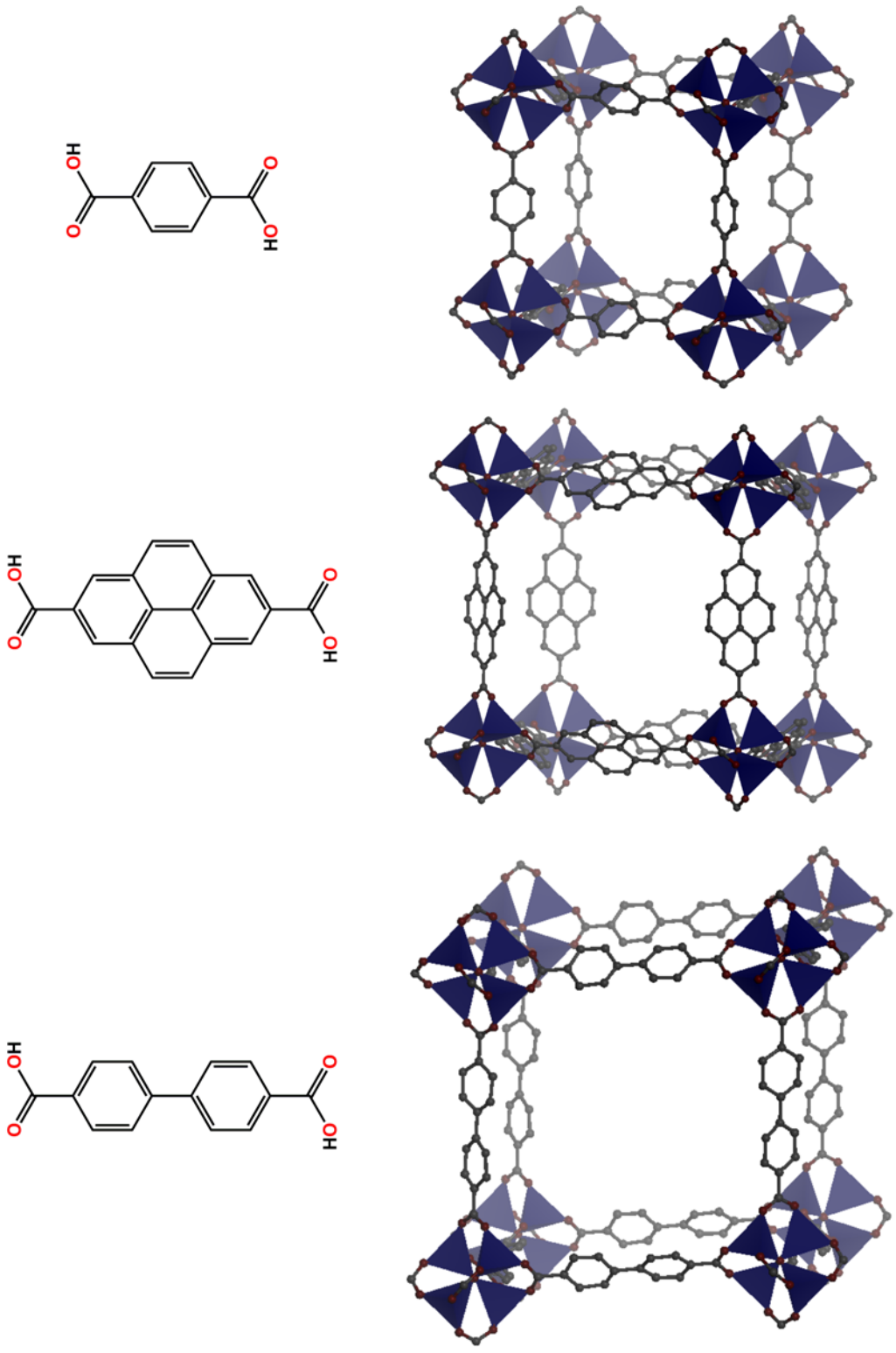

Figure 1.2. Isoreticular series based on $Zn_4O(COO)_6$ with benzenedicarboxylate (BDC, top), pyrenedicarboxylate (PDC, middle), and biphenyldicarboxylate (BPDC, bottom) (right; C, grey; O, red; Zn^{2+}polyhedra, blue)

Inifinite SBUs do not have as well-established syntheses for targeting specific SBUs, but a survey of the literature indicates that MOF reactions with longer ligands often result in the formation of frameworks with infinite SBUs. Longer ligands are not as rigid as shorter ligands and this can result in structure collapse upon solvent removal. Consequently, a greater possibility exists that the ligands will overlap with one another and participate in CH-π and π–π stacking[5] to provide additional stability to the framework.[6,7] Part of this thesis focuses on targeting infinite SBUs for the purpose of studying the impact π–π stacking has on the photophysical properties of lanthanide containing MOFs.

1.1.2 Applications of MOFs

MOFs exhibit properties that make them suitable for potential applications in gas storage,[8] sensing,[9-12] catalysis,[13,14] and drug delivery.[15-19] One of the more advantageous features of MOF chemistry is the ability to impart function into the structure for a desired application via judicious selection of metal ions and ligand. For example, because of their intrinsic porosity and extremely high surface areas, MOFs are ideal materials for gas storage. To increase the surface area, Yaghi *et al*. used a larger ligand than previously studied BDC and BPDC, benzene 1,3-tribenzoate (BTB) (Figure 1.3). This tritopic ligand promoted large cavities and yielded a material of extremely high surface area of 4500 m^2/g.[20]

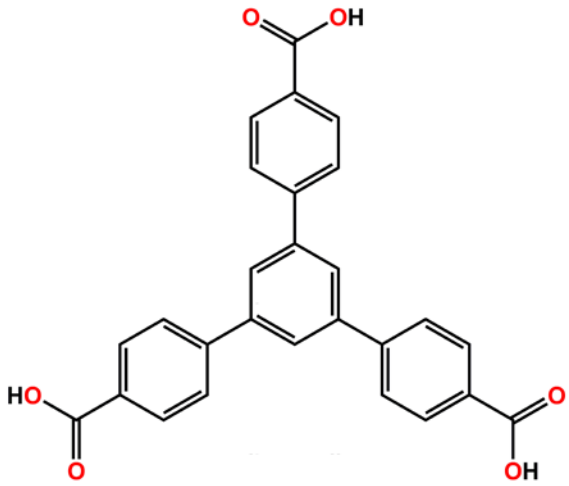

Figure 1.3. Tritopic linker, benzene 1,3-tribenzoic acid (BTB)

Another example of choosing a ligand for a specific application is for CO_2 capture, which is extremely important due to global warming. CO_2 has strong Lewis acid-Lewis base interactions with nitrogen atoms. An et al. has utilized these strong interactions by synthesizing a MOF with Co^{2+} and adenine, a nucleobase that contains multiple nitrogen atoms (Figure 1.4).[21] The adeninate MOF showed high selectivity for CO_2 over N_2. Computational studies on CO_2 interactions within the adeninate framework further support these results.[22]

Figure 1.4. Adenine for enhanced CO_2 capture

These are only two examples of the many MOFs that have been designed for various applications. Other examples include 1) enantioselective catalysis utilizing chiral building blocks,[13,14,23,24] 2) magnetism using paramagnetic metals such as iron and gadolinium,[25,26] and 3) drug delivery by incorporating biologically active molecules.[15-19] In this thesis, we target lanthanide-based MOFs to yield luminescent materials with highly tailorable structures and therefore tunable properties, in this case photophysical properties. We design these materials for potential applications such as security tags, bioanalytical labels, and biological imaging probes.

1.2 LANTHANIDES

Lanthanide metals comprise elements with atomic numbers 57 to 71, lanthanum to lutecium, of the periodic table. (Figure 1.5). Aside from La, which has the electronic configuration [Xe] $5d^1$ $6s^2$, electrons add to the 4f orbitals with increasing atomic number. Lanthanides predominantly exist in their trivalent state, Ln^{III} ([Xe]$4f^n$), and the filled 5s and 5p orbitals shield the 4*f* orbitals from the environment. This shielding causes a lack of 4*f* orbital overlap with the coordinated ligand's orbitals, resulting in little observable crystal field splitting. The similar reactivity of all of the lanthanides can be attributed to this shielding, as well. Their reactivity can vary if size is an important parameter due to the lanthanide contraction, as the radius decreases from 103 pm for La^{3+} to 86 pm for Lu^{3+}. Lanthanides typically have a high coordination number (8-12)[27] making their reactivity quite different than transition metals, which have a typical coordination number of 4 or 6.

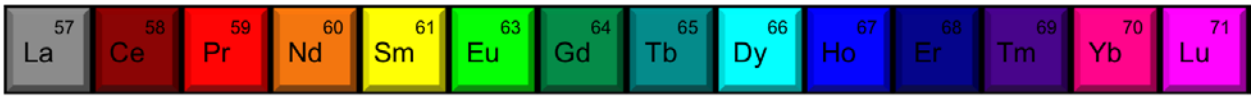

Figure 1.5. Lanthanide series

1.2.1 Advantages of lanthanide luminescence

Lanthanides have unique luminescence due to their electronic structure.[28] Since the 4*f* electrons are well shielded from the environment, small crystal field splitting occurs within the 4*f* shell. As a result, the emission spectra have characteristic narrow bands, resembling those of the corresponding free atoms, and these emission bands are not dependent upon experimental parameters such as pH, temperature, and biological environment. The emission bands do not overlap significantly with the emission bands of other lanthanide ions, allowing for incorporation of multiple lanthanides into one material to generate a discernible spectroscopic barcode. The luminescence spans from the visible[29] to near-infrared (NIR)[30] region of the spectrum, rendering them useful in a variety of applications (Figure 1.6).

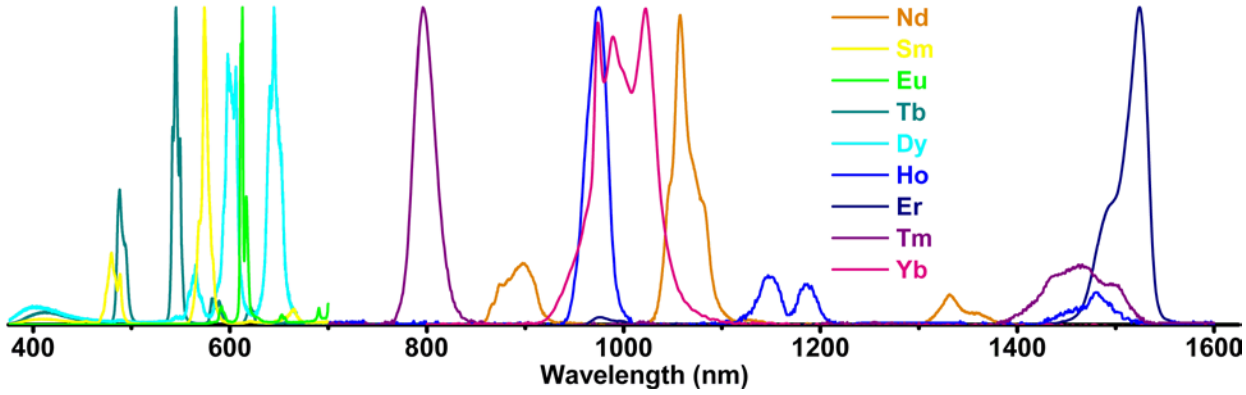

Figure 1.6. Normalized lanthanide emission spectra

NIR emitting lanthanide cations consist of neodymium, holmium, erbium, thulium, and ytterbium. Their NIR emissions are advantageous for biological measurements, because NIR photons can penetrate deeply in tissue (several centimeters)[31,32] and have less scattering than visible photons, making it possible to obtain images with improved resolution. Since naturally-occurring molecules seldom have native NIR luminescence[33], detection of analytes using NIR signal output results in improved signal-to-noise ratio and corresponding detection sensitivity. Lanthanide cations also have much longer luminescence lifetimes (μs-ms)[34,35] than organic fluorophores (ps-ns). The longer lifetimes can help discriminate the signal in biological media by collecting time-resolved measurements.[36, 37] Another advantage of lanthanide cations is that, unlike fluorophores, they are highly resistant to photobleaching, allowing for extended storage time and repeated exposure to excitation sources. All of these properties demonstrate why lanthanide cations make useful components of various applications such as photonics and biological imaging.

1.2.2 Challenges of lanthanide luminescence

Several challenges must be overcome to effectively harness and utilize lanthanide luminescence. For example, free lanthanide cations have weak absorptivity because *f-f* transitions are Laporte-forbidden. This effectively limits their luminescence intensity.[28,38] The "antenna effect"[39] has become a broadly applied strategy to improve the efficiency of lanthanide luminescence.[30,40-47] In this approach, lanthanide cations are placed in proximity to antennae, chromophoric molecules with high absorptivity that transfer energy to sensitize the lanthanide

cations (Figure 1.7). Upon excitation, the antenna transfers energy from its excited triplet or singlet state to the lanthanide (Figure 1.8).[48]

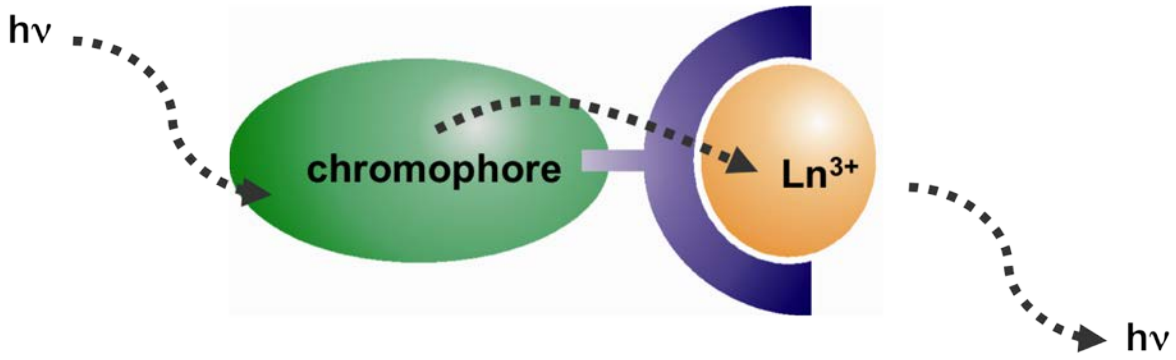

Figure 1.7. Antenna effect: upon excitation, a chromophore in close proximity to the lanthanide ion transfers its energy resulting in lanthanide luminescence

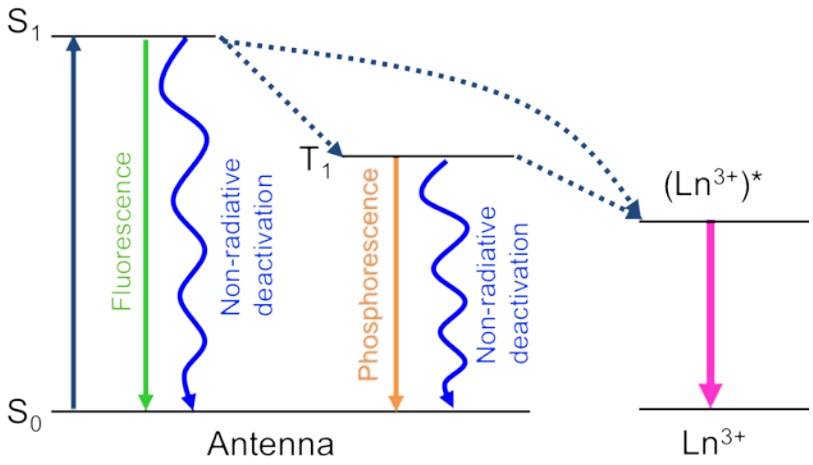

Figure 1.8. Jablonski diagram demonstrating both the mechanism of sensitization of Ln^{3+} via the antenna effect and the potential for relaxation via radiative and non-radiative deactivation

The coordination environment around lanthanide cations and thus the organization of antennae, significantly impacts the luminescent properties of the complex. The antennae serve not only to transfer energy to the lanthanide, but also to protect the lanthanide from O-H, N-H, and to a lesser extent C-H vibrations, whose overtones quench luminescence intensity and decrease luminescence lifetimes. However, designing complexes in which the lanthanide is both effectively sensitized and shielded is challenging, because lanthanide cations generally exhibit low stereochemical requirements and therefore it can be difficult to control the organization of the ligands (antennae) around the metal ion.

A suitable antenna should combine several characteristics and ideally overcome the aforementioned drawbacks of lanthanide luminescence. The antenna should have a high molar absorption coefficient. The brightness of the complex depends on the quantum yield, the molar absorption coefficient of the ligand,[48] and the number of lanthanide emitters per unit volume. Thus, a strongly absorbing ligand and/or a polymetallic complex can overcome a low quantum yield to allow for its use in biological applications. Lanthanide metals are hard acids, so, antennae should contain hard bases, like oxygen or nitrogen to form strong bonds. Cryptates, porphyrins, and dendrimers have been incorporated into many lanthanide complexes because of their multiple nitrogen binding sites.[46,49-51] Also, the antennae should fill the coordination sphere of the lanthanide to protect the lanthanide from quenching from any water or solvent.[27,28] To date, most antennae excite in the UV, with a few exceptions excitable in the visible range.[50,52-55] Exciting in the UV for NIR emission is not energy efficient, and for biological purposes, the excitation energy of the antennae should be in the visible, or ideally, NIR range so that it can penetrate tissue with some depth.

1.3 MOF-BASED APPROACH FOR TUNING PHOTOPHYSICAL PROPERTIES OF NIR EMITTING LANTHANIDE CATIONS

This thesis describes utilizing metal-organic framework (MOF) materials as a means to sensitize lanthanides in the NIR and optimize their excitation and emission properties. MOFs have several advantages that make them an attractive class of materials for sensitizing lanthanide cations. First, they have rigid structures in which the metal ions and ligands are well organized and spatially constrained. With fewer structural vibrations, the energy transfer from the antenna to the lanthanide cation should be more efficient than occurs within a simple lanthanide complex. In Chapter 2, we illustrate the impact of the crystalline MOF structure by showing a red-shifted excitation energy of the antenna compared to that of a lanthanide complex. Moreover, MOFs can exhibit a variety of topologies and in some cases the topological features of a MOF can be designed. Therefore, the positions of the metal ions and ligands within a MOF can be finely controlled, which permits precise tuning of MOF properties. Also in Chapter 2, we modulate the structure of a NIR-emitting MOF to improve the photophysical properties of the lanthanide cation without having to change the sensitizer.

MOF structures can incorporate a large number of metal cations per unit volume and the metal ion coordination spheres are often completely saturated by the ligands. In the context of lanthanide sensitization and luminescence, these features are important because increasing the density of lanthanide cations within a material will improve emission intensities.[51] The high number of chromophoric groups (ligands) surrounding each lanthanide will help maximize the absorption of a larger amount of excitation light, leading to more intense lanthanide luminescence. Also, MOFs can protect the lanthanide cations from quenching solvent molecules, leading to bright emission intensities. Chapter 2 and Chapter 4 illustrate these

advantageous features with quantum yield values amongst the highest reported for Yb^{3+} and Er^{3+} complexes while under solvent. Also in Chapter 5, Nd^{3+} and Yb^{3+} exhibit an uncommon luminescence while the MOFs are suspended under water, demonstrating the overall brightness of the MOF materials.

Multiple metal ion MOFs[56] can be targeted, allowing for the incorporation of multiple luminescent lanthanides and multiple signals into a single material. Chapters 3, 4, and 5 all demonstrate the impact of having multiple lanthanide cations incorporated into one framework. In Chapter 3 we demonstrate the first example of a MOF designed to be a luminescent barcode.[57] In Chapter 4, we investigate tuning the ratio of Yb^{3+}/Er^{3+} in order to utilize a common Yb^{3+}-Er^{3+} energy transfer for optimizing erbium emission. In Chapter 5, we improve upon the barcoded MOFs in Chapter 3 by synthesizing a water stable barcoded MOF with emissions from three lanthanide cations. We also generate a more biocompatible MOF through the synthesis of nanoMOFs, resulting in the first example of a barcoded NIR emitting nanoMOF system.

In Chapter 6, we present the results from a second project that also involves the use of a chromophoric ligand molecule. Interestingly, it can be used to prepare highly porous macrocyclic structures. We present these novel results and investigate the unique porosity and stability of this material.

1.4 LANTHANIDE METAL-ORGANIC FRAMEWORKS

When we initiated this work, few examples of near-infrared (NIR) emitting MOFs[58,59] had been published in the literature and very little work had been published on how to use MOFs to improve upon the photophysical properties of lanthanide cations. However, several

lanthanide-containing MOFs had been prepared,[60] and sensing applications based on their visible emission properties were explored.[10,12] A brief overview will be provided to give background in regards to 1) tuning the photophysical properties of lanthanide MOFs and 2) utilizing multiple-lanthanide MOFs. Thereafter, we will present background on preparing MOFs to be more compatible for biomedical applications.

1.4.1 Tuning the photophysical properties of Ln-MOFs

To the best of our knowledge, the first example of tuning the photophysical properties of a NIR emitting MOF was published in 2006.[58] Chen et al. synthesized an Er^{3+}-MOF with benzene dicarboxylate (BDC). NIR emission was achieved through erbium's direct excitation band, not through the antenna effect. Erbium is easily quenched from O-H and C-H vibrations, common vibrations in complexing organic ligands/sensitizers and surrounding solvent molecules. However, since C-F vibrations do not quench erbium's luminescence to a great extent, a commonly employed technique for improving the photophysical properties of erbium is to use perfluoronated ligands. Chen demonstrated this increase in luminescence upon changing the ligand from BDC to its perfluoronated variation. While this method does improve lanthanide emission, creating perfluoronated versions of coordinating ligands can be difficult, costly, and time consuming. The electronic differences between the two ligands can make producing the same MOF challenging, as well. Improving the photophysical properties of lanthanide cations without having to alter the chromophore is a highly advantageous strategy that we explore in Chapter 2.

Lu et al. demonstrated increasing the luminescence of Tb^{3+} upon cation exchange.[61] The anionic framework was synthesized with K^+ ions in the pores. Upon exchanging K^+ for Ca^{2+}, an

increase in luminescence was observed. Most other metals had no impact and a few actually decreased the emission intensity. However, the large Ca^{2+} ions are thought to interact with the flexible oxolate ligand, making a more rigid structure and a brighter lanthanide emission. While this can just act as a sensor for Ca^{2+} ions, this is also an interesting method of improving the luminescence of lanthanide metals.

Another example of improving lanthanide emission within a MOF is through dehydration. Upon heating, coordinated water molecules can be removed leading to enhanced photophysical properties.[62] However, this method can also result in collapse of the structure, resulting in a decrease in lanthanide emission.[63]We improve upon this method by modifying synthetic conditions to prevent coordination of water molecules to the lanthanide centers, as explained in Chapter 2.

1.4.2 Multiple lanthanide MOFs

While we demonstrate the first example of a barcoded MOF by incorporating multiple lanthanide cations, other examples of multiple lanthanide MOFs are in the literature. A few of these use the bi-metallic MOFs for sensing (Section 1.5.2), and other examples only exhibit emission from one lanthanide. Some also study Ln-Ln interactions, but do not demonstrate enhancement of erbium's luminescence through energy transfer as we do in Chapter 4.

A few MOFs have been synthesized with Er^{3+} and Yb^{3+} to study their Ln-Ln interactions. In a recent example, Haquini et al. attempted to improve the NIR emission of an Er^{3+}-MOF through doping with Yb^{3+}.[64] However, no enhancement was observable and upon doping with more than 50 % of ytterbium ions, a structural change occurred. Yb^{3+}-Er^{3+} upconversion properties of multiple lanthanide MOFs also have been studied.[65] For example, a MOF

synthesized using oxalic acid, 4,4'-oxybis(benzoic acid), and yttrium was co-doped with Er^{3+} and Yb^{3+} and demonstrated upconversion from Yb^{3+} to Er^{3+} for visible emission.[65] However, no study was done to optimize the photophysical properties upon varying the dopant amounts. In Chapter 4, we demonstrate optimization of Er^{3+} luminescence through enhanced emission from Yb^{3+} down-conversion energy transfer.

Multiple MOFs have been synthesized containing both Tb^{3+} and Eu^{3+}, two visible light emitters.[66-68] Terbium and europium are commonly incorporated into materials for potential white light emission because of the strong green and red emissions from Tb^{3+} and Eu^{3+}, respectively. Terbium and europium both have direct excitation bands. While there is weak absorption through direct excitation, this is a novel method for demonstrating Tb^{3+}-Eu^{3+} energy transfer. Upon direct excitation of Tb^{3+}, Tb^{3+} and Eu^{3+} emissions are visible, providing evidence of energy transfer within a MOF. Recent advances in Tb_xEu_{1-x}-MOFs have included the incorporation of a third lanthanide[67] for an additional color, blue Ce^{3+} into a framework and the fabrication of nanoscale Tb_xEu_{1-x}MOF thin films[68] for potential white light emitting applications.

While much progress is needed on how to effectively use a MOF for enhancing the photophysical properties of lanthanide ions, one other important area of MOF research involves making them more compatible for specific applications. One method of making MOFs more biocompatible is by preparing them in nanocrystalline form.

1.5 NANOMOFS

A new class of smaller MOFs, known as nanoMOFs, has been synthesized recently for biological applications. NanoMOFs are typically 50-300 nm as opposed to bulk MOFs that can be hundreds

of micrometers.[16] A common nanoMOF synthesis uses a water-in-oil reverse microemulsion method that results in crystalline powder materials.[16] The "identity" and purity of these nanomaterials are characterized by powder X-ray diffraction and compared to the simulated powder pattern of the known single crystal bulk material.

1.5.1 NanoMOFs for drug delivery

The porosity of MOFs has been studied for drug delivery applications. However, many of these materials might be too large for drug delivery and they contain metals that are not biocompatible, such as Co^{2+}, Ni^{2+}, and Cr^{2+}.[15] Ferey et al. synthesized nanoparticle materials of previously published MOFs, such as MIL-100 and MIL-88A, and replaced potentially toxic metals with Fe^{3+}, which is already found in the blood stream.[69] These materials successfully loaded antitumoural and antiviral drugs that had previously showed low drug loading in other materials (less than 5 wt%). The nanoMOFs were nontoxic, had good stability in biological media, and demonstrated controlled delivery of these materials.

Wenbin Lin's group has also demonstrated drug delivery via nanoMOF carriers.[19,70] However, as opposed to encapsulating the drug inside the pore, he incorporated a drug molecule as part of the framework and in another instance, post-synthetically attached an anticancer drug, to an Fe-BDC nanoMOF.[70] Post-synthetic modification and drug loading offer the synthetic advantage of using previously synthesized materials that could by carriers for a variety of drug molecules, as opposed to incorporating one specific drug molecule into the framework.

1.5.2 Lanthanide nanoMOFs

Lanthanide cations have also been utilized in nanoMOFs for imaging and sensing applications. Gadolinium is a highly paramagnetic lanthanide that can increase water proton relaxation rates. Water proton rates differ for normal and diseased tissue. So by increasing the relaxation rates, images with better contrast are yielded. Lin et al. synthesized a nanoscale Gd^{3+}-MOF and because of the high density of metals, the nanoMOF material effectively increased the relaxtivity rate much more so than current Gd_2O_3 nanoparticles.[71,72]

The Gd^{3+}-MOFs were also doped with Eu^{3+} and Tb^{3+} to take advantage of lanthanide luminescence. They exhibited luminescence upon UV excitation, making them candidates for biological imaging agents. Sensing was another area explored with the Eu^{3+}-doped Gd^{3+}-MOF.[11] The nanoMOF was functionalized with a Tb^{3+}-EDTM molecule because Tb^{3+} acts as a sensing agent for anthrax derivatives, such as DPA. Before any DPA is added to the solution of Tb^{3+}-EDTM-functionalized-nanoMOF, only Eu^{3+}emission is observable. Upon adding DPA and its subsequent binding to Tb^{3+}-EDTM, Tb^{3+} becomes luminescent with its emission proportional to the amount of binding DPA, while the Eu^{3+} concurrently continues to luminesce and acts as an internal standard. A few other applications of nanoMOFs include post-synthetically attaching fluorophores for imaging,[70] using manganese for MRI,[73] and using an iodinated benzoic acid MOF for computed tomography.[74]

1.6 REFERENCES

(1) Ferey, G. *Chem. Soc. Rev.* **2008**, *37*, 191.
(2) Kitagawa, S.; Kitaura, R.; Noro, S. *Angew. Chem. Int. Ed.* **2004**, *43*, 2334.
(3) Eddaoudi, M.; Moler, D. B.; Li, H.; Chen, B.; Reineke, T. M.; O'Keeffe, M.; Yaghi, O. M. *Acc. Chem. Res.* **2001**, *34*, 319.
(4) Eddaoudi, M.; Kim, J.; Rosi, N.; Vodak, D.; Wachter, J.; O'Keefe, M.; Yaghi, O. M. *Science* **2002**, *295*, 469.
(5) Hunter, C. A.; Sanders, J. K. M. *J. Am. Chem. Soc.* **1990**, *112*, 5525.
(6) Rosi, N. L.; Kim, J.; Eddaoudi, M.; Chen, B. L.; O'Keeffe, M.; Yaghi, O. M. *J. Am. Chem. Soc.* **2005**, *127*, 1504.
(7) Rosi, N. L.; Eddaoudi, M.; Kim, J.; O'Keeffe, M.; Yaghi, O. M. *Angew. Chem. Int. Ed.* **2001**, *41*, 284.
(8) Lin, X. A.; Champness, N. R.; Schroder, M. In *Functional Metal-Organic Frameworks: Gas Storage, Separation and Catalysis*; Springer-Verlag Berlin: Berlin, 2010; Vol. 293, p 35.
(9) Chen, B. L.; Xiang, S. C.; Qian, G. D. *Acc. Chem. Res.* **2010**, *43*, 1115.
(10) Chen, B. L.; Yang, Y.; Zapata, F.; Lin, G. N.; Qian, G. D.; Lobkovsky, E. B. *Adv. Mater.* **2007**, *19*, 1693.
(11) Rieter, W. J.; Taylor, K. M. L.; Lin, W. B. *J. Am. Chem. Soc.* **2007**, *129*, 9852.
(12) Wong, K. L.; Law, G. L.; Yang, Y. Y.; Wong, W. T. *Adv. Mater.* **2006**, *18*, 1051.
(13) Liu, Y.; Xuan, W. M.; Cui, Y. *Adv. Mater.* **2010**, *22*, 4112.
(14) Seo, J. S.; Whang, D.; Lee, H.; Jun, S. I.; Oh, J.; Jeon, Y. J.; Kim, K. *Nature* **2000**, *404*, 982.
(15) Horcajada, P.; Serre, C.; Vallet-Regi, M.; Sebban, M.; Taulelle, F.; Ferey, G. *Angew. Chem. Int. Ed.* **2006**, *45*, 5974.
(16) Lin, W. B.; Rieter, W. J.; Taylor, K. M. L. *Angew. Chem. Int. Ed.* **2009**, *48*, 650.
(17) McKinlay, A. C.; Morris, R. E.; Horcajada, P.; Ferey, G.; Gref, R.; Couvreur, P.; Serre, C. *Angew. Chem. Int. Ed.* **2010**, *49*, 6260.
(18) An, J.; Geib, S. J.; Rosi, N. L. *J. Am. Chem. Soc.* **2009**, *131*, 8376.
(19) Rieter, W. J.; Pott, K. M.; Taylor, K. M. L.; Lin, W. B. *J. Am. Chem. Soc.* **2008**, *130*, 11584.
(20) Chae, H. K.; Siberio-Perez, D. Y.; Kim, J.; Go, Y.; Eddaoudi, M.; Matzger, A. J.; O'Keeffe, M.; Yaghi, O. M. *Nature* **2004**, *427*, 523.
(21) An, J.; Geib, S. J.; Rosi, N. L. *J. Am. Chem. Soc.* **2010**, *132*, 38.
(22) Chen, Y. F.; Jiang, J. W. *ChemSusChem* **2010**, *3*, 982.
(23) Wu, C.-D. H., A.; Zhang, L.; Lin, W. *J. Am. Chem. Soc.* **2005**, *127*, 8940.
(24) Ma, L. Q.; Falkowski, J. M.; Abney, C.; Lin, W. B. *Nat. Chem.* **2010**, *2*, 838.
(25) Agusti, G.; Munoz, M. C.; Gaspar, A. B.; Real, J. A. *Inorg. Chem.* **2009**, *48*, 3371.
(26) Batten, S. R.; Murray, K. S. *Coord. Chem. Rev.* **2003**, *246*, 103.
(27) Parker, D.; Dickins, R. S.; Puschmann, H.; Crossland, C.; Howard, J. A. K. *Chem. Rev.* **2002**, *102*, 1977.
(28) Bünzli, J.-C. G.; Piguet, C. *Chem. Soc. Rev.* **2005**, *34*, 1048.

(29) Petoud, S.; Cohen, S. M.; Bunzli, J. C. G.; Raymond, K. N. *J. Am. Chem. Soc.* **2003**, *125*, 13324.
(30) Zhang, J.; Badger, P. D.; Geib, S. J.; Petoud, S. *Angew. Chem. Int. Ed.* **2005**, *44*, 2508.
(31) Ballou, B.; Ernst, L. A.; Waggoner, A. S. *Curr. Med. Chem.* **2005**, *12*, 795.
(32) Weissleder, R.; Tung, C.-H.; Mahmood, U.; Bogdanov, A., Jr. *Nat. Biotechnol.* **1999**, *17*, 375.
(33) Mahmood, U.; Weissleder, R. *Molecular Cancer Therapeutics* **2003**, *2*, 489.
(34) Beeby, A.; Clarkson, I. M.; Dickins, R. S.; Faulkner, S.; Parker, D.; Royle, L.; de Sousa, A. S.; Williams, J. A. G.; Woods, M. *J. Chem. Soc., Perkin Trans. 2* **1999**, 493.
(35) Horrocks, W. D.; Sudnick, D. R. *J. Am. Chem. Soc.* **1979**, *101*, 334.
(36) Yuan, J.; Wang, G. *Trends Anal. Chem.* **2006**, *25*, 490.
(37) Bünzli, J.-C. G. In *Lanthanide Probes in Life, Chemical and Earth Sciences*; Bünzli, J.-C. G., Choppin, G. R., Eds.; Elsevier Science Publishers B.V.: Amsterdam, 1989, p 219.
(38) de Sa, G. F.; Malta, O. L.; Donega, C. D.; Simas, A. M.; Longo, R. L.; Santa-Cruz, P. A.; da Silva, E. F. *Coord. Chem. Rev.* **2000**, *196*, 165.
(39) Weissman, S. I.; AIP: 1942; Vol. 10, p 214.
(40) Beeby, A.; Dickins, R. S.; Faulkner, S.; Parker, D.; Williams, J. A. G. *Chem. Commun.* **1997**, 1401.
(41) Comby, S.; Imbert, D.; Chauvin, A.-S.; Bünzli, J.-C. G. *Inorg. Chem.* **2006**, *45*, 732.
(42) Gunnlaugsson, T.; Stomeo, F. *Org. Biomol. Chem.* **2007**, *5*, 1999.
(43) Hebbink, G. A.; Grave, L.; Woldering, L. A.; Reinhoudt, D. N.; van Veggel, F. C. J. M. *J. Phys. Chem. A* **2003**, *107*, 2483.
(44) Ronson, T. K.; Lazarides, T.; Adams, H.; Pope, S. J. A.; Sykes, D.; Faulkner, S.; Coles, S. J.; Hursthouse, M. B.; Clegg, W.; Harrington, R. W.; Ward, M. D. *Chem. Eur. J.* **2006**, *12*, 9299.
(45) Van Deun, R.; Fias, P.; Nockemann, P.; Van Hecke, K.; Van Meervelt, L.; Binnemans, K. *Inorg. Chem.* **2006**, *45*, 10416.
(46) Vicinelli, V.; Ceroni, P.; Maestri, M.; Balzani, V.; Gorka, M.; Voegtle, F. *J. Am. Chem. Soc.* **2002**, *124*, 6461.
(47) Zhang, J.; Petoud, S. *Chem. Eur. J.* **2008**, *14*, 1264.
(48) Werts, M. H. V. *Sci. Prog.* **2005**, *88*, 101.
(49) Sabbatini, N.; Guardigli, M.; Lehn, J. M. *Coord. Chem. Rev.* **1993**, *123*, 201.
(50) Beeby, A.; Dickins, R. S.; FitzGerald, S.; Govenlock, L. J.; Parker, D.; Williams, J. A. G.; Maupin, C. L.; Riehl, J. P.; Siligardi, G. *Chem. Commun.* **2000**, 1183.
(51) Cross, J. P.; Lauz, M.; Badger, P. D.; Petoud, S. *J. Am. Chem. Soc.* **2004**, *126*, 16278.
(52) Gerald A. Hebbink, S. I. K., Lennart Grave, Patrick G. B. Oude Alink, Frank C. J. M. van Veggel *ChemPhysChem* **2002**, *3*, 1014.
(53) Hebbink, G. A.; Grave, L.; Woldering, L. A.; Reinhoudt, D. N.; Veggel, F. C. J. M. v. *J. Phys. Chem. A* **2003**, *107*, 2483.
(54) Raymond F. Ziessel, G. U. L. C. D. I. R. S. J.-C. G. B. n. *Chem. Eur. J.* **2006**, *12*, 5060.
(55) Shavaleev, N. M.; Pope, S. J. A.; Bell, Z. R.; Faulkner, S.; Ward, M. D. *Dalton T.* **2003**, 808.
(56) Chen, B. L.; Fronczek, F. R.; Maverick, A. W. *Inorg. Chem.* **2004**, *43*, 8209.
(57) White, K. A.; Chengelis, D. A.; Gogick, K. A.; Stehman, J.; Rosi, N. L.; Petoud, S. *J. Am. Chem. Soc.* **2009**, *131*, 18069.

(58) Chen, B.; Yang, Y.; Zapata, F.; Qian, G.; Luo, Y.; Zhang, J.; Lobkovsky, E. B. *Inorg. Chem.* **2006**, *45*, 8882.
(59) Zhang, Z.-H.; Song, Y.; Okamura, T.-a.; Hasegawa, Y.; Sun, W.-Y.; Ueyama, N. *Inorg. Chem.* **2006**, *45*, 2896.
(60) Ma, L.; Evans, O. R.; Fowman, B. M.; Lin, W. B. *Inorg. Chem.* **1999**, *38*, 5837.
(61) Pan, L.; Adams, K. M.; Hernandez, H. E.; Wang, X.; Zheng, C.; Hattori, Y.; Kaneko, K. *J. Am. Chem. Soc.* **2003**, *125*, 3062.
(62) de Lill, D. T.; de Bettencourt-Dias, A.; Cahill, C. L. *Inorg. Chem.* **2007**, *46*, 3960.
(63) Lu, W. G.; Jiang, L.; Feng, X. L.; Lu, T. B. *Inorg. Chem.* **2009**, *48*, 6997.
(64) Shi, F. N.; Cunha-Silva, L.; SaFarreira, R. A.; Mafra, L.; Trindade, T.; Carlos, L. D.; AlmeidaPaz, F. A.; Rocha, J. *J. Am. Chem. Soc.* **2008**, *130*, 150.
(65) Zhu, W. H.; Wang, Z. M.; Gao, S. *Inorg. Chem.* **2007**, *46*, 1337.
(66) Haquin, V.; Gumy, F.; Daiguebonne, C.; Bunzli, J. C.; Guillou, O. *Eur. J. Inorg. Chem.* **2009**, 4491.
(67) Sun, C. Y.; Zheng, X. J.; Chen, X. B.; Li, L. C.; Jin, L. P. *Inorg. Chim. Acta* **2009**, *362*, 325.
(68) Soares-Santos, P. C. R.; Cunha-Silva, L.; Paz, F. A. A.; Ferreira, R. A. S.; Rocha, J.; Trindade, T.; Carlos, L. D.; Nogueira, H. I. S. *Crystal Growth & Design* **2008**, *8*, 2505.
(69) Kerbellec, N.; Kustaryono, D.; Haquin, V.; Etienne, M.; Daiguebonne, C.; Guillou, O. *Inorg. Chem.* **2009**, *48*, 2837.
(70) Guo, H.; Zhu, Y.; Qiu, S.; Lercher, J. A.; Zhang, H. *Adv Mater* **2010**, *22*, 4190.
(71) Horcajada, P.; Chalati, T.; Serre, C.; Gillet, B.; Sebrie, C.; Baati, T.; Eubank, J. F.; Heurtaux, D.; Clayette, P.; Kreuz, C.; Chang, J. S.; Hwang, Y. K.; Marsaud, V.; Bories, P. N.; Cynober, L.; Gil, S.; Ferey, G.; Couvreur, P.; Gref, R. *Nat. Mater.* **2010**, *9*, 172.
(72) Taylor-Pashow, K. M. L.; Della Rocca, J.; Xie, Z. G.; Tran, S.; Lin, W. B. *J. Am. Chem. Soc.* **2009**, *131*, 14261.
(73) Rieter, W. J.; Taylor, K. M. L.; An, H. Y.; Lin, W. L.; Lin, W. B. *J. Am. Chem. Soc.* **2006**, *128*, 9024.
(74) Taylor, K. M. L.; Jin, A.; Lin, W. B. *Angew. Chem. Int. Ed.* **2008**, *47*, 7722.
(75) Taylor, K. M. L.; Rieter, W. J.; Lin, W. B. *J. Am. Chem. Soc.* **2008**, *130*, 14358.
(76) Dekrafft, K. E.; Xie, Z. G.; Cao, G. H.; Tran, S.; Ma, L. Q.; Zhou, O. Z.; Lin, W. B. *Angew. Chem. Int. Ed.* **2009**, *48*, 9901.

2.0 NEAR-INFRARED (NIR) EMITTING YTTERBIUM METAL-ORGANIC FRAMEWORKS WITH TUNABLE PROPERTIES

Part of this chapter has been published as Kiley A. White, Demetra A. Chengelis, Matthias Zeller, Steven J. Geib, Jessica Szakos, Stéphane Petoud, and Nathaniel L. Rosi, *Chem. Comm.*, **2009**, 4506-4508.

This work was done in collaboration with Demetra Chengelis (Stéphane Petoud Research Group, University of Pittsburgh), who performed the luminescence measurements.

Steven J. Geib (X-ray crystallographer, University of Pittsburgh) solved the crystal structure of **Yb-PVDC-1.**
Matthias Zeller (X-ray crystallographer, Youngstown State University) solved the crystal structure of **Yb-PVDC-2.**

2.1 INTRODUCTION

Several lanthanide-containing MOFs emitting in the visible have been prepared and characterized spectroscopically.[1] However, very few near-infrared (NIR)[2] emitting MOFs have been synthesized. NIR emitting Ln-MOFs offer properties that might be useful for a variety of new applications, such as photonic materials and optical telecommunication devices, as well as bioanalytical and biological imaging probes and sensors.[3,4]

Before lanthanide cations can be incorporated as functional components in materials with real-world applications, their photophysical properties should be optimized. These properties can be adversely affected by the lanthanide environment, such as O-H, N-H, and C-H vibrational overtones from organic solvents and antennae that quench luminescence intensity.[3] Thus, it is crucial to control the environment around these cations; however, lanthanides have low stereochemical requirements. Their coordination must be tridimensionally manipulated by the design of the overall molecular complex in which the antennae are arranged to provide control of the photophysical properties and protection of the metal cations. Additionally, for practical applications, control over the excitation wavelength, which is determined by the electronic properties of the ligand and any ligand/ligand interactions, is advantageous. Whether an "invisble" UV, a low energy visible, or a NIR excitation wavelength is desired, the ability to tune the wavelength without having to find a different sensitizer would be optimal.

In Chapter 2, we use a novel metal-organic framework (MOF) approach[5-10] to achieve control of lanthanide luminescence properties. Our results demonstrate for the first time that modification of our MOF structure, without changing the chromophore linker, allows for tuning of the luminescence properties of the resulting Yb^{3+} MOFs. The fundamental strategies presented

herein will be useful for creating, optimizing, and tailoring lanthanide-based materials for NIR applications.

2.2 RESULTS AND DISCUSSION

2.2.1 H_2-PVDC

We initiated this work by identifying a ligand that could both sensitize a NIR-emitting lanthanide cation and direct its assembly into an extended porous network. 4,4'-[(2,5-dimethoxy-1,4-phenylene)di-2,1-ethenediyl]bis-benzoic acid (**H_2-PVDC**) (Figure 2.1) was chosen because it absorbs strongly in the visible range; it could promote the formation of extended MOF structures; and our preliminary studies demonstrated that it was capable of sensitizing NIR-emitting Yb^{3+}, Ho^{3+}, Er^{3+}, and Nd^{3+}.

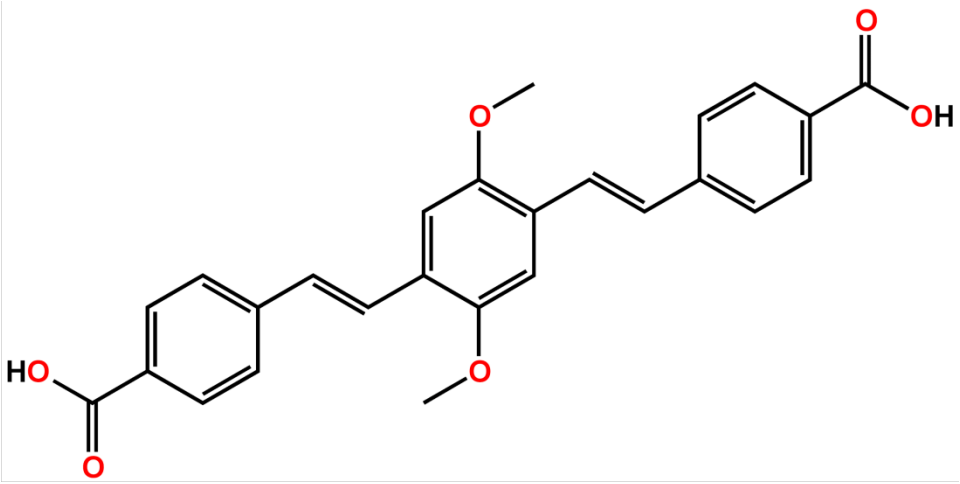

Figure 2.1. H_2-PVDC

2.2.1.1 Synthesis of H_2-PVDC

H_2-PVDC had never been synthesized previously. Synthetic details can be found Section 2.4.4 including ^{1}H and ^{13}C NMR spectra. This molecule was designed with specific attributes: 1) both oxygen atoms can bond strongly to lanthanide cations upon deprotonation of the carboxylic acid; 2) the trans olefin bonds promote planarity and complete conjugation throughout the molecule, leading to enhanced electronic and fluorescent properties; and 3) the methoxy groups enhance the solubility and allow for the PVDC to be dissolved in common organic solvents. Originally the same ligand without the methoxy moieties was synthesized, and that compound was found to be insoluble in most standard organic solvents, making it difficult to perform reactions with that ligand.

The four-step synthesis (Scheme 2.1) began with a bromomethylation of 1,4 dimethoxybenzene using HBr and acetic acid to produce 1,4-bis(bromomethyl)-2,5-dimethoxybenzene (**1**).[11] The phosphonium salt **(2)** was then synthesized in preparation for a standard Wittig reaction. The Wittig reaction yielded a mixture of E,E, Z,E, and Z,Z products of the methyl-ester-terminated phenylene vinylene.[12] All three stereoisomers were subsequently isomerized to the trans, trans isomer by refluxing in I_2 and toluene.[13] Post isomerization, the IR spectrum shows only the trans H-C=C-H vibration at ~960 cm^{-1}; the cis out-of-plane H-C=C-H stretch, originally present at 564 cm^{-1} in the IR spectrum of the initial mixture of products, is now absent, indicating a pure trans, trans product, dimethyl 4,4'-(1*E*,1'*E*)-2,2'-(2,5-dimethoxy-1,4-phenylene)bis(ethane-2,1-diyl)dibenzoate **(3)** (confirmed by ^{1}H NMR, as well).[13] The final product **(4)** is obtained by hydrolyzing the methoxy ester with excess base, KOH. Crystallization from DMF yields the pure product, 4,4'-(1*E*, 1'*E*)-2,2'-(2,5-dimethoxy-1,4-phenylene)bis(ethene-2,1-diyl)dibenzoic acid (H_2-PVDC), as confirmed by ^{1}H NMR and ^{13}C NMR.

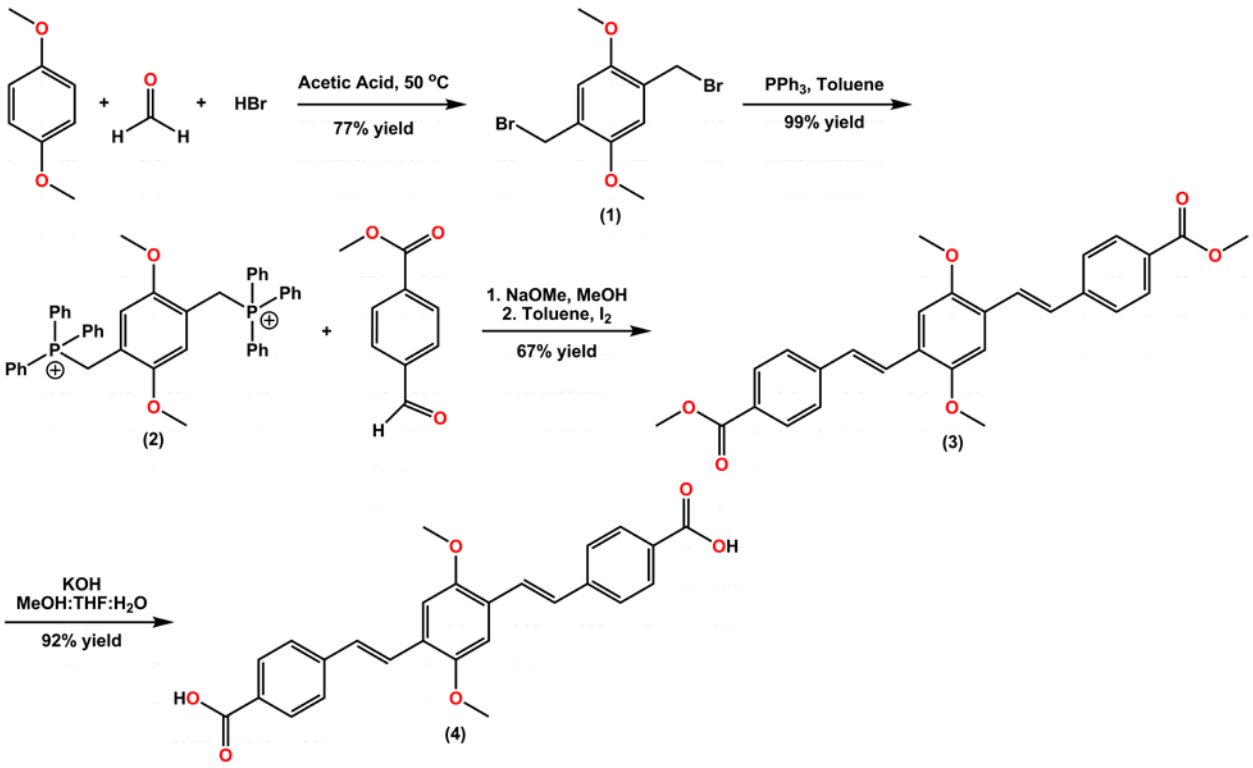

Scheme 2.1. Synthesis of H_2-PVDC

2.2.1.2 Photophysical properties of H_2-PVDC

H_2-PVDC was dissolved in DMSO and its excitation, fluorescence, and absorbance spectra were collected. The excitation spectrum of **H_2-PVDC** displays two bands with apparent maxima centered at 340 and 420 nm (Figure 2.2). Excitation through either of these bands produces a fluorescence band centered at 485 nm. **H_2-PVDC** displays a strong absorption spectrum with maxima similar to the excitation spectrum (Figure 2.3). This strong absorbance is ideal for antennae that are used for lanthanide sensitization in order to maximize absorption of incoming light and the amount of resulting energy transferred to the lanthanide cation.

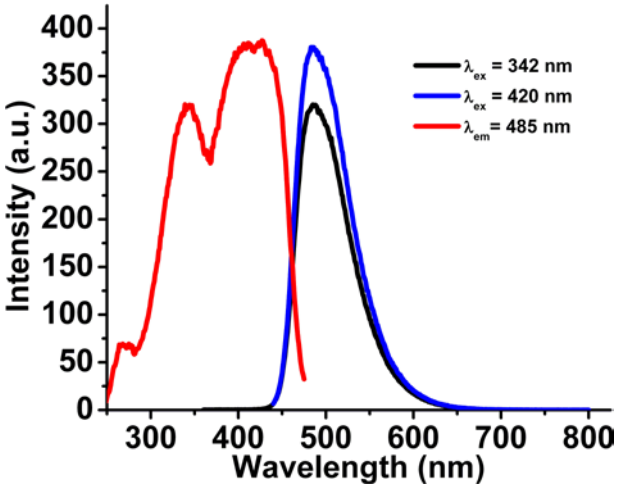

Figure 2.2. Excitation (red, λ_{em} = 485 nm) and emission spectra (black, λ_{ex} = 342 nm; blue, λ_{ex} = 420 nm) of H_2-PVDC in DMSO

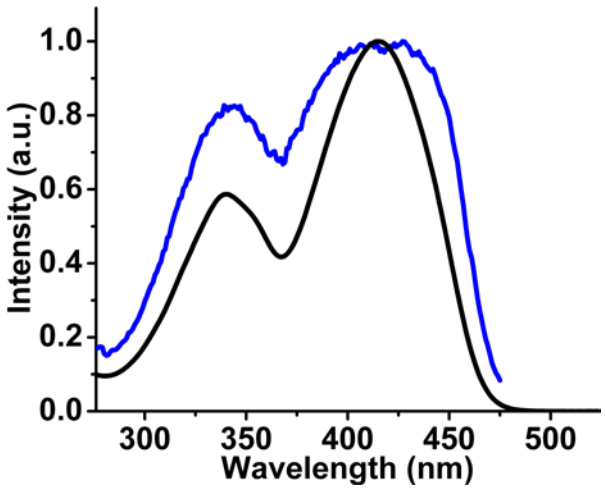

Figure 2.3. Absorbance (black) and excitation (blue; λ_{em} = 485 nm) spectra of H_2-PVDC in DMSO

2.2.2 Ln-PVDC molecular complexes

Molecular complexes of **H_2-PVDC** and $LnCl_3$ salts were prepared in solution to test the ability of bond formation and the luminescence spectra were collected to determine any lanthanide sensitization. Upon exciting the Yb-PVDC molecular complex at 420 nm (Figure 2.4), Yb^{3+} emission centered at 980 nm was observed (Figure 2.4). To determine if the emission was via the antenna effect, the excitation spectrum for the complex was collected while monitoring the 980 nm emission band of ytterbium. The excitation spectrum contains two bands centered at 340 and 415 nm that adopt the same profile as the absorption of **H_2-PVDC**, indicating that PVDC sensitizes the lanthanide via the antenna effect (Figures 2.4). The photophysical properties of the remaining molecular complexes were then investigated and sensitization was achieved resulting in typical emission bands of NIR emitting Yb^{3+}, Er^{3+}, Nd^{3+}, and Ho^{3+} (Figure 2.5).

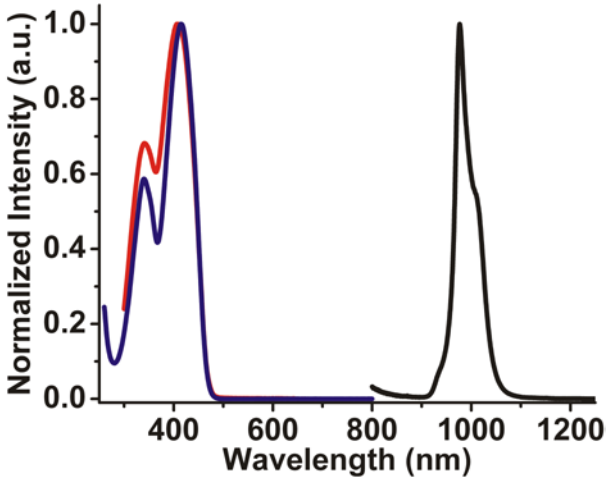

Figure 2.4. Excitation spectrum (red; λ_{em} = 980 nm) and emission spectrum (black; λ_{ex} = 420 nm) for the Yb-PVDC complex in DMSO, and absorbance (blue) of H_2-PVDC

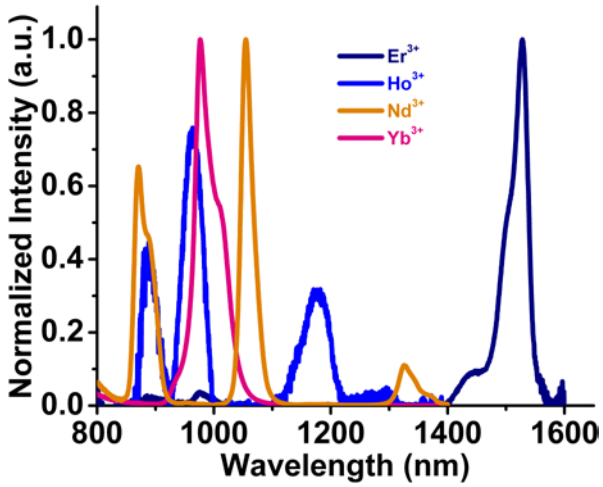

Figure 2.5. Normalized NIR spectra (λ_{ex} = 410 nm) of Ln-PVDC complexes in DMSO showing Er^{3+} emission (royal; 1530 nm), Ho^{3+} emission (blue; 890, 975, and 1195 nm), Nd^{3+} emission (orange; 875, 1060, and 1330 nm), and Yb^{3+} emission (980 nm)

2.2.3 Yb-PVDC-1

After concluding that sensitization was achieved with **H_2-PVDC** and NIR-emitting lanthanide cations, MOF reactions were begun. Reacting $Yb(NO_3)_3 \cdot 5H_2O$ with **H_2-PVDC** yielded yellow needles of **Yb-PVDC-1**, $Yb_2(C_{26}H_{20}O_6)_3(H_2O)_2 \cdot (DMF)_6(H_2O)_{8.5}$. Single crystal X-ray diffraction analysis revealed that **Yb-PVDC-1** crystallizes in the high symmetry *F*ddd space group and is composed of infinite Yb-carboxylate chains aligned along the *a* crystallographic direction (Figure 2.6 and 2.7).[14] The chains consist of alternating octa- and hexa-coordinated Yb^{3+}, bridged in a di-monodentate fashion via the carboxylates of three different PVDC linkers (Figure 2.7). Two water molecules terminally coordinate to the octa-coordinate Yb^{3+}. The chains are connected along [110] via the phenylene vinylene portion of the ligand resulting in the formation of large 24 x 40 Å channels (Figure 2.6). The material maintains its crystallinity in a variety of solvents, as confirmed by powder X-ray diffraction studies of solvent exchanged samples (Figure 2.8).

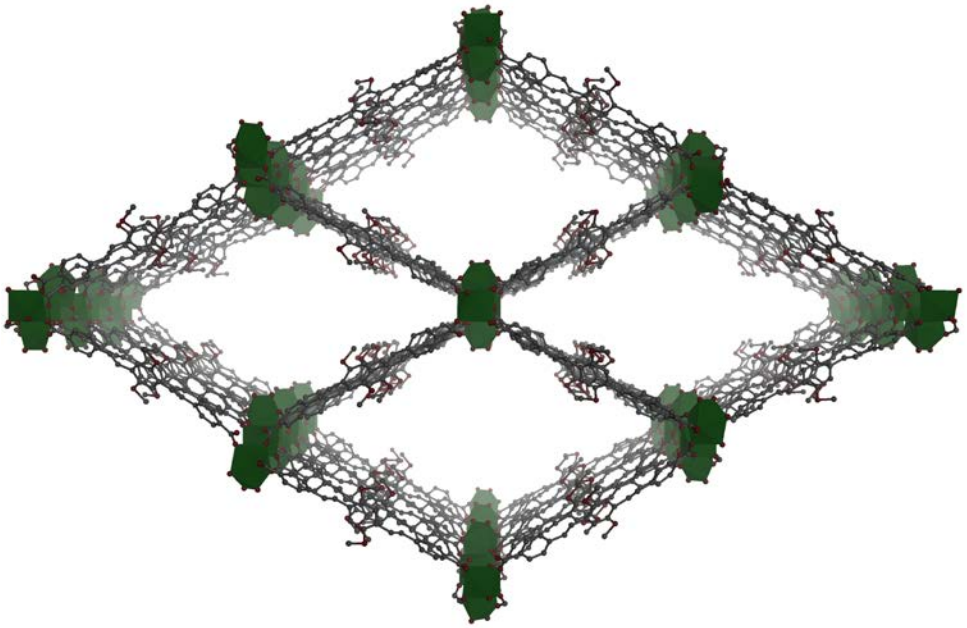

Figure 2.6. Projection view of Yb-PVDC-1 viewed along the *a* crystallographic direction with Yb^{3+} shown as polyhedra (C, grey; O, red; Yb^{3+}, dark green)

.

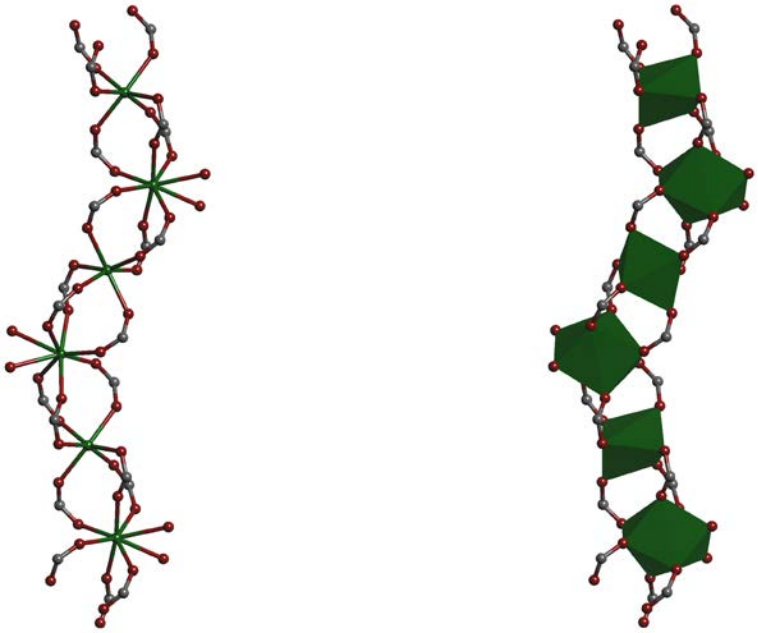

Figure 2.7. Ball and stick depiction of infinite SBU (left) and SBU with Yb^{3+} shown as polyhedra (right) within Yb-PVDC-1 (C, grey; O, red; Yb^{3+}, dark green)

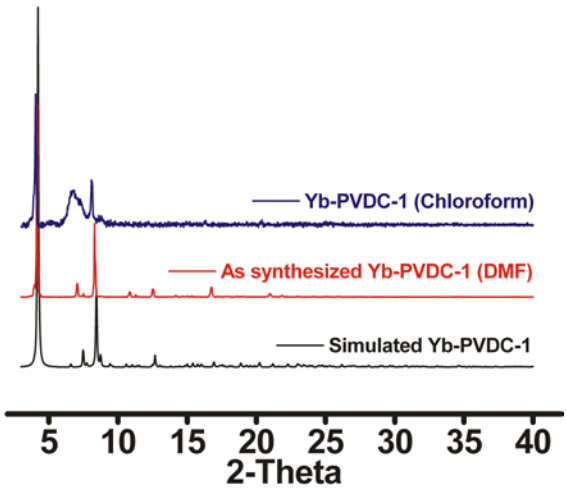

Figure 2.8. Powder X-ray diffraction patterns of Yb-PVDC-1

The emission and excitation spectra were measured for **Yb-PVDC-1** and compared to corresponding spectra recorded for **H_2-PVDC** and the 1:1 Yb-PVDC molecular complex to determine how the MOF structure impacts the luminescence properties of the system. Luminescence analysis was performed on **Yb-PVDC-1** suspended under chloroform (Figure 2.9) and displays Yb^{3+} luminescence in the NIR (Figure 2.10). The MOF excitation spectrum displays bands with maxima at 370 and 470 nm, notably red-shifted from 415 nm for the Yb-PVDC complex (Figure 2.9). Although the Yb-PVDC complex experiments were performed in DMSO due to solubility constraints, this observed shift of over 50 nm cannot solely be attributed to a solvatochromic effect. We tentatively attribute a significant component of this shift to organizational constraints that the MOF architecture imparts on the phenylene vinylene linkers. In **Yb-PVDC-1**, the ligands are arranged in parallel along [110], which may allow for weak interactions between neighboring chromophoric ligands (Figure 2.11). These interactions are hypothesized to affect the electronic structure of the chromophore, resulting in decreased excitation energy.

Figure 2.9. Yb-PVDC-1 crystals suspended under chloroform

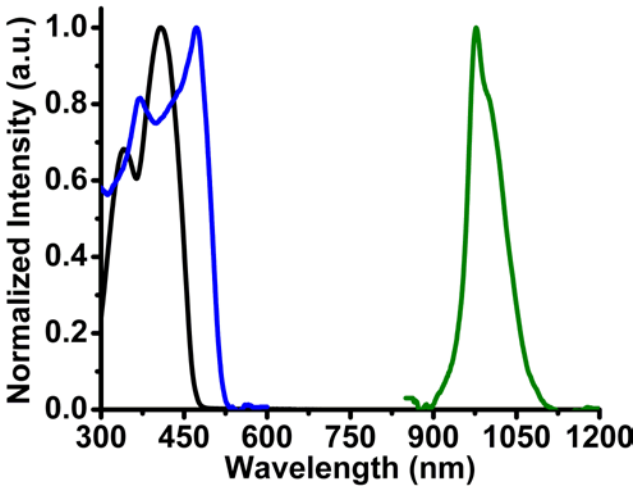

Figure 2.10. Excitation profile of the Yb-PVDC molecular complex (black; λ_{em} = 980 nm), excitation profile of Yb-PVDC-1 (blue; λ_{em}= 980 nm) and Yb^{3+} emission of Yb-PVDC-1 (green; λ_{ex} = 470 nm)

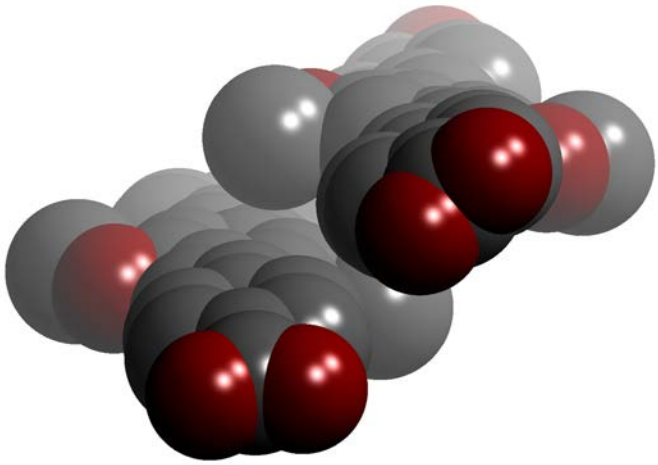

Figure 2.11. Ligand stacking motif within Yb-PVDC-1 along [110]

2.2.4 Yb-PVDC-2

To evaluate the extent to which ligand-ligand interactions impact the excitation and emission properties of Yb-PVDC systems, we prepared a second MOF, **Yb-PVDC-2**, $Yb_2(C_{26}H_{20}O_6)_3 \cdot (DMF)_{12}(H_2O)_{10}$. **Yb-PVDC-2** crystallizes in the orthorhombic *Pnna* space group and also exhibits infinite Yb-carboxylate SBUs (Figure 2.12 and 2.13). However, the connectivity within the SBU differs from that of **Yb-PVDC-1**. The SBU is composed of alternating octa- and hexa-coordinated Yb^{3+}. The Yb^{3+} are bridged by two carboxylates in a di-mondodentate fashion and by a third carboxylate that chelates the octa-coordinate Yb^{3+} and coordinates in a monodentate fashion to the hexa-coordinate Yb^{3+} (Figure 2.12). These coordination modes result in a chain of corner-sharing polyhedral Yb^{3+}. Each chain is linked to six other chains via the phenylene vinylene portion of the PVDC linkers (Figure 2.13). The linkers connecting the chains along the [001] stack in parallel, while those that connect the chains in the [011] form criss-crossing pairs with close π-π interactions[15] (perpendicular distance between planes: 3.6 Å) between the central phenyl rings of the PVDC linkers (Figure 2.14). Because each infinite SBU is connected to six other SBUs, the resulting triangular channels are smaller than those observed for **Yb-PVDC-1**, measuring ~13-14 Å from corner to edge (Figure 2.12). **Yb-PVDC-2** also maintains its crystallinity in a variety of solvents, as confirmed by powder X-ray diffraction studies of solvent-exchanged samples (Figure 2.15).

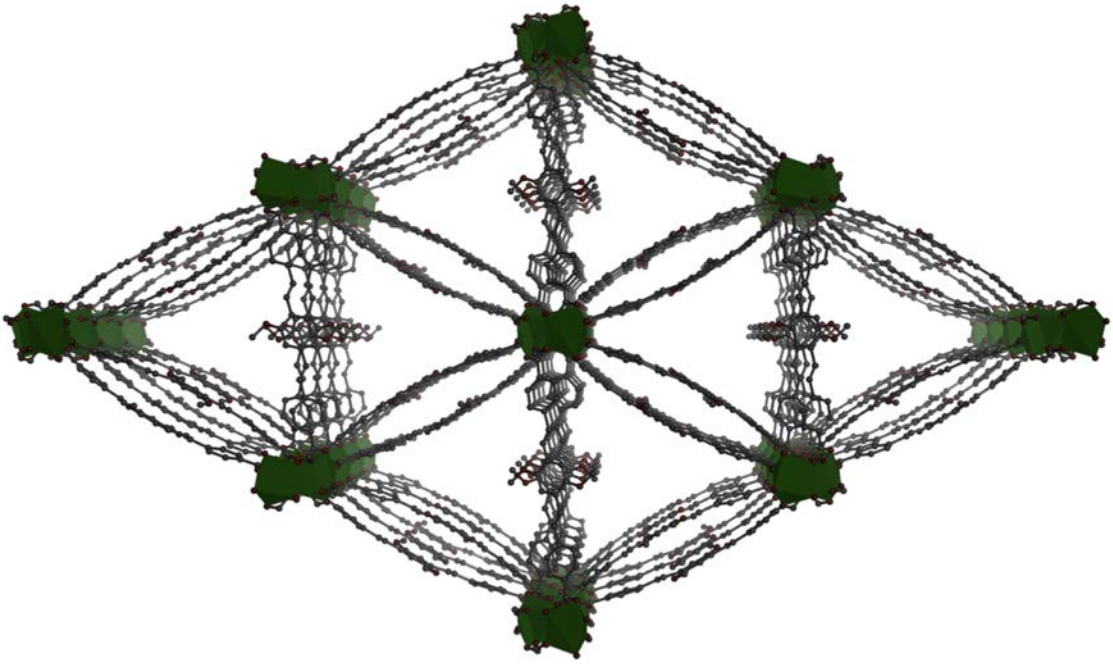

Figure 2.12. Projection view of Yb-PVDC-2 viewed along the *a* crystallographic direction with Yb^{3+} shown as polyhedra (C, grey; O, red; Yb^{3+}, dark green)

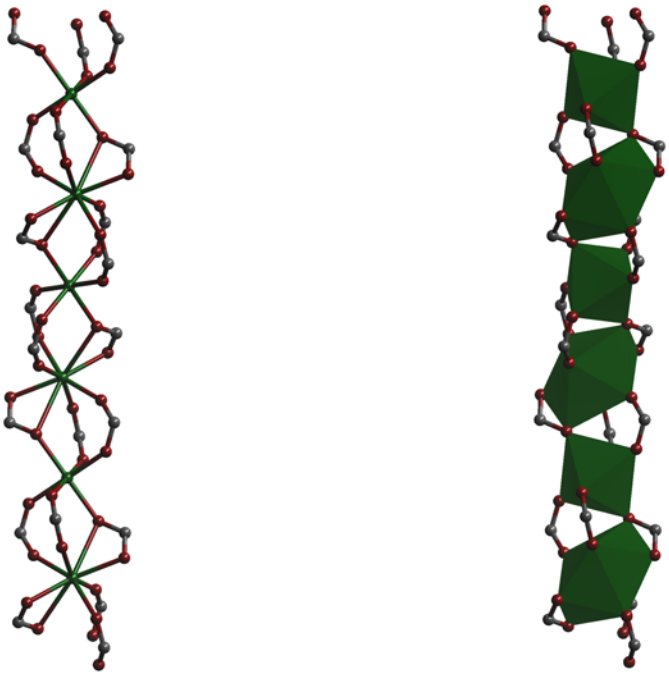

Figure 2.13. Ball and stick depiction of infinite SBU (left) and SBU with Yb^{3+} shown as polyhedra (right) within Yb-PVDC-2 (C, grey; O, red; Yb^{3+}, dark green)

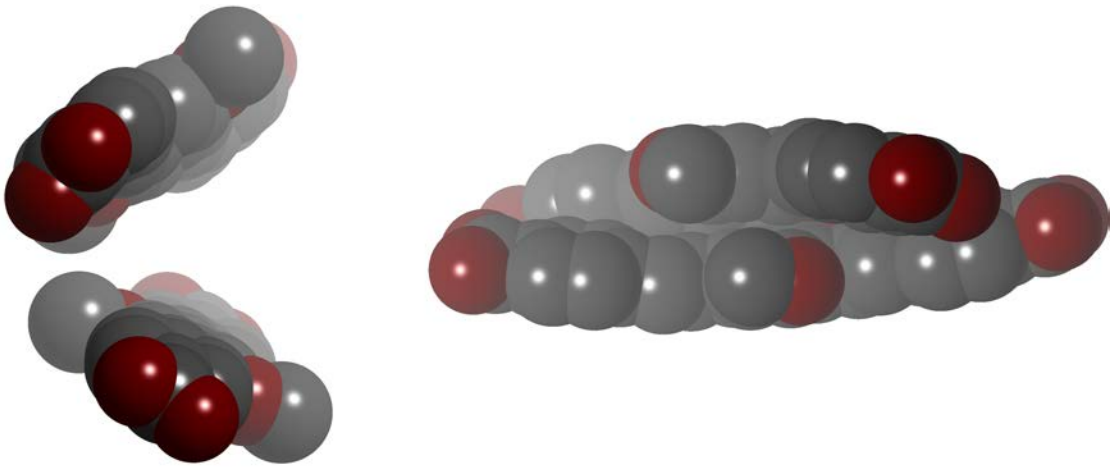

Figure 2.14. Ligand stacking motif within Yb-PVDC-2 along the [001] (left) and [011] (right)

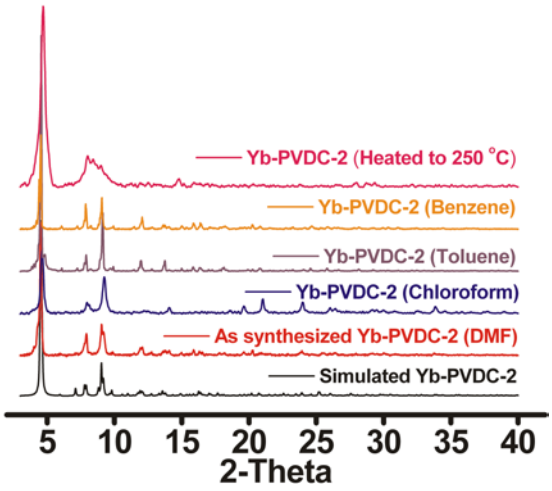

Figure 2.15. Powder X-ray diffraction patterns of Yb-PVDC-2 solvent-exchanged materials

The luminescent properties of **Yb-PVDC-2** (chloroform-exchanged material) were examined to determine the impact the structural changes have on the photophysical properties of this system. **Yb-PVDC-2,** while suspended under chloroform, appears yellow-orange (Figure 2.16) as opposed to the bright yellow color of **Yb-PVDC-1**, indicating variations between their photophysical properties. The excitation spectrum collected upon monitoring the emission intensity of Yb^{3+} luminescence at 980 nm displayed apparent band maxima centered at 370 and

500 nm (Figure 2.17). The emission spectra collected in the NIR range upon excitation at these wavelengths shows characteristic Yb^{3+} emission at 980 nm. Interestingly, the lowest energy excitation band of **Yb-PVDC-2** is further red-shifted to 500 nm from 470 nm in **Yb-PVDC-1**, which explains the color difference between the crystals. We tentatively propose that the close π-π interactions between the PVDC linkers decrease the energy of the π→π* transition, resulting in a lowered excitation energy.

Figure 2.16. Yb-PVDC-2 suspended in chloroform

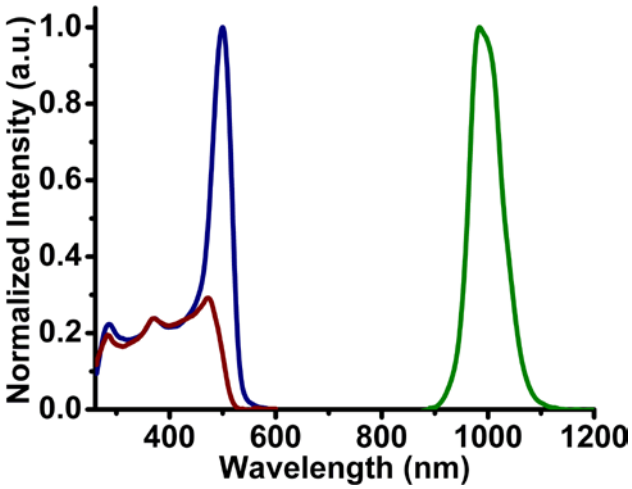

Figure 2.17. Luminescence data comparing the excitation profiles of Yb-PVDC-1 (red; λ_{em} = 980 nm) to Yb-PVDC-2 (blue; λ_{em} = 980 nm) and displaying Yb^{3+} emission of Yb-PVDC-1 (green; λ_{ex} = 500 nm)

2.2.5 Lifetimes and quantum yields

To determine whether the MOF architecture provides efficient protection for the lanthanide cations from solvent quenching and to quantify the intramolecular energy transfer of the systems, we measured quantum yield values using an integration sphere (Table 2.1). The quantum yield of **Yb-PVDC-2** is five times higher than **Yb-PVDC-1** when excited through the lower energy band (490 nm). The quantum yield of **Yb-PVDC-2** is among the highest values reported for ytterbium systems under solvent.[16-18] These quantum yields are global: the excitation is performed through the sensitizer and the emission is observed through the Yb^{3+} cations that have different coordination environments and levels of protection in both MOFs. In **Yb-PVDC-1**, the octa-coordinate Yb^{3+} cations coordinate two water molecules which quench ytterbium emission and lower the global quantum yield.

We monitored ytterbium centered luminescence lifetimes in order to further determine the effectiveness of the MOFs in protecting the lanthanide cations from non-radiative deactivation. Both MOFs displayed multi-exponential decay patterns and were best fit with four components (Table 2.1), which are attributed to four different lanthanide environments: the hexa-coordinate and octa-coordinate Yb^{3+} sites within the core of the MOF structures and those along the terminating edges of the crystals, where the lanthanide cations are more exposed to sources of non-radiative deactivation. The long component values are up to two times longer than the longest lifetimes reported for Yb^{3+} molecular species in solution.[19-20] These luminescence lifetimes demonstrate that MOFs can provide coordination environments with improved protection from quenching than molecular complexes.

Table 2.1. Absolute emission quantum yields (Φ, λ_{ex} = 490 nm) and luminescent lifetimes (τ_x, μs, λ_{ex} = 354 nm) of Yb^{3+} centered emission at 980 nm for the MOFs as crystalline solids under chloroform with error included in parentheses

MOF	Φ_{Yb}	τ_1	τ_2	τ_3	τ_4
Yb-PVDC-1	3.3 (±0.5)×10^{-3}	29 (±2)	10 (±1)	1.5 (±0.5)	0.34 (±0.06)
Yb-PVDC-2	1.8 (±0.2)×10^{-2}	22 (±4)	5.6 (±1.5)	1.7 (±0.3)	0.61 (±0.17)

2.2.6 Solvent studies

Powder X-ray diffraction studies confirmed that **Yb-PVDC-2** maintains its crystallinity in a variety of solvents, such as chloroform, toluene, benzene, and dimethylformamide. In order to confirm that solvent effects were not responsible for the shift in excitation wavelength, luminescence spectra and quantum yields were measured for **Yb-PVDC-2** solvent-exchanged. The excitation spectra of the sensitized ytterbium emission at 980 nm in these different solvents were collected (Figure 2.18). All excitation spectra have similar profiles, with maxima centered at the same wavelengths. There are some variations in the intensities at higher energy, which is likely due to differences in the solvent absorption. However, no major shifts exist in the locations of the excitation maxima between solvents, which confirms that the dramatic difference in excitation wavelengths for the MOFs compared to the molecular complex cannot be due to solvatochromic effects.

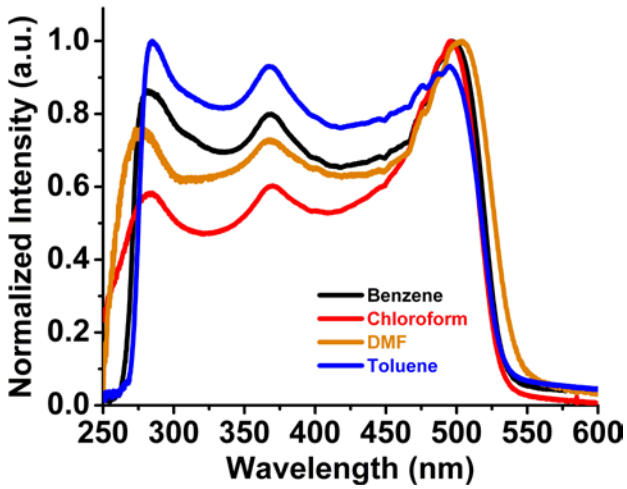

Figure 2.18. Yb^{3+} excitation spectra (λ_{em} = 980 nm) for Yb-PVDC-2 suspended under benzene (black), chloroform (red), dimethylformamide (orange), and toluene (blue)

The quantum yields were also measured (Table 2.2). The values among benzene, toluene, and chloroform are within error of each other, which is rational since none of these solvents contain highly quenching modes. However, the quantum yield under DMF is much lower, which is likely due to the instability of this compound in this solvent rather than quenching effects. After a few days under DMF, the solvent became yellow, indicating breakdown of the crystal structure, which did not occur in the other solvents. Alternatively, DMF is a highly hygroscopic solvent so the water content may be much larger which could also lead to decreased quantum yields.

Table 2.2. Absolute emission quantum yields (Φ) for Yb^{3+} luminescence in Yb-PVDC-2 under different solvents (λ_{ex} = 490 nm) with error included in parentheses

Solvent	Φ_{Yb}
Benzene	1.5 (± 0.1) %
Toluene	1.6 (± 0.1) %
Chloroform	1.8 (± 0.2) %
DMF	0.4 (± 0.2) %

2.3 CONCLUSION

We have synthesized an antenna, **H_2-PVDC**, suitable for sensitizing four NIR emitting lanthanide cations: Ho^{3+}, Nd^{3+}, Er^{3+} and Yb^{3+}. We have also illustrated the validity of a MOF-based approach to sensitize NIR emitting Yb^{3+}, which results in materials with enhanced and controlled luminescence properties. Specifically, we have shown that a chromophoric antenna molecule and NIR emitting Yb^{3+} can be assembled into rigid MOF structures that effectively control the coordination environments around the lanthanide cations and the arrangement of chromophoric antennae. Using this strategy, we obtained a lower energy excitation wavelength by modifying the three-dimensional MOF structure to allow for close π-π interactions between the chromophores. The possibility to have different excitation ranges without altering the structure of the sensitizer provides a new route for controlling the photophysical properties of lanthanide complexes, in contrast to more traditional approaches, which involve changing the antenna's structure. The intrinsic structures of the MOFs also provide protection of the lanthanide cations from solvent vibrations. The ability to design MOFs and control their structural features makes them ideal materials for carefully controlling and optimizing the photophysical properties of lanthanide cations. We further illustrate this capability in Chapter 3 when we incorporate multiple lanthanides into MOF materials for barcoding applications and in Chapter 4 when we investigate Ln-Ln interactions within a MOF.

2.4 EXPERIMENTAL

2.4.1 Reagents

Dimethoxybenzene, paraformaldehyde, triphenylphosphine, methanol, NaOMe, THF, DMF, anhydrous methanol, anyhydrous benzene, $NdCl_3 \bullet 6H_2O$, $YbCl_3 \bullet 6H_2O$, $ErCl_3 \bullet 6H_2O$, $HoCl_3 \bullet 6H_2O$, 0.1 N KOH in methanolic solution, and tetrabutylammonium hydroxide were purchased from Aldrich. $Yb(NO_3)_3 \bullet 5H_2O$ was purchased from Strem Chemicals. Glacial acetic acid and hydrochloric acid were purchased from Fisher. Hyrdobromic acid (33% in AcOH) was purchased from Fluka. Anhydrous toluene (99.8%) and anhydrous chloroform (99.8%) were purchased from Acros. Argon gas was purchased from Valley National. Methyl 4-formylbenzoate was purchased from TCI. Ethanol was purchased from Pharmco. KOH was purchased from Alfa Aesar. All reagents were used as received without further purification.

2.4.2 General procedures

^{1}H NMR (300 MHz) and ^{13}C NMR (75 MHz) were recorded on a Bruker Avance 300. Fourier transform infrared (FT-IR) spectra were measured on a Nicolet Avatar 360 FT-IR spectrometer using KBr pellet samples. Absorptions are described as very strong (vs), strong (s), medium (m), weak (w), shoulder (sh), and broad (br) and stretches (st) are labeled symmetric (sym) or asymmetric (as). Data was analyzed using the Omnic Software Package. Mass spectra were obtained with a VG AutoSpec Q.

X-ray powder diffraction patterns were taken using a Bruker AXS D_8 Discover powder diffractometer at 40 kV, 40 mA for Cu Kα, (λ = 1.5406 Å) with a scan speed of 0.20 sec/step

and a step size of .02018º. The data were analyzed for d-spacing measurements using the EVA program from the Bruker Powder Analysis Software package. The simulated powder patterns were calculated using PowderCell 2.4. The purity and homogeneity of the bulk products were determined by comparison of the simulated and experimental X-ray powder diffraction patterns. Solvent exchange of the DMF and H_2O guest molecules in **Yb-PVDC-1** and **Yb-PVDC-2** was performed using anhydrous solvents as follows: 30 min soak in exchange solvent (ES) followed by solvent removal (3X); overnight soak in ES and then solvent removal; 24 h soak in ES and solvent removal; addition of fresh solvent. The elemental microanalysis was performed by the University of Illinois, Department of Chemistry, Microanalytical Laboratory using an Exeter Analytical CE440.

2.4.3 Spectroscopic procedures

Absorption spectra were recorded on a Perkin-Elmer Lambda 9 Spectrometer coupled with a personal computer using software supplied by Perkin-Elmer. For analysis of the photophysical properties of **H_2-PVDC**, a solution of 5.0×10^{-4} M was prepared by dissolving 1.50 mg of the ligand in 6.97 mL of dimethylsulfoxide (DMSO). This stock solution was diluted for UV-visible absorbance measurements and fluorescence analysis

Emission and excitation spectra in the visible range were measured using a Varian Cary Eclipse Fluorescence Spectrophotometer coupled to a personal computer with software provided by Varian. Spectra in the near infrared range were measured using a Jobin Yvon–Horiba Fluorolog-322 spectrofluorimeter equipped with an Electro-Optical Systems, Inc. DSS-IGA020L detector for the NIR domain. Emission and excitation spectra of the **Yb-PVDC-1** and **Yb-PVDC-2** were collected as solid samples under chloroform on the JY Horiba Fluorolog-322

Spectrofluorimeter fitted with an integrating sphere developed by Prof. Frédéric Gumy and Prof. Jean-Claude G. Bünzli (Laboratory of Lanthanide Supramolecular Chemistry, École Polytechnique Féderale de Lausanne (EPFL), BCH 1402, CH-1015 Lausanne, Switzerland) as an accessory to the Fluorolog FL3-22 spectrometer (Patent pending) using quartz tube sample holders.

Relative quantum yield measurements were obtained with the integration sphere on the Jobin Yvon-Horiba Fluorolog-322. For quantum yield measurements in the NIR range with the integration sphere, the analysis is more complex as two different detectors are used, a visible detector to determine the absorbance of light and a NIR detector to monitor the sample emission. It is necessary to measure a relative quantum yield using a sample with a known value. The procedure is described below, using ytterbium or erbium tropolonate, $[Ln(trop)_4]^-$ in DMSO ($\Phi_{Yb} = 1.9x10^{-2}$, $\Phi_{Er} = 1.7x10^{-4}$)[7] as the reference.

1) To determine the amount of light absorbed by the sample and the reference, emission spectra are collected of the excitation light from the lamp for the sample (ExS) and the reference (ExR), as well as an empty cuvette (ExB). Due to the high intensity of the lamp, neutral density filters are employed and the integrated values are corrected accordingly. The light absorbed is given by: $Ex_B - Ex_S$ and $Ex_B - Ex_R$.

2) Emission spectra are collected in the NIR range of the sample (I_S) and the reference (I_R), as well as of an empty cuvette (I_B). If the sample and reference emission spectra are collected with different excitation or emission wavelengths, two corresponding emission spectra of the empty cuvette will be necessary. To eliminate second order bands, glass cut on filters are placed before the detector. The spectra are corrected for lamp variation, detector response and signal attenuation from the cut on filters. The emission bands for

the sample, reference, and blank(s) are integrated, and total emission is given by: $I_S - I_B$ and $I_R - I_B$.

3) Using the known quantum yield of the reference, a scalar ($X_{NIR\text{-}VIS}$) is created to offset the NIR emission spectra to the same scale as the visible spectra of the excitation, as shown in Equation 2.1.

$$\textbf{(2.1)}\ X_{NIR\text{-}VIS} = [\Phi(Ex_B - Ex_R)] / (I_R - I_B)$$

4) The quantum yield (Φ) is calculated using Equation 2.2.

$$\textbf{(2.2)}\ \Phi = [X_{NIR\text{-}VIS}(I_S - I_B)] / (Ex_B - Ex_S)$$

Lanthanide luminescence lifetimes were measured using a Nd:YAG Continuum Powerlite 8010 laser (354 nm, 3rd harmonic) as the excitation source. Emission was collected at a right angle to the excitation beam, and wavelengths were selected by a Spectral Products CM 110 1/8 meter monochromator. The signal was monitored by a Hamamatsu R316-02 photomultiplier tube for the NIR range, and was collected on a 500 MHz band pass digital oscilloscope (Tektronix TDS 754D). Alternatively, luminescence lifetimes in the visible range were measured using an Oriel 79110 Nitrogen laser (λ_{ex}: 337 nm) or the flash lamp of the JY Horriba fluorimeter as the excitation source, and the emission signal was collected at a 90 degree angle with the SPEX Fluorolog detector. The signal was monitored with the same oscilloscope. Signals from >1000 flashes were collected and averaged. Luminescence decay curves were treated with Origin 7.0 software using exponential fitting models. Three decay curves were collected on each sample, and reported lifetimes are an average of at least two independent measurements.

2.4.4 Synthesis of H_2-PVDC

1,4-Bis(bromomethyl)-2,5-dimethoxybenzene (**1**):

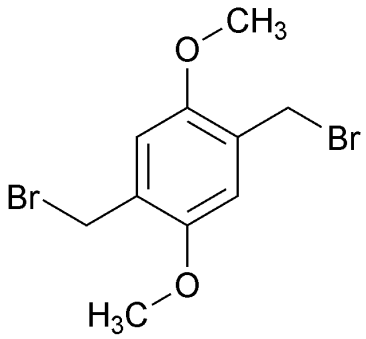

(1)

This intermediate was prepared following an established procedure,[11] which is detailed below. To a stirred solution of 1,4-dimethoxybenzene (Aldrich, 10.00 g, 72.37 mmol) in glacial acetic acid (Fisher, 50 mL), paraformaldehyde (Aldrich, 4.27 g, 144.75 mmol) and HBr/AcOH (Fluka, 33%, 30 mL) were added slowly. The mixture was stirred at 50 ºC for one hour and hydrolyzed in water (200 mL) after cooling to room temperature. The white solid was collected by filtration, suspended in $CHCl_3$ (50 mL), and refluxed for 10 min. After cooling to room temperature, the white solid was again collected by filtration and washed with water (15.75 g, 67%). ^{1}H NMR (300 MHz, $CDCl_3$) δ 6.88 (s, 2H), 4.54 (s, 4H), 3.87 (s, 6H) ppm; ^{13}C NMR (75 MHz, $CDCl_3$) δ 151.9, 128.0, 114.5, 56.9, 29.1 ppm; FTIR (KBr pellet): 2962 (w), 2934 (w), 2834 (w), 1509 (vs), 1461 (s), 1428 (w), 1404 (vs), 1319 (m), 1228 (vs), 1205 (s), 1179 (w), 1103 (w), 890 (w), 874 (w), 718 (w) cm^{-1}. HRMS (EI+) Calcd for $C_{10}H_{12}O_2Br_2$ $[M]^+$ 321.9204, found 321.9209.

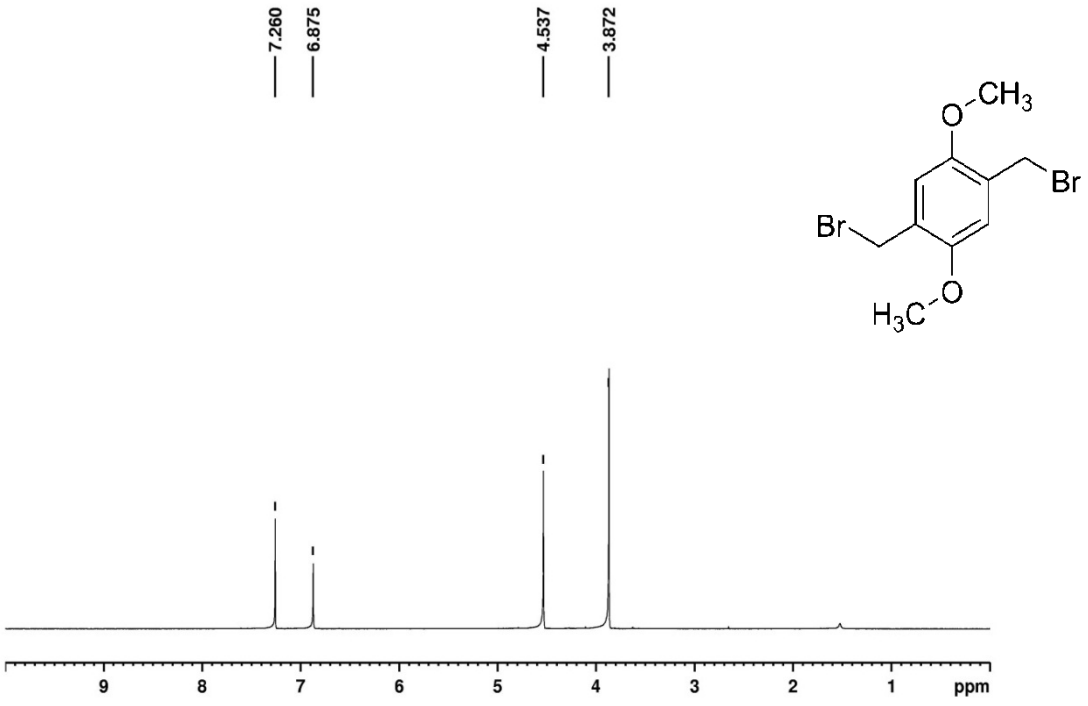
7.260
6.875
4.537
3.872
O
CH3
Br
Br
H3C
O
9
8
7
6
5
4
3
2
1
ppm

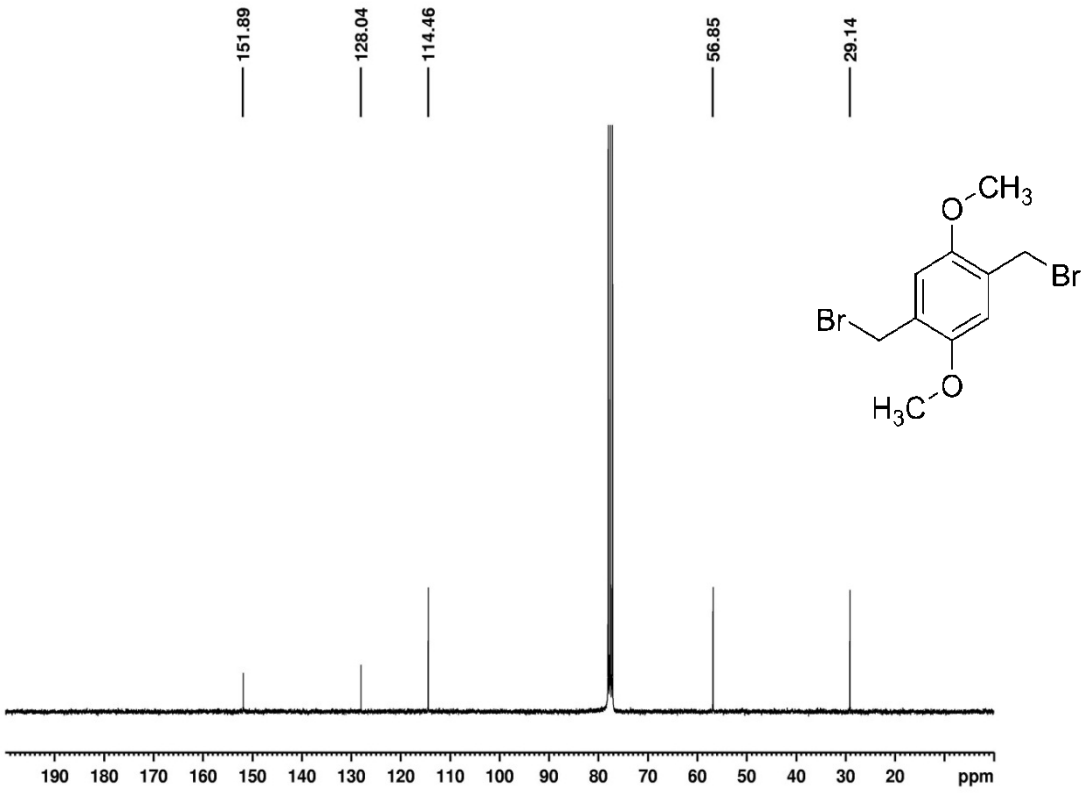
151.89
128.04
114.46
56.85
29.14
O
CH3
Br
Br
H3C
O
190
180
170
160
150
140
130
120
110
100
90
80
70
60
50
40
30
20
ppm

(2,5-Dimethoxy-1,4-phenylene)bis(methylene)bis(triphenylphosphonium bromide) (**2**):

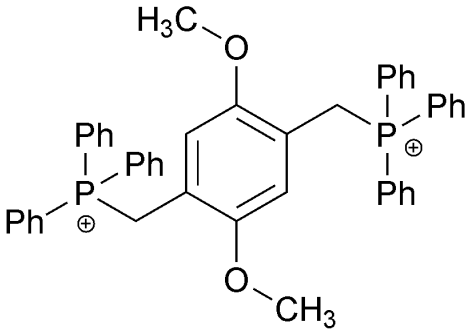

(2)

A mixture of 1,4-bis(bromomethyl)-2,5-dimethoxybenzene **1** (9.59 g, 29.60 mmol) and triphenylphosphine (Aldrich, 18.63 g, 71.04 mmol) was refluxed in dry toluene (Acros, 99.8%, 80 mL) under Argon for 6 hours. The crude white powder was obtained by filtration and used for subsequent reaction without further purification.

Dimethyl 4,4'-(1*E*,1'*E*)-2,2'-(2,5-dimethoxy-1,4-phenylene)bis(ethane-2,1-diyl)dibenzoate (**3**):

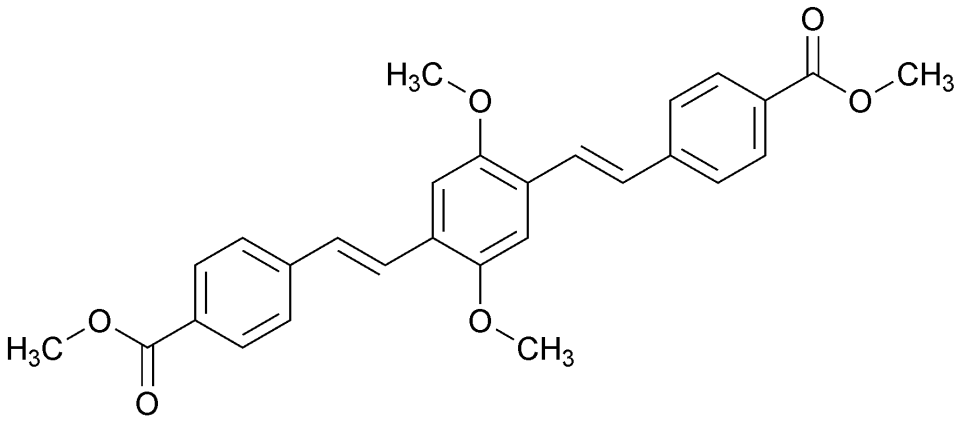

(3)

The following procedure was adapted from a previously reported synthesis.[12] A mixture of (2,5-Dimethoxy-1,4-phenylene)bis(methylene)bis(triphenylphosphonium bromide) **2** (25.68g, 30.26 mmol) and methyl 4-formylbenzoate (TCI, 12.42 g, 75.66 mmol) were dissolved in dry methanol (Aldrich, 99.8%, 120 mL) under argon. NaOMe (Aldrich, 0.5 M in methanol, 160 mL) was added via cannula. A yellow precipitate formed immediately. The reaction was stirred under argon for 4 h. After addition of water (140 mL), the yellow powder was filtered and washed with aqueous ethanol (60%, x 75 mL). Pure trans product was isolated via crystallization from toluene in the presence of few crystals of iodine[13] (11.95 g, 86%) ^{1}H NMR (300 MHz, $CHCl_3$) δ 8.02 (d, J=8.7, 4H), 7.59 (m, 6H), 7.16 (m, 4H), 3.95 (s, 6H), 3.93 ppm (s, 6H); ^{13}C NMR (75 MHz,$CHCl_3$) δ 167.5, 152.4, 142.9, 130.6, 129.4, 128.8, 127.2, 127.0, 126.3, 109.9, 56.9, 52.66 ppm; FTIR (KBr pellet): 3007 (w), 2943 (w), 2835 (w), 1714 (vs), 1604 (m), 1493 (w), 1464 (w), 1437 (sh), 1410 (m), 1277 (vs), 1209 (s), 1183 (m), 1111 (s), 1041 (m), 1014 (w), 971 (trans =C-H, w), 875 (sh), 849 (w), 766 (m), 702 cm^{-1} (w). HRMS (EI+) Calcd for $C_{28}H_{26}O_6$ $[M]^+$ 458.1729, found 458.1727.

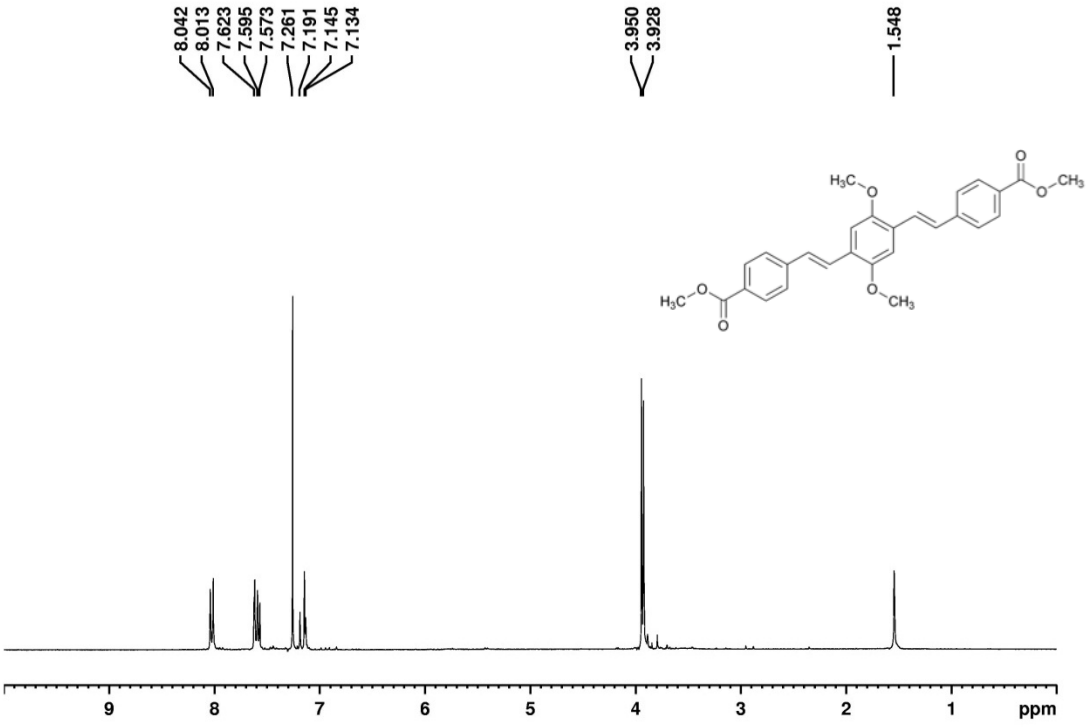
8.042
8.013
7.623
7.595
7.573
7.261
7.191
7.145
7.134
3.950
3.928
1.548
9
8
7
6
5
4
3
2
1
ppm

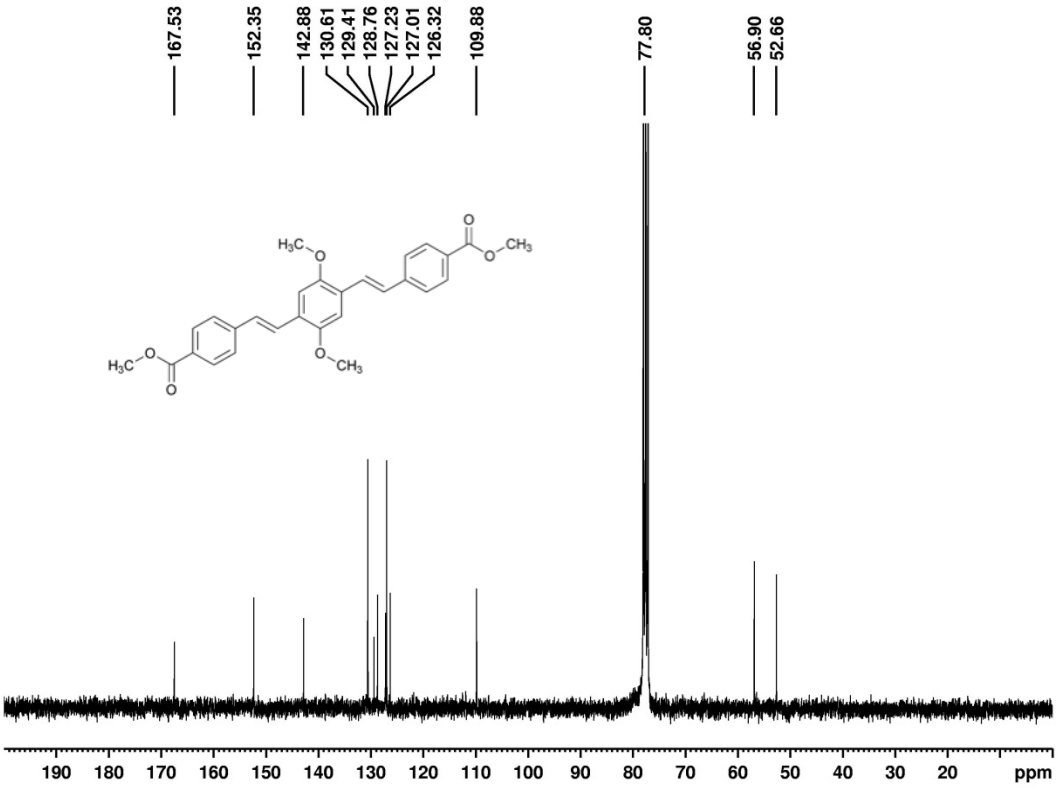
167.53
152.35
142.88
130.61
129.41
128.76
127.23
127.01
126.32
109.88
77.80
56.90
52.66
190
180
170
160
150
140
130
120
110
100
90
80
70
60
50
40
30
20
ppm

4,4'-(1*E*, 1'*E*)-2,2'-(2,5-dimethoxy-1,4-phenylene)bis(ethene-2,1-diyl)dibenzoic acid (**4**):

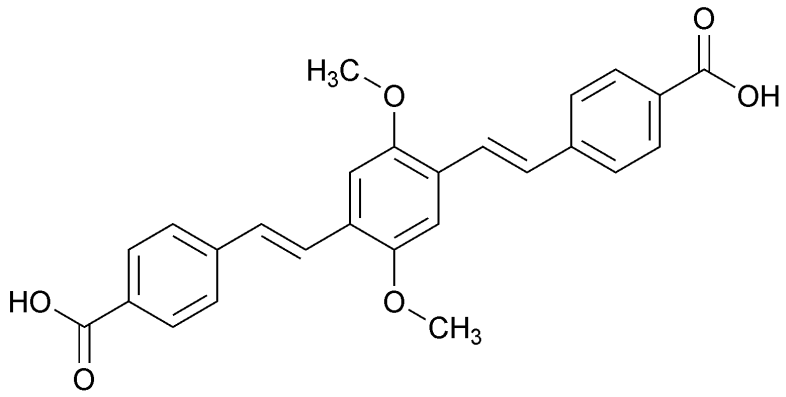

(4)

To dimethyl 4,4'-(1*E*, 1'*E*)-2,2'-(2,5-dimethoxy-1,4-phenylene)bis(ethane-2,1-diyl)dibenzoate (5.46 g, 11.9 mmol) was added KOH (Alfa Aesar, 6.2 g, 121 mmol), methanol (60 mL), THF (60 mL), and H_2O (30 mL). The mixture was refluxed overnight, cooled, and H_2O (60 mL) was added, resulting in a clear yellow solution. The solution was acidified with 2N HCl and the resulting yellow solid was collected by filtration and was then recrystallized from DMF to yield a bright yellow powder (4.24 g, 83%). ^{1}H NMR (300 MHz, DMSO) δ 12.87 (s, 2H), 7.95 (d, J=7.5, 4H), 7.70 (d, J=8.4, 4H), 7.51 (d, J=21.9, 2H), 7.45 (d, J=15.9, 2H), 7.39 (s, 2H), 3.93 ppm (s, 6H); ^{13}C NMR (75 MHz, DMSO) δ 168.14, 152.30, 142.64, 130.94, 130.43, 129.33, 127.45, 126.94, 126.01, 110.59, 57.27 ppm; FTIR (KBr pellet): 2938 (b), 2831 (b), 2543 (m), 2361 (w), 1680 (C=O, s), 1600 (s), 1536 (w), 1491 (w), 1462 (m), 1315 (m), 1290 (s), 1209 (m), 1045 (m), 959 (trans =C-H, w), 859 (w), 771 cm^{-1} (w). HRMS (EI+) Calcd for $C_{26}H_{22}O_6$ $[M]^+$ 430.1416, found 430.1401.

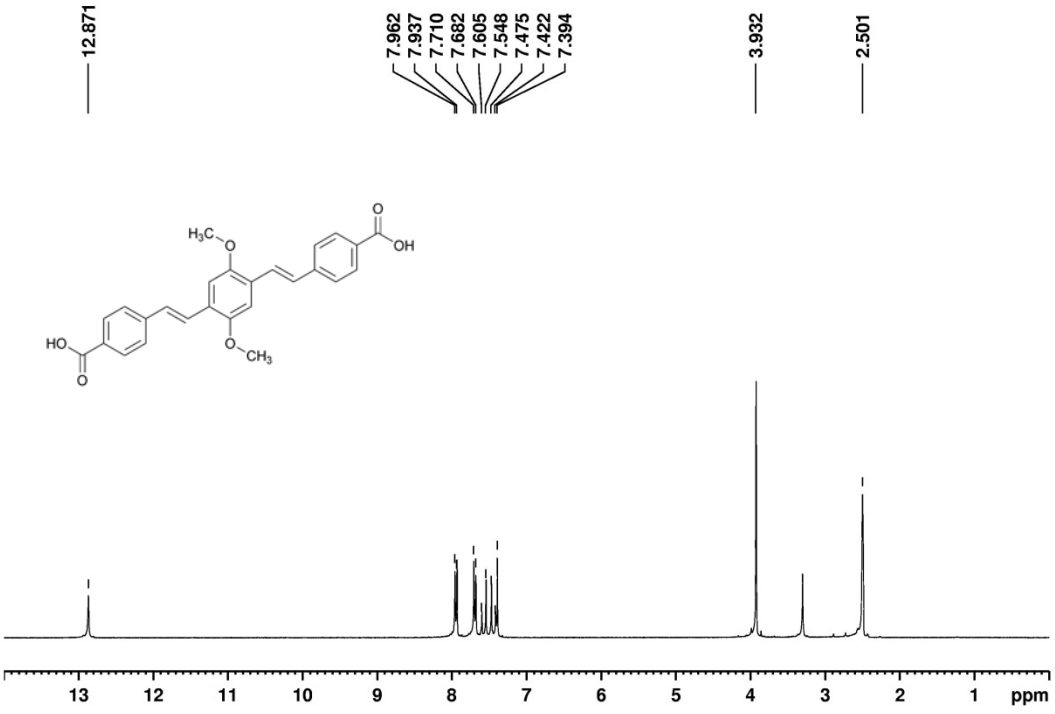
12.871
7.962
7.937
7.710
7.682
7.605
7.548
7.475
7.422
7.394
3.932
2.501
HO
O
H3C
O
O
OH
O
CH3
13
12
11
10
9
8
7
6
5
4
3
2
1
ppm

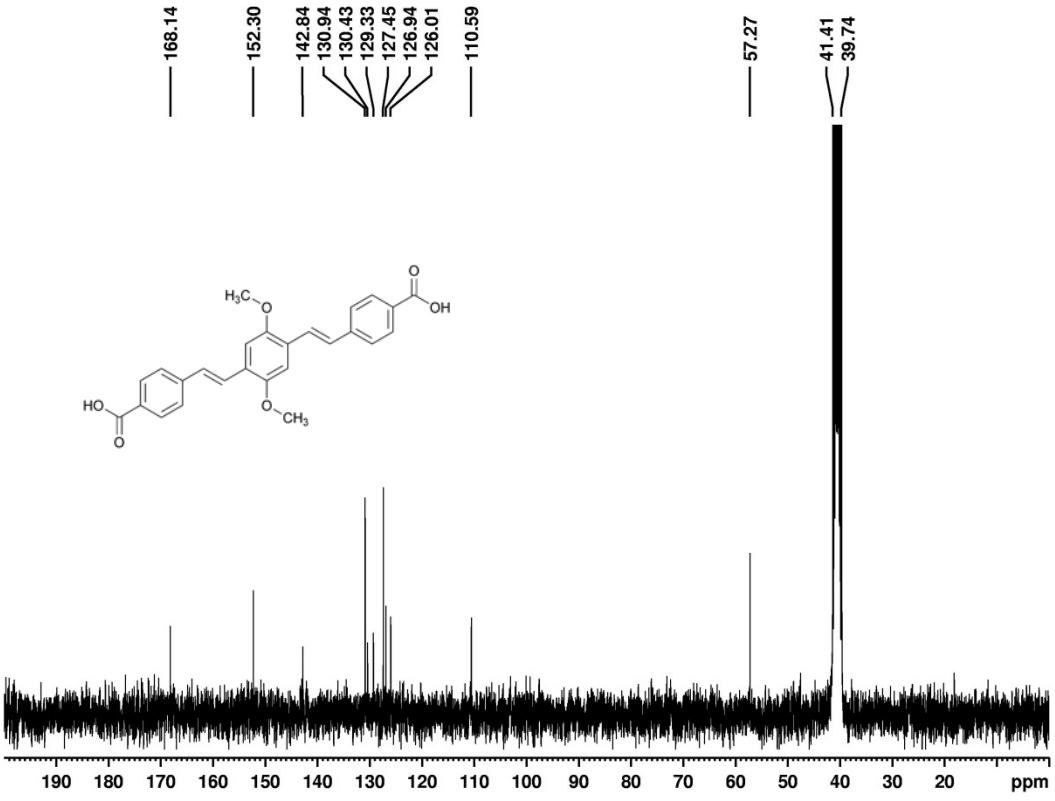
168.14
152.30
142.84
130.94
130.43
129.33
127.45
126.94
126.01
110.59
57.27
41.41
39.74
HO
O
H3C
O
O
OH
O
CH3
190
180
170
160
150
140
130
120
110
100
90
80
70
60
50
40
30
20
ppm

2.4.5 Ln-PVDC molecular complexes

In order to investigate the ability of **H_2-PVDC** to bind to and sensitize Yb^{3+} cations, solutions were prepared in the following manner: 0.60 mL of 5×10^{-4}M **H_2-PVDC** was deprotonated with 1 equivalent of tetraethylamine hydroxide (0.1 M solution in DMSO). 1 equivalent of ytterbium cation (from chloride salt in DMSO solution) was added to this solution to yield a final stoichiometric ratio of 1:1, metal to ligand. The solution was then diluted with DMSO to bring the total volume to 3.0 mL and the final concentration to 1.0×10^{-4} M for each reagent. The solution was allowed to stand overnight to allow complete complexation prior to analysis. This complex was analyzed by mass spectrometry, which revealed that the ytterbium cation binds to PVDC in a stoichiometric ratio of 1:1 metal to ligand. HRMS (EI+) Calcd for $C_{26}H_{21}O_6Yb$ $[M]^+$ 599.0686, found 599.0677. The Yb-PVDC solution was analyzed in 1.0 mm path length quartz cuvettes (purchased from NSG Precision Cells, Inc).

2.4.6 Synthesis of Yb-PVDC-1: $Yb_2(C_{26}H_{20}O_6)_3(H_2O)_2\bullet(DMF)_6(H_2O)_{8.5}$

In a glass vial (4 mL), a solution of 4,4'-(1*E*,1'*E*)-2,2'-(2,5-dimethoxy-1,4-phenylene)bis(ethene-2,1-diyl)dibenzoic acid (**H_2-PVDC**) (8.60 mg, 0.020 mmol) in DMF (0.4 mL) was added to a solution of $Yb(NO_3)_3\bullet 5H_2O$ (6.75 mg, 0.015 mmol) and 1M $HNO_{3(aq)}$ (20.0 μL) in DMF (0.3 mL) to produce a neon green solution. The vial was capped and placed in an 85 ºC isotemp oven for 48 hours to produce yellow crystalline needles of the product. The crystals were collected, washed with DMF (4 x 3 mL), and air dried (8.6 mg, 42.4 %).

EA Calcd. (%) for $Yb_2(C_{26}H_{20}O_6)_3(H_2O)_2\bullet(DMF)_6(H_2O)_{8.5}$: C, 51.04; H, 5.49; N, 3.72. Found: C, 50.97; H, 4.57; N, 3.91. EA. Calcd. (%) for the chloroform exchange product,

$Yb_2(C_{26}H_{20}O_6)_3(H_2O)_2\bullet(CHCl_3)_{2.75}(DMF)_{0.3}$: C, 48.61; H, 3.44; N, 0.21. Found: C, 48.79; H, 3.10; N, 0.21.FT-IR (KBr 4000-700 cm^{-1}): 3432 (br), 2933 (w), 1665 (DMF C=O, m), 1600 (m), 1538 (s), 1414 (COO^-, vs), 1256 (w), 1209 (s), 1180 (w), 1106 (w), 1042 (s), 962 (m), 861 (w), 780 (trans C=C-H, s), 709 cm^{-1}(w).

2.4.7 Synthesis of Yb-PVDC-2: $Yb_2(C_{26}H_{20}O_6)_3\bullet(DMF)_{12}(H_2O)_{10}$

In a glass vial (20 mL), a solution of 4,4'-(1*E*, 1'*E*)-2,2'-(2,5-dimethoxy-1,4-phenylene)bis(ethene-2,1-diyl)dibenzoic acid (**H_2-PVDC**) (86.0 mg, 0.20 mmol) in DMF (4 mL) was added to a solution of $Yb(NO_3)_3\bullet5H_2O$ (22.5 mg, 0.05 mmol) and 1M $HNO_{3(aq)}$ (10 μL) in DMF (1 mL) to yield a neon green solution. The vial was capped and placed in an 105 ºC isotemp oven for 36 hours to produce orange block-like crystals of the product. The crystals were collected, washed with DMF (4 x 5 mL) and air dried (48 mg, 51.9 %).

EA Calcd. (%) for $Yb_2(C_{26}H_{20}O_6)_3\bullet(DMF)_{12}(H_2O)_{10}$: C, 50.93; H, 6.15; N, 6.25. Found: C, 50.95; H, 5.40; N, 6.47. EA. Calcd. (%) for the chloroform exchange product, $Yb_2(C_{26}H_{20}O_6)_3\bullet(CHCl_3)_{7.5}(H_2O)_{0.5}(DMF)_{0.5}$: C, 40.62; H, 2.82; N, 0.27. Found: C, 40.66; H, 2.75; N, 0.23. FT-IR (KBr 4000-700 cm^{-1}): 3433 (br), 2930 (w), 1655 (DMF C=O, m), 1602 (s), 1536 (m), 1418 (COO^-,vs), 1208 (s), 1180 (w), 1103 (w), 1041 (w), 960 (trans =C-H, w), 862 (w), 780 cm^{-1} (m).

2.4.8 Single crystal X-ray diffraction studies

Single crystal XRD data was collected on a Bruker SMART APEX II CCD-based X-ray diffractometer equipped with a normal focus Mo-target X-ray tube (λ =0.71073Å) operated at

2000 W power (45 kV and 35 mA). The detector was placed at a distance of 6.002 cm from the crystal. 1800 frames were collected with a scan width of 0.3° in omega and phi with an exposure time of 10 s/frame. Crystals were mounted in glass capillaries, and the X-ray intensities were measured at 253K and 298K for **Yb-PVDC-1** and **Yb-PVDC-2**, respectively.

2.4.8.1 Single crystal X-ray diffraction studies of Yb-PVDC-1

An X-ray crystal structure was determined for $C_{39}H_{30}O_{10}Yb$, **Yb-PVDC-1**, using a single crystal on a Bruker Smart Apex CCD diffractmeter with graphite-monochromated MoKα (λ= 0.71073 Å) radiation. The parameters used during the collection of diffraction data are summarized in Appendix A. The crystal was mounted in a glass capillary and placed in a cold N_2 stream (253 K) for data collection.

Unit-cell parameters and systematic absences indicated **Yb-PVDC-1** crystallized in orthorhombic *F*ddd. Unit-cell dimensions were derived from the least-squares fit of the angular settings of 2973 reflections. Data were corrected for absorption using the Bruker program Sadabs. The crystal was weakly diffracting with no observed intensities beyond 2θ=46°

The structure was solved via direct methods, which located Yb^{3+} and most of the remaining non-hydrogen atoms. All non-hydrogen atoms except C(10) were refined anisotropically. Idealized atom positions were calculated for all hydrogen atoms (*d*-(C_{methyl}-H) = 0.96Å, d-C_{phenyl}-H)=0.93 Å, $U = 1.2U_{iso}$of attached carbon).

Calculations from Platon indicated solvent accessible voids accounting for 64.5% of the unit-cell volume (eight voids measuring 5175 $Å^3$ with 790 electrons each). We were unable to identify or model specific solvent molecules within the voids. The diffuse electron density was treated with the SQUEEZE routine from the PLATON software package.

The large voids in the structure allow for considerable flexing and uncertainty in the positions of the framework atoms and this is evidenced in large atomic displacement parameters for many of the benzene carbons and a large number of atypical bond lengths and angles. It was necessary to fit the rings to rigid hexagons (*d*C-C = 1.39 Å) and constrain a number of other bond lengths in the structure in order get a stable refinement. Several 1,3 distances were restrained to provide reasonable geometries. The numerous checkcif alerts are attributable to the uncertainty in the atomic positions and the low percentage of observed diffraction intensities.

The final Fourier map showed maximum and minimum peaks of 0.531 and -0.258$e^{-}Å^{-3}$, respectively, which were close to Yb(2). All computer programs used in the data collection and refinements are contained in the Bruker program packages SMART (vers. 5.625), SAINT (vers. 6.22), and SHELXTL (vers. 6.14) and Platon.[13]

2.4.8.2 Single crystal X-ray diffraction studies of Yb-PVDC-2

An amber block-shaped crystal (0.45 x 0.5 x 0.45 mm) of $Yb_2(C_{26}H_{20}O_6)_3$, **Yb-PVDC-2**, was mounted in a glass capillary on a Bruker SMART APEX II CCD-based X-ray diffractometer equipped with a normal focus Mo-target X-ray tube (λ = 0.71073 Å) operated at 2000 W power (45 kV and 35 mA). The X-ray intensities were measured at 298 K. The detector was placed at a distance of 6.002 cm from the crystal. 1800 frames were collected with a scan width of 0.3 degrees in omega and phi with an exposure time of 10 s/frame.

An initial unit cell was established using the Apex2 software proved to be ambiguous and thus 708 reflections were read in form several hundred frames and were exported into Cell-Now, resulting in a suggested I centered orthorhombic unit cell with the dimensions a = 16.063, b = 22.697, c = 38.454, α = 90.07, β = 90.03, γ = 89.93. 5.5% of the reflections were not consistent

with an I centered lattice (versus 50% for e.g. a C-centered lattice), and the unit cell was integrated in this setting, a unit cell was assigned in XPREP and attempts were made to solve the structure. These attempts, however, failed, and thus the data were again integrated using a primitive orthorhombic instead of the I centered orthorhombic cell with the same metric parameters as that established by Cell_Now. Inspection in XPREP then also suggested an I-centered orthorhombic cell with I/sigma for reflections obeying I centering being 1.7 versus 5.2 for all reflections, but again the primitive cell was chosen instead. Based on systematic absences the space group Pnna was chosen and the data were cut off at a d-spacing of 0.75.

The structure was then solved with the help of Patterson methods using the program XS, which revealed two ytterbium atoms and some of the metal bound oxygen atoms. Using Fourier transform recycling additional possible oxygen atoms were identified during the next refinement cycles. Tentatively correct oxygen positions were chosen based on the Yb-O distances and angles. Successive improvement of the difference map then allowed for the identification of the aromatic rings bonded to the carboxylate groups, and the model was augmented to include all of the O_2C-C_6H_4 groups. At this point it became obvious that the remainder of the linking molecules exhibit large vibrational motion with less than atomic resolution for the 2,5-dimethoxy phenylene units. The overall electron density nevertheless allowed for identification of the units as a whole and disorder for one of the two crystallographically independent linkers became obvious. The - caused by flip disorder of one of the two ethylene units - involves both etheylene units of this linker, the 2,5-dimethoxy phenylene and one of the carboxylate bonded aromatic rings, and the occupancy ratio refined to 0.63(1) to 0.37(1). The other linker - located on a crystallographical inversion center - showed no disorder but only very pronounced thermal motion.

In order to obtain a chemically meaningful model and refinement a range of restraints was introduced at this point. For the benzene ring located on the inversion center all 1,1 and 1,2 C-C distances were restrained to be each the same (the respective symmetry operator was used to do this across the inversion center). All other benzene rings were restrained to resemble ideal hexagons with C-C distances of 1.39 Å. All carbon atoms but the carboxylate ones were restrained to be isotropic within a standard deviation of 0.02 $Å^2$, and all carbon and oxygen atoms were restrained to have similar ADPs as their neighbors (SIMU and DELU restraints with a standard deviation of 0.03 each). Chemically equivalent 1,1 and 1,2 C-C distances to the ethylene carbon atoms in all units were restrained to be the same within a standard deviation of 0.02 Å. The methoxy units were restrained to have the same 1,1 and 1,2 distances in all units and to lie within the planes of the phenylene units they are bonded to. The carbon atoms C2a to C7a were set to have the same ADPs as their disordered counterparts C2b to C7b (which they significantly overlap). Application of these restraints did not cause any significant increase in R values or decrease in any other structure quality indicators, and none of the restraints applied had an error significantly larger than 0.1 Å or $Å^2$ for bond distance and ADP restraints, respectively.

The residual electron density in the voids between the inorganic-organic hybrid network did not exhibit any chemically meaningful pattern and was ignored during the refinement process. No correction was applied for the residual electron density. The two largest peaks exhibit electron densities of 2.44 and 1.89 electrons per cubic Ångstrom.

2.5 REFERENCES

(1) Rieter, W. J.; Taylor, K. M. L.; Lin, W. B. *J. Am. Chem. Soc.* **2007**, *129*, 9852.
(2) Allendorf, M. D.; Bauer, C. A.; Bhakta, R. K.; Houk, R. J. T. *Chem. Soc. Rev.* **2009**, *38*, 1330.
(3) Bünzli, J.-C. G.; Piguet, C. *Chem. Soc. Rev.* **2005**, *34*, 1048.
(4) Comby, S.; Bünzli, J.-C. G. In *Handbook on the Physics and Chemistry of Rare Earths*; Gschneidner, K. A., Jr., Bünzli, J.-C. G., Pecharsky, V., Ed.; Elsevier: Amsterdam, 2007; Vol. 37.
(5) Rowsell, J. L. C.; Yaghi, O. M. *Micropor. Mesopor. Mat.* **2004**, *73*, 3.
(6) Moulton, B.; Zaworotko, M. J. *Chem. Rev.* **2001**, *101*, 1629.
(7) Maspoch, D.; Ruiz-Molina, D.; Veciana, J. *Chem. Soc. Rev.* **2007**, *36*, 770.
(8) Kitagawa, S.; Kitaura, R.; Noro, S. *Angew. Chem. Int. Ed.* **2004**, *43*, 2334.
(9) Ferey, G. *Chem. Soc. Rev.* **2008**, *37*, 191.
(10) Brant, J. A.; Liu, Y. L.; Sava, D. F.; Beauchamp, D.; Eddaoudi, M. *J. Mol. Struct.* **2006**, *796*, 160.
(11) Irngartinger, H.; Herpich, R. *Eur. J. Org. Chem.* **1998**, 595.
(12) Stammel, C.; Frohlich, R.; Wolff, C.; Wenck, H.; de Meijere, A.; Mattay, J. *Eur. J. Org. Chem.* **1999**, 1709.
(13) McManis, G. E. *Appl. Spectrosc.* **1970**, *24*, 495.
(14) Rosi, N. L.; Kim, J.; Eddaoudi, M.; Chen, B. L.; O'Keeffe, M.; Yaghi, O. M. *J. Am. Chem. Soc.* **2005**, *127*, 1504.
(15) Hunter, C. A.; Sanders, J. K. M. *J. Am. Chem. Soc.* **1990**, *112*, 5525.
(16) Rusakova, N. V.; Korovin, Y. V.; Zhilina, Z. I.; Vodzinskii, S. V.; Ishkov, Y. V. *J. Appl. Spectrosc.* **2004**, *71*, 506.
(17) Davies, G. M.; Aarons, R. J.; Motson, G. R.; Jeffery, J. C.; Adams, H.; Faulkner, S.; Ward, M. D. *Dalton T.* **2004**, 1136.
(18) Hebbink, G. A.; Grave, L.; Woldering, L. A.; Reinhoudt, D. N.; Veggel, F. C. J. M. v. *J. Phys. Chem. A* **2003**, *107*, 2483.
(19) Foley, T. J.; Harrison, B. S.; Knefely, A. S.; Abboud, K. A.; Reynolds, J. R.; Schanze, K. S.; Boncella, J. M. *Inorg. Chem.* **2003**, *42*, 5023.
(20) Goncalves e Silva, F. R.; Malta, O. L.; Reinhard, C.; Guedel, H.-U.; Piguet, C.; Moser, J. E.; Bünzli, J.-C. G. *J. Phys. Chem. A* **2002**, *106*, 1670.

3.0 NEAR-INFRARED LUMINESCENT LANTHANIDE MOF BARCODES

This chapter has been published as Kiley A. White, Demetra A. Chengelis-Czegan, Kristy A. Gogick, Jack Stehman, Nathaniel L. Rosi, and Stéphane Petoud, *J. Am. Chem. Soc.*, **2009**, 131 (50), 18069-18071.

This work was done in collaboration with Demetra Chengelis and Kristy Gogick (Stéphane Petoud Research Group, University of Pittsburgh), who performed the luminescence measurements.

3.1 INTRODUCTION

Barcoded materials are attractive as labels in multiplexed bioanalytical assays and as encryption tags.[1-9] Such systems provide an unambiguous way to recognize the identity of a biological entity or of an object. These materials can play an important role in applications related to national security purposes, such as for tracking and identifying objects at airports, in transit, in storage, and on the battlefield. An ideal barcoded material should meet the following specifications. It should be robust, available in large scale, and its synthesis should be straightforward, highly reproducible, and configurable to provide numerous possible encoding combinations. In addition, its spectral signature should be easily and rapidly acquired and unambiguously interpreted with inexpensive and portable equipment.

In this chapter, we report a new conceptual approach for creating luminescent barcoded systems based on using metal-organic frameworks (MOFs) which contain multiple near-infrared (NIR) emitting lanthanides and that have well-controlled compositions and photophysical properties (Scheme 3.1).[10-18]

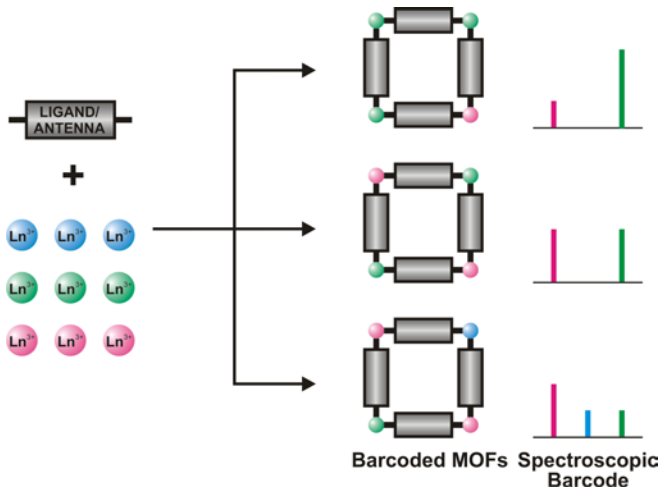

Scheme 3.1. Controlled preparation of barcoded MOFs

Luminescent lanthanide cations have unique advantages for the creation of barcoded luminescent materials. They exhibit sharp, non-overlapping, and easily identifiable emission bands in both the visible (vis)[19] and near-infrared (NIR).[20,21] More specifically, they have much narrower bandwidths than organic fluorophores and semi-conductor fluorescent nanocrystals (NCs) (Figure 3.1). In addition, the wavelengths of the emission bands of lanthanide cations are not affected by their environment,[22] unlike those of organic fluorophores and NCs that may change emission wavelengths based on conditions such as the nature of the solvent[23] or pH. These advantages permit their use in various materials and solvents where their emission wavelength depends only on the nature of the lanthanide, not on its environment. Since free lanthanides have very low extinction coefficients, chromophoric molecules ('antennae') must be placed at close proximity of the lanthanides to allow for their sensitization so that the compound may emit a sufficient number of photons for sensitive detection.[24]

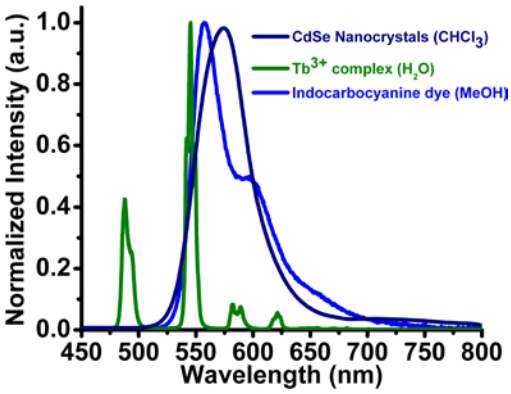

Figure 3.1. Normalized emission spectra of an organic indocarbocyanine dye (C3), CdSe nanocrystals, and a Tb^{3+} complex in solution allowing for comparison of the emission bandwidth.

For practical applications, a common antenna for the sensitization of several different lanthanide cations would be advantageous in order to generate simultaneous emission of several

wavelengths using one excitation wavelength. In addition, it is beneficial if all lanthanide cations are embedded in a well-defined unit that can be well-characterized and retains its properties with time. However, creating polymetallic lanthanide compounds with well-defined and easily reproducible structures is challenging. The synthesis of barcoded polymetallic lanthanide complexes as metal-organic frameworks (MOFs) addresses these challenges and is attractive for several reasons. i) Unlike lanthanide-doped nanocrystals,[25-27] MOFs have easily characterizable crystalline structures, which allow for a high degree of spatial organization of multiple different cations[17,28]and organic sensitizers.[29] The crystalline nature of these materials allows for unambiguous determination of their structures in terms of the precise locations of the cations and sensitizers. This aspect permits reproducible formation of the material and rationalization of its luminescence properties based on its structure.[18] ii) MOFs have a high density of lanthanide cations and sensitizers and can therefore emit a large number of photons per unit of volume.[18,30] Herein we report highly reproducible barcoded MOF materials with NIR emissions based on the controlled composition of MOFs incorporating several different lanthanide cations.

3.2 RESULTS AND DISCUSSION

3.2.1 Barcoded MOFs composed of two lanthanides: Er^{3+} and Yb^{3+}

Here, we have adapted our synthesis of **Yb-PVDC-1** (Figure 3.2) to yield barcoded frameworks containing both Yb^{3+} and Er^{3+}. Ytterbium and erbium were chosen because they have very distinguishable emission profiles in the NIR and have similar radii. Specifically, we reacted our chosen antenna, **H_2-PVDC**, with $Er(NO_3)_3 \bullet 5H_2O$ and $Yb(NO_3)_3 \bullet 5H_2O$ to produce yellow

needles of four luminescent frameworks with varying lanthanide ion stoichiometries: **$Er_{0.32}Yb_{0.68}$-PVDC-1**, **1**; **$Er_{0.58}Yb_{0.42}$-PVDC-1**, **2**; **$Er_{0.70}Yb_{0.30}$-PVDC-1**, **3**; and **$Er_{0.81}Yb_{0.19}$-PVDC-1**, **4**. Each framework is isostructural with **Yb-PVDC-1**, as revealed by comparison of their powder X-ray diffraction (PXRD) patterns (Figure 3.3).

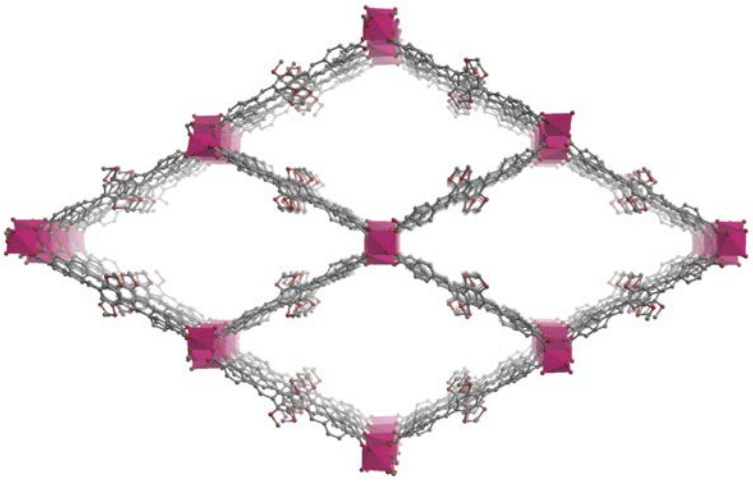

Figure 3.2. Crystal structure of Yb-PVDC-1 viewed along the *c* crystallographic direction with Yb^{3+} shown as polyhedra (C, grey; O, red; Yb^{3+}, pink)

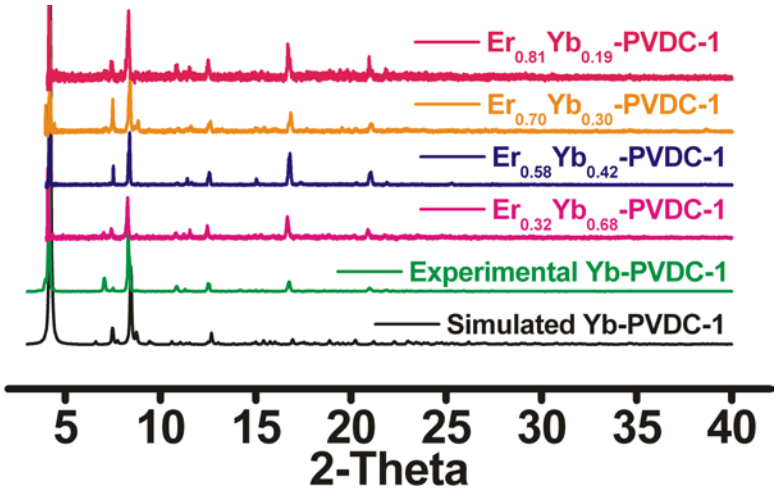

Figure 3.3. Powder X-ray diffraction patterns of Yb-PVDC-1 and barcoded analogues 1-4

The lanthanide compositions in the resulting products were determined by energy dispersive X-ray spectroscopy (EDS) and directly correlated to the amounts of each lanthanide salt used during the corresponding syntheses (Table 3.1). The EDS measurements were performed on a minimum of four independently synthesized samples for each MOF and showed highly reproducible results for each lanthanide composition. These results indicate that any desired lanthanide composition in the final product can be obtained in a predictable and reproducible fashion by simply controlling the stoichiometry of the reactants. Moreover, they suggest that the MOF structure does not preferentially include either lanthanide cation and thus that any Er:Yb ratio can be obtained. This predictable aspect of the synthesis is highly advantageous for a barcoded material, and in this case it allows for the preparation of multiple barcodes simply by varying the ratios of two emitters.

Table 3.1. Relative Ln^{3+} content for the Er_xYb_{1-x}-PVDC-1 MOFs 1-4 during synthesis (theor) and as determined by EDS and ICP analysis of the final product with errors given in parentheses

	synthesis amount (mmol)		% Er^{3+}		
MOF	$Er(NO_3)_3$	$Yb(NO_3)_3$	theor	EDS	ICP
1	0.00125	0.0025	33	32 (± 2)	30
2	0.00375	0.0025	60	58 (± 2)	63
3	0.00625	0.0025	71	70 (± 2)	68
4	0.00625	0.00125	83	81 (± 3)	78

Photoluminescence studies were performed on each sample to determine whether the different lanthanide compositions would result in materials having unique and discernible barcoded signals. MOFs **1-4** were suspended in chloroform and their respective excitation and

emission spectra were recorded. The MOFs display sharp signals from both erbium and ytterbium. The excitation spectrum of either the erbium or ytterbium emission band contains two similar bands with apparent maxima at 370 and 470 nm, as observed for **Yb-PVDC-1**. These results indicate that the chromophore embedded in the MOF is able to sensitize these two different cations. Excitation through either of these bands simultaneously produces the characteristic Yb^{3+} emission band centered at 980 nm and the Er^{3+} band centered at 1530 nm. As expected, upon increasing the amount of Er^{3+} and decreasing the amount of Yb^{3+}, their respective emission intensities increase and decrease accordingly (Figure 3.4). Thus, we have demonstrated that by controlling the lanthanide composition, we can quantitatively control the resulting luminescence intensities of the individual signal of both NIR emitting lanthanide cations.

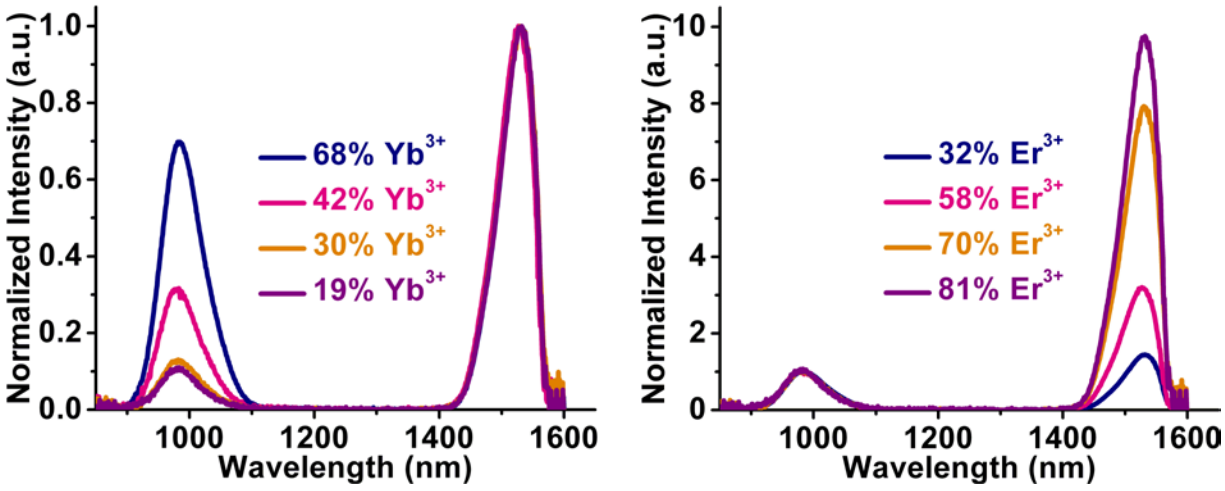

Figure 3.4. Yb^{3+} (980 nm) and Er^{3+} (1530 nm) emission spectra recorded upon 490 nm excitation normalized to the Er^{3+} signal (left) and normalized to the Yb^{3+} signal (right)

A plot of the ratio of the integrated intensities of the emissions of the two different lanthanides with respect to their metal cation ratio reveals a linear relationship between 32:68 and 81:19 Er:Yb (Figure 3.5). This trend is similar when either excitation band is used and is reproducible

across multiple samples. This feature provides the advantage of offering two excitation wavelengths for verifying the authenticity of an encryption tag. Importantly, PXRD shows that these materials maintain their crystallinity throughout the photoluminescence experiments, demonstrating the possibility for extended use, which is another important requirement for applications (Figure 3.6).

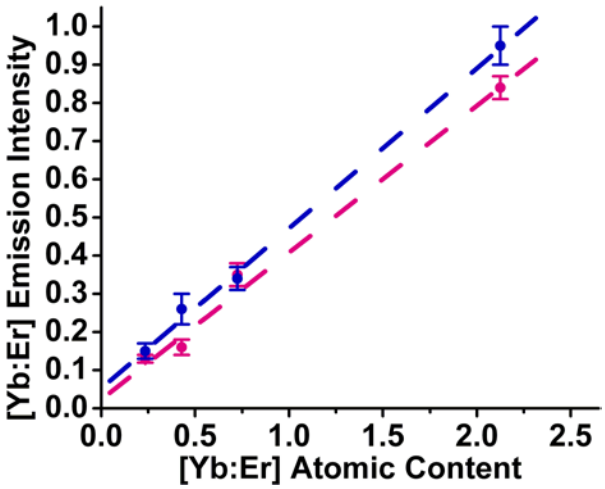

Figure 3.5. Plot of the Yb:Er ratio of integrated emission intensities vs. their atomic content ratio as measured by EDS (blue, λ_{ex} = 370 nm; pink, λ_{ex} = 490 nm)

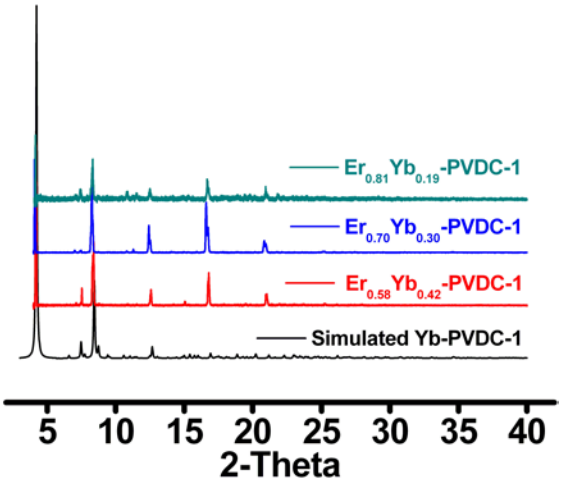

Figure 3.6. Powder X-ray diffraction patterns of Er_xYb_{1-x}-PVDC-1 post-luminescence measurements

To facilitate interpretation, we generated a color-coded barcode readout (Figure 3.7), because the Er^{3+} and Yb^{3+} luminescence bands in the NIR range cannot be detected by the naked eye. Therefore, the signal can only be spectroscopically monitored and the signal intensities artificially correlated with two different visible colors for facile human interpretation and quantification. Here, purple is used to represent the Er^{3+} signal and green the Yb^{3+} signal. Their relative intensities are reflected in the display, creating four distinct barcodes, one correlating to each MOF.

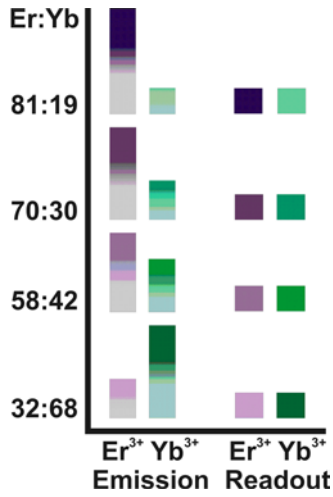

Figure 3.7. Color-coded schematic of the barcode readout.

For practical applications, barcoded materials need to be incorporated into objects (e.g. money or clothing) in ways that do not detrimentally affect their signal. To evaluate this possibility, we coated **2** in Superglue and then investigated its luminescence properties. Upon excitation at 490 nm, the Yb^{3+}/Er^{3+} barcode was easily detected in the NIR range (Figure 3.8).

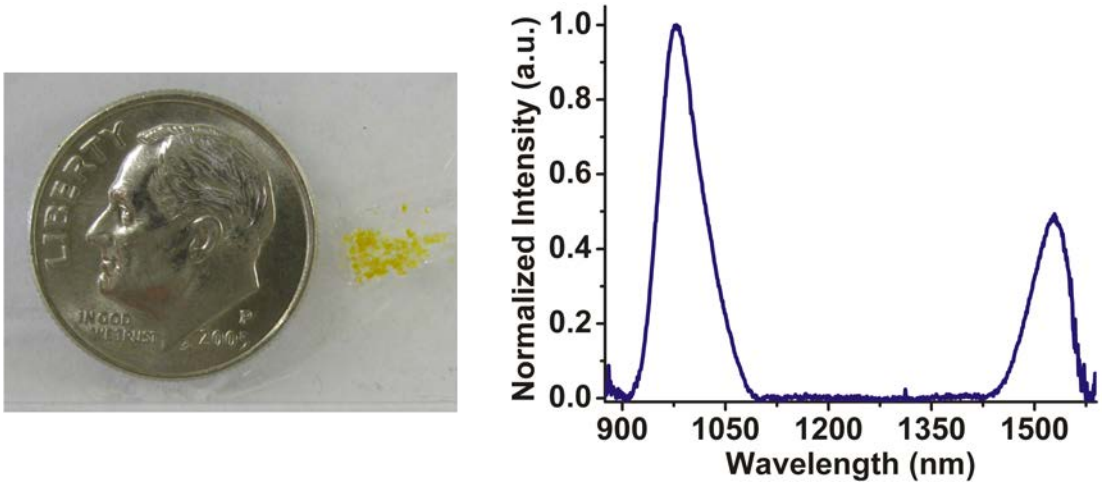

Figure 3.8. Sample of $Er_{0.58}Yb_{0.42}$-PVDC-1 dried and glued to a microscope slide (left; dime is included for size perspective) and Yb^{3+} (980 nm) and Er^{3+} (1530 nm) emission spectra for this sample (right; λ_{ex} = 490 nm)

3.2.2 Barcoded MOFs composed of three lanthanides: Er^{3+}, Yb^{3+}, and Nd^{3+}

The number and diversity of barcodes can be increased by using a larger number of Ln:Ln ratios or by incorporating additional lanthanide cations into the material. As a first step in this direction, we demonstrated the latter concept by preparing **$Nd_{0.09}Er_{0.55}Yb_{0.36}$-PVDC-1**, **5** (Figure 3.9). As expected, it displays a more sophisticated barcode signal consisting of NIR signals from its three component lanthanide cations (Figure 3.10). However, predicting the resulting neodymium amount in this system may be harder due to possible size selectivity.

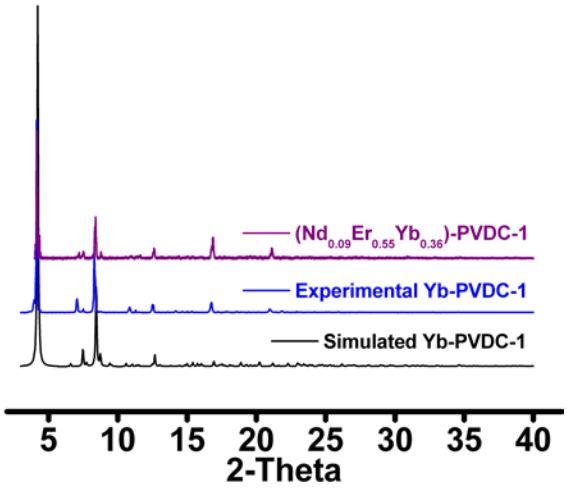

Figure 3.9. Powder X-ray diffraction pattern comparison of $Nd_{0.09}Er_{0.55}Yb_{0.36}$-PVDC-1 to Yb-PVDC-1.

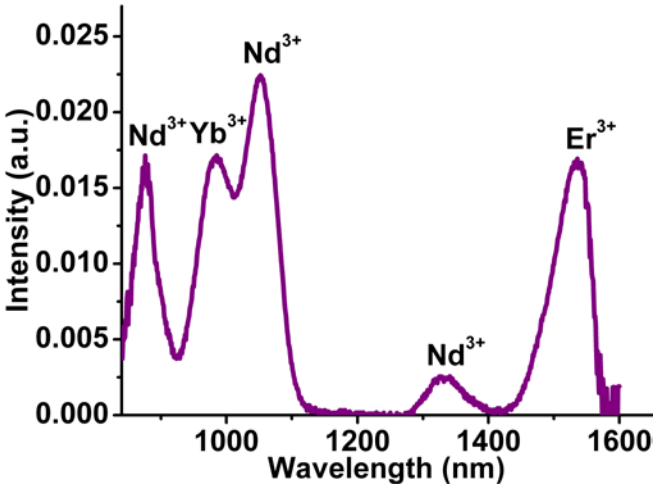

Figure 3.10. Yb^{3+}, Er^{3+}, and Nd^{3+} emission from 5 (λ_{ex} = 490 nm).

3.3 CONCLUSION

Whereas in Chapter 2 we reported two new Yb^{3+}-based MOFs (**Yb-PVDC-1** and **Yb-PVDC-2**) and demonstrated that we can i) use the chromophoric group within these MOFs to sensitize Yb^{3+} and ii) tune and optimize their luminescence properties by tailoring the MOF

architecture,[18] in Chapter 3 we have created a new barcoded system based on polymetallic lanthanide MOFs which simultaneously emit several independent NIR signals arising from different lanthanide cations. We have demonstrated that by controlling reactant stoichiometry we can predict and tune the lanthanide composition of the MOF and therefore control the resulting individual emission intensities. Further, we showed that excitation at a single wavelength produces concurrent ytterbium and erbium emission bands that are linearly correlated to the lanthanide ratio. An investigation of the possible ytterbium to erbium energy transfer for these systems will be discussed in Chapter 4. **Er_xYb_{1-x}-PVDC-1** MOFs have the required properties to serve as barcoded luminescent materials, and we expect that these materials and others produced using the concepts forwarded herein will be useful for many practical applications. In Chapter 5 we synthesize and characterize a more water-stable barcoded MOF and demonstrate its potential for biological applications.

3.4 EXPERIMENTAL

3.4.1 Reagents

Starting materials and reagents were obtained from commercial sources or synthesized by procedures noted below. **H_2-PVDC** was synthesized as described in Section 2.4.4. Dimethoxybenzene, paraformaldehyde, triphenylphosphine, methanol, NaOMe, THF, DMF, anhydrous methanol, and $Er(NO_3)_3 \cdot 5H_2O$ were purchased from Aldrich. $Yb(NO_3)_3 \cdot 5H_2O$ was purchased from Strem Chemicals. Glacial acetic acid and hydrochloric acid were purchased from Fisher. Hyrdobromic acid (33% in AcOH) was purchased from Fluka. Anhydrous toluene

(99.8%) and anhydrous chloroform (99.8%), were purchased from Acros. Argon gas was purchased from Valley National. Methyl 4-formylbenzoate was purchased from TCI. KOH was purchased from Alfa Aesar. All reagents were used as received without further purification.

3.4.2 General procedures

Fourier transform infrared (FT-IR) spectra were measured on a Nicolet Avatar 360 FT-IR spectrometer using KBr pellet samples. Absorptions are described as very strong (vs), strong (s), medium (m), weak (w), shoulder (sh), and broad (br) and stretches (st) are labeled symmetric (sym) or asymmetric (as). Data was analyzed using the Omnic Software Package.

X-ray powder diffraction patterns were collected using a Bruker AXS D_8 Discover powder diffractometer at 40 kV, 40 mA for Cu Kα, (λ = 1.5406 Å) with a scan speed of 0.20 sec/step and a step size of .02018º. The data were analyzed for d-spacing measurements using the EVA program from the Bruker Powder Analysis Software package. The purity and homogeneity of the bulk products were determined by comparison to the simulated and experimental X-ray powder diffraction patterns of Yb-PVDC-1. Solvent exchange of the DMF and H_2O guest molecules in **$Er_{0.32}Yb_{0.68}$-PVDC-1**, **$Er_{0.58}Yb_{0.42}$-PVDC-1, $Er_{0.70}Yb_{0.30}$-PVDC-1, $Er_{0.81}Yb_{019}$-PVDC-1** was performed using anhydrous solvents as follows: 30 min soak in exchange solvent (ES) followed by solvent removal (3X); overnight soak in ES and then solvent removal; 24 h soak in ES and solvent removal; addition of fresh solvent. The elemental microanalysis (CHN) and ICP-OES ($Er^{3+}Yb^{3+}$) were performed by the University of Illinois, Department of Chemistry, Microanalytical Laboratory using an Exeter Analytical CE440.

Energy-dispersive X-ray analysis (EDX) was measured on a Philips XL 30 SEM equipped with an EDAX CDU leap detector.

3.4.3 Spectroscopic measurements

Absorption spectra were recorded on a Perkin-Elmer Lambda 9 Spectrometer coupled with a personal computer using software supplied by Perkin-Elmer.

Emission and excitation spectra in the visible range were measured using a Varian Cary Eclipse Fluorescence Spectrophotometer coupled to a personal computer with software provided by Varian. Spectra in the near infrared range were measured using a Jobin Yvon–Horiba Fluorolog-322 spectrofluorimeter equipped with an Electro-Optical Systems, Inc. DSS-IGA020L detector for the NIR domain. Emission and excitation spectra of the **$Er_{0.32}Yb_{0.68}$-PVDC-1**, **$Er_{0.58}Yb_{0.42}$-PVDC-1, $Er_{0.70}Yb_{0.30}$-PVDC-1, $Er_{0.81}Yb_{019}$-PVDC-1** were collected as solid samples under chloroform on the JY Horiba Fluorolog-322 Spectrofluorimeter fitted with an integrating sphere developed by Frédéric Gumy and Prof. Jean-Claude G. Bünzli (Laboratory of Lanthanide Supramolecular Chemistry, École Polytechnique Féderale de Lausanne (EPFL), BCH 1402, CH-1015 Lausanne, Switzerland) as an accessory to the Fluorolog FL3-22 spectrometer (Patent pending) using quartz tube sample holders.

3.4.4 Syntheses of Er_xYb_{1-x}-PVDC-1

3.4.4.1 Synthesis of $Er_{0.32}Yb_{0.68}$-PVDC-1 (1)

In a glass vial (4 mL), a solution of 4,4'-(1*E*,1'*E*)-2,2'-(2,5-dimethoxy-1,4-phenylene)bis(ethene-2,1-diyl)dibenzoic acid (**H_2-PVDC**)[18] (8.60 mg, 0.020 mmol) in DMF (0.4

mL) was added to a solution of $Yb(NO_3)_3 \bullet 5H_2O$ (1.02 mg, 0.0025 mmol) in DMF (0.050 mL), $Er(NO_3)_3 \bullet 5H_2O$ (0.55 mg, 0.00125 mmol) in DMF (0.025 mL), and 1M $HNO_{3(aq)}$ (10.0 μL) to produce a neon green solution. The vial was capped and placed in a 100 ºC isotemp oven for 72 hours to produce yellow crystalline needles. The crystals were collected, washed with DMF (4 x 3 mL), and air dried (2.1 mg, 52.8%).

EA Calcd. (%) for $(Er_{0.32}Yb_{0.68})_2(C_{26}H_{20}O_6)_3(H_2O)_2 \bullet (DMF)_5(H_2O)_5$: C, 52.71; H, 5.18; N, 3.30. Found: C, 52.79; H, 4.33; N, 2.94. FT-IR (KBr 4000-700 cm^{-1}): 3381 (br), 2933 (w), 1659 (DMF C=O, m), 1600 (s), 1536 (s), 1413 (COO^-, vs), 1258 (w), 1209 (s), 1180 (m), 1105 (w), 1042 (s), 962 (m), 865 (w), 780 (trans C=C-H, s), 709 cm^{-1}(w). ICP analysis showed that the molar ratio of Yb^{3+}/Er^{3+} was 11.58:4.92, corresponding to 30% Er^{3+} of the total metal composition.

3.4.4.2 Synthesis of $Er_{0.58}Yb_{0.42}$-PVDC-1 (2)

In a glass vial (4 mL), a solution of 4,4'-(1*E*,1'*E*)-2,2'-(2,5-dimethoxy-1,4-phenylene)bis(ethene-2,1-diyl)dibenzoic acid (**H_2-PVDC**) (8.60 mg, 0.020 mmol) in DMF (0.4 mL) was added to a solution of $Yb(NO_3)_3 \bullet 5H_2O$ (1.02 mg, 0.0025 mmol) in DMF (0.050 mL), $Er(NO_3)_3 \bullet 5H_2O$ (1.66 mg, 0.00375 mmol) in DMF (0.075 mL), and 1M $HNO_{3(aq)}$ (10.0 μL) to produce a neon green solution. The vial was capped and placed in a 100 ºC isotemp oven for 72 hours to produce yellow crystalline needles. The crystals were collected, washed with DMF (4 x 3 mL), and air dried (4.6 mg, 31.4%).

EA Calcd. (%) for $(Er_{0.58}Yb_{0.42})_2(C_{26}H_{20}O_6)_3(H_2O)_2 \bullet (DMF)_{8.5}(H_2O)_5$: C, 52.41; H, 5.67; N, 5.02. Found: C, 52.50; H, 4.87; N, 4.45. FT-IR (KBr 4000-700 cm^{-1}): 3433 (br), 2934 (w), 1658 (DMF C=O, m), 1602 (s), 1534 (s), 1418 (COO^-, vs), 1256 (w), 1210 (s), 1181 (w), 1106

(w), 1043 (s), 963 (m), 866 (w), 781 (trans C=C-H, s), 709 cm^{-1}(w). ICP analysis showed that the molar ratio of Yb^{3+}/Er^{3+} was 6.06:10.29, corresponding to 63% Er^{3+} of the total metal composition.

3.4.4.3 Synthesis of $Er_{0.70}Yb_{0.30}$-PVDC-1 (3)

In a glass vial (4 mL), a solution of 4,4'-(1*E*,1'*E*)-2,2'-(2,5-dimethoxy-1,4-phenylene)bis(ethene-2,1-diyl)dibenzoic acid (**H_2-PVDC**) (8.60 mg, 0.020 mmol) in DMF (0.4 mL) was added to a solution of $Yb(NO_3)_3 \bullet 5H_2O$ (1.02 mg, 0.0025 mmol) in DMF (0.050 mL), $Er(NO_3)_3 \bullet 5H_2O$ (2.77 mg, 0.00625 mmol) in DMF (0.125 mL), and 1M $HNO_{3(aq)}$ (10.0 μL) to produce a neon green solution. The vial was capped and placed in a 100 ºC isotemp oven for 72 hours to produce yellow crystalline needles. The crystals were collected, washed with DMF (4 x 3 mL), and air dried (2.3 mg, 9.9%).

EA Calcd. (%) for$(Er_{0.70}Yb_{0.30})_2(C_{26}H_{20}O_6)_3(H_2O)_2 \bullet (DMF)_{12}(H_2O)_7$: C, 51.43; H, 6.13; N, 6.31. Found: C, 51.42; H, 5.51; N, 6.65. FT-IR (KBr 4000-700 cm^{-1}): 3436 (br), 2935 (w), 1656 (DMF C=O, m), 1602 (s), 1542 (s), 1411 (COO^-, vs), 1259 (w), 1209 (s), 1180 (w), 1104 (w), 1043 (s), 947 (m), 865 (w), 780 (trans C=C-H, s), 709 cm^{-1}(w). ICP analysis showed that the molar ratio of Yb^{3+}/Er^{3+} was 5.46:11.56, corresponding to 68% Er^{3+} of the total metal composition.

3.4.4.4 Synthesis of $Er_{0.81}Yb_{0.19}$-PVDC-1 (4)

In a glass vial (4 mL), a solution of 4,4'-(1*E*,1'*E*)-2,2'-(2,5-dimethoxy-1,4-phenylene)bis(ethene-2,1-diyl)dibenzoic acid (**H_2-PVDC**) (8.60 mg, 0.020 mmol) in DMF (0.4 mL) was added to a solution of $Yb(NO_3)_3 \bullet 5H_2O$ (0.56 mg, 0.00125 mmol) in DMF (0.025 mL),

$Er(NO_3)_3 \bullet 5H_2O$ (2.77 mg, 0.00625 mmol) in DMF (0.125 mL), and 1M $HNO_{3(aq)}$ (10.0 μL) to produce a neon green solution. The vial was capped and placed in a 100 ºC isotemp oven for 72 hours to produce yellow crystalline needles. The crystals were collected, washed with DMF (4 x 3 mL), and air dried (5.8 mg, 70.7%).

EA Calcd. (%) for $(Er_{0.81}Yb_{0.19})_2(C_{26}H_{20}O_6)_3(H_2O)_2 \bullet (DMF)_6(H_2O)_5$: C, 52.73; H, 5.35; N, 3.84. Found: C, 52.87; H, 4.73; N, 4.35. FT-IR (KBr 4000-700 cm^{-1}): 3399 (br), 2933 (w), 1656 (DMF C=O, m), 1602 (s), 1535 (s), 1416 (COO^-, vs), 1259 (w), 1209 (s), 1180 (w), 1106 (w), 1043 (s), 962 (m), 865 (w), 779 (trans C=C-H, s), 709 cm^{-1}(w). ICP analysis showed that the molar ratio of Yb^{3+}/Er^{3+} was 3.82:13.49, corresponding to 78% Er^{3+} of the total metal composition.

3.5 REFERENCES

(1) Kim, S. K.; Lee, S. B. *J. Mater. Chem.* **2009**, *19*, 1381.
(2) Chan, W. C. W.; Maxwell, D. J.; Gao, X. H.; Bailey, R. E.; Han, M. Y.; Nie, S. M. *Curr. Opin. Biotechnol.* **2002**, *13*, 40.
(3) Chang, S.; Zhou, M.; Grover, C. P. *Opt. Express* **2004**, *12*, 143.
(4) Finkel, N. H.; Lou, X. H.; Wang, C. Y.; He, L. *Anal. Chem.* **2004**, *76*, 353A.
(5) Jaiswal, J. K.; Simon, S. M. *Trends Cell Biol.* **2004**, *14*, 497.
(6) Wang, J. *J. Mater. Chem.* **2008**, *18*, 4017.
(7) Nicewarner-Pena, S. R.; Freeman, R. G.; Reiss, B. D.; He, L.; Pena, D. J.; Walton, I. D.; Cromer, R.; Keating, C. D.; Natan, M. J. *Science* **2001**, *294*, 137.
(8) Han, M. Y.; Gao, X. H.; Su, J. Z.; Nie, S. *Nat. Biotechnol.* **2001**, *19*, 631.
(9) Vancaeyzeele, C.; Ornatsky, O.; Baranov, V.; Shen, L.; Abdelrahman, A.; Winnik, M. A. *J. Am. Chem. Soc.* **2007**, *129*, 13653.
(10) Rowsell, J. L. C.; Yaghi, O. M. *Micropor. Mesopor. Mat.* **2004**, *73*, 3.
(11) Ferey, G. *Chem. Soc. Rev.* **2008**, *37*, 191.
(12) Moulton, B.; Zaworotko, M. J. *Chem. Rev.* **2001**, *101*, 1629.
(13) Kitagawa, S.; Kitaura, R.; Noro, S. *Angew. Chem. Int. Ed.* **2004**, *43*, 2334.
(14) Reineke, T. M.; Eddaoudi, M.; O'Keeffe, M.; Yaghi, O. M. *Angew. Chem. Int. Ed.* **1999**, *38*, 2590.
(15) Allendorf, M. D.; Bauer, C. A.; Bhakta, R. K.; Houk, R. J. T. *Chem. Soc. Rev.* **2009**, *38*, 1330.
(16) Chen, B. L.; Yang, Y.; Zapata, F.; Qian, G. D.; Luo, Y. S.; Zhang, J. H.; Lobkovsky, E. B. *Inorg. Chem.* **2006**, *45*, 8882.
(17) Rieter, W. J.; Taylor, K. M. L.; An, H. Y.; Lin, W. L.; Lin, W. B. *J. Am. Chem. Soc.* **2006**, *128*, 9024.
(18) White, K. A.; Chengelis, D. A.; Zeller, M.; Geib, S. J.; Szakos, J.; Petoud, S.; Rosi, N. L. *Chem. Commun.* **2009**, 4506.
(19) Petoud, S.; Cohen, S. M.; Bünzli, J.-C. G.; Raymond, K. N. *J. Am. Chem. Soc.* **2003**, *125*, 13324.
(20) Zhang, J.; Badger, P. D.; Geib, S. J.; Petoud, S. *Angew. Chem. Int. Ed.* **2005**, *44*, 2508.
(21) da Vila, L. D.; Gomes, L.; Tarelho, L. V. G.; Ribeiro, S. J. L.; Messadeq, Y. *J. Appl. Phys.* **2003**, *93*, 3873.
(22) Bunzli, J. C. G.; Piguet, C. *Chem. Soc. Rev.* **2005**, *34*, 1048.
(23) Lee, J. A.; Mardyani, S.; Hung, A.; Rhee, A.; Klostranec, J.; Mu, Y.; Li, D.; Chan, W. C. W. *Adv. Mater.* **2007**, *19*, 3113.
(24) Weissman, S. I. *J. Chem. Phys.* **1942**, *10*, 214.
(25) Zhang, J.; Shade, C. M.; Chengelis, D. A.; Petoud, S. *J. Am. Chem. Soc.* **2007**, *129*, 14834.
(26) Chengelis, D. A.; Yingling, A. M.; Badger, P. D.; Shade, C. M.; Petoud, S. *J. Am. Chem. Soc.* **2005**, *127*, 16752.
(27) Wang, F.; Liu, X. G. *Chem. Soc. Rev.* **2009**, *38*, 976.
(28) Weng, D. F.; Zheng, X. J.; Jin, L. P. *Eur. J. Inorg. Chem.* **2006**, 4184.
(29) de Lill, D. T.; de Bettencourt-Dias, A.; Cahill, C. L. *Inorg. Chem.* **2007**, *46*, 3960.
(30) Cross, J. P.; Lauz, M.; Badger, P. D.; Petoud, S. *J. Am. Chem. Soc.* **2004**, *126*, 16278.

4.0 YTTERBIUM-ERBIUM ENERGY TRANSFER WITHIN POLYMETALLIC LANTHANIDE MOFS

4.1 INTRODUCTION

Lanthanide cations have ideal photophysical properties such as long luminescence lifetimes and sharp emission bands that result from the forbidden 4*f*-4*f* transition. These properties render them useful as components of many applications such as biological imaging, photonics, and telecommunications.[1] However, their luminescence can be quenched by O-H, N-H, and C-H vibrations of the surrounding solvent or attached ligands. Being able to improve these properties while still in the presence of quenching molecules has proved challenging. While in Chapter 2 we discussed how MOF chemistry allows for the enhancement of photophysical properties through modifications of the synthesis resulting in optimal ligand-ligand interactions, in Chapter 4 we discuss using lanthanide-lanthanide (Ln-Ln) interactions for improving photophysical properties. Specifically we show that by doping an Er^{3+}-MOF with Yb^{3+}, the Yb^{3+} will transfer some of its energy to the Er^{3+} and increase the brightness of Er^{3+}. Importantly, we have already shown in Chapter 3 that we have a method for controlled preparation of multiple lanthanide frameworks and can target various amounts of dopant.

Erbium is of particular interest because of its very low energy emission in the NIR; however, it is highly susceptible to quenching from C-H and O-H vibrations. Since sensitized emission arises from complexing organic molecules to the erbium cations, the C-H vibrations of the organic molecule decrease erbium's emission intensity. One common method to decrease this quenching is to use perfluoronated organic molecules, because the second vibrational overtone of C-F bonds does not quench the erbium luminescence as strongly as C-H overtones.[2] However, these complexes can be difficult to form and are unstable. More recently an erbium-perfluoronated complex that was encapsulated into a zeolite showed high quantum yield and long luminescence lifetimes.[3] Another method for improving erbium's photophysical properties

is through a doping method utilizing Yb^{3+} for Yb^{3+}-Er^{3+} energy transfer. This method has been explored for its use in improving erbium's properties in telecommunication applications. Erbium-doped fiber amplifiers (EDFA) are common components used to amplify signal in telecommunication applications.[4] Erbium's emission at 1.54 μm corresponds to the optical transmission window of silica fibers. By doping fibers with erbium, stimulated emission can occur upon laser excitation, which results in enhancement of the optical signal. This Yb^{3+}-Er^{3+} energy transfer has also been studied by others in a YAG matrix,[5] in glass,[6] in thin films,[7] and in crystals[8] with an aim toward being able to increase the emission of Er^{3+} for use in lasers and telecommunication devices.

Bi-metallic MOFs have been synthesized previously with transition metals,[9-11] transition and lanthanide metals,[12] and lanthanides metals.[13-20] Few studies have examined Ln-Ln interactions within a MOF. Of these, most were focused on upconversion properties and Tb-Eu energy transfer.[16,17,21] One attempt at doping an Er^{3+}-MOF with Yb^{3+} to increase erbium's luminescence was ineffective and ultimately resulted in a structural change of the MOF upon addition of too much ytterbium.[22]

MOFs are ideal systems for energy transfer studies because 1) their crystalline nature allows us to know exactly where the metal cations are located, 2) MOF chemistry permits the design of structures to vary the distance between lanthanide cations, and 3) dopant concentration can be well-controlled.

4.2 RESULTS AND DISCUSSION

Yb-PVDC-1 and four barcoded **Er_xYb_{1-x}-PVDC-1** MOFs had already been synthesized.[19] The luminescence spectra for the barcoded MOFs showed a linear dependence on lanthanide content. However, the erbium emission signal appeared stronger or just as strong in all of the samples, even for **$Er_{0.32}Yb_{0.68}$-PVDC-1**. To determine if this was simply because **H_2-PVDC**sensitizes erbium more efficiently, pure **Er-PVDC-1** needed to be synthesized and characterized.

4.2.1 Er-PVDC-1

H_2-PVDC and $Er(NO_3)_3 \bullet 5H_2O$ in DMF and ethanol were heated to yield yellow crystals of $Er_2(C_{26}H_{20}O_6)_3(H_2O)_2 \bullet (DMF)_3(H_2O)_4$. Powder X-ray diffraction studies show that **Er-PVDC-1** is isostructural with **Yb-PVDC-1** and **Er_xYb_{1-x}-PVDC-1** (Figure 4.1). Its photophysical properties were then studied.

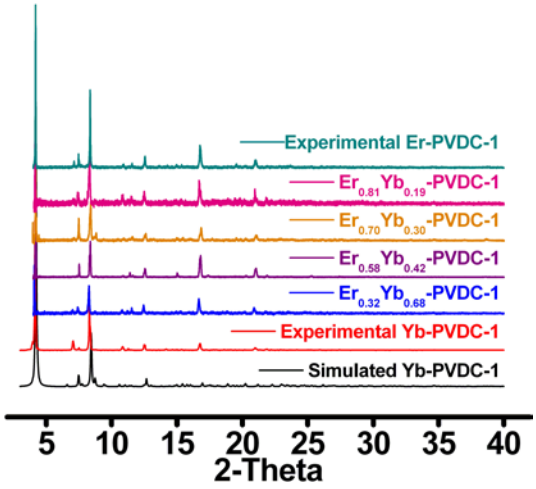

Figure 4.1. Powder X-ray diffraction patterns comparing Er-PVDC-1 to Yb-PVDC-1 and barcoded Er_xYb_{1-x}-PVDC-1 analogues

Excitation and emission spectra were collected of **Er-PVDC-1** as a solid under chloroform in the same manner as **Yb-PVDC-1** and **Er_xYb_{1-x}-PVDC-1**. Upon monitoring erbium emission at 1525 nm, an excitation spectrum was collected and showed maxima centered at 370 nm, 470 nm, 520 nm, and 650 nm. The 370 nm and 470 nm excitation bands correspond well to the excitation spectrum of **Yb-PVDC-1**. The bands with maxima centered at 520 nm and 650 nm are due to direct excitation of erbium. The 470 nm band appears more intense than for the **Yb-PVDC-1** sample because, in this case, the 470 nm and 520 nm bands overlap. Excitation at 370 nm and 470 nm both produce erbium emission centered at 1525 nm indicating sensitization via the antenna effect.

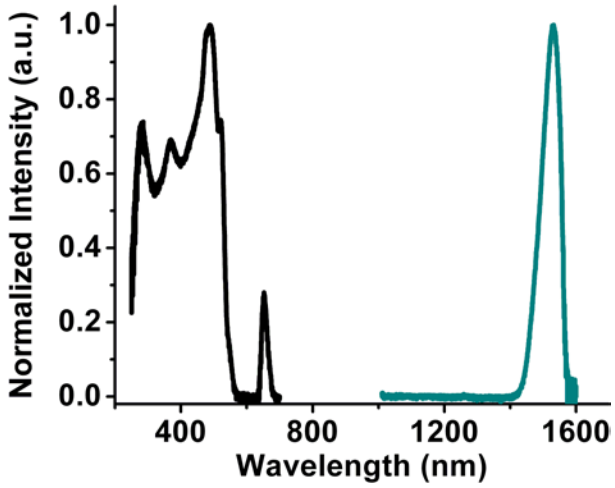

Figure 4.2. Excitation spectrum (black, λ_{em} = 1525 nm) and erbium sensitized emission (cyan, λ_{ex} = 470 nm) of Er-PVDC-1 collected as a solid under chloroform.

The quantum yield was measured through excitation at 490 nm instead of 470 nm in order to be consistent with our previous measurements on the **Ln-PVDC-1** system. The erbium quantum yield was determined to be 8.5 (± 0.4) x 10^{-5}. This value is in the same range as the highest values reported for erbium complexes in solution,[23,24] which indicates that the MOF

provides good protection of the Er^{3+} cations. However, this value is lower than the quantum yield of ytterbium in **Yb-PVDC-1**, 3.3(±0.5) $\times 10^{-3}$, indicating the PVDC sensitizes Yb^{3+} more efficiently than it does Er^{3+}. This could be due to Er^{3+} being more easily quenched by O-H vibrational overtones. The octa-coordinated lanthanide within the MOF has two water molecules bound to it and these vibrations could result in the lower quantum yield. This result along with the emission spectra presented in Chapter 3 prompted us to do a more thorough photophysical study of the barcoded MOFs to determine the cause in variations of emission intensities.

4.2.2 Energy transfer studies

To quantify the overall efficiency of the antenna effect in the MOF materials, quantum yields of all barcoded MOFs under chloroform were collected using a 490 nm excitation wavelength. If no energy transfer was occurring, the quantum yields for ytterbium and erbium should follow a linear pattern with the corresponding lanthanide composition. However, the quantum yields suggest that Yb^{3+}-Er^{3+} energy transfer is occurring (Table 4.1, Figure 4.3 and 4.4). The quantum yield for Yb^{3+} decreases drastically to a value of 6.5 (± 0.8) x 10^{-4} for **$Er_{0.32}Yb_{0.68}$-PVDC-1** from a value of 3.3 (±0.5) $\times 10^{-3}$ for **Yb-PVDC-1**. The Er^{3+} quantum yield initially decreases, but as more Yb^{3+} is doped into **Er-PVDC-1**, the quantum yields actually increase to a higher quantum yield than **Er-PVDC-1**.

Table 4.1. Quantum yield measurements with errors in parentheses (λ_{ex} = 490 nm).

MOF	$Er^{3+}\Phi$	$Yb^{3+}\Phi$
Yb-PVDC-1	-	3.3 (±0.5) x 10^{-3}
$Er_{0.32}Yb_{0.68}$-PVDC-1	1.8 (±0.4) x 10^{-4}	6.5 (±0.8) x 10^{-4}
$Er_{0.58}Yb_{0.42}$-PVDC-1	1.7 (±0.4) x 10^{-4}	1.8 (±0.4) x 10^{-4}
$Er_{0.70}Yb_{0.30}$-PVDC-1	9.98 (±0.9) x 10^{-5}	8.0 (±0.2) x 10^{-5}
$Er_{0.81}Yb_{0.19}$-PVDC-1	6.0 (±1.2) x 10^{-5}	3.4 (±0.4) x 10^{-5}
Er-PVDC-1	8.5 (±0.4) x 10^{-5}	-

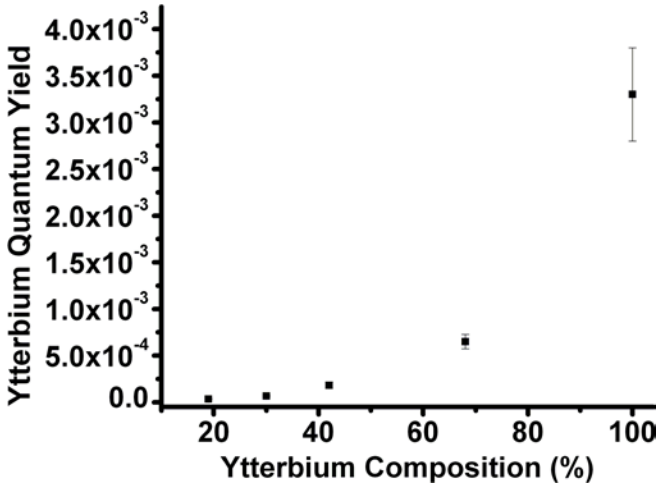

Figure 4.3. Yb^{3+} quantum yield values (λ_{ex} = 490 nm).

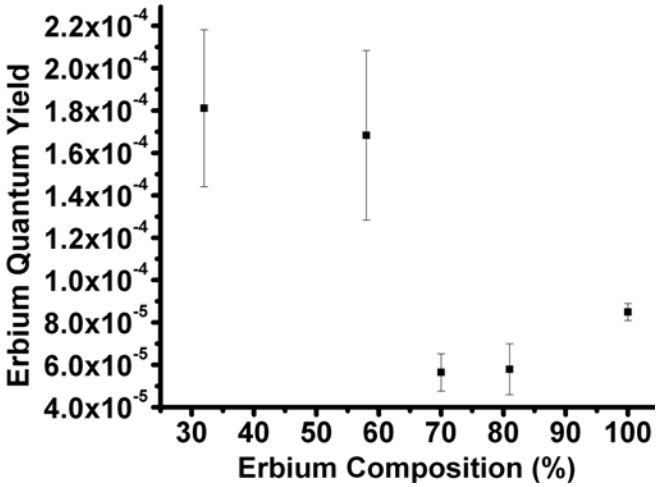

Figure 4.4. Er^{3+} quantum yield values (λ_{ex} = 490 nm).

We rationalize this increase as a result of energy transfer from the $^2F_{5/2}$ donor level of Yb^{3+} to the $^4I_{11/2}$ accepting level of Er^{3+} (Figure 4.5).[6] The energy gaps between the $^2F_{7/2}$ and $^2F_{5/2}$ levels of Yb^{3+} correspond well with the $^4I_{15/2}$ and $^4I_{11/2}$ levels of Er^{3+} making Yb^{3+}-Er^{3+} transfer likely when the metals are in close proximity to one another. In **Ln-PVDC-1**, a distance of 4.4 Å separates lanthanide ions within one SBU and a distance of approximately 24 Å separates lanthanides in neighboring SBUs. While we hypothesize that energy transfer within one SBU is more likely than between two SBUs, the distance dependence on Ln-Ln energy transfer is not well understood yet.

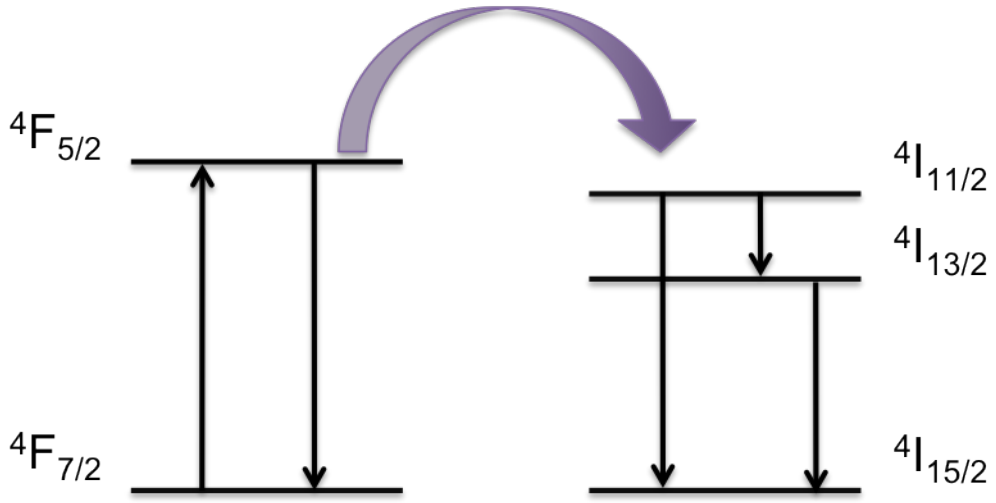

Figure 4.5. Energy level diagram of Yb^{3+} and Er^{3+} with arrows showing the different possible processes.

To further investigate possible energy transfer in **Er_xYb_{1-x}-PVDC-1**, luminescent lifetimes of Yb^{3+} in **$Er_{0.30}Yb_{0.70}$-PVDC-1** were measured, and displayed biexponetial behavior with values of 0.27 (±0.03) μs and 0.77 (±0.09) μs. Luminescence lifetime measurements for Yb^{3+}were also conducted on **$Er_{0.81}Yb_{0.19}$-PVDC-1**; however, the signal was too weak to be

discriminated from the background. These values reflect a significant quenching from the long-lived values reported for **Yb-PVDC-1** in Table 2.1. Moreover, the decrease in the number of luminescence lifetimes is also indicative of energy transfer. Measurements of the luminescence lifetimes of Yb^{3+} and Er^{3+} are currently underway. We expect the luminescence lifetimes of Er^{3+} to be longer lived in the barcoded MOFs than **Er-PVDC-1**, which would be confirmation of Yb^{3+}-Er^{3+} energy transfer.

4.3 CONCLUSION

We have demonstrated a new method for enhancing the NIR emission of erbium in the solid state. A MOF-based approach allows for the incorporation of both ytterbium and erbium cations in controlled amounts that permit tuning of the photophysical properties. **Er-PVDC-1** was successfully synthesized and characterized. Erbium sensitization is achieved via the antenna effect and its quantum yield ranks high amongst others measured in solution. Higher quantum yields are obtained upon doping **Er-PVDC-1** with ytterbium cations. This increase in quantum yield for erbium and big decrease for ytterbium is indicative of energy transfer. The shortened luminescence lifetimes of ytterbium support this energy transfer, although, luminescence lifetimes of erbium will further confirm this conclusion.

While in Chapter 2 we demonstrated that the photophysical properties of lanthanide cations can be tuned by controlling ligand-ligand interactions within a MOF, in Chapter 4 we demonstrated this by controlling Ln-Ln interactions within a MOF. To the best of our knowledge, this is the first example of a bi-metallic lanthanide MOF that uses a doping method

to optimize the photophysical properties of a NIR emitting lanthanide cation. While this system only incorporates ytterbium and erbium, this method is versatile and could be expanded to include any lanthanide metals.

4.4 EXPERIMENTAL

4.4.1 Reagents

Starting materials and reagents were obtained from commercial sources or synthesized by procedures noted below. **H_2-PVDC** was synthesized as described in Section 2.4.4. Dimethoxybenzene, paraformaldehyde, triphenylphosphine, methanol, ethanol NaOMe, THF, DMF, anhydrous methanol, and $Er(NO_3)_3 \bullet 5H_2O$were purchased from Aldrich. $Yb(NO_3)_3 \bullet 5H_2O$ was purchased from Strem Chemicals. Glacial acetic acid and hydrochloric acid were purchased from Fisher. Hyrdobromic acid (33% in AcOH) was purchased from Fluka. Anhydrous toluene (99.8%) and anhydrous chloroform (99.8%) were purchased from Acros. Argon gas was purchased from Valley National. Methyl 4-formylbenzoate was purchased from TCI. KOH was purchased from Alfa Aesar. All reagents were used as received without further purification.

4.4.2 Physical characterization

Fourier transform infrared (FT-IR) spectra were measured on a Nicolet Avatar 360 FT-IR spectrometer using KBr pellet samples. Absorptions are described as very strong (vs), strong (s), medium (m), weak (w), shoulder (sh), and broad (br) and stretches (st) are labeled symmetric

(sym) or asymmetric (as). Data was analyzed using the Omnic Software Package. X-ray powder diffraction patterns were collected using a Bruker AXS D_8 Discover powder diffractometer at 40 kV, 40 mA for Cu Kα, (λ = 1.5406 Å) with a scan speed of 0.20 sec/step and a step size of .02018º. The data were analyzed for d-spacing measurements using the EVA program from the Bruker Powder Analysis Software package. The purity and homogeneity of the bulk products were determined by comparison to the simulated and experimental X-ray powder diffraction patterns of **Yb-PVDC-1**.

4.4.3 Spectroscopic methods

Emission and excitation spectra in the visible range were measured using a Varian Cary Eclipse Fluorescence Spectrophotometer coupled to a personal computer with software provided by Varian. Spectra in the near infrared range were measured using a Jobin Yvon–Horiba Fluorolog-322 spectrofluorimeter equipped with an Electro-Optical Systems, Inc. DSS-IGA020L detector for the NIR domain. Emission and excitation spectra of **Er-PVDC-1**, **Yb-PVDC-1**, and **Er_xYb_{1-x}-PVDC-1** were collected as a solid sample under chloroform on the JY Horiba Fluorolog-322 Spectrofluorimeter fitted with an integrating sphere developed by Frédéric Gumy and Prof. Jean-Claude G. Bünzli (Laboratory of Lanthanide Supramolecular Chemistry, École Polytechnique Féderale de Lausanne (EPFL), BCH 1402, CH-1015 Lausanne, Switzerland) (ref Aebischer, A.; Gumy, F.; Bünzli, J.-C. G. Phys. Chem. Chem. Phys. 2009, 11, 1346-1353.) as an accessory to the Fluorolog FL3-22 spectrometer (Patent pending) using quartz tube sample holders.

Relative quantum yield measurements were obtained with the integration sphere on the Jobin Yvon-Horiba Fluorolog-322 using ytterbium tropolonate and erbium tropolonate as the

references for these experiments ($[Ln(trop)_4]^-$ in DMSO, $\Phi_{Yb} = 1.9 \times 10^{-2}$, $\Phi_{Er} = 1.7 \times 10^{-4}$).[23] Measurements of the near infrared luminescence lifetimes were performed using a Nd:YAG Continuum Powerlite 8010 laser (354nm, third harmonic) as the excitation source. Emission was collected at a right angle to the excitation beam, and wavelengths were selected by a Spectral Products CM 110 1/8 meter monochromator. The signal was monitored by a Hamamatsu R316-02 photomultiplier tube coupled to a 500 MHz band pass digital oscilloscope (Tektronix TDS 754D). Signals from >1000 flashes were collected and averaged. The results have been obtained from data resulting from at last three independent experiments. Luminescence decay curves were treated with Origin 7.0 software using exponential fitting models.

4.4.4 Synthesis of Er-PVDC-1

In a glass vial (4 mL), a solution of 4,4'-(1*E*,1'*E*)-2,2'-(2,5-dimethoxy-1,4-phenylene)bis(ethene-2,1-diyl)dibenzoic acid (**H_2-PVDC**) (8.60 mg, 0.020 mmol) in DMF (0.4 mL) and a solution of $Er(NO_3)_3 \bullet 5H_2O$ (4.43 mg, 0.01 mmol) in DMF (0.2 mL) were combined with ethanol (95 %, 100.0 μL) to produce a neon green solution. The vial was capped and placed in an 100 ºC isotemp oven for 12 hours to produce yellow crystalline needles of the product. The crystals were collected, washed with DMF (4 x 3 mL), and air dried (2.3 mg, 11.8 %).

EA Calcd. (%) for $Er_2(C_{26}H_{20}O_6)_3(H_2O)_2 \bullet (DMF)_3(H_2O)_4$: C, 53.66; H, 4.81; N, 2.16. Found: C, 53.54; H, 4.28; N, 2.20. EA. Calcd. (%) for the chloroform exchange product, $Er_2(C_{26}H_{20}O_6)_3(H_2O)_2 \bullet (CHCl_3)_{2.50}(DMF)_{0.25}$: C, 49.47; H, 3.49; N, 0.18. Found: C, 49.92; H, 3.59; N, 0.15. FT-IR (KBr 4000-700 cm^{-1}): 3309 (br), 1658 (DMF C=O, m), 1601 (m), 1541 (s) 1415 (COO^-, vs), 1209 (s), 1180 (w), 1107 (w), 1043 (s), 967 (m), 867 (w), 781 cm^{-1} (trans C=C-H, s,).

4.5 REFERENCES

(1) Comby, S.; Bünzli, J.-C. G. In *Handbook on the Physics and Chemistry of Rare Earths*; Gschneidner, K. A., Jr., Bünzli, J.-C. G., Pecharsky, V., Ed.; Elsevier: Amsterdam, 2007; Vol. 37.

(2) Mancino, G.; Ferguson, A. J.; Beeby, A.; Long, N. J.; Jones, T. S. *J. Am. Chem. Soc.* **2005**, *127*, 524.

(3) Mech, A.; Monguzzi, A.; Meinardi, F.; Mezyk, J.; Macchi, G.; Tubino, R. *J. Am. Chem. Soc.* **2010**, *132*, 4574.

(4) Meinardi, F.; Colombi, N.; Destri, S.; Porzio, W.; Blumstengel, S.; Cerminara, M.; Tubino, R. *Synth. Met.* **2003**, *137*, 959.

(5) Vega-Duran, J. T.; Barbosa-Garcia, O.; Diaz-Torres, L. A.; Meneses-Nava, M. A.; Sumida, D. S. *Appl. Phys. Lett.* **2000**, *76*, 2032.

(6) da Vila, L. D.; Gomes, L.; Tarelho, L. V. G.; Ribeiro, S. J. L.; Messadeq, Y. *J. Appl. Phys.* **2003**, *93*, 3873.

(7) Suarez-Garcia, A.; Serna, R.; de Castro, M. J.; Afonso, C. N.; Vickridge, I. *Appl. Phys. Lett.* **2004**, *84*, 2151.

(8) You, W.; Huang, Y.; Chen, Y.; Lin, Y.; Luo, Z. *Optics Communications* **2008**, *281*, 4936.

(9) Agusti, G.; Munoz, M. C.; Gaspar, A. B.; Real, J. A. *Inorg. Chem.* **2009**, *48*, 3371.

(10) Gu, Z. G.; Sevov, S. C. *J. Mater. Chem.* **2009**, *19*, 8442.

(11) Colacio, E.; Lloret, F.; Kivekas, R.; Suarez-Varela, J.; Sundberg, M. R.; Uggla, R. *Inorg. Chem.* **2003**, *42*, 560.

(12) Rieter, W. J.; Pott, K. M.; Taylor, K. M. L.; Lin, W. B. *J. Am. Chem. Soc.* **2008**, *130*, 11584.

(13) Rieter, W. J.; Taylor, K. M. L.; An, H. Y.; Lin, W. L.; Lin, W. B. *J. Am. Chem. Soc.* **2006**, *128*, 9024.

(14) Rieter, W. J.; Taylor, K. M. L.; Lin, W. B. *J. Am. Chem. Soc.* **2007**, *129*, 9852.

(15) Guo, H.; Zhu, Y.; Qiu, S.; Lercher, J. A.; Zhang, H. *Adv Mater* **2010**, *22*, 4190.

(16) Sun, C. Y.; Zheng, X. J.; Chen, X. B.; Li, L. C.; Jin, L. P. *Inorg. Chim. Acta* **2009**, *362*, 325.

(17) Weng, D. F.; Zheng, X. J.; Chen, X. B.; Li, L.; Jin, L. P. *Eur. J. Inorg. Chem.* **2007**, 3410.

(18) Luo, F.; Batten, S. R. *Dalton T.* **2010**, *39*, 4485.

(19) White, K. A.; Chengelis, D. A.; Gogick, K. A.; Stehman, J.; Rosi, N. L.; Petoud, S. *J. Am. Chem. Soc.* **2009**, *131*, 18069.

(20) Yuan, W.; O'Connor, J.; James*, S. L. *CrystEngComm* **2010**, *12*, 3515.

(21) Weng, D. F.; Zheng, X. J.; Jin, L. P. *Eur. J. Inorg. Chem.* **2006**, 4184.

(22) Haquin, V.; Gumy, F.; Daiguebonne, C.; Bunzli, J. C.; Guillou, O. *Eur. J. Inorg. Chem.* **2009**, 4491.

(23) Zhang, J.; Badger, P. D.; Geib, S. J.; Petoud, S. *Angew. Chem. Int. Ed.* **2005**, *44*, 2508.

(24) Zhang, J.; Petoud, S. *Chem. Eur. J.* **2008**, *14*, 1264.

5.0 NEAR-INFRARED EMITTING WATER-STABLE MOF AND NANOMOF BARCODES

The spectroscopic data was done in collaboration with Kristy Gogick (Stéphane Petoud Research Group, Department of Chemistry, University of Pittsburgh),

Steven J. Geib (X-ray crystallographer, University of Pittsburgh) solved the crystal structure of **Ho-PVDC-3**, **Tb-PVDC-3**, **Nd-PVDC-3**, **Er-PVDC-3**, and **Yb-PVDC-3**.

5.1 INTRODUCTION

Metal-organic frameworks (MOFs) have many properties that make them great candidates for biomedical applications. First, MOFs can be designed to exhibit low toxicity by incorporating metal ions that are already in the body, such as Zn^{2+} or Fe^{3+}, as opposed to ones that are known to be toxic like Cd^{2+}. A more biocompatible MOF can be synthesized by choosing a nucleobase[1] or amino acid[2] for the organic linker. Moreover, the porosity of the MOF can be utilized for a drug delivery system.[3] The ability to post-synthetically modify the MOF allows for another method for delivering drug molecules or to attach a fluorophore for biological imaging.[4] In addition to low toxicity, other criteria must be met to utilize MOFs for intracellular applications. The MOF must be adequately stable in water or biological media for a suitable duration, which will depend on the application, and it must be sufficiently small to cross cell membranes.[5]

In Chapter 5, we incorporate near-infrared (NIR) emitting lanthanide metals into MOFs because they have several advantages over other components frequently used in biological imaging materials, such as fluorophores and quantum dots. Lanthanide emission arises from the Laporte forbidden 4*f*-4*f* transition. These electrons are well shielded from the environment by the 5s and 5p electrons, resulting in atom-like, characteristic emission bands specific for each lanthanide, unlike the broad emission bands of fluorophores. The emission bands are also sharper than those of quantum dots, which would allow for a higher number of barcoded materials for multiplexing assays (Figure 3.1). Unlike quantum dots, Ln^{3+} emission bands are not affected by environmental conditions,[6] such as pH or solvent,[7] nor are the emission dependent on the size of the material.

Moreover, the luminescence lifetimes of lanthanide cations (μs – ms),[8,9] are much longer than those of organic fluorophores (ps – ns), which is beneficial for cellular imaging. The long luminescence lifetimes allow for time resolved experiments to discriminate lanthanide luminescence from background autofluorescence.[10] NIR emission is particularly useful because biological tissue has a low absorptivity of NIR light.[11] Consequently, NIR light can penetrate more deeply, allowing for a less invasive imaging technique.[12,13] Finally, NIR photons can provide images with better resolution than organic fluorophores because NIR photons are scattered less than those in the visible region.

In Chapter 5, we discuss the synthesis of a NIR emitting lanthanide framework that appears to be stable and luminescent while suspended in water, demonstrating again that MOF materials provide good protection from quenching of lanthanide cations. We then address the size requirement by utilizing a reverse microemulsion process that allows for the miniaturization of these MOFs, resulting in materials referred to as nanoMOFs. Finally, we also synthesize the barcoded bulk MOF and corresponding nanomaterials. Unlike Ln-PVDC-1, Ln-PVDC-3 does not show any size selectivity allowing for incorporation of neodymium in addition to ytterbium and erbium. These materials should have great potential for imaging and multiplexing assays.

5.2 RESULTS AND DISCUSSION

5.2.1 A Ho^{3+}-MOF with water stability

We adapted the synthesis of **Yb-PVDC-1** and **Yb-PVDC-2** by adding more water or acid to solutions of $Ln(NO_3)_3$ salts and **H_2-PVDC** to yield a new family of 3-dimensional crystals: **Ln-PVDC-3**. $Ho(NO_3)_3 \bullet 5H_2O$ was reacted with **H_2-PVDC** in DMF and nitric acid at 105 °C for 12 hours to yield yellow needles of product. **Ho-PVDC-3** crystallizes in low symmetry space group P-1 and exhibits infinite Ho-carboxylate SBUs along the *a* crystallographic direction (Figure 5.1 and 5.2). The SBU consists of only one metal center (octa-coordinated, Figure 5.2), as opposed as to the two metal centers (octa-coordinated and hexa-coordinated) that alternate in **Yb-PVDC-1** and **Yb-PVDC-2**. Ho^{3+} is octa-coordinated with 6 carboxylates from 3 ligands, an oxygen atom from one water molecule, and an oxygen atom from one DMF molecule (Figure 5.2). The three-dimensional structure of **Ho-PVDC-3** is depicted in Figure 5.1. **Ho-PVDC-3** is stable in a variety of solvents, including water, as confirmed by powder X-ray diffraction (Figure 5.3). Even after soaking in water for a month, the material maintains its original crystallinity.

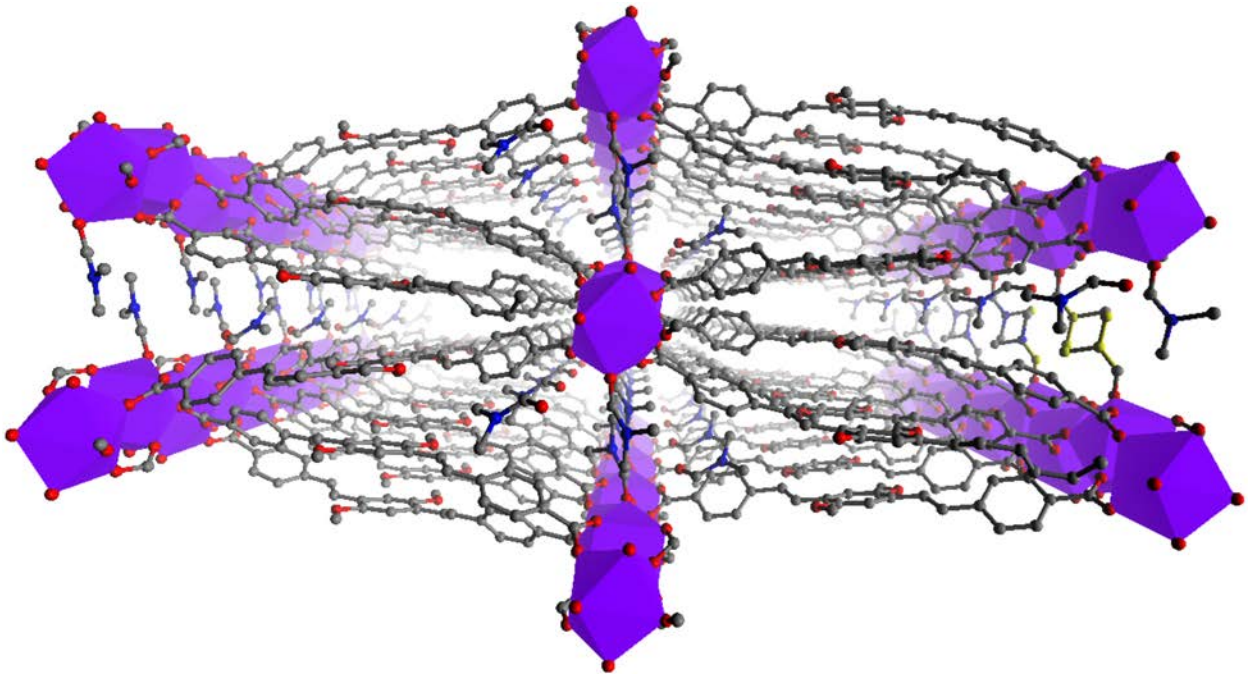

Figure 5.1. Perspective view of Ho-PVDC-3 down the *a* crystallographic direction with Ho^{3+} shown as polyhedra (C, grey; O, red; N, blue; Ho^{3+}, purple)

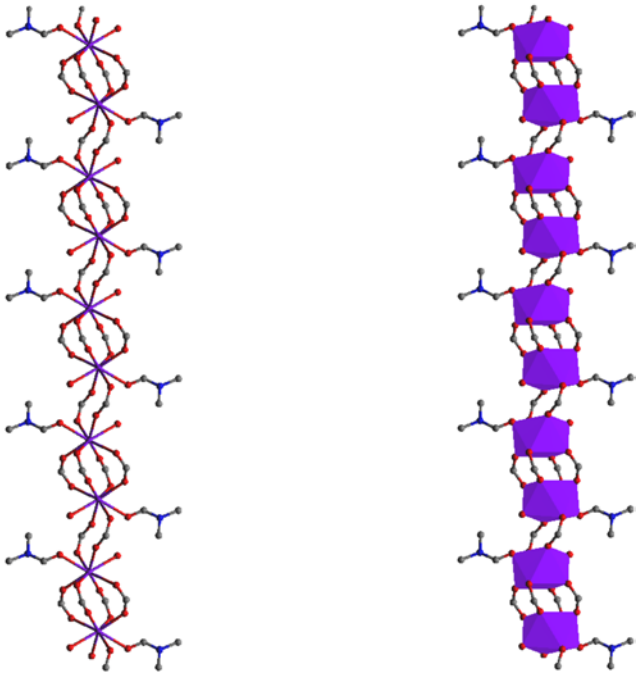

Figure 5.2. Ball and stick depiction of infinite SBU (left) and SBU with Ho^{3+} shown as polyhedra (right) (C, grey; O, red; N, blue; Ho^{3+}, purple).

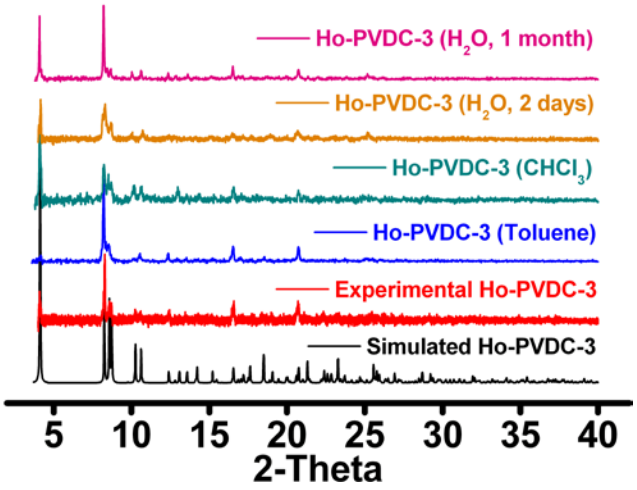

Figure 5.3. Powder X-ray diffraction patterns of Ho-PVDC-3 solvent-exchanged materials.

We also prepared isostructural analogues to **Ho-PVDC-3** by using other lanthanide cations. Specifically, the Tb^{3+}, Yb^{3+}, Nd^{3+}, and Er^{3+} analogues were prepared using only slightly modified syntheses compared to that of **Ho-PVDC-3.** The identity of each analogue was confirmed by single-crystal X-ray studies.

5.2.2 Luminescent Nd^{3+}, Er^{3+}, Yb^{3+}-MOFs with water stability

Reacting **H_2-PVDC** with $Nd(NO_3)_3 \bullet 6H_2O$, $Er(NO_3)_3 \bullet 5H_2O$, and $Yb(NO_3)_3 \bullet 5H_2O$ yielded **Nd-PVDC-3**, **Er-PVDC-3**, and **Yb-PVDC-3**, respectively. Reaction conditions were similar to that of **Ho-PVDC-3** with slight variations in co-solvents (Table 5.1). Water was used in place of nitric acid for **Nd-PVDC-3**, and a slight increase in nitric acid was used for **Er-PVDC-3** and **Yb-PVDC-3**. Crystal structure data was collected and solved, demonstrating that **Nd-PVDC-3**, **Er-PVDC-3**, and **Yb-PVDC-3** all formed isostructural MOFs (Unit cell summary in Table 5.2).

The structure of **Nd-PVDC-3** (Figure 5.4) contains the same basic formula as **Ho-PVDC-3** and **Tb-PVDC-3** of $Ln_1(PVDC)_{1.5}(DMF)_1(H_2O)_1$ with one DMF molecule and one water molecule coordinated to the Nd^{3+} (Figure 5.5 and 5.6). However, **Er-PVDC-3** and **Yb-PVDC-3** differ slightly in that each metal center is coordinated by two water molecules instead of one water molecule and one DMF molecule (Figure 5.6). With guest solvent molecules the formulae of **Nd-PVDC-3**, **Er-PVDC-3**, and **Yb-PVDC-3** are $Nd_1(C_{26}H_{20}O_6)_{1.5}(DMF)_1(H_2O)_1\bullet(DMF)_{0.5}(H_2O)_2$, $Er_1(C_{26}H_{20}O_6)_{1.5}(H_2O)_2\bullet(DMF)_{1.5}$, and $Yb_1(C_{26}H_{20}O_6)_{1.5}(H_2O)_2\bullet(DMF)_{1.5}$, respectively.

Table 5.1. Synthetic conditions for Ln-PVDC-3

Ln	Ln (mmol)	PVDC (mmol)	HNO_3 (1M) (mL)	H_2O (mL)
Nd	0.05	0.20	-	0.5
Tb	0.15	0.20	0.75	-
Ho	0.15	0.20	0.5	0.5
Er	0.05	0.20	1.0	-
Yb	0.05	0.20	1.0	-

Table 5.2. Unit cell data for Ln-PVDC-3 with errors in parentheses

MOF	a (Å)	b(Å)	c (Å)	α °	β °	γ °
Nd-PVDC-3	9.258(2)	10.765(3)	21.866(6)	78.623(5)	88.322(5)	79.430(5)
Tb-PVDC-3	9.1655(18)	10.667(2)	21.774(4)	78.12(3)	87.89(3)	79.41(3)
Ho-PVDC-3	9.202(3)	10.702(4)	21.866(8)	78.019(7)	87.845(6)	79.438(7)
Er-PVDC-3	8.942(4)	10.817(6)	21.818(11)	78.278(9)	87.967(9)	78.977(10)
Yb-PVDC-3	8.811(2)	10.951(3)	21.944(5)	77.152(5)	87.703(5)	78.251(6)

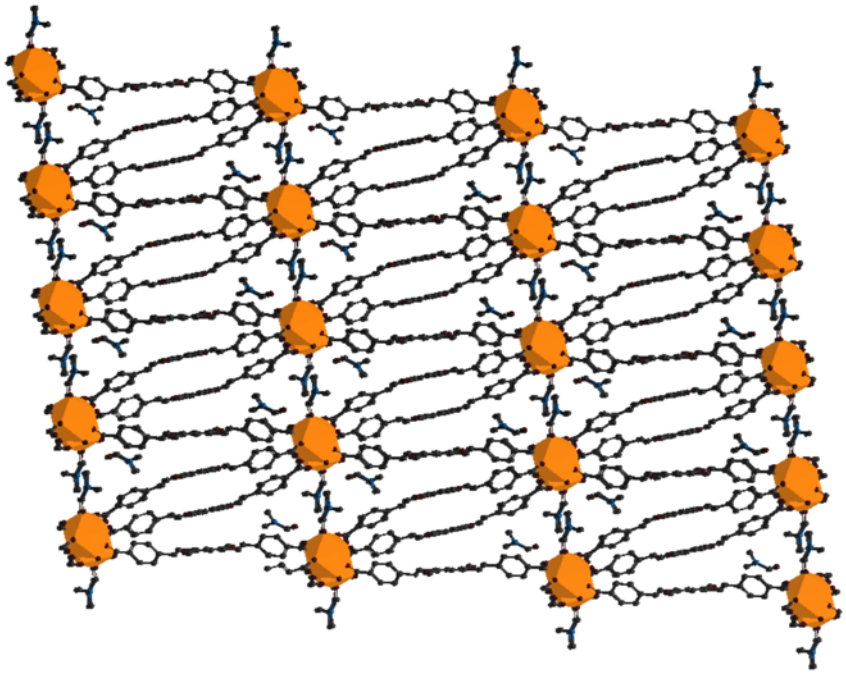

Figure 5.4. Perspective view of Nd-PVDC-3 down the *a* crystallographic direction with Nd^{3+} shown as polyhedra (C, grey; O, red; N, blue; Nd^{3+}, orange).

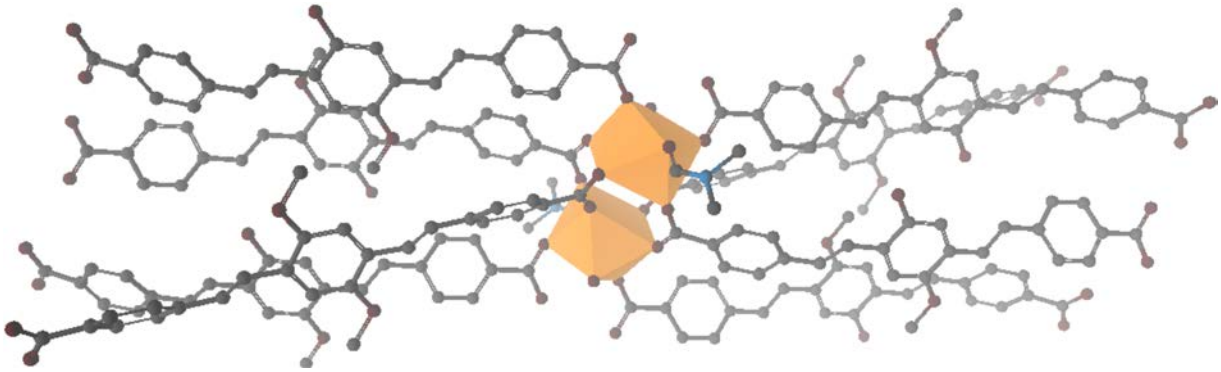

Figure 5.5. Connectivity within Nd-PVDC-3 with Nd^{3+} shown as polyhedra (C, grey; O, red; N, blue; Nd^{3+}, orange)

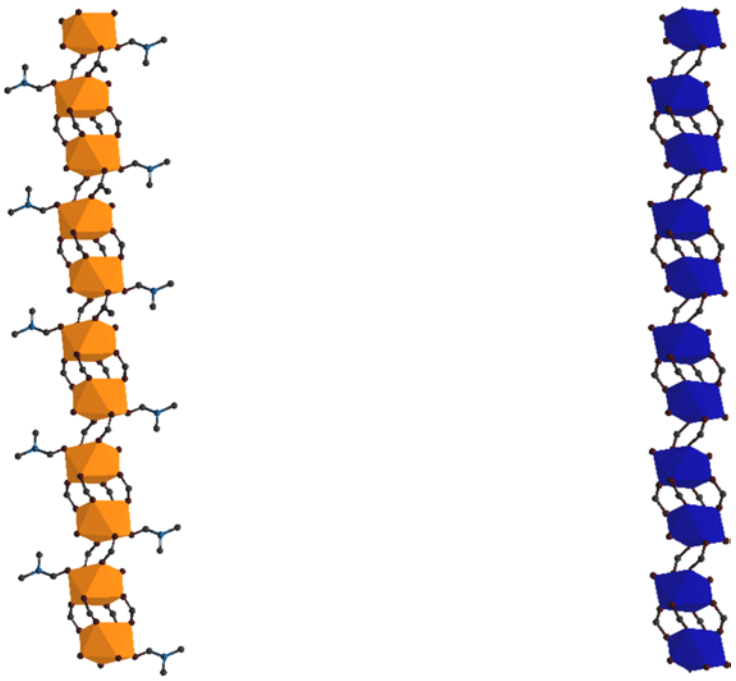

Figure 5.6. Comparison of SBUs: Nd^{3+} (orange) has one coordinated water molecule and one coordinated DMF molecule (left) and Er^{3+}(royal blue) has two coordinated water molecules

The thermogravimetric analysis (TGA) data reflects this difference in that both patterns show a weight loss that plateaus around 120 °C corresponding to the removal of guest molecules. Upon further heating, the DMF and water molecules are not removed until 225°C (Figure 5.7) and the two water molecules are removed at 200°C (Figure 5.8). When **Nd-PVDC-3** is heated to 120 °C, guest molecule evacuate the cavities and the weight loss measured by TGA is 9.5 % (calc'd, 8 %). The heated sample was submitted for C, H, N elemental analysis and calculated and measured CHN data correspond well for the evacuated framework $Nd_1(PVDC)_{1.5}(DMF)_1(H_2O)_1$ (Calc'd: C, 57.46; H, 4.48; N,1.60; Found: C, 57.52; H, 4.11; N,1.78). Upon further heating to 225 °C, TGA data shows a weight loss of 17.0 % (calc'd: 17.3%). However, a smaller total weight loss of 15% at 200 °C is observed for **Yb-PVDC-3**,

which corresponds to the calculated weight loss off 15% upon removal of guest molecules and two coordinated water molecules.

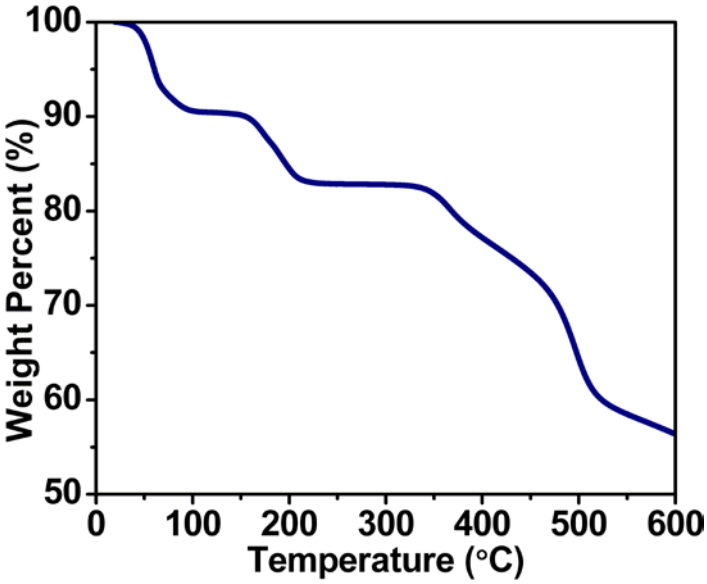

Figure 5.7. TGA of Nd-PVDC-3

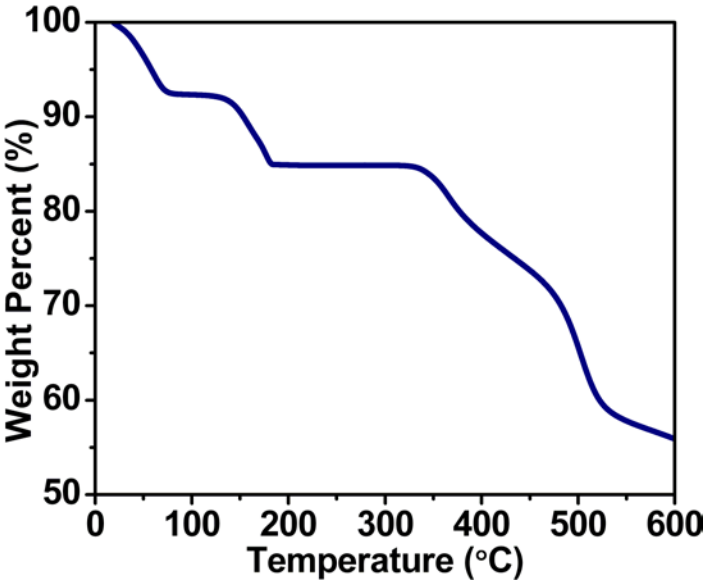

Figure 5.8. TGA of Yb-PVDC-3

In order to elucidate the solvent stability of **Nd-PVDC-3**, **Er-PVDC-3**, and **Yb-PVDC-3**, solvent exchanges were performed with chloroform and water. Powder X-ray diffraction patterns were collected and demonstrated that these materials appear to maintain their crystallinity upon solvent-exchange (Figure 5.9, 5.10, and 5.11). C, H, N elemental analysis of the water-exchanged materials of **Nd-PVDC-3**, **Er-PVDC** and **Yb-PVDC-3** showed that some residual DMF resided in the pores and that these materials were not completely water-exchanged with resulting formulae of $Nd_1(C_{26}H_{20}O_6)_{1.5}(H_2O)_2\bullet(DMF)_{0.25}(H_2O)_{3,}$, $Er_1(C_{26}H_{20}O_6)_{1.5}(H_2O)_2\bullet(DMF)_{0.5}(H_2O)_2$, and $Yb_1(C_{26}H_{20}O_6)_{1.5}(H_2O)_2\bullet(DMF)_{0.25}(H_2O)_{2.25}$, respectively.

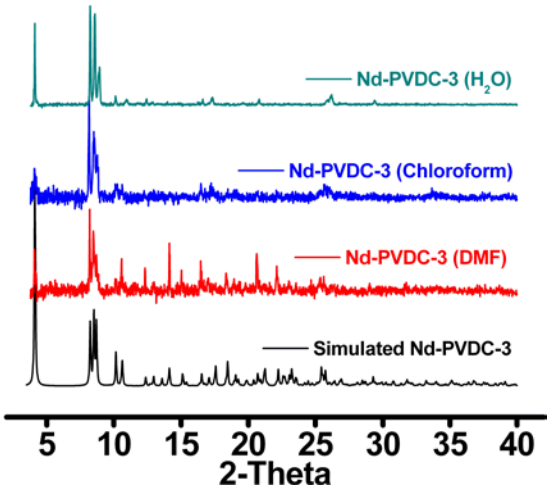

Figure 5.9. Powder X-ray diffraction pattern of Nd-PVDC-3 solvent-exchanged materials

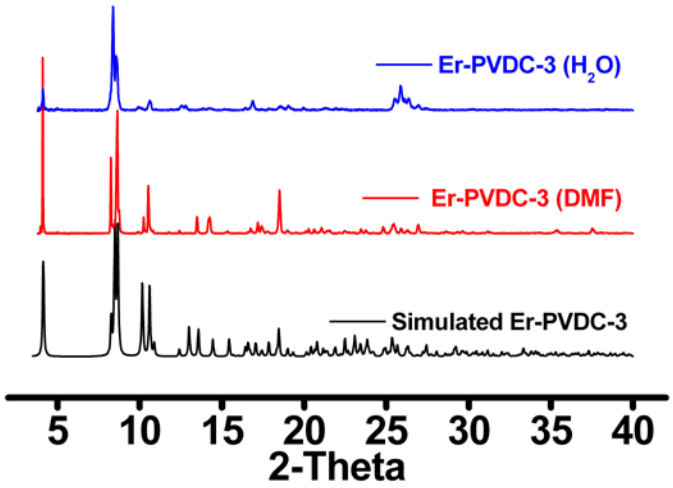

Figure 5.10. Powder X-ray diffraction pattern of Er-PVDC-3 solvent-exchanged materials

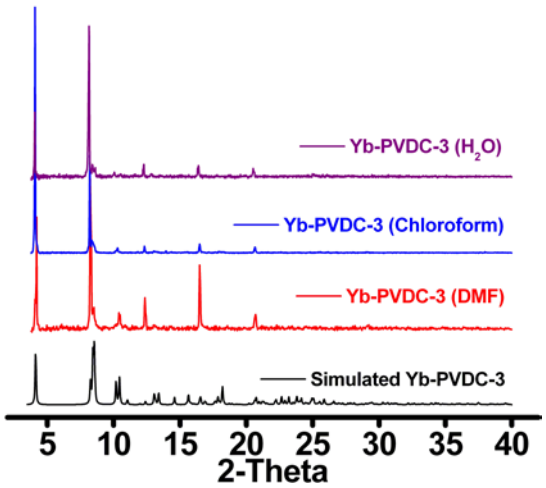

Figure 5.11. Powder X-ray diffraction pattern of Yb-PVDC-3 solvent-exchanged materials

Luminescent studies were performed on the solvent exchange materials to reveal the impact that solvent has on **Ln-PVDC-3**. Upon monitoring Yb^{3+} emission at 980 nm, an excitation spectrum was collected and showed apparent maxima at 280 nm, 370 nm, and 450 nm (Figure 5.12).

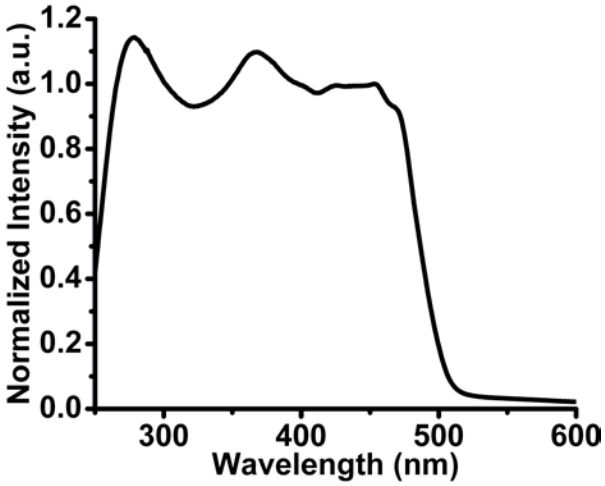

Figure 5.12. Excitation plot of Yb-PVDC-3 while monitoring ytterbium luminescence in DMF (λ_{em} = 980 nm)

Upon excitation through the 280 nm, 370nm, and 450 nm bands, sensitized ytterbium emission is observed (Figure 5.13). As expected, exciting **Nd-PVDC-3** and **Er-PVDC-3** through any of those bands also results in lanthanide emission of Nd^{3+} (875, 1060, and 1330 nm), respectively (Figure 5.14 and 5.15).

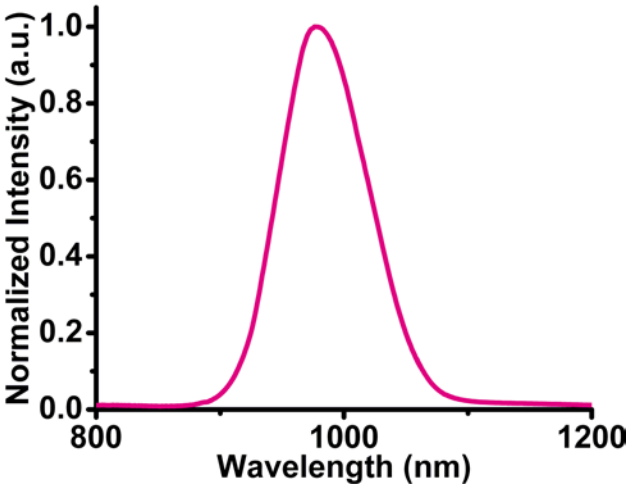

Figure 5.13. Ytterbium emission (980 nm) in Yb-PVDC-3 while suspended under DMF (λ_{ex} = 450 nm)

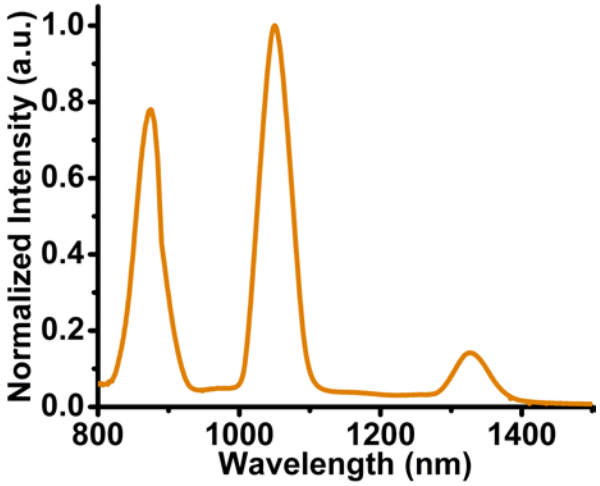

Figure 5.14. Neodymium emission (875, 1060, and 1330 nm) in Nd-PVDC-3 while suspended under DMF (λ_{ex} = 450 nm).

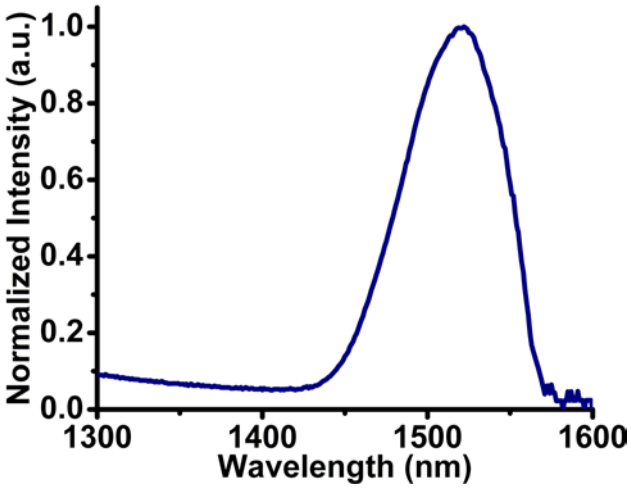

Figure 5.15. Erbium emission (1530 nm) in Er-PVDC-3 (λ_{ex} = 450 nm) while suspended under DMF

The photoluminescence properties of the water-exchanged materials were studied. Upon excitation at 450 nm, **Nd-PVDC-3** and **Yb-PVDC-3** both displayed their typical emission bands (Figure 5.16). However, no Er^{3+} luminescence was observable. This can be attributed to the

luminescence of Er^{3+} being more easily quenched than that of Nd^{3+} and Yb^{3+}. The 2nd vibrational overtone of O-H is close in energy to the $^4I_{15/2}$ excited state of erbium (Figure 5.17).

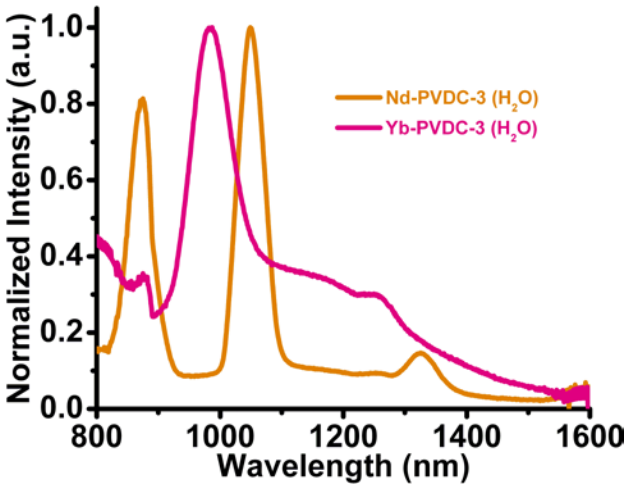

Figure 5.16. Ytterbium emission (980 nm) in Yb-PVDC-3 (pink) and neodymium emission (875, 1060, and 1330 nm) in Nd-PVDC-3 (orange) while suspended under water (λ_{ex} = 450 nm)

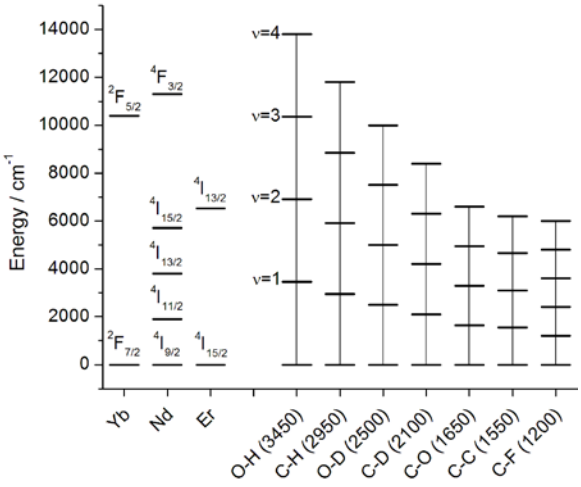

Figure 5.17. Energy level diagram showing quenching vibrations of common organic bonds

5.2.3 Single lanthanide-containing nanoMOFs

The stability of Ln-PVDC-3 in water and the luminescence of **Yb-PVDC-3** and **Nd-PVDC-3** while suspended in water prompted us to miniaturize Ln-PVDC-3 into a nanoMOF. NanoMOF synthesis allows us make materials sufficiently small for biological applications. One nanoMOF synthesis employs a water-in-oil reverse microemulsion method. An aliquot of an aqueous solution of the methylammonium salt of **H_2-PVDC** and an aliquot of an aqueous solution of $LnCl_3$ salt are added to separate flasks each containing an aliquot of CTAB/Hexanol/Heptane solution. They are stirred individually and then combined. The ratio (*W*) of the aqueous reagent to the CTAB greatly affects the resulting crystal formation.

5.2.3.1 Uncoated nanoMOFs

The water-in-oil ratio (*W*) is determined by ($[H_2O]/[CTAB]$). Analogous to the role solvent and co-solvents play in standard MOF synthesis, the *W* value greatly affects the resulting nanoMOFs structure. Neodymium nanoMOFs were prepared with w = 5, 10, and 15 (Figure 5.18). Powder X-ray diffraction patterns were collected and compared to the pattern simulated from the single crystal X-ray diffraction of the bulk material **Nd-PVDC-3.** The diffraction pattern for w = 15 does not contain peaks coinciding with the bulk material. While the pattern for w = 5 has many of the same peaks that appear for the bulk material, other peaks exist that indicate either a different crystal structure or a mixture of **Nd-PVDC-3** and another material. The diffraction pattern for w = 10 corresponds well with the simulated pattern, indicating we had synthesized **Nd-PVDC-3 nMOF.** Reactions with $YbCl_3$ and $ErCl_3$ using w = 10 also yielded Ln-PVDC-3 nMOF materials as confirmed by powder X-ray diffraction patterns (Figure 5.19).

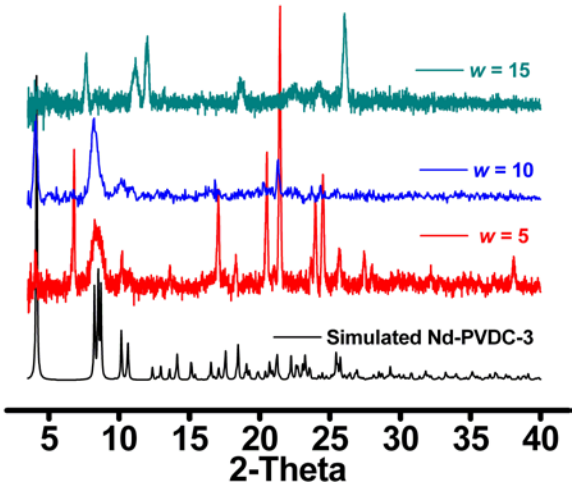

Figure 5.18. Powder X-ray diffraction patterns of Nd-PVDC-3 nMOF with different *W* values

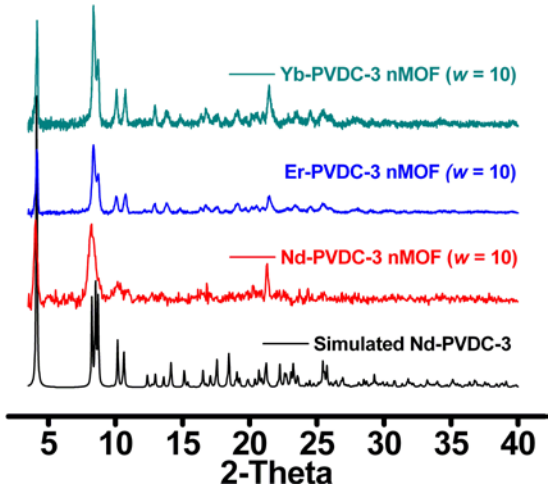

Figure 5.19. Powder X-ray diffraction pattern of Ln-PVDC-3 nMOF with *W* = 10

Luminescence properties of **Nd-PVDC-3 nMOF**, **Yb-PVDC-3 nMOF**, and **Er-PVDC-3 nMOF** were then studied as solid-state samples and while suspended under water. The excitation profile showed the same apparent maxima as the corresponding bulk material (Figure 5.20). Upon excitation through the low energy 450 nm band, Nd^{3+} and Yb^{3+} emission was observed for **Nd-PVDC-3 nMOF** (Figure 5.21) and **Yb-PVDC-3 nMOF** (Figure 5.22),

respectively. Upon excitation of **Er-PVDC-3 nMOF**, no Er^{3+} emission was observed as expected.

Quantum yield measurements were performed on **Nd-PVDC-3 nMOF** and **Yb-PVDC-3 nMOF** as powders suspended under water. These measurements revealed quantum yield values of is 1.17 x 10^{-4} and 9.3 x 10^{-5} for **Nd-PVDC-3 nMOF** and **Yb-PVDC-3 nMOF**, respectively. Neodymium's quantum yield is par for reported systems under water; however, ytterbium's quantum yield is low.[14]

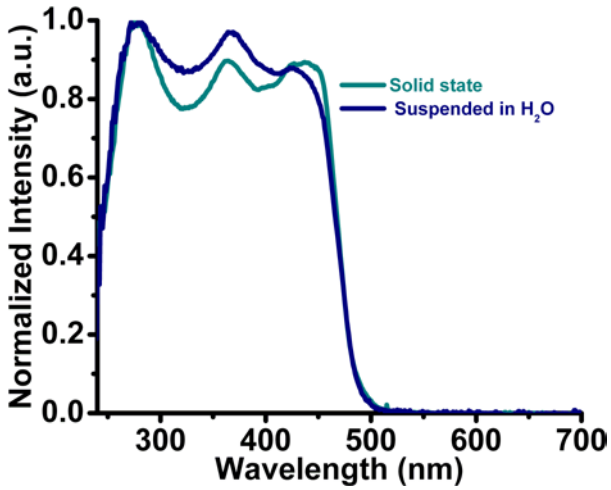

Figure 5.20. Excitation profile for Yb-PVDC-3 nMOF as a dry powder (green; λ_{em} = 980 nm) and while suspended under water (blue; λ_{em} = 980 nm).

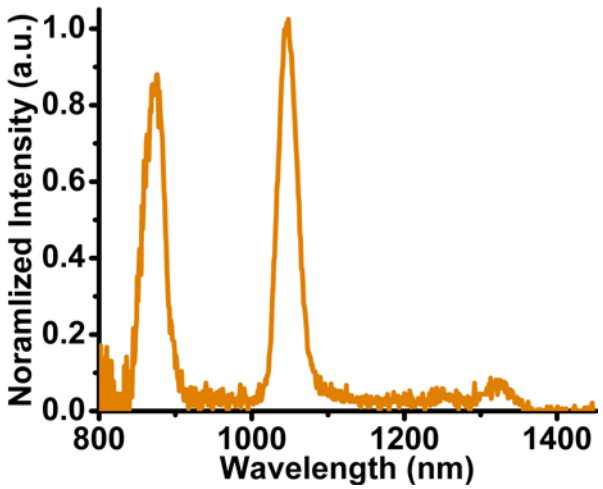

Figure 5.21. Nd-PVDC-3 nMOF emission (875, 1060, and 1330 nm) while suspended in H_2O (λ_{ex} = 450 nm).

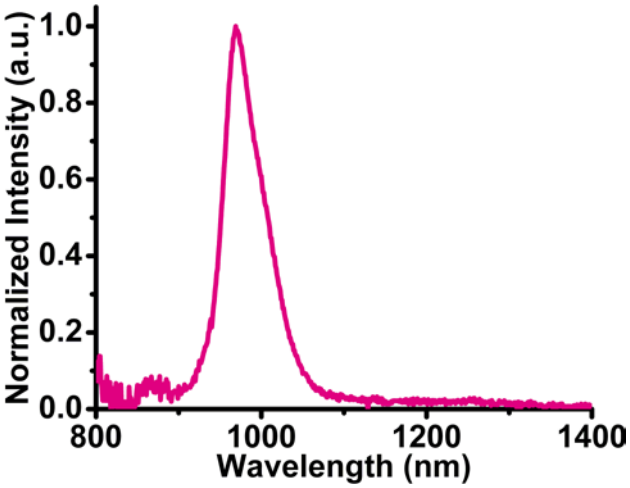

Figure 5.22. Yb-PVDC-3 nMOF emission (980 nm) while suspended in H_2O (λ_{ex}= 450 nm).

SEM was performed on the powder samples. After a reaction time of only 30 minutes, formation of nanorods is observed and elongation of the nanorods is observed after 4 hours, as shown for **Nd-PVDC-3 nMOF**. The particles have a smallest dimension of approximately 50 nm for **Nd-PVDC-3 nMOF** (Figure 5.23), 100 nm for **Yb-PVDC-3 nMOF** (Figure 5.24), and 120 nm for **Er-PVDC-3 nMOF** (Figure 5.25). However, aggregation of particles in solution was evident, which would most likely hinder their mobility across cellular membranes.[5]

Attempts at re-dispersing the material in water or ethanol, even with sonication, proved to be very difficult. Zeta potentials measured on **Nd-PVDC-3 nMOF** samples were inconsistent and close to zero (-4.9, +10.0, +3.7, and -12.8 mv), indicating aggregation.[15]

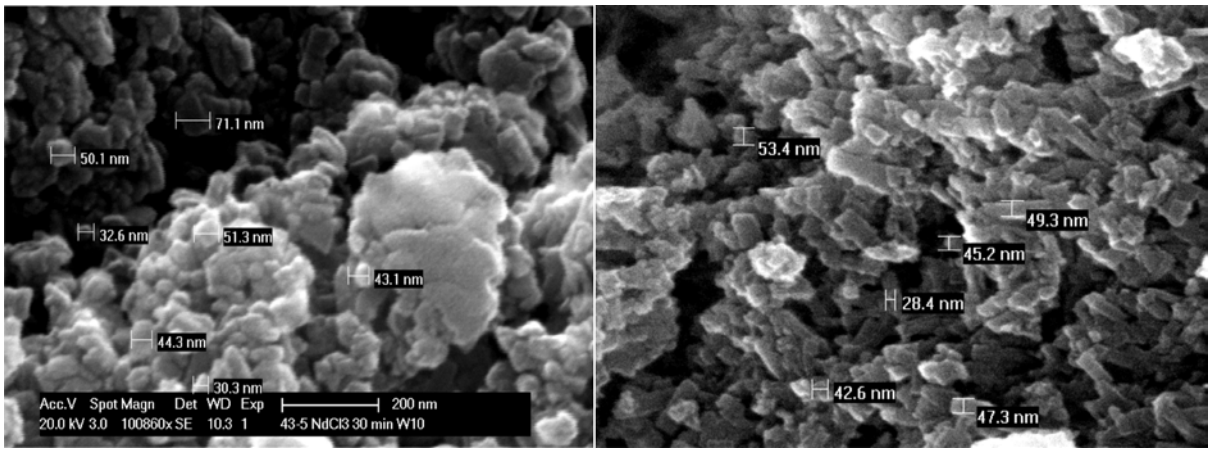

Figure 5.23. SEM images of Nd-PVDC-3 nMOF after 30 min (left) and after 4 hours (right)

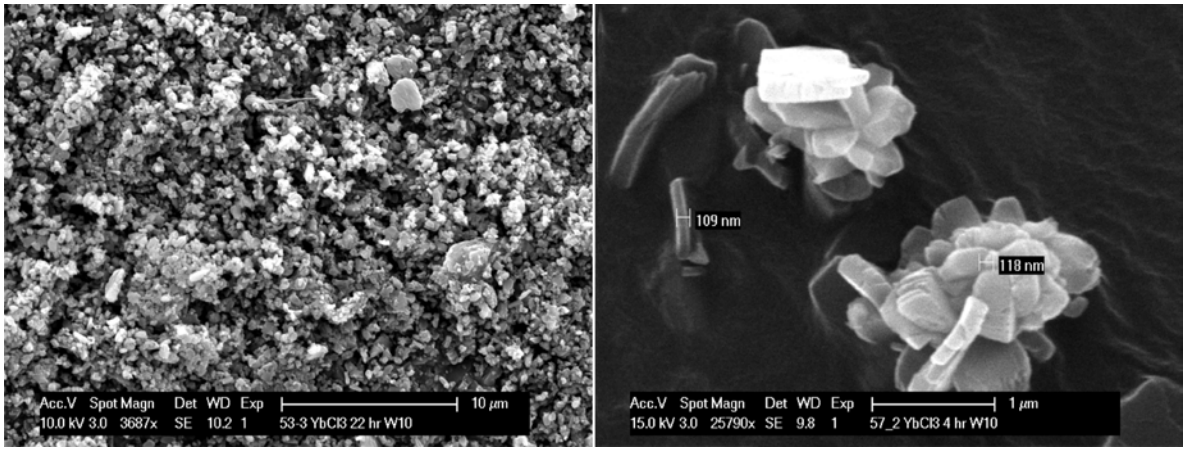

Figure 5.24. SEM images of Yb-PVDC-3 nMOF

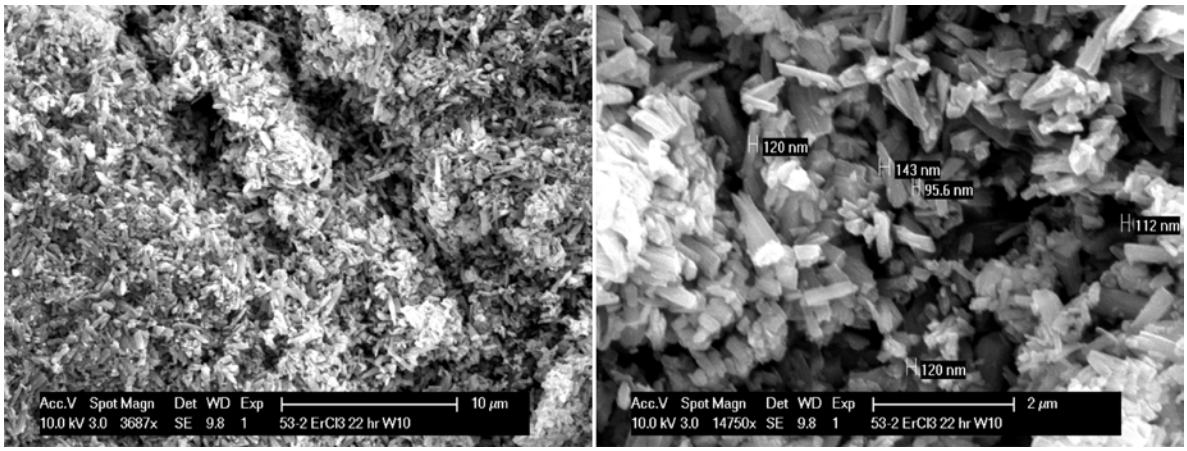

Figure 5.25. SEM images of Er-PVDC-3 nMOF

5.2.3.2 PVP and SiO_2 coated nanoMOFs

A common method to improve aggregation is to coat nanoparticles with a steric stabilizer, such as polyvinyl pyrrolidone (PVP). PVP also helps when coating the material with a silica shell. Silica provides many advantages for nanomaterials such as enhanced water stability, improved dispersity, and facile covalent functionalization. PVP-40 was added into the nanoMOFs suspension after 1 hour of reaction time. The reaction mixture was then stirred for an additional 20 hours to ensure adhesion of the PVP. The particles were easily redispersed in ethanol, and then using an adapted Stöber method, were coated with a SiO_2 shell.[16] SEM images of Nd-PVDC-3 nMOF coated with PVP shows the lack of aggregation (Figure 5.26). However, due to the longer reaction time, **Nd-PVDC-3 nMOF** increased in size to approximately 120 nm. Powder X-ray diffraction confirmed that after coating silica, the **Nd-PVDC-3 nMOF @SiO_2** maintained its crystallinity (Figure 5.27). SEM images of **Yb-PVDC-3 nMOF** still showed some aggregation (Figure 5.28). However, the zeta potential of **Yb-PVDC-3 nMOF@SiO_2** is -35.5 mV, which is indicative of dispersed particles in solution. Powder X-ray diffraction indicates crystallinity of these silica coated particles (Figure 5.29). The synthesis and

characterization of water-stable barcoded Ln-PVDC-3 systems and then their nanocomposite materials are described next.

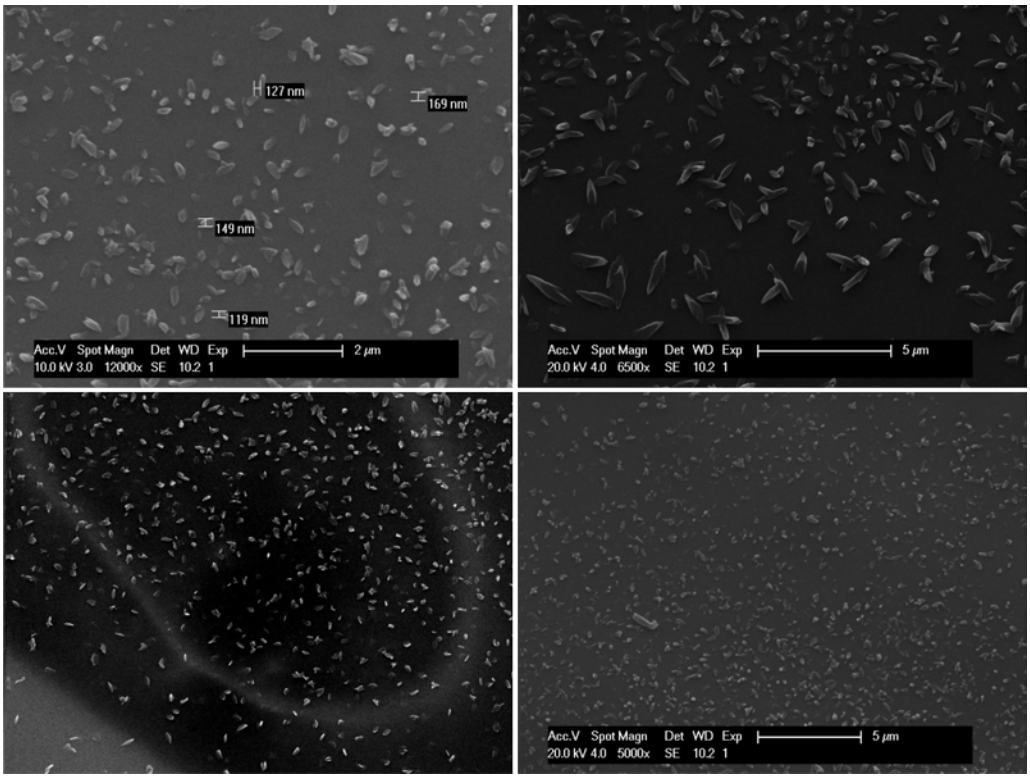

Figure 5.26. SEM images of PVP-Nd-PVDC-3 nMOF

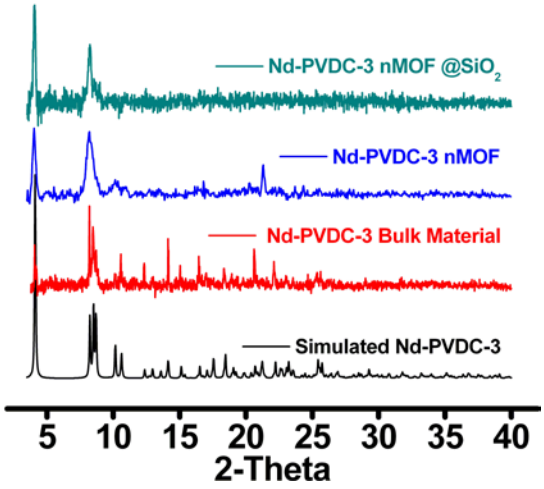

Figure 5.27. Powder X-ray diffraction patterns of Nd-PVDC-3 materials

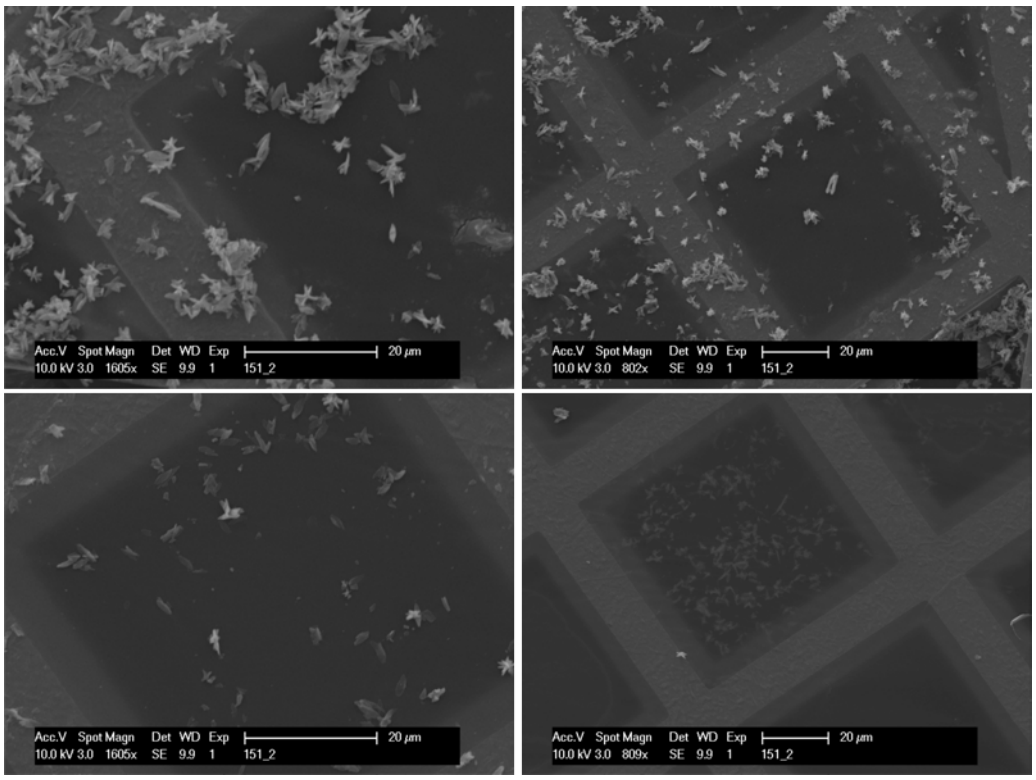

Figure 5.28. SEM images of PVP-Yb-PVDC-3 nMOF

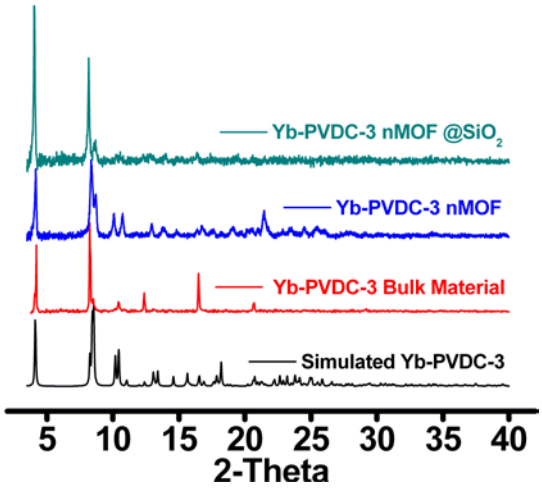

Figure 5.29. Powder X-ray diffraction patterns of Yb-PVDC-3 materials

5.2.4 Barcoded Er_xYb_{1-x}-PVDC-3 and $Er_xNd_yYb_z$-PVDC-3 MOFs

The synthesis of **Yb-PVDC-3** and **Er-PVDC-3** was utilized to synthesize barcoded materials of Er^{3+}/Yb^{3+}, Nd^{3+}/Yb^{3+}, and $Er^{3+}/Nd^{3+}/Yb^{3+}$. The ligand to metal ratio is 4:1 and kept constant for all materials. For example, the synthesis of **$Nd_{0.75}Yb_{0.25}$-PVDC-3** includes 4 mL of **H_2-PVDC** (0.05 M), 0.75 mL of $Nd(NO_3)_3$ (0.05 M) and 0.25 mL $Yb(NO_3)_3$ (0.05 M). This system is an improvement upon Er_xYb_{1-x}-PVDC-1, in which the ligand to metal ratio changed with varying metal ratios.

5.2.4.1 Er_xYb_{1-x}-PVDC-3

To probe the feasibility of making Ln-PVDC-3 into a barcoded system, we first used Er^{3+} and Yb^{3+} because 1) they are close in size so size selectivity should not be an issue, 2) they had previously been incorporated into a barcoded MOF system, and 3) their emission bands do not overlap. Reacting $Er(NO_3)_3 \bullet 5H_2O$, and $Yb(NO_3)_3 \bullet 5H_2O$ with **H_2-PVDC** produced three barcoded MOFs: **$Er_{0.25}Yb_{0.75}$-PVDC-3**, **$Er_{0.50}Yb_{0.50}$-PVDC-3**, and **$Er_{0.75}Yb_{0.25}$-PVDC-3**. Powder X-ray diffraction patterns confirmed that these materials were isostructural with the other Ln-PVDC-3 materials (Figure 5.30). Energy dispersive spectroscopy (EDS) was measured to determine the lanthanide content. These materials, similar to Er_xYb_{1-x}-PVDC-1, demonstrate the ability to produce these materials in a controlled fashion (Table 5.3).

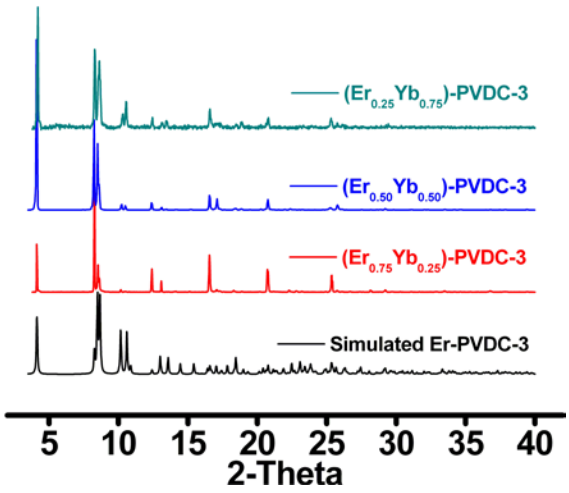

Figure 5.30. Powder X-ray diffractions patterns of barcoded Er_xYb_{1-x}-PVDC bulk MOFs

Table 5.3. Relative Ln^{3+} content of Er_xYb_{1-x}-PVDC-3 bulk materials corresponding to synthetic (theoretical) and as determined by EDS with errors in parentheses

Theoretical %		EDS %	
Er^{3+}	**Yb^{3+}**	**Er^{3+}**	**Yb^{3+}**
75	25	77 (±3)	23 (±3)
50	50	52 (±2)	48 (±2)
25	75	26 (±2)	74 (±2)

Luminescence studies of the materials suspended under DMF showed sensitized Er^{3+} (1530 nm) and Yb^{3+} (980 nm) emission upon excitation at 450 nm. As expected, emission intensities varied with the lanthanide content as shown in plots normalized to the Er^{3+} and Yb^{3+} signals (Figure 5.31). These emission intensities vary linearly, as well (Figure 5.32). The water-exchanged materials were also studied. While the pure **Er-PVDC-3** did not show luminescence while suspended under water, we hypothesized that perhaps erbium emission would be apparent in the barcoded MOF due to energy transfer from the ytterbium. However, upon exciting at 450 nm, no Er^{3+} emission was observed.

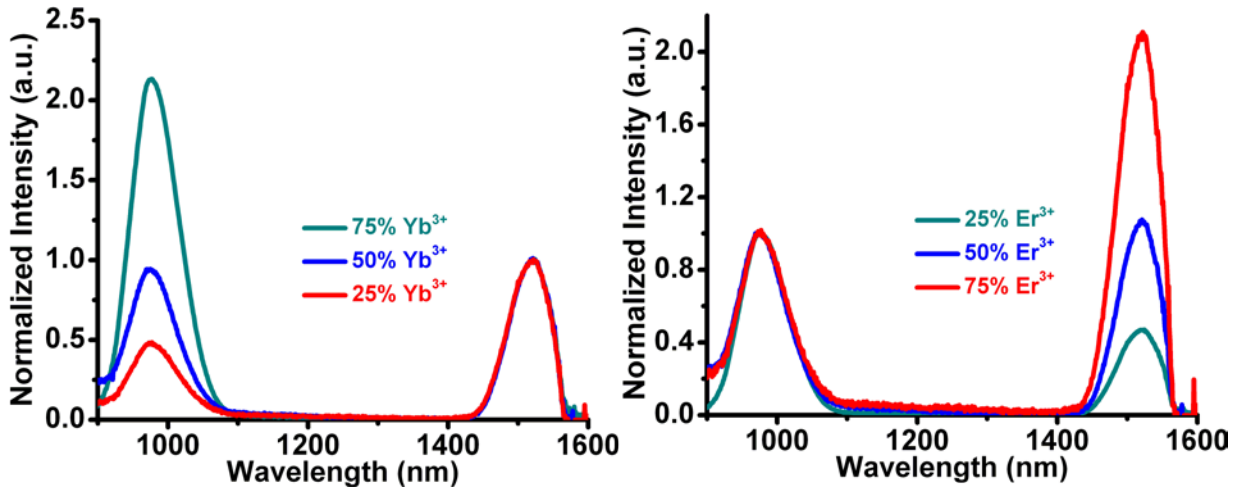

Figure 5.31. Yb^{3+} (980 nm) and Er^{3+} (1025 nm) emission normalized to the erbium signal (left) and the ytterbium signal (right) for Er_xYb_{1-x}-PVDC-3 bulk MOFs (λ_{ex} = 450 nm)

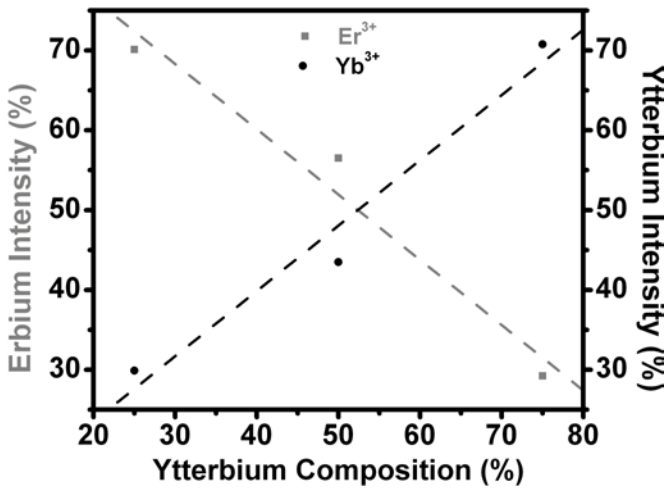

Figure 5.32. Linear relationship between Ln^{3+} composition and emission intensities for Er^{3+}(grey) and Yb^{3+}(black) of Er_xYb_{1-x}-PVDC-3 bulk MOFs

5.2.4.2 $Er_xNd_yYb_z$-PVDC-3 (x + y + z = 1)

The ability to synthesize **Nd-PVDC-3** prompted us to incorporate Nd^{3+} into the Ln-PVDC-3 barcoded system. Inclusion of a third metal expands upon the number of barcoded materials one could synthesize and also permits utilizing one metal as an internal standard and varying the ratio of the other two metals. For example, Er^{3+} could be kept constant at 50 % the total lanthanide content and only the amounts of Nd^{3+} and Yb^{3+} would vary. Erbium's emission would remain the same while the emission intensities for Nd^{3+} and Yb^{3+} would create the barcode. This provides for a more sophisticated system.

$Nd(NO_3)_3 \bullet 6H_2O$, $Er(NO_3)_3 \bullet 5H_2O$, $Yb(NO_3)_3 \bullet 5H_2O$ and **H_2-PVDC** were reacted together to yield **$Er_{0.50}Nd_{0.25}Yb_{0.25}$-PVDC-3**, **$Er_{0.25}Nd_{0.50}Yb_{0.25}$-PVDC-3**, **$Er_{0.25}Nd_{0.25}Yb_{0.50}$-PVDC-3**. Powder X-ray diffraction confirms these are isostructural with the single lanthanide MOFs (Figure 5.33). EDS data shows that the lanthanide content corresponds to the synthetic amounts with no apparent size selectivity was apparent (Table 5.4). Upon 450 nm excitation, photoluminescence of these materials showed characteristic bands for Nd^{3+} (890, 1060, and 1330 nm) Yb^{3+} (980 nm) and Er^{3+} (1530 nm) with varying intensities (Figure 5.34); however, the integrated ratios are still being calculated. Erbium's emission appears very weak, even in the 50% Er^{3+} sample.

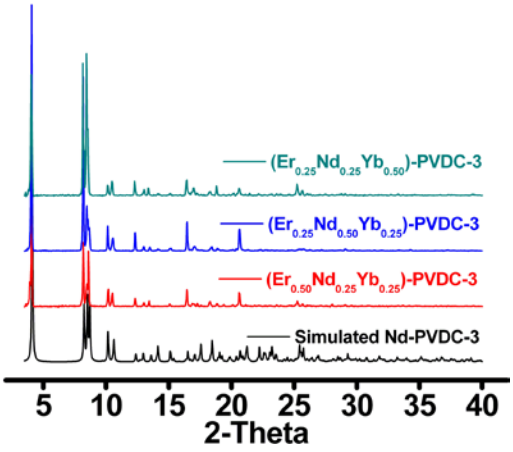

Figure 5.33. Powder X-ray diffraction patterns of $Er_xNd_yYb_z$-PVDC-3 MOFs

Table 5.4. Relative Ln^{3+} content $Er_xNd_yYb_z$-PVDC-3 bulk materials corresponding to synthetic (theoretical) and as determined by EDS with errors in parentheses

Theoretical %			EDS %		
Er^{3+}	Nd^{3+}	Yb^{3+}	Er^{3+}	Nd^{3+}	Yb^{3+}
25	25	50	25 (±1)	29 (±2)	45 (±1)
25	50	25	26 (±1)	54 (±1)	21 (±1)
50	25	25	52 (±2)	28 (±1)	20 (±2)

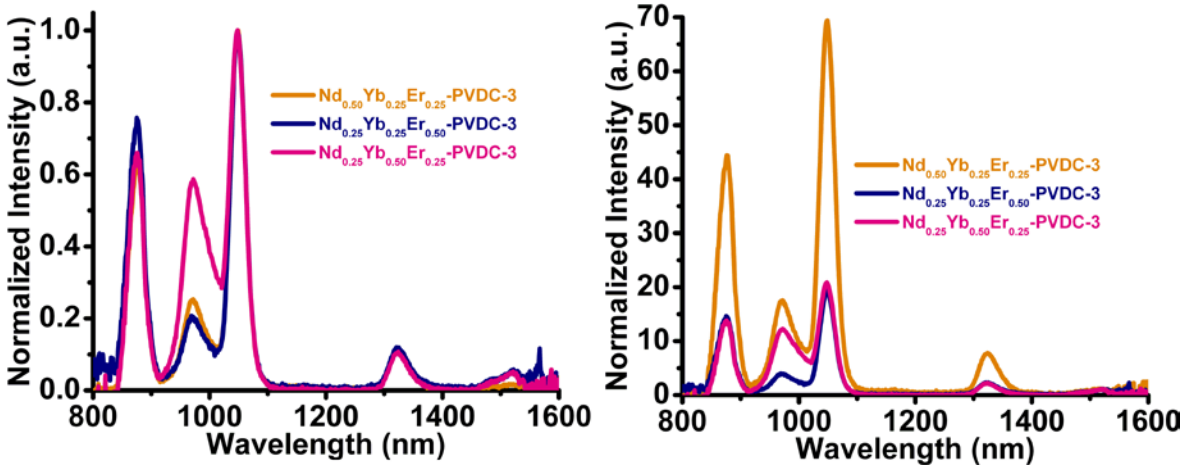

Figure 5.34. $Er_xNd_yYb_z$-PVDC-3 emission while suspended under DMF normalized to Nd^{3+} (1060 nm; left) and Er^{3+} (1530 nm; right) (λ_{ex} = 450 nm)

5.2.5 Barcoded Nd_xYb_{1-x}-PVDC-3

5.2.5.1 Nd_xYb_{1-x}-PVDC-3 bulk materials.

Due to the weak emission of erbium in barcoded **$Er_xNd_yYb_z$-PVDC-3** and its lack of emission while suspended under water, a potential barcoded nanoMOFs system should incorporate Yb^{3+} and Nd^{+}. Barcoded **$Nd_{0.25}Yb_{0.75}$-PVDC-3**, **$Nd_{0.50}Yb_{0.50}$-PVDC-3**, and **$Nd_{0.75}Yb_{0.25}$-PVDC-3** were prepared as confirmed by powder X-ray diffraction studies (Figure 5.35). The TGA data shows the second weight loss ends at approximately 200 °C, indicating two water molecules are coordinated to the lanthanide centers like that of **Er-PVDC-3** and **Yb-PVDC-3** since (Figure 5.36).

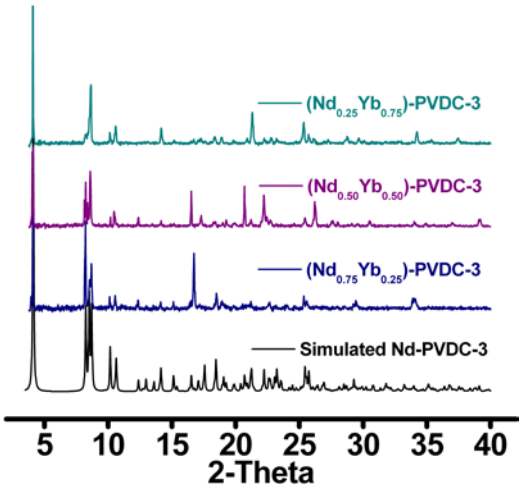

Figure 5.35. Powder X-ray diffraction patterns of Nd_xYb_{1-x}-PVDC-3 bulk materials

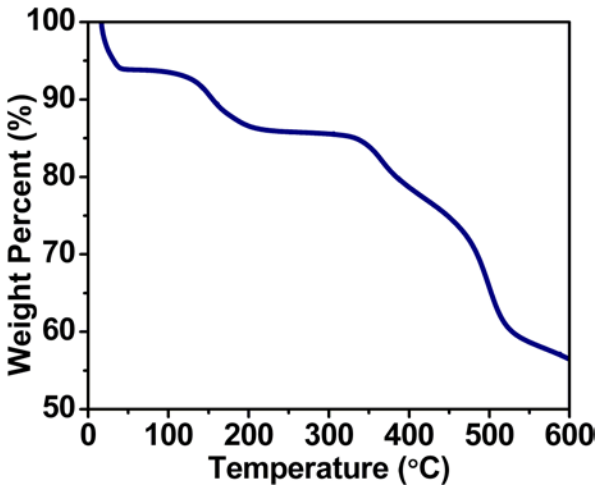

Figure 5.36. TGA of $Nd_{0.25}Yb_{0.75}$-PVDC-3 showing the second weight loss ends at approximately 200 °C, indicating that two water molecules are coordinated to the lanthanide centers.

No lanthanide selectivity was demonstrated, as EDS and ICP confirm the lanthanide content corresponds to the synthetic conditions (Table 5.5). Samples were suspended under DMF and their luminescent properties were examined. Upon 450 nm excitation, both neodymium and ytterbium emission bands were displayed. The varying intensities corresponded to decreasing and increasing amounts of lanthanide as demonstrated in the plots normalized to neodymium, 1060 nm, and ytterbium, 980 nm (Figure 5.37). Moreover, upon integration, these emission intensities vary linearly with lanthanide content (Figure 5.38).

Table 5.5. Relative Ln^{3+} content Nd_xYb_{1-x}-PVDC-3 bulk materials corresponding to synthetic (theoretical) and as determined by EDS and ICP with errors in parentheses

Theoretical %		Measured %			
		EDS		ICP	
Nd^{3+}	**Yb^{3+}**	**Nd^{3+}**	**Yb^{3+}**	**Nd^{3+}**	**Yb^{3+}**
75	25	77 (±4)	23 (±4)	73.86	26.14
50	50	57 (±3)	43 (±3)	49.57	50.43
25	75	30 (±2)	70 (±2)	24.49	75.51

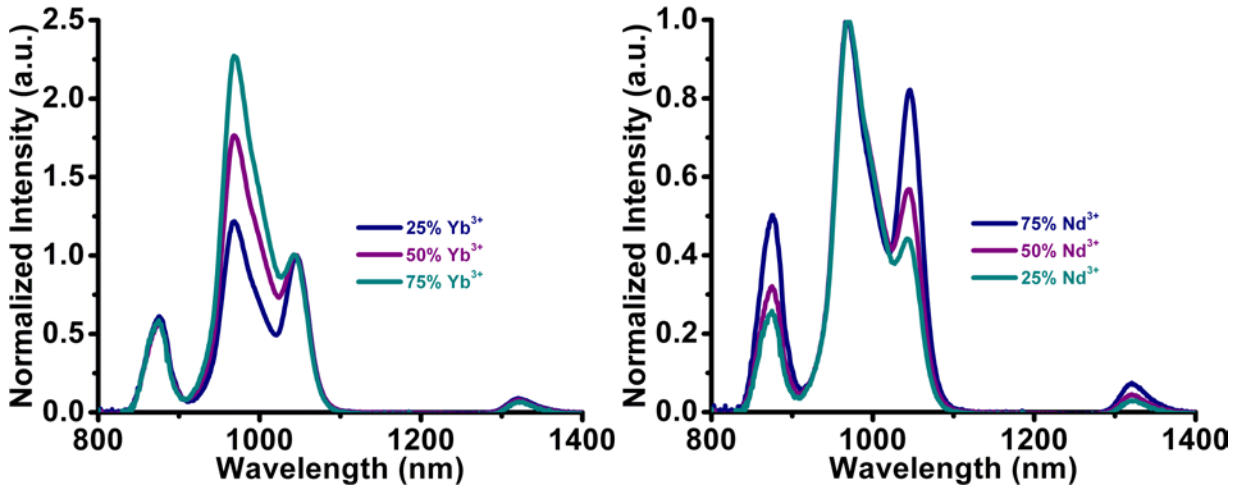

Figure 5.37. Normalized emission of Nd_xYb_{1-x}-PVDC-3 materials (λ_{ex} = 450 nm) while suspended under DMF

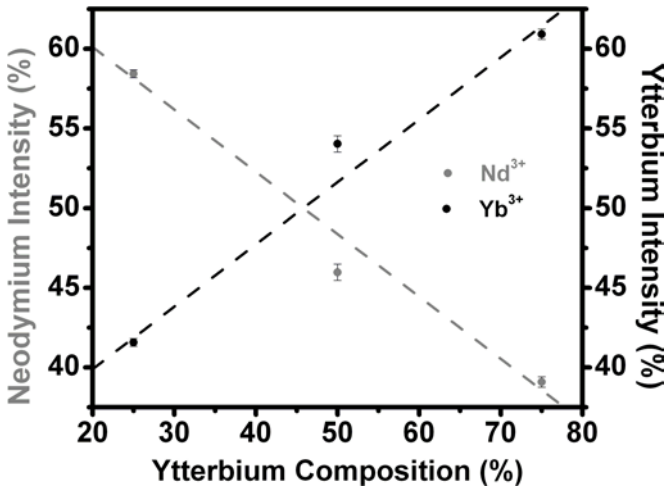

Figure 5.38. Nd^{3+} emission (grey) and Yb^{3+} emission (black) versus Yb^{3+} composition demonstrate a linear relationship for Nd_xYb_{1-x}-PVDC-3 bulk MOFs (λ_{ex} = 450 nm).

5.2.5.2 Nd_xYb_{1-x}-PVDC-3 nanoMOFs

The nanoMOFs of barcoded **Nd_xYb_{1-x}-PVDC-3** materials were synthesized using the reverse microemulsion (W = 10) with $NdCl_3$ and $YbCl_3$. Powder X-ray diffraction shows they are isostructural with the bulk materials (Figure 5.39). While many bi-metallic lanthanide nanoMOFs have been synthesized previously, this is the first example of a barcoded NIR

emitting nanoMOF system. TGA shows the same weight loss pattern as the bulk material with the second weight loss step corresponding to the removal of coordinated water molecules from the lanthanide cations (Figure 5.40). EDS measurements confirm the lanthanide compositions correspond to the synthetic amounts (Table 5.6).

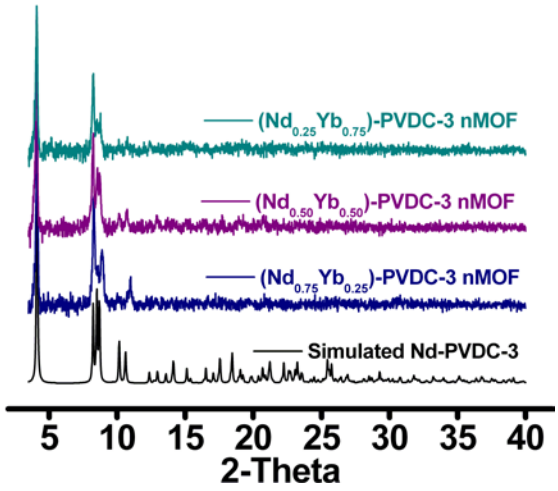

Figure 5.39. Powder X-ray diffraction patterns of Nd_xYb_{1-x}-PVDC-3 nMOF materials

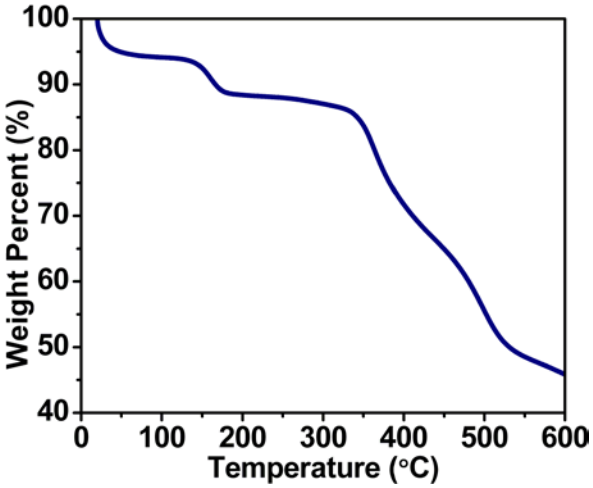

Figure 5.40. TGA of $Nd_{0.50}Yb_{0.50}$-PVDC-3 nMOF.

Table 5.6. Relative Ln^{3+} content of Nd_xYb_{1-x}-PVDC-3 nMOFs corresponding to synthetic (theoretical) and as determined by EDS

Theoretical %		EDS Measured %	
Nd^{3+}	Yb^{3+}	Nd^{3+}	Yb^{3+}
75	25	74	26
50	50	50	50
25	75	30	70

The luminescence properties of the nanoMOFs were explored while the nanoMOFs were suspended under water. Upon excitation at 450 nm, both Yb^{3+} (980 nm) and Nd^{3+} (875, 1060 and 1330 nm) emissions are observed. The varying emission intensities Yb^{3+} and Nd^{3+} correspond to decreasing and increasing amounts of lanthanide as demonstrated in the plots normalized to neodymium, 1060 nm, and ytterbium, 980 nm (Figure 5.41). The emission of Nd^{3+} is much brighter than that of Yb^{3+}, as expected since the quantum yield for **Nd-PVDC-3 nMOF** is larger than that of **Yb-PVDC-3 nMOF**. The plot of integrated emission intensities against Ln^{3+} composition appears linear, demonstrating the potential for this nanoMOF barcode (Figure 5.42).

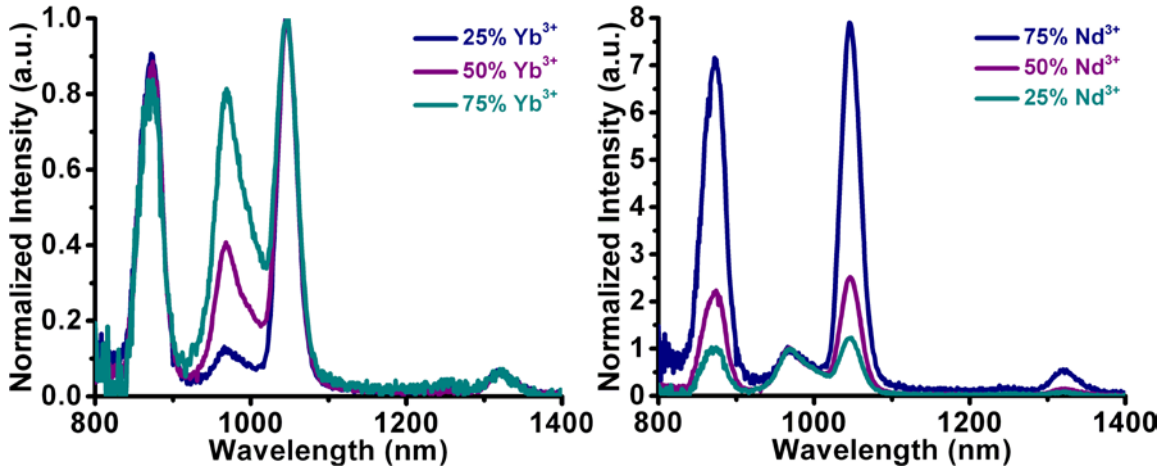

Figure 5.41. NIR emission of barcoded Nd_xYb_{1-x}-PVDC-3 nMOF materials with spectra normalized to neodymium (left; 1060 nm) and ytterbium (right; 980 nm) (λ_{ex} = 450 nm) while suspended under water

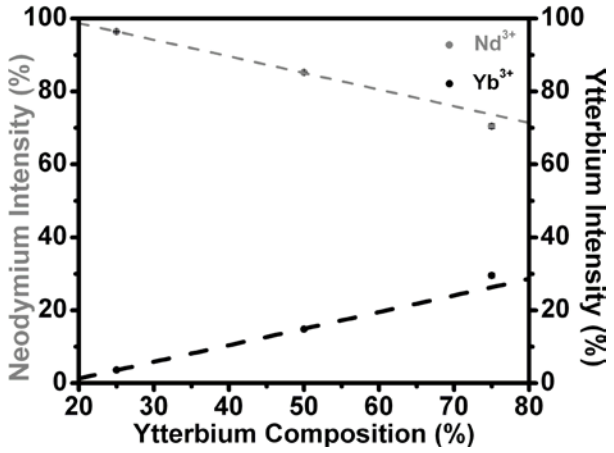

Figure 5.42. Nd^{3+} emission (grey) and Yb^{3+} emission (black) versus Yb^{3+} composition demonstrate a linear relationship for Nd_xYb_{1-x}-PVDC-3 nanoMOFs (λ_{ex} = 450 nm)

Representative SEM images are shown of **$Nd_{0.25}Yb_{0.75}$-PVDC-3 nMOF** (Figure 5.43), **$Nd_{0.50}Yb_{0.50}$-PVDC-3 nMOF** (Figure 5.44), and **$Nd_{0.75}Yb_{0.25}$-PVDC-3 nMOF** (Figure 5.45). Upon coating with silica, the nanoMOFs maintain their crystallinity (Figure 5.46). Zeta potential values of -39.8, -34.8, and -31.3 mV were measured on **$Nd_{0.25}Yb_{0.75}$-PVDC-3 nMOF @SiO_2**, **$Nd_{0.50}Yb_{0.50}$-PVDC-3 nMOF @SiO_2**, and **$Nd_{0.75}Yb_{0.25}$-PVDC-3 nMOF @SiO_2**, respectively. These values indicate that the nanoMOFs are not aggregating while in solution.

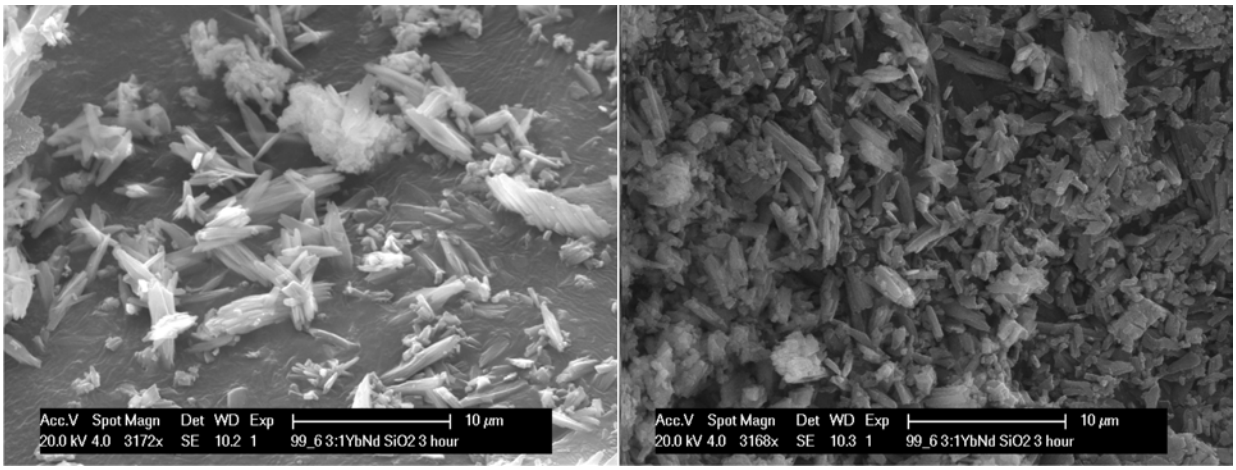

Figure 5.43. SEM images of $Nd_{0.25}Yb_{0.75}$-PVDC-3 nMOF

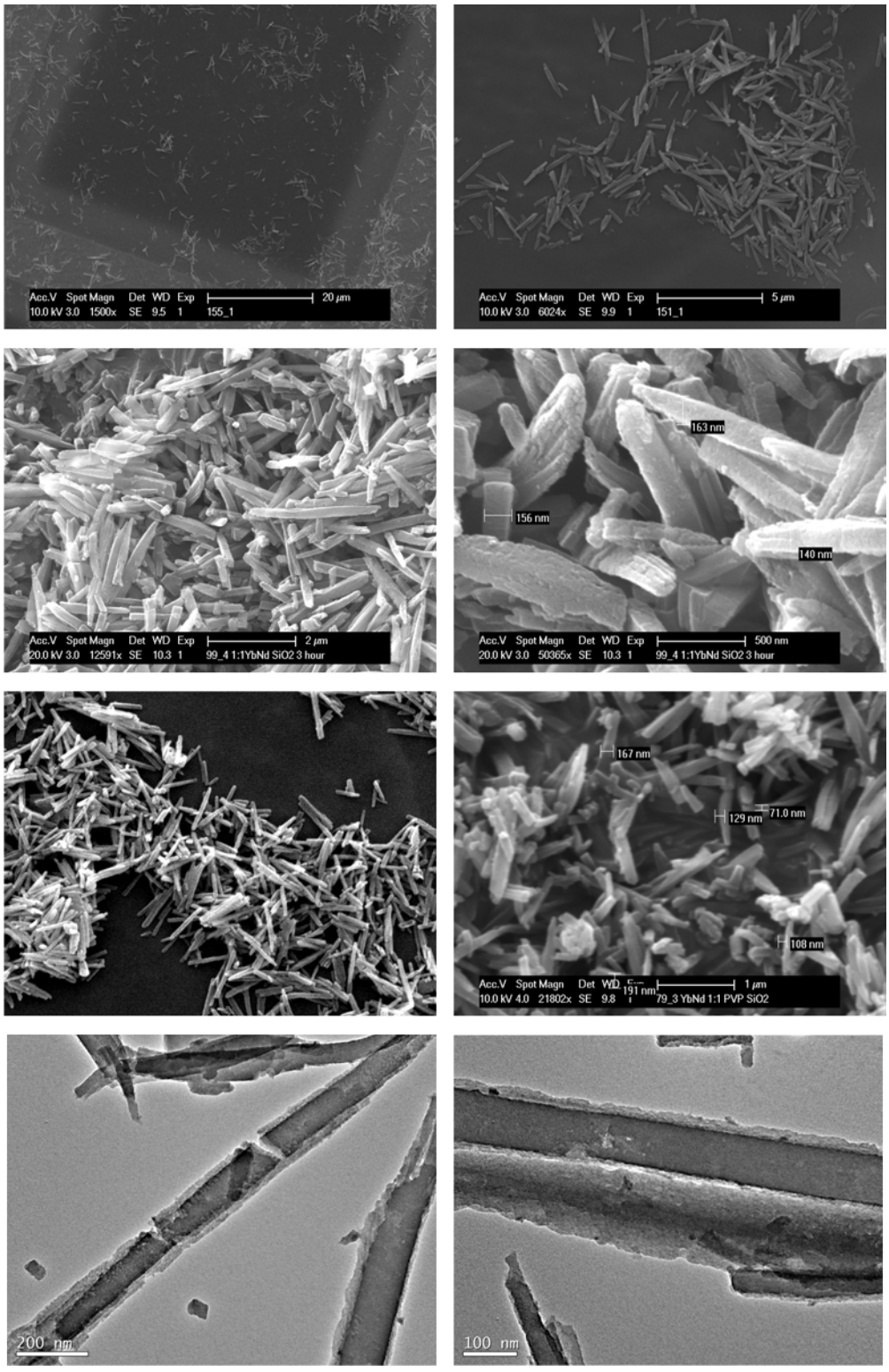

Figure 5.44. SEM images (top 6) and TEM images (bottom 2) of $Nd_{0.50}Yb_{0.50}$-PVDC-3 nMOF

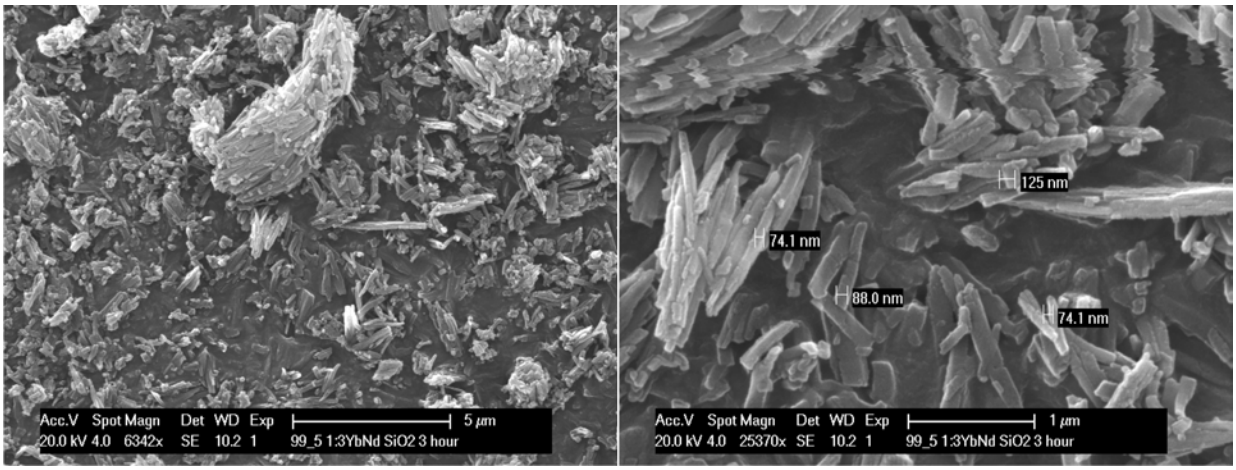

Figure 5.45. SEM images of $Nd_{0.75}Yb_{0.25}$-PVDC-3 nMOF

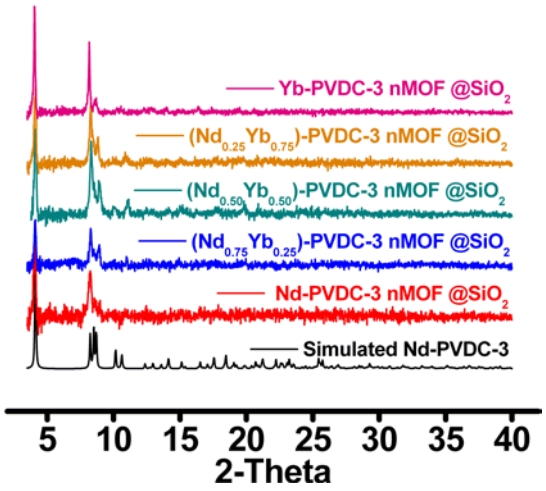

Figure 5.46. Powder X-ray diffraction patterns of Nd_xYb_{1-x}-PVDC-3 nMOFs @SiO_2

5.2.6 Stability studies

Stability studies were done on both **$Nd_{0.50}Yb_{0.50}$-PVDC-3 nMOF** and **$Nd_{0.50}Yb_{0.50}$-PVDC-3 nMOF @SiO_2** in water and in HEPES buffer solution. Materials were suspended in solution for various durations, centrifuged, and supernatant was removed and analyzed by ICP. After one week, the solutions remained clear to the naked eye, unlike the usual green color observed upon

break-down. ICP analysis revealed that very little dissociation had occurred with slightly less dissociation for the materials coated in a silica shell (Table 5.7). Toxicity and intracellular imaging experiments are currently underway. Preliminary studies indicate that the silica-coated nanoparticles show very little toxicity to HeLA cells.

Table 5.7. Stability studies of $Nd_{0.50}Yb_{0.50}$-PVDC-3 nMOF

SiO_2	Solvent	ICP (Ppb)	% dissociation
No	H_2O	0.08	3.58E-04
No	HEPES	0.24	1.07E-03
Yes	H_2O	0.07	3.13E-04
Yes	HEPES	0.18	8.05E-04

5.3 CONCLUSION

In conclusion, we have developed a new family of crystals including: **Ho-PVDC-3**, **Tb-PVDC-3**, **Nd-PVDC-3**, **Er-PVDC-3**, and **Yb-PVDC-3**. These are stable in a variety of solvents including water. No lanthanide luminescence was observed for Ho^{3+} or Tb^{3+}, however, Nd^{3+}, Er^{3+}, Yb^{3+} all exhibited NIR emission via the antenna affect. Moreover, Nd^{3+} and Yb^{3+} are luminescent while suspended under water. Barcoded MOFs were synthesized with Nd^{3+}/Yb^{3+}, Er^{3+}/Yb^{3+}, and $Nd^{3+}/Er^{3+}/Yb^{3+}$. EDS and ICP showed no size selectivity. These materials were synthesized into nanoMOFs via a reverse microemulsion. Nd^{3+} and Yb^{3+} exhibited luminescence as dry powders and while suspended under water. We produced the first example of a barcoded nanoMOFs system, which could have the potential for biological applications. Coating with a steric stabilizer, PVP, decreased the amount of aggregation of the nanoMOFs. The nanoMOFs

are stable in water and HEPES for a minimum of a week, which is longer than necessary for biological experiments.

5.4 EXPERIMENTAL

5.4.1 Reagents

Starting materials and reagents were obtained from commercial sources or synthesized by procedures noted below. **H_2-PVDC** was synthesized as described in Section 2.4.4. Dimethoxybenzene, paraformaldehyde, triphenylphosphine, PVP-40, tetraethyl orthosilicate, methanol, ethanol, NaOMe (0.05 M MeOH), THF, DMF, hexanol, heptane, anhydrous methanol (99.8%), anhydrous toluene (99.8%), anhydrous benzene (99.8%), methylamine (40 wt%), $Er(NO_3)_3 \bullet 5H_2O$, $Nd(NO_3)_3 \bullet 6H_2O$, $Tb(NO_3)_3 \bullet 5H_2O$, $YbCl_3 \bullet 6H_2O$, $ErCl_3 \bullet 6H_2O$, $NdCl_3 \bullet 6H_2O$ were purchased from Aldrich. $Yb(NO_3)_3 \bullet 5H_2O$ was purchased from Strem Chemicals. Dry ethanol was purchased from Pharmco. Glacial acetic acid, ammonium hydroxide (29% weight), and hydrochloric acid were purchased from Fisher. Hyrdobromic acid (33% in AcOH) was purchased from Fluka. Anhydrous chloroform (99.9%), was purchased from Acros. Argon gas was purchased from Valley National. Methyl 4-formylbenzoate was purchased from TCI. KOH and $Ho(NO_3)_3 \cdot 5H_2O$ were purchased from Alfa Aesar. TEM grids (carbon film on 300 square mesh copper grid) were purchased from Electron Microscopy Sciences. All reagents were used as received without further purification.

5.4.2 General procedures

Fourier transform infrared (FT-IR) spectra were measured on a Nicolet Avatar 360 FT-IR spectrometer using KBr pellet samples. Absorptions are described as very strong (vs), strong (s), medium (m), weak (w), shoulder (sh), and broad (br) and stretches (st) are labeled symmetric (sym) or asymmetric (as). Data was analyzed using the Omnic Software Package.

X-ray powder diffraction patterns were collected using a Bruker AXS D_8 Discover powder diffractometer at 40 kV, 40 mA for Cu Kα, (λ = 1.5406 Å) with a scan speed of 0.20 sec/step and a step size of .02018º. The data were analyzed for d-spacing measurements using the EVA program from the Bruker Powder Analysis Software package. The purity and homogeneity of the bulk products were determined by comparison to the simulated and experimental X-ray powder diffraction patterns of Ln-PVDC-3. Solvent exchange of the DMF and H_2O guest molecules in **Ho-PVDC-3**, **Tb-PVDC-3**, **Nd-PVDC-3**, **Er-PVDC-3**, and **Yb-PVDC-3** was performed using anhydrous solvents as follows: 30 min soak in exchange solvent (ES) followed by solvent removal (3X); overnight soak in ES and then solvent removal; 24 h soak in ES and solvent removal; addition of fresh solvent. The elemental microanalysis (CHN) and ICP-OES ($Er^{3+}Yb^{3+}$) were performed by the University of Illinois, Department of Chemistry, Microanalytical Laboratory using an Exeter Analytical CE440. SEM samples were coated with palladium for 100 seconds prior to analysis. Energy-dispersive X-ray analysis (EDX) was measured on a Philips XL 30 SEM equipped with an EDAX CDU leap detector.

5.4.3 Spectroscopic methods

Emission and excitation spectra in the visible range were measured using a Varian Cary Eclipse Fluorescence Spectrophotometer coupled to a personal computer with software provided by Varian. Spectra in the near infrared range were measured using a Jobin Yvon–Horiba Fluorolog-322 spectrofluorimeter equipped with an Electro-Optical Systems, Inc. DSS-IGA020L detector for the NIR domain. Emission and excitation spectra were collected as solid samples under solvent on the JY Horiba Fluorolog-322 Spectrofluorimeter fitted with an integrating sphere developed by Prof. Frédéric Gumy and Prof. Jean-Claude G. Bünzli (Laboratory of Lanthanide Supramolecular Chemistry, École Polytechnique Féderale de Lausanne (EPFL), BCH 1402, CH-1015 Lausanne, Switzerland) as an accessory to the Fluorolog FL3-22 spectrometer (Patent pending) using quartz tube sample holders.

Spectra were corrected according to the following procedure. MOF and control (i.e., solvent) spectra were collected using the same instrumental parameters for both. The MOF and control spectra were each offset to zero at 1600 nm and corrected for variations in the lamp intensity. The control spectrum was subtracted from the MOF spectrum using a scaling factor, *k*. The value of *k* was calculated using the equation $Ck=S$, where *C* represents the control and *S* represents the sample, using the intensities of the respective spectra at 1550 nm (chosen because there is no Ln^{3+} signal in that region). The value of *k* was optimized in order to achieve the flattest baseline. The resulting spectrum was then corrected for the detector.

The spectra had to be deconvoluted in order to integrate the overlapping Nd^{3+} and Yb^{3+} bands. Three Nd^{3+} bands were integrated; the band centered at 880 nm was integrated over the range 820-910 nm, and the band centered at 1330 nm was integrated over the range 1265-1385 nm. The Yb^{3+} band centered at 980 nm overlapped with the Nd^{3+} band centered at 1060 nm, so

the spectrum was deconvoluted using the software supplied by Jobin Yvon-Horiba. The deconvolution function was applied in the region 1018-1100 nm for Nd^{3+} and 910-1018 nm for Yb^{3+}. The resulting deconvoluted spectra were integrated over the entire range.

Relative quantum yield measurements were obtained with the integration sphere on the Jobin Yvon-Horiba Fluorolog-322. For quantum yield measurements in the NIR range with the integration sphere, the analysis is more complex as two different detectors are used, a visible detector to determine the absorbance of light and a NIR detector to monitor the sample emission. It is necessary to measure a relative quantum yield using a sample with a known value. The procedure is described below, using ytterbium or erbium tropolonate, $[Ln(trop)_4]^-$ in DMSO ($\Phi_{Yb} = 1.9x10^{-2}$, $\Phi_{Nd} = 2.1 \times 10^{-3}$)[7] as the reference.

1) To determine the amount of light absorbed by the sample and the reference, emission spectra are collected of the excitation light from the lamp for the sample (ExS) and the reference (ExR), as well as an empty cuvette (ExB). Due to the high intensity of the lamp, neutral density filters are employed and the integrated values are corrected accordingly. The light absorbed is given by: $Ex_B - Ex_S$ and $Ex_B - Ex_R$.

2) Emission spectra are collected in the NIR range of the sample (I_S) and the reference (I_R), as well as of an empty cuvette (I_B). If the sample and reference emission spectra are collected with different excitation or emission wavelengths, two corresponding emission spectra of the empty cuvette will be necessary. To eliminate second order bands, glass cut on filters are placed before the detector. The spectra are corrected for lamp variation, detector response and signal attenuation from the cut on filters. The emission bands for the sample, reference, and blank(s) are integrated, and total emission is given by: $I_S - I_B$ and $I_R - I_B$.

3) Using the known quantum yield of the reference, a scalar ($X_{NIR\text{-}VIS}$) is created to offset the NIR emission spectra to the same scale as the visible spectra of the excitation, as shown in Equation 4.1.

$$(\mathbf{4.1})\ X_{NIR\text{-}VIS} = [\Phi(Ex_B - Ex_R)] / (I_R - I_B)$$

4) The quantum yield (Φ) is calculated using Equation 2.2.

$$(\mathbf{4.2})\ \Phi = [X_{NIR\text{-}VIS}(I_S - I_B)] / (Ex_B - Ex_S)$$

5.4.4 Syntheses of Ln-PVDC-3

5.4.4.1 Synthesis of Ho-PVDC-3

In a glass vial (20 mL), a solution of 4,4'-(1*E*,1'*E*)-2,2'-(2,5-dimethoxy-1,4-phenylene)bis(ethene-2,1-diyl)dibenzoic acid (**H_2-PVDC**) (86.0 mg, 0.20 mmol) in DMF (4.0 mL) was added to a solution of $Ho(NO_3)_3 \bullet 5H_2O$ (66.2 mg, 0.15 mmol) in DMF (1.0 mL) and HNO_3 (0.5 mL, 1M aq) to produce a neon green solution. The vial was capped and placed in a 105 ºC isotemp oven for 12 hours to produce yellow crystalline needles of the product. The crystals were collected, washed with DMF (4 x 5 mL), and air dried.

5.4.4.2 Synthesis of Tb-PVDC-3

In a glass vial (20 mL), a solution of 4,4'-(1*E*,1'*E*)-2,2'-(2,5-dimethoxy-1,4-phenylene)bis(ethene-2,1-diyl)dibenzoic acid (**H_2-PVDC**) (86.0 mg, 0.20 mmol) in DMF (4.0 mL) was added to a solution of $Tb(NO_3)_3 \bullet 5H_2O$ (65.3 mg, 0.15 mmol) in DMF (1.0 mL) and HNO_3(0.75 mL, 1M aq) to produce a neon green solution. The vial was capped and placed in a

105 ºC isotemp oven for 12 hours to produce yellow crystalline needles of the product. The crystals were collected, washed with DMF (4 x 5 mL), and air dried.

5.4.4.3 Synthesis of Nd-PVDC-3

In a glass vial (20 mL), a solution of 4,4'-(1*E*,1'*E*)-2,2'-(2,5-dimethoxy-1,4-phenylene)bis(ethene-2,1-diyl)dibenzoic acid (**H_2-PVDC**) (86.0 mg, 0.20 mmol) in DMF (4.0 mL) was added to a solution of $Nd(NO_3)_3 \bullet 6H_2O$ (21.9 mg, 0.05 mmol) in DMF (1.0 mL) and water(0.50 mL) to produce a neon green solution. The vial was capped and placed in a 105 ºC isotemp oven for 12 hours to produce yellow crystalline needles of the product. The crystals were collected, washed with DMF (4 x 5 mL), and air dried (29.5 mg, 62.1%).

EA. Calcd. (%) for$Nd_1(C_{26}H_{20}O_6)_{1.5}(H_2O)_1(DMF)_1 \bullet (DMF)_{0.5}(H_2O)_2$: C, 54.96; H, 4.93; N, 2.21. Found: C, 54.79; H, 4.45; N, 2.39.EA. Calcd. (%) for the water exchange product, $Nd_1(C_{26}H_{20}O_6)_{1.5}(H_2O)_2 \bullet (DMF)_{0.25}(H_2O)_3$: C, 52.70; H, 4.42; N, 0.39. Found: C, 53.15; H, 4.00; N, 0.35. FT-IR (KBr 4000-700 cm^{-1}): 3442 (br), 3056 (w), 2998 (w), 2932 (w), 2830 (w), 1658 (DMF C=O, m), 1581 (m), 1537 (m), 1407 (COO^-, vs), 1338 (w), 1261 (w), 1210 (s), 1181 (m), 1102 (w), 1043 (s), 965 (m), 859 (w), 780 (trans C=C-H, s), 710 cm^{-1}(w).

5.4.4.4 Synthesis of Er-PVDC-3

In a glass vial (20 mL), a solution of 4,4'-(1*E*,1'*E*)-2,2'-(2,5-dimethoxy-1,4-phenylene)bis(ethene-2,1-diyl)dibenzoic acid (**H_2-PVDC**) (86.0 mg, 0.20 mmol) in DMF (4.0 mL) was added to a solution of $Er(NO_3)_3 \bullet 5H_2O$ (22.2 mg, 0.05 mmol) in DMF (1.0 mL) and HNO_3(1 mL, 1M aq) to produce a neon green solution. The vial was capped and placed in a 105

ºC isotemp oven for 12 hours to produce yellow crystalline needles of the product. The crystals were collected, washed with DMF (4 x 5 mL), and air dried (33.4 mg, 69.9%).

EA Calcd. (%) for $Er_1(C_{26}H_{20}O_6)_{1.5}(H_2O)_2\bullet(DMF)_{1.5}$: C, 54.68; H, 4.69; N, 2.20. Found: C, 55.25; H, 4.26; N, 2.69. EA. Calcd. (%) for the water exchange product, $Er_1(C_{26}H_{20}O_6)_{1.5}(H_2O)_2\bullet(DMF)_{0.5}(H_2O)_2$: C, 52.96; H, 4.55; N, 0.76. Found: C, 53.06; H, 4.00; N, 0.73.FT-IR (KBr 4000-700 cm^{-1}): 3430 (br), 3050 (w), 2997 (w), 2932 (w), 2831 (w), 1670 (DMF C=O, m), 1584 (m), 1540 (m), 1413 (COO^-, vs), 1338 (w), 1260 (w), 1211 (s), 1181 (m), 1105 (w), 1044 (s), 964 (m), 860 (w), 780 (trans C=C-H, s), 710 cm^{-1}(w).

5.4.4.5 Synthesis of Yb-PVDC-3

In a glass vial (20 mL), a solution of 4,4'-(1*E*,1'*E*)-2,2'-(2,5-dimethoxy-1,4-phenylene)bis(ethene-2,1-diyl)dibenzoic acid (H_2-PVDC) (86.0 mg, 0.20 mmol) in DMF (4.0 mL) was added to a solution of $Yb(NO_3)_3\bullet5H_2O$ (22.5 mg, 0.05 mmol) in DMF (1.0 mL) and HNO_3(1 mL, 1M aq) to produce a neon green solution. The vial was capped and placed in a 105 ºC isotemp oven for 12 hours to produce yellow crystalline needles of the product. The crystals were collected, washed with DMF (4 x 5 mL), and air dried(29.7 mg, 61.8%).

EA Calcd. (%) for $Yb_1(C_{26}H_{20}O_6)_{1.5}(H_2O)_2\bullet(DMF)_{1.5}$: C, 54.35; H, 4.67; N, 2.19. Found: C, 54.87; H, 4.22; N, 2.51. EA. Calcd. (%) for the water exchange product, $Yb_1(C_{26}H_{20}O_6)_{1.5}(H_2O)_2\bullet(DMF)_{0.25}(H_2O)_{2.25}$: C, 52.43; H, 4.46; N, 0.38. Found: C, 52.12; H, 3.68; N, 0.30. FT-IR (KBr 4000-700 cm^{-1}): 3424 (br), 3054 (w), 2998 (w), 2936 (w), 2830 (w), 1665 (DMF C=O, m), 1601 (m), 1544 (m), 1413 (COO^-, vs), 1338 (w), 1260 (w), 1211 (s), 1181 (m), 1108 (w), 1044 (s), 965 (m), 861 (w), 779 (trans C=C-H, s), 709 cm^{-1}(w).

5.4.5 Syntheses of Nd_xYb_{1-x}-PVC-3

5.4.5.1 Synthesis of $Nd_{0.25}Yb_{0.75}$-PVDC-3

In a glass vial (20 mL), a solution of 4,4'-(1*E*,1'*E*)-2,2'-(2,5-dimethoxy-1,4-phenylene)bis(ethene-2,1-diyl)dibenzoic acid (**H_2-PVDC**) (86.0 mg, 0.20 mmol) in DMF (4.0 mL) was added to a solution of $Yb(NO_3)_3 \bullet 5H_2O$ (16.7 mg, 0.0375 mmol) and $Nd(NO_3)_3 \bullet 6H_2O$ (5.5 mg, 0.0125 mmol) in DMF (1.0 mL) and HNO_3 (1 mL, 1M aq) to produce a neon green solution. The vial was capped and placed in a 105 ºC isotemp oven for 12 hours to produce yellow crystalline needles of the product. The crystals were collected, washed with DMF (4 x 5 mL), and air dried(33.4 mg, 69.4%).

EA Calcd. (%) for $Nd_{0.25}Yb_{0.75}(C_{26}H_{20}O_6)_{1.5}(H_2O)_2 \bullet (DMF)_{1.5}(H_2O)_{0.5}$: C, 54.25; H, 4.76; N, 2.18. Found: C, 54.18; H, 4.28; N, 2.21. FT-IR (KBr 4000-700 cm^{-1}): 3407 (br), 2929 (w), 1657 (DMF C=O, m), 1583 (m), 1542 (s), 1492 (w), 1409 (COO^-, vs), 1260 (w), 1210 (s), 1180 (m), 1103 (w), 1043 (s), 964 (m), 860 (w), 779 (trans C=C-H, s), 709 cm^{-1}(w). ICP analysis showed that the molar ratio of Nd^{3+}/Yb^{3+} was 4.20/12.95 corresponding to 24.5 % Nd^{3+} of the total metal composition.

5.4.5.2 Synthesis of $Nd_{0.50}Yb_{0.50}$-PVDC-3

In a glass vial (20 mL), a solution of 4,4'-(1*E*,1'*E*)-2,2'-(2,5-dimethoxy-1,4-phenylene)bis(ethene-2,1-diyl)dibenzoic acid (**H_2-PVDC**) (86.0 mg, 0.20 mmol) in DMF (4.0 mL) was added to a solution of $Yb(NO_3)_3 \bullet 5H_2O$ (11.3 mg, 0.025 mmol) and $Nd(NO_3)_3 \bullet 6H_2O$ (10.9 mg, 0.025 mmol) in DMF (1.0 mL) and HNO_3 (1 mL, 1M aq) to produce a neon green solution. The vial was capped and placed in a 105 ºC isotemp oven for 12 hours to produce

yellow crystalline needles of the product. The crystals were collected, washed with DMF (4 x 5 mL), and air dried (32.1 mg, 67.2%).

EA Calcd. (%) for $Nd_{0.50}Yb_{0.50}(C_{26}H_{20}O_6)_{1.5}(H_2O)_2 \bullet (DMF)_{1.5}(H_2O)_{0.5}$: C, 54.65; H, 4.80; N, 2.20. Found: C, 54.62; H, 4.37; N, 2.41. FT-IR (KBr 4000-700 cm^{-1}): 3416 (br), 2928 (w), 1655 (DMF C=O, m), 1583 (m), 1541 (m), 1409 (COO^-, vs), 1258 (w), 1210 (s), 1180 (m), 1100 (w), 1043 (s), 965 (m), 860 (w), 780 (trans C=C-H, s), 710 cm^{-1}(w). ICP analysis showed that the molar ratio of Nd^{3+}/Yb^{3+} was 8.10/8.24 corresponding to 49.6 % Nd^{3+} of the total metal composition.

5.4.5.3 Synthesis of $Nd_{0.75}Yb_{0.25}$-PVDC-3

In a glass vial (20 mL), a solution of 4,4'-(1*E*,1'*E*)-2,2'-(2,5-dimethoxy-1,4-phenylene)bis(ethene-2,1-diyl)dibenzoic acid (H_2-PVDC) (86.0 mg, 0.20 mmol) in DMF (4.0 mL) was added to a solution of $Yb(NO_3)_3 \bullet 5H_2O$ (5.6 mg, 0.0125 mmol) and $Nd(NO_3)_3 \bullet 6H_2O$ (16.4 mg, 0.0375 mmol) in DMF (1.0 mL) and HNO_3 (1 mL, 1M aq) to produce a neon green solution. The vial was capped and placed in a 105 ºC isotemp oven for 12 hours to produce yellow crystalline needles of the product. The crystals were collected, washed with DMF (4 x 5 mL), and air dried(23.6 mg, 49.7%).

EA Calcd. (%) for $Nd_{0.75}Yb_{0.25}(C_{26}H_{20}O_6)_{1.5}(H_2O)_2 \bullet (DMF)_{1.5}(H_2O)_{0.5}$: C, 55.07; H, 4.83; N, 2.21. Found: C, 55.35; H, 4.45; N, 2.45. FT-IR (KBr 4000-700 cm^{-1}): 3734 (w), 3450 (br), 2360 (w), 1655 (DMF C=O, m), 1582 (m), 1536 (m), 1409 (COO^-, vs), 1210 (s), 1041 (s), 965 (m), 780 (trans C=C-H, s), 710 cm^{-1}(w). ICP analysis showed that the molar ratio of Nd^{3+}/Yb^{3+} was 11.33/4.01 corresponding to 73.9 % Nd^{3+} of the total metal composition.

5.4.6 Syntheses of Er_xYb_{1-x}-PVDC-3 ($Er_{0.25}Yb_{0.75}$-PVDC-3, $Er_{0.50}Yb_{0.50}$-PVDC-3, $Er_{0.75}Yb_{0.25}$-PVDC-3) and $Er_xNd_yYb_z$-PVDC-3 ($Er_{0.50}Nd_{0.25}Yb_{0.25}$-PVDC-3, $Er_{0.25}Nd_{0.50}Yb_{0.25}$-PVDC-3, $Er_{0.25}Nd_{0.25}Yb_{0.50}$-PVDC-3)

In a glass vial (20 mL), a solution of 4,4'-(1*E*,1'*E*)-2,2'-(2,5-dimethoxy-1,4-phenylene)bis(ethene-2,1-diyl)dibenzoic acid (**H_2-PVDC**) (86.0 mg, 0.20 mmol) in DMF (4.0 mL) was added to a solution of $Yb(NO_3)_3 \bullet 5H_2O$ (11.25 mg, 0.025 mmol) and $Er(NO_3)_3 \bullet 5H_2O$ (11.1 mg, 0.025 mmol) in DMF (1.0 mL) and HNO_3(1 mL, 1M aq) to produce a neon green solution. The vial was capped and placed in a 105 ºC isotemp oven for 12 hours to produce yellow crystalline needles of the product. The crystals were collected, washed with DMF (4 x 5 mL), and air dried (19.6 mg, 40.5%).

EA Calcd. (%) for $Er_{0.50}Yb_{0.50}(C_{26}H_{20}O_6)_{1.5}(H_2O)_2 \bullet (DMF)_{1.5}(H_2O)_{1.5}$: C, 53.02; H, 4.86; N, 213. Found: C, 53.02; H, 4.15; N, 2.34. FT-IR (KBr 4000-700 cm^{-1}): 3402 (br), 3058 (w), 2939 (w), 2835 (w), 1665 (DMF C=O, m), 1602 (m), 1544 (m), 1412 (COO^-, vs), 1260 (w), 1211 (s), 1182 (m), 1104 (w), 1044 (s), 1014 (w), 967 (m), 864 (w), 780 cm^{-1} (trans C=C-H, s).

5.4.7 NanoMOF synthesis

The methylammonium salt of the phenylene vinylene dicarboxylic acid (**H_2-PVDC**) was prepared by dissolving **H_2-PVDC** in methylamine (40 wt % in water) and isolating the salt by solvent removal under reduced pressure. The salt was then dissolved in a known amount of water to make a 0.05 M solution. The $LnCl_3$ salt solution was prepared by dissolving the metal in a known amount of water to make a 0.05 M solution. A 0.05 M surfactant mixture was made from combining cetyltrimethylammonium bromide (CTAB) (9.112 g, 0.025 mol), 1-hexanol

(38.318 g, 0.375 mol), and heptane (296.36 g, 2.957 mol) and stirring for at least 30 minutes. Two microemulsions were prepared by combining each aqueous reactant to an aliquot of the surfactant mixture corresponding to a particular *w* value ([H2O]/[CTAB]). Both solutions were stirred for at least 10 minutes until they were visibly clear. The metal solution was then added to the ligand solution, where upon the solution became cloudy indicating nanoparticle formation. A yellow powder was isolated via centrifugation and washed with ethanol.

5.4.7.1 Synthesis of Nd-PVDC-3 nMOF

A *w* = 10 mixture was prepared by addition of $NdCl_3 \bullet 6H_2O$ (225μL, 0.05 M H_2O) to a flask containing the cationic CTAB mixture (25 mL, 0.05 M Heptane/Hexanol) and stirred for at least 10 minutes until clear. PVDC-$(NH_2CH_3)_2$ (225 μL, 0.05 M H_2O) was added to another flask containing the cationic CTAB mixture (25 mL, 0.05 M Heptane/Hexanol) and stirred for at least 10 minutes until clear. The Nd^{3+} solution was then added to the PVDC mixture and stirred at room temperature. The yellow powder product was isolated via centrifugation 4000 RPM for 30 min followed by washing with ethanol.

5.4.7.2 Synthesis of Yb-PVDC-3 nMOF

A *w* = 10 mixture was prepared by addition of $YbCl_3 \bullet 6H_2O$ (225 μL, 0.05 M H_2O) to a flask containing the cationic CTAB mixture (25 mL, 0.05 M Heptane/Hexanol) and stirred for at least 10 minutes until clear. PVDC-$(NH_2CH_3)_2$ (225 μL, 0.05 M H_2O) was added to another flask containing the cationic CTAB mixture (25 mL, 0.05 M Heptane/Hexanol) and stirred for at least 10 minutes until clear. The Yb^{3+} solution was then added to the PVDC mixture and stirred

at room temperature. The yellow powder product was isolated via centrifugation 4000 RPM for 30 min followed by washing with ethanol.

5.4.7.3 Synthesis of Er-PVDC-3 nMOF

A w = 10 mixture was prepared by addition of $ErCl_3 \bullet 6H_2O$ (225 μL, 0.05 M H_2O) to a flask containing the cationic CTAB mixture (25 mL, 0.05 M Heptane/Hexanol) and stirred for at least 10 minutes until clear. PVDC-$(CH_3NH_2)_2$ (225 μL, 0.05 M H_2O) was added to another flask containing the cationic CTAB mixture (25 mL, 0.05 M Heptane/Hexanol) and stirred for at least 10 minutes until clear. The Er^{3+} solution was then added to the PVDC mixture and stirred at room temperature. The yellow powder product was isolated via centrifugation 4000 RPM for 30 min followed by washing with ethanol.

5.4.7.4 Synthesis of $Nd_{0.25}Yb_{0.75}$-PVDC-3 nMOF

A w = 10 mixture was prepared by addition of $NdCl_3 \bullet 6H_2O$ (56 μL, 0.05 M H_2O) and $YbCl_3 \bullet 6H_2O$ (168 μL, 0.05 M H_2O) to a flask containing the cationic CTAB mixture (25 mL, 0.05 M Heptane/Hexanol) and stirred for at least 10 minutes until clear. PVDC-$(NH_2CH_3)_2$ (225 μL, 0.05 M H_2O) was added to another flask containing the cationic CTAB mixture (25 mL, 0.05 M Heptane/Hexanol) and stirred for at least 10 minutes until clear. The Nd^{3+} solution was then added to the PVDC mixture and stirred at room temperature. The yellow powder product was isolated via centrifugation 4000 RPM for 30 min followed by washing with ethanol.

5.4.7.5 Synthesis of $Nd_{0.50}Yb_{0.50}$-PVDC-3 nMOF

A *w* = 10 mixture was prepared by addition of $NdCl_3 \bullet 6H_2O$ (112 μL, 0.05 M H_2O) and $YbCl_3 \bullet 6H_2O$ (112 μL, 0.05 M H_2O) to a flask containing the cationic CTAB mixture (25 mL, 0.05 M Heptane/Hexanol) and stirred for at least 10 minutes until clear. PVDC-$(NH_2CH_3)_2$ (225 μL, 0.05 M H_2O) was added to another flask containing the cationic CTAB mixture (25 mL, 0.05 M Heptane/Hexanol) and stirred for at least 10 minutes until clear. The Nd^{3+} solution was then added to the PVDC mixture and stirred at room temperature. The yellow powder product was isolated via centrifugation 4000 RPM for 30 min followed by washing with ethanol.

5.4.7.6 Synthesis of $Nd_{0.75}Yb_{0.25}$-PVDC-3 nMOF

A *w* = 10 mixture was prepared by addition of $NdCl_3 \bullet 6H_2O$ (168 μL, 0.05 M H_2O) and $YbCl_3 \bullet 6H_2O$ (56 μL, 0.05 M H_2O) to a flask containing the cationic CTAB mixture (25 mL, 0.05 M Heptane/Hexanol) and stirred for at least 10 minutes until clear. PVDC-$(NH_2CH_3)_2$ (225 μL, 0.05 M H_2O) was added to another flask containing the cationic CTAB mixture (25 mL, 0.05 M Heptane/Hexanol) and stirred for at least 10 minutes until clear. The Nd^{3+} solution was then added to the PVDC mixture and stirred at room temperature. The yellow powder product was isolated via centrifugation 4000 RPM for 30 min followed by washing with ethanol.

5.4.8 PVP-NanoMOF synthesis

NanoMOFs were coated with 40K-PVP to prevent their aggregation. PVP-40 (1 mL, 0.005 M H_2O) was added to the nanoMOF solution after 1 hour of reaction time. The solution was stirred at room temperature for an additional 20-24 hours to allow for complete adhesion. A

yellow powder was then isolate via centrifugation and subsequently washed with ethanol. These materials were then coated with silica.

5.4.9 NanoMOF @SiO_2 synthesis

The PVP coated nanoMOFs were further encapsulated with silica in order to improve their stability. PVP coated nanoMOFs were reacted with 100% ethanol (5mL/mg), NH_4OH (4% v/v), and tetraethyl orthosilicate (TEOS) (5μl/mg) and stirred for 2 hours. After 2 hours, additional TEOS (5μl/mg) was added and the reaction mixture was stirred for 2 more horus for a total reaction time of 4 hours. The mixture was then centrifuged (1 hr x 4000 RPM), followed by removal of supernatant and washing with 100% ethanol. EDS measurements gave a 2.1 Si/Ln ratio corresponding to an approximate 10 nm SiO_2 shell as measured from a TEM image.

5.4.10 Single crystal X-ray diffraction studies

Single crystal XRD data was collected on a Bruker SMART APEX II CCD-based X-ray diffractometer equipped with a normal focus Mo-target X-ray tube (λ =0.71073 Å) operated at 2000 W power (45 kV and 35 mA). The detector was placed at a distance of 6.002 cm from the crystal. 1800 frames were collected with a scan width of 0.3° in omega and phi with an exposure time of 10 s/frame. Crystals were mounted in a glass loop and placed in a cold N_2 stream for data collection and the X-ray intensities were measured at 203K for **Ho-PVDC-3**, **Tb-PVDC-3**, **Nd-PVDC-3**, **Er-PVDC-3**, and **Yb-PVDC-3**.

5.4.10.1 Single crystal X-ray diffraction studies for Ho-PVDC-3

An X-ray crystal structure was determined for $C_{45}H_{43}N_2O_{12}Ho$, **Ho-PVDC-3**, using a single crystal on a Bruker Smart Apex CCD diffractometer with graphite-monochromated MoK_α (λ = 0.71073 Å) radiation. The parameters used during the collection of diffraction data are summarized in Appendix A. The crystal was mounted in a glass loop and placed in a cold N_2 stream (203 K) for data collection.

Unit-cell determination required the use of the Bruker AXS Cell_now program. Out of 999 reflections input to Cell_now, 827 reflections were used to determine the triclinic cell listed in Appendix A. A minor twin component, rotated 179.5 degrees about the reciprocal axis 0,0,1 was made up of 152 of the remaining reflections. The major component's unit-cell and orientation matrix was used in the integration, solution and refinement.

Unit-cell parameters and lack of systematic absences indicated **Ho-PVDC-3** crystallized in triclinic space groups P 1 or P-1; centrosymmetric P-1 was chosen based on E-values and the successful solution and refinement of the structure. Unit-cell dimensions were derived from the least-squares fit of the angular settings of 4752 reflections. Data were corrected for absorption using the Bruker program Sadabs. The structure was solved via direct methods, which located Ho and most of the remaining non-hydrogen atoms. Remaining non-hydrogen atoms were gradually found from several subsequent difference Fourier syntheses. All non-hydrogen atoms except for O(10) were refined anisotropically. Idealized atom positions were calculated for all hydrogen atoms (d-(C_{methyl}-H) = 0.96 Å, d-C_{phenyl}-H)=0.93 Å, U = 1.2$Uiso$ of attached carbon).

The final Fourier map shows very large maximum peak of 10.27 $e^-/Å^{-3}$ which is close to Ho, and is likely due to contributions from Ho in the minor twin component. All computer

programs used in the data collection and refinements are contained in the Bruker program packages SMART (vers. 5.625), SAINT (vers. 6.22), and SHELXTL (vers. 6.14) and Platon.

5.4.10.2 Single crystal X-ray diffraction studies for Tb-PVDC-3

An X-ray crystal structure was determined for $C_{45}H_{43}N_2O_{12}Tb$, **Tb-PVDC-3**, using a single crystal on a Bruker Smart Apex CCD diffractometer with graphite-monochromated MoK_α (λ = 0.71073 Å) radiation. The parameters used during the collection of diffraction data are summarized in Appendix A. The crystal was mounted in a glass loop and placed in a cold N_2 stream (203 K) for data collection.

Unit-cell determination required the use of the Bruker AXS Cell_now program. Out of 999 reflections input to Cell_now, 646 reflections were used to determine the triclinic cell listed in Appendix A. A minor twin component, rotated 179.5 degrees about the reciprocal axis 0,1,0 was made up of 353 of the remaining reflections. The major component's unit-cell and orientation matrix was used in the integration, solution and refinement.

Unit-cell parameters and lack of systematic absences indicated **Tb-PVDC-3** crystallized in triclinic space groups P 1 or P-1; centrosymmetric P-1 was chosen based on E-values and the successful solution and refinement of the structure. Unit-cell dimensions were derived from the least-squares fit of the angular settings of 3580 reflections. Data were corrected for absorption using the Bruker program Sadabs. The structure was solved via direct methods, which located Tb^{3+} and most of the remaining non-hydrogen atoms. Remaining non-hydrogen atoms were gradually found from several subsequent difference Fourier syntheses. All non-hydrogen atoms were refined anisotropically. Idealized atom positions were calculated for all hydrogen atoms (*d*-(C_{methyl}-H) = 0.96 Å, d-C_{phenyl}-H)=0.93 Å, U = 1.2*Uiso* of attached carbon).

The final Fourier map shows very large maximum peak of 8.99 $e^-/Å^{-3}$ which is close to Tb, and is likely due to contributions from Tb in the minor twin component. All computer programs used in the data collection and refinements are contained in the Bruker program packages SMART (vers. 5.625), SAINT (vers. 6.22), and SHELXTL (vers. 6.14) and Platon.

5.4.10.3 Single crystal X-ray diffraction studies for Nd-PVDC-3

An X-ray crystal structure was determined for $C_{45}H_{43}N_2O_{12}Nd$, **Nd-PVDC-3**, using a single crystal on a Bruker Smart Apex CCD diffractometer with graphite-monochromated MoK_α (λ = 0.71073 Å) radiation. The parameters used during the collection of diffraction data are summarized in Appendix A. The crystal was mounted in a glass loop and placed in a cold N_2 stream (203 K) for data collection.

Unit-cell parameters and lack of systematic absences indicated **Nd-PVDC-3** crystallized in triclinic space groups P 1 or P-1; centrosymmetric P-1 was chosen based on E-values and the successful solution and refinement of the structure. Unit-cell dimensions were derived from the least-squares fit of the angular settings of 2782 reflections. Data were corrected for absorption using the Bruker program Sadabs. The structure was solved via direct methods, which located Nd^{3+} and most of the remaining non-hydrogen atoms. Remaining non-hydrogen atoms were gradually found from several subsequent difference Fourier syntheses. All non-hydrogen atoms were refined anisotropically. Idealized atom positions were calculated for all hydrogen atoms (*d*-(C_{methyl}-H) = 0.96 Å, d-C_{phenyl}-H)=0.93 Å, U = 1.2*Uiso* of attached carbon).

The final Fourier map shows very large maximum peak of 4.34 $e^-/Å^{-3}$ which is close to Nd. All computer programs used in the data collection and refinements are contained in the Bruker program packages SMART (vers. 5.625), SAINT (vers. 6.22), and SHELXTL (vers. 6.14) and Platon.

5.4.10.4 Single crystal X-ray diffraction studies for Er-PVDC-3

An X-ray crystal structure was determined for $C_{42}H_{36}NO_{12}Er$, **Er-PVDC-3**, using a single crystal on a Bruker Smart Apex CCD diffractometer with graphite-monochromated MoK_α (⌊= 0.71073 Å) radiation. The parameters used during the collection of diffraction data are summarized in Appendix A. The crystal was mounted in a glass loop and placed in a cold N_2 stream (203 K) for data collection. Crystals of this compound diffracted very weakly, with no observed intensities beyond $2\theta=46^\circ$.

Unit-cell parameters and lack of systematic absences indicated **Er-PVDC-3** crystallized in triclinic space groups P 1 or P-1; centrosymmetric P-1 was chosen based on E-values and the successful solution and refinement of the structure. Unit-cell dimensions were derived from the least-squares fit of the angular settings of 2782 reflections. Data were corrected for absorption using the Bruker program Sadabs. The structure was solved via isomorphous replacement; coordinates for the metal and PVDC carbon atoms were obtained from the isomorphous **Yb-PVDC-3** structure. Remaining non-hydrogen atoms were gradually found from several subsequent difference Fourier syntheses. Non-hydrogen atoms (except for C(8), C(9), C(10), C(13), C(15), C(16), C(17), O(6), O(8), and O(10)) were refined anisotropically, although an isotropic restraint (SHELXTL ISOR command) was used on all non-hydrogens to avoid going non-positive definite. Idealized atom positions were calculated for all hydrogen atoms (*d*-(Cmethyl-H) = 0.96 Å, d-Cphenyl-H)=0.93 Å, $U = 1.2Uiso$ of attached carbon).

The final Fourier map shows a very large maximum peaks (max. 3.56 $e^-/Å^{-3)}$ which is close to Er^{3+} and not chemically significant. All computer programs used in the data collection and refinements are contained in the Bruker program packages SMART (vers. 5.625), SAINT (vers. 6.22), and SHELXTL (vers. 6.14) and Platon.

5.4.10.5 Single crystal X-ray diffraction studies for Yb-PVDC-3

An X-ray crystal structure was determined for $C_{42}H_{36}NO_{12}Yb$, **Yb-PVDC-3**, using a single crystal on a Bruker Smart Apex CCD diffractometer with graphite-monochromated MoK_α (λ = 0.71073 Å) radiation. The parameters used during the collection of diffraction data are summarized in Appendix A. The crystal was mounted in a glass loop and placed in a cold N_2 stream (203 K) for data collection.

Unit-cell parameters and lack of systematic absences indicated **Yb-PVDC-3** crystallized in triclinic space groups P 1 or P-1; centrosymmetric P-1 was chosen based on E-values and the successful solution and refinement of the structure. Unit-cell dimensions were derived from the least-squares fit of the angular settings of 2782 reflections. Data were corrected for absorption using the Bruker program Sadabs. The structure was solved via direct methods, which located Yb and most of the remaining non-hydrogen atoms. Yb is found to be disordered over at least two sites. The two Yb sites are occupied at 57% and 43%Remaining non-hydrogen atoms were gradually found from several subsequent difference Fourier syntheses. All non-hydrogen atoms were refined anisotropically excepting O(6), O(12), N, C(24), C(27), C(37), C(38), C(40), C(41), and C(42). Idealized atom positions were calculated for all hydrogen atoms (*d*-(C_{methyl}-H) = 0.96 Å, d-C_{phenyl}-H)=0.93 Å, *U* = 1.2*Uiso* of attached carbon). The coordinated DMF seen in other Ln-PVDC isomorphs could not be resolved in this structure, probably because of overlap with the disordered Yb sites.

The final Fourier map shows very large maximum peak of 2.29 $e^-/Å^{-3}$ which is close to the Yb sites. All computer programs used in the data collection and refinements are contained in the Bruker program packages SMART (vers. 5.625), SAINT (vers. 6.22), and SHELXTL (vers. 6.14) and Platon.

5.5 REFERENCES

(1) An, J.; Geib, S. J.; Rosi, N. L. *J. Am. Chem. Soc.* **2009**, *131*, 8376.
(2) Sarma, D.; Ramanujachary, K. V.; Lofland, S. E.; Magdaleno, T.; Natarajan, S. *Inorg. Chem.* **2009**, *48*, 11660.
(3) Horcajada, P.; Chalati, T.; Serre, C.; Gillet, B.; Sebrie, C.; Baati, T.; Eubank, J. F.; Heurtaux, D.; Clayette, P.; Kreuz, C.; Chang, J. S.; Hwang, Y. K.; Marsaud, V.; Bories, P. N.; Cynober, L.; Gil, S.; Ferey, G.; Couvreur, P.; Gref, R. *Nat. Mater.* **2010**, *9*, 172.
(4) Taylor-Pashow, K. M. L.; Della Rocca, J.; Xie, Z. G.; Tran, S.; Lin, W. B. *J. Am. Chem. Soc.* **2009**, *131*, 14261.
(5) Zhang, S. L.; Li, J.; Lykotrafitis, G.; Bao, G.; Suresh, S. *Adv. Mater.* **2009**, *21*, 419.
(6) Bünzli, J.-C. G.; Piguet, C. *Chem. Soc. Rev.* **2005**, *34*, 1048.
(7) Lee, J. A.; Mardyani, S.; Hung, A.; Rhee, A.; Klostranec, J.; Mu, Y.; Li, D.; Chan, W. C. W. *Adv. Mater.* **2007**, *19*, 3113.
(8) Beeby, A.; Clarkson, I. M.; Dickins, R. S.; Faulkner, S.; Parker, D.; Royle, L.; de Sousa, A. S.; Williams, J. A. G.; Woods, M. *J. Chem. Soc., Perkin Trans. 2* **1999**, 493.
(9) Horrocks, W. D.; Sudnick, D. R. *J. Am. Chem. Soc.* **1979**, *101*, 334.
(10) Bünzli, J.-C. G. In *Lanthanide Probes in Life, Chemical and Earth Sciences*; Bünzli, J.-C. G., Choppin, G. R., Eds.; Elsevier Science Publishers B.V.: Amsterdam, 1989, p 219.
(11) Mahmood, U.; Weissleder, R. *Molecular Cancer Therapeutics* **2003**, *2*, 489.
(12) Ballou, B.; Ernst, L. A.; Waggoner, A. S. *Curr. Med. Chem.* **2005**, *12*, 795.
(13) Weissleder, R.; Tung, C.-H.; Mahmood, U.; Bogdanov, A., Jr. *Nat. Biotechnol.* **1999**, *17*, 375.
(14) Imbert, D.; Comby, S.; Chauvin, A. S.; Bunzli, J. C. G. *Chem. Commun.* **2005**, 1432.
(15) Bagwe, R. P.; Hilliard, L. R.; Tan, W. H. *Langmuir* **2006**, *22*, 4357.
(16) Graf, C.; Vossen, D. L. J.; Imhof, A.; van Blaaderen, A. *Langmuir* **2003**, *19*, 6693.

6.0 A MESOPOROUS MACROCYCLE WITH PERMANENT POROSITY

This chapter utilizes another ligand, **H-TPY**, that was originally chosen because it sensitizes four visible emitting lanthanide cations: Dy^{3+}, Eu^{3+}, Sm^{3+}, and Tb^{3+}. However, a former member of the Rosi Group, Dr. Chunlong Chen, synthesized a crystal with **H-TPY** and Zn^{2+}. I optimized the synthesis of this material and fully characterized it, discovering that it exhibits unique gas adsorption properties.

6.1 INTRODUCTION

Macrocyclic species can potentially stack together in three dimensions to yield 3-D assembled structures. If the 'empty' centers of the macrocycles align along a specific crystallographic direction, the 3-D assembled structures can exhibit 1-D channels. However, few of these structures are permanently porous;[1-4] that is, upon removal of solvent guest molecules via heating/activation prior to gas adsorption measurements, the macrocycles may shift with respect to one another within the material, resulting in destruction or occlusion of the channels. In order for assembled macrocyclic structures to maintain their porosity, the interactions between neighboring macorcycles within the structures must be sufficiently strong so that the 3-D structure is maintained during the solvent evacuation process prior to gas adsorption. Here, we present a strategy for assembling macrocycles into permanently porous 3-D crystalline structures that relies on strong inter-macrocycle π-π interactions. We demonstrate that this material exhibits permanent mesoporosity. To our knowledge, this is the first mesoporous macrocycle-based crystalline material. We created a highly stable mesoporous macrocycle by utilizing a large aromatic ligand, terpyridal benzoic acid (**H-TPY,** Figure 6.1).[5]

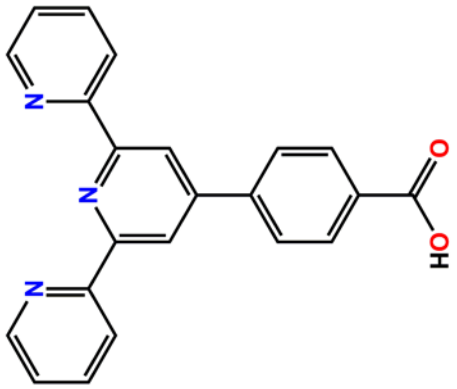

Figure 6.1. H-TPY

6.2 RESULTS AND DISCUSSION

6.2.1 Syntheses of hexameric Zn-TPY-1 and Zn-TPY-2

A solvothermal reaction between **H-TPY** and $Zn(CF_3COO)_2 \bullet 2H_2O$ in the presence of trifluoracetic acid and water was heated at 85 °C to yield yellow hexagonal crystals of the macrocycle **Zn-TPY-1** (Figure 6.2), formulated $Zn_6(C_{22}H_{14}N_3O_2)_6(CF_3COO)_6 \bullet (DMF)_7(H_2O)_9$. Single crystal X-ray diffraction revealed that **Zn-TPY-1** crystallizes in the space group R-3. The hexameric macrocycle contains six Zn^{2+} metals bridged by six TPY molecules. Each zinc is bound by three nitrogen atoms of one TPY molecule, a carboxylate oxygen of another TPY molecule, and an oxygen from the trifluoroacetate (Figure 6.4). Electron density was found in the cavity approximately 3.0 Å from the TPY carbonyl oxygen, indicating it is most likely hydrogen bonding to a water molecule. The macrocycles stack in an a-b-c fashion (Figure 6.5) in order to gain stability through π-π stacking of TPY molecules of alternating layers (3.7 Å) (Figure 6.4). These layers form 1-D channels that measure approximately 25.9 Å in diameter.

The large 1-D pores prompted us to characterize the material for gas sorption studies. We expected **Zn-TPY-1** to have high selectivity for CO_2 over N_2, because of the polarity of the CF_3 groups.[6] In order to fully investigate the impact of the CF_3 groups, we also prepared the non-fluorinated version of **Zn-TPY-1**. Replacing zinc trifluoracetate with zinc acetate and trifluoracetic with acetic acid yielded **Zn-TPY-2**, formulated $Zn_6(C_{22}H_{14}N_3O_2)_6(CH_3COO)_6 \bullet (DMF)_2(H_2O)_{33}$. Powder X-ray diffraction indicates both **Zn-TPY-1** and **Zn-TPY-2** are stable in acetonitrile (Figure 6.6 and 6.7).

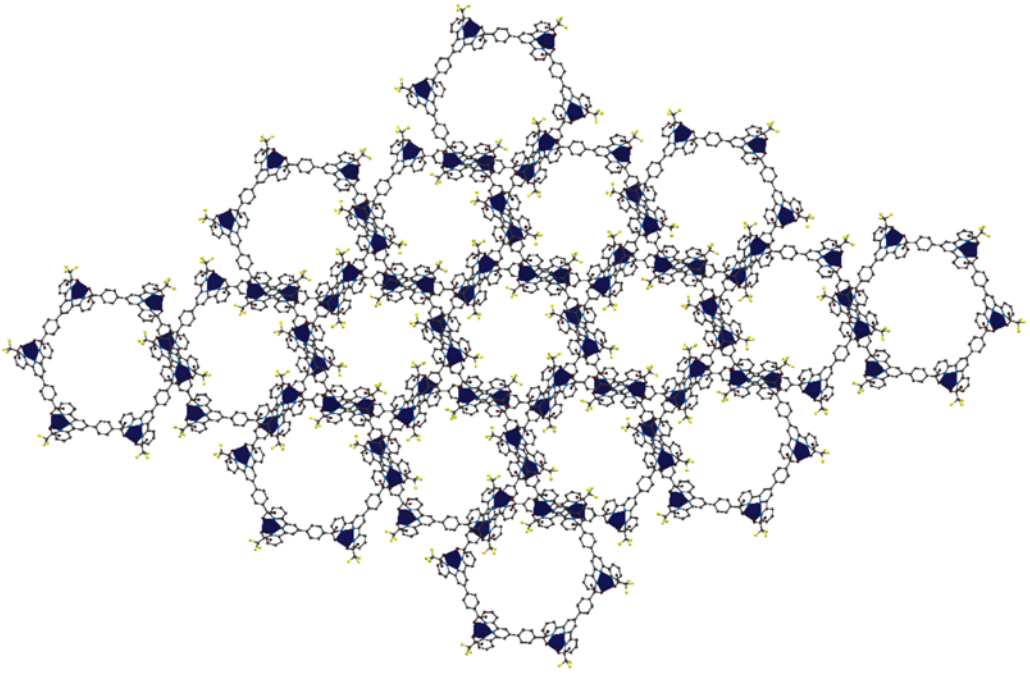

Figure 6.2. Perspective view of Zn-TPY-1 down the *c* crystallographic direction with Zn^{2+} shown as polyhedra (C, grey; O, red; N, blue; F, yellow; Zn^{2+}, royal blue)

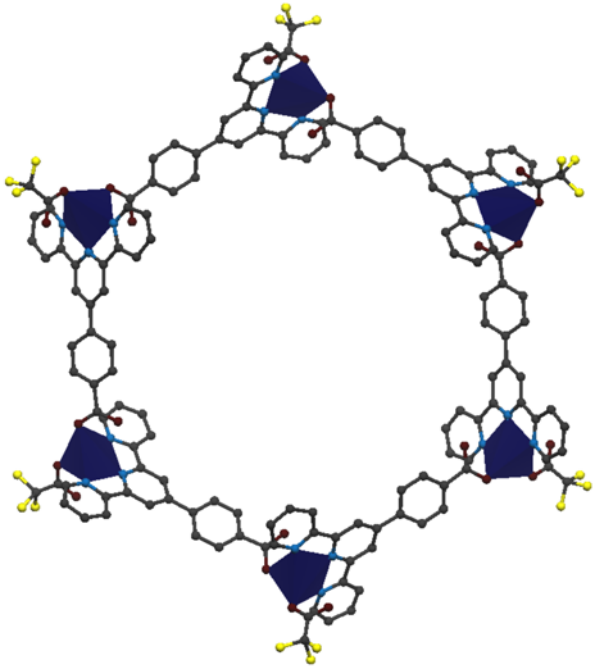

Figure 6.3. Marocycle with Zn^{2+} shown as polyhedra (C, grey; O, red; N, blue; F, yellow; Zn^{2+}, royal blue)

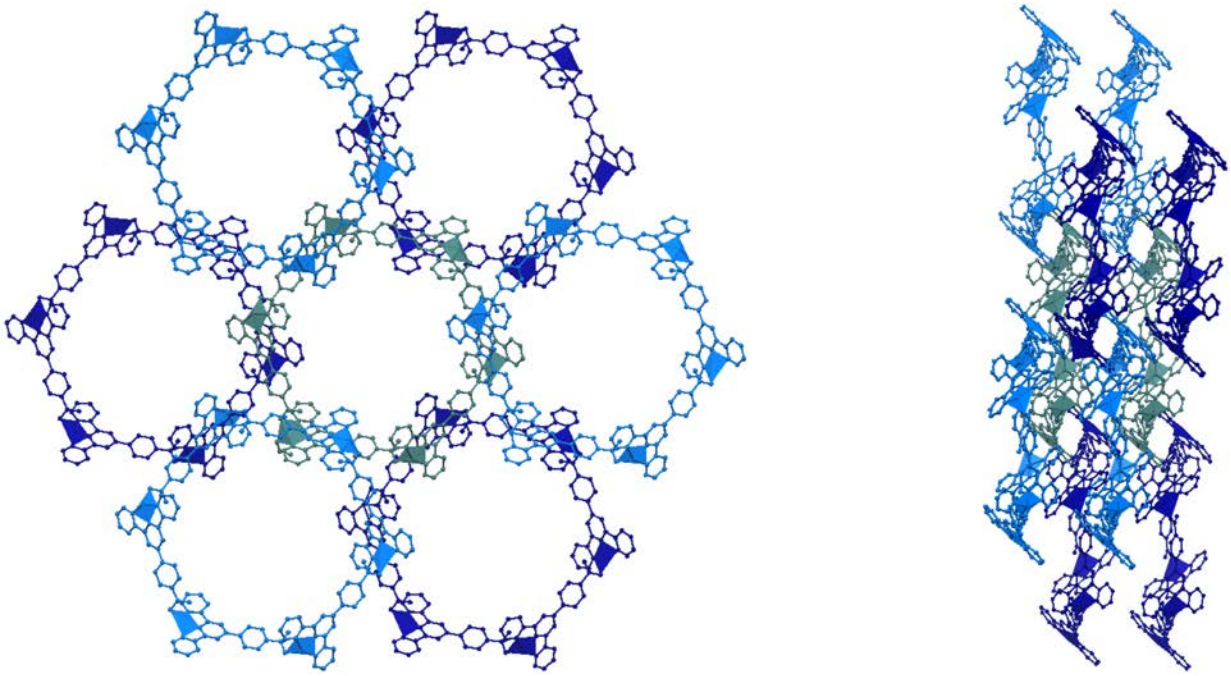

Figure 6.4. Packing in an a-b-c- fashion down the *c* crystallographic direction (left) and *b* crystallographic direction (right)

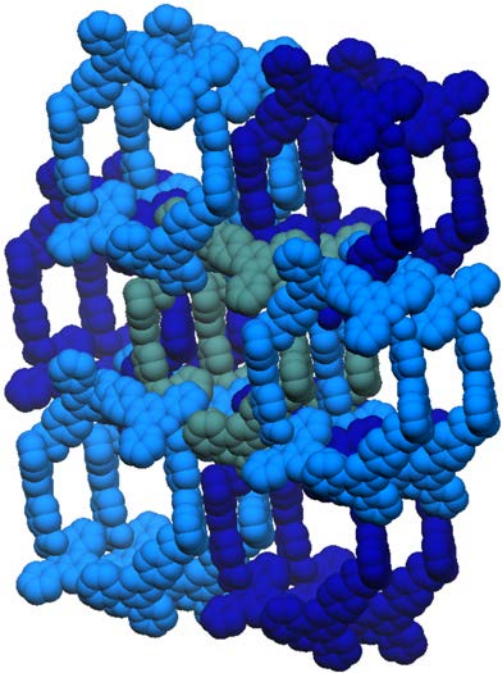

Figure 6.5. Packing in an a-b-c fashion shown with space filling model

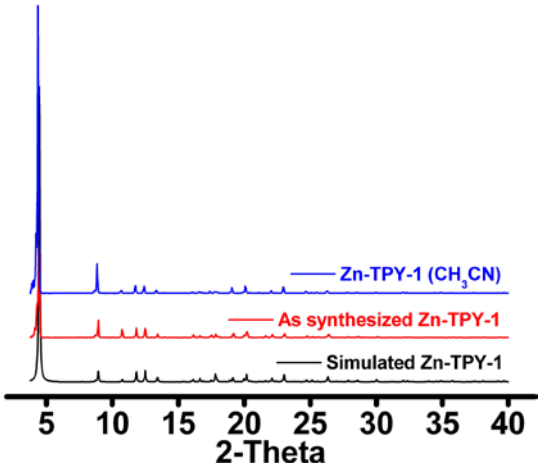

Figure 6.6. Powder X-ray diffraction patterns of Zn-TPY-1

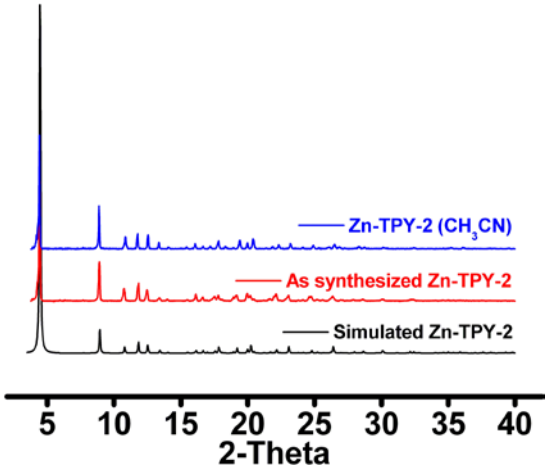

Figure 6.7. Powder X-ray diffraction patterns of Zn-TPY-2

6.2.2 Gas adsorption studies of Zn-TPY-1 and Zn-TPY-2

For the gas adsorption studies, all of the solvent molecules should be removed for maximum gas uptake. Thermogravimentric analysis (TGA) shows the weight loss profile upon heating. By correlating the TGA elemental analysis data, we determined the optimal activation temperature. EA data suggests 7 DMF molecules and 9 water molecules reside in the pore (Calc'd.: C, 51.36; H, 3.94; N, 9.08; Found: C, 51.17; H, 4.08; N, 9.26) The **Zn-TPY-1** TGA

shows two weight loss steps: the first corresponding to the free solvent molecules (calc'd, 18%; measured, 19%) and the second at 250 °C corresponding to the loss of the trifluoroacetate molecules for a total weight loss of 31% (calc'd, 36%) (Figure 6.8). For **Zn-TPY-2**, the TGA displays the same profile as the TGA of **Zn-TPY-1**, with a smaller second weight loss due to the lighter acetate molecules (Figure 6.9). EA data suggests 33 water molecules and 2 DMF molecules reside in the pore (calc'd, 50.02; H, 5.09; N, 7.78; Found, C, 49.94; H, 4.21; N, 8.27). The first weight loss corresponds to loss of the free solvent molecules (calc'd, 21%; measured: 24%). The second weight loss is from the coordinated acetate molecules resulting in a total weight loss of 29 % (calc'd, 30 %).

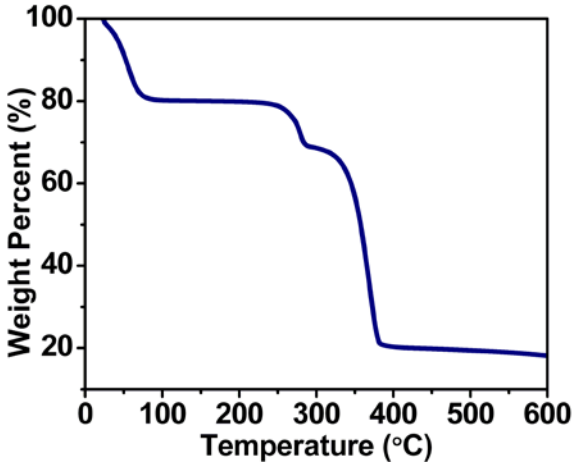

Figure 6.8. TGA of Zn-TPY-1 as synthesized material

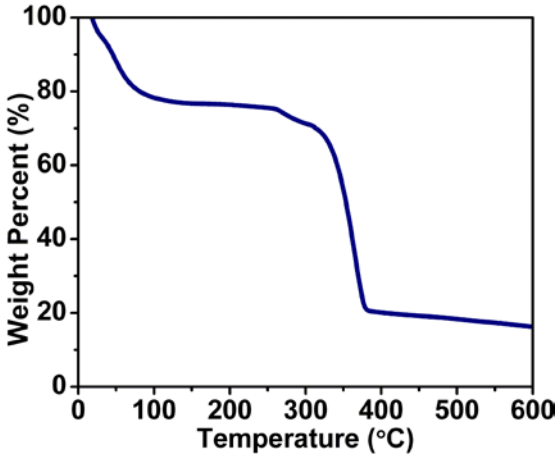

Figure 6.9. TGA of Zn-TPY-2 as synthesized material

Zn-TPY-1 was activated at 200 °C to ensure removal of all guest molecules. Despite the large pores, the nitrogen isotherm (Figure 6.10, circles, 77K) showed a small amount of adsorbed N_2, a large hysteresis, and a very small Brunauer-Emmett-Teller (BET) surface area of 37 m^2/g. Repeating this adsorption experiment resulted in a similar isotherm but an overall higher amount of gas adsorption and a higher BET surface area of 138 m^2/g (Figure 6.10, triangles, 77K). We hypothesized that this inconsistency is due to the partial removal of trifluoroacetate molecules.

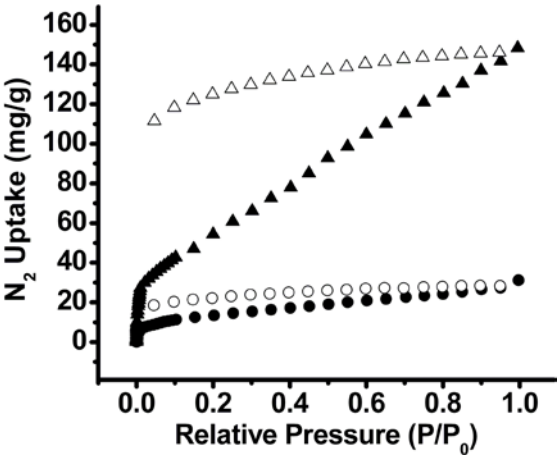

Figure 6.10. N_2 adsorption (filled) and desorption (open) for Zn-TPY-1 upon activation at 200 °C for sample 1 (circles) and sample 2 (triangles)

The TGA data suggests that the removal of trifluoroacetate molecules does not begin until 250 °C; however, heating the material at 200 °C for 24 hours results in a weight loss attributed to some of the trifluoroacetate molecules (Figure 6.11 left). We hypothesized that different amounts of trifluoroacetate molecules led to the different surface areas. We subsequently determined that 260 °C activation yielded accurate and repeatable results. Heating the acetonitrile-exchanged **Zn-TPY-1** at 260 °C for 48 hours allowed for the complete removal of the trifluoroacetate molecules (TGA weight loss: 22.2% and calculated weight loss: 21.3%) (Figure 6.11). The slight discrepancy is most likely due to some residual water molecules.

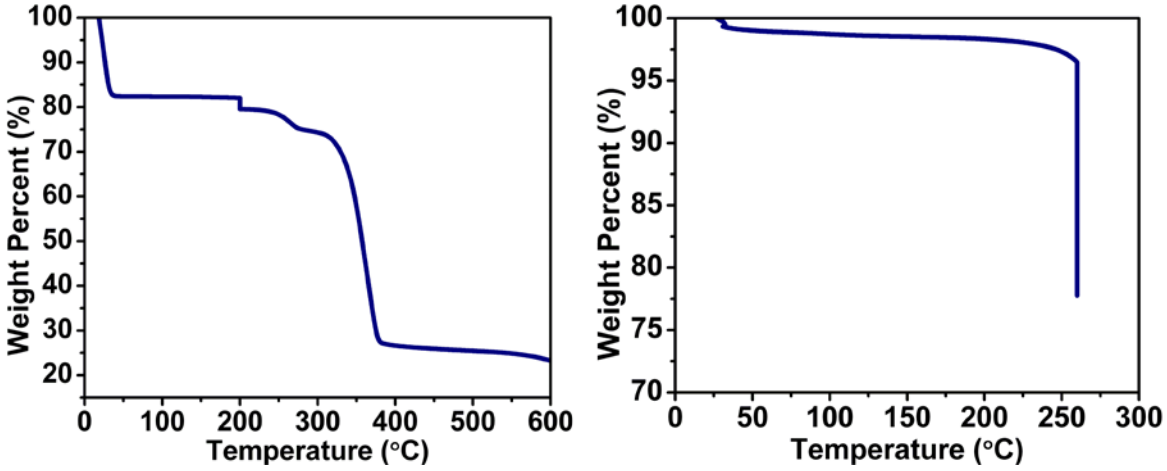

Figure 6.11. TGA of acetonitrile-exchanged material of Zn-TPY-1, showing removal of TFA molecules when the temperature is held constant at 200 °C (left) and 260 °C (right)

The material was activated at 260 °C and the resulting nitrogen isotherm showed a typical type IVA isotherm for a mesoporous material with cylindrical cavities, as one would expect from the crystal structure data. The extreme hysteresis at higher temperatures is typical for mesoporous materials that contain 1-D cylindrical channels. Activation at 260 °C resulted in an increase of BET surface area to 290 m^2/g and maximum N_2 uptake of 438 mg/g with

repeatable results. Surprisingly, the nitrogen isotherm did not show hysteresis at low relative pressures (0.02 – 0.004) upon desorption, which is common for unstable macrocycle-based structures which undergo structural rearrangement or structural shear upon desorption. The enhanced stability of **Zn-TPY-1** is likely due to the strong π–π interactions between neighboring macrocycles within the structure. The powder pattern collected after sorption also showed that the material still maintained its crystalline properties. **Zn-TPY-2** showed the same mesoporosity upon N_2 sorption, as expected since **Zn-TPY-1** and **Zn-TPY-2** are essentially the same material after activation (Figure 6.14).

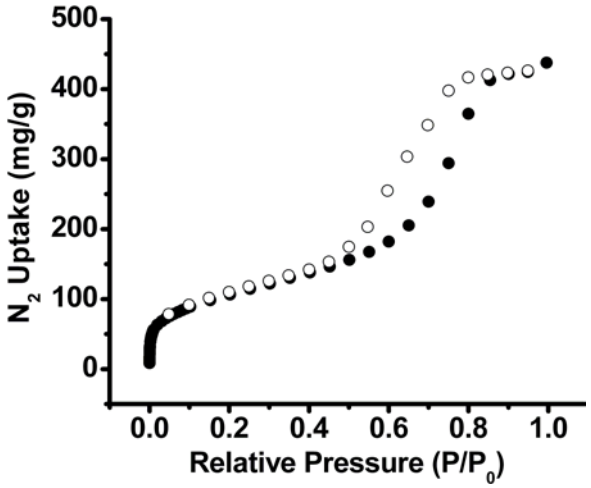

Figure 6.12. N_2 isotherm of Zn-TPY-1 upon 260 °C activation showing adsorption (filled circles) and desorption (open circles), 77K.

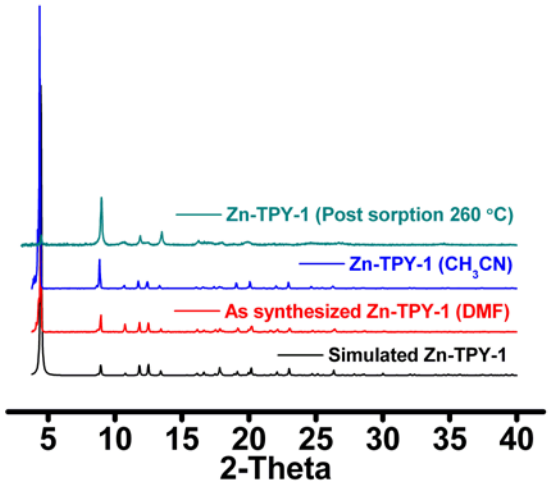

Figure 6.13. Powder X-ray diffraction pattern for Zn-TPY-1 post-sorption experiments

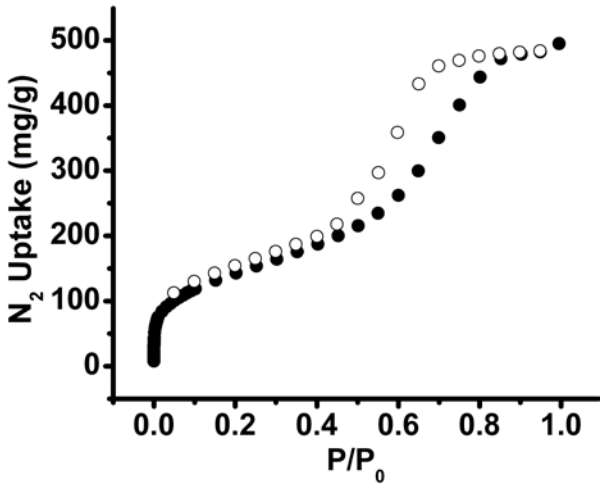

Figure 6.14. N_2 isotherm of Zn-TPY-2 upon 260 °C activation showing adsorption (filled circles) and desorption (open circles), 77K

CO_2 and H_2 isotherms were also collected on the acetonitrile-exchange **Zn-TPY-1**. **Zn-TPY-1** shows a small uptake of CO_2 with a maximum of 35 cm^3/g at 760 Torr. (Figure 6.15). Although the removal of the trifluoroacetate molecules allowed for open metal sites, which are known to potentially lead to a high H_2 uptake,[6] **Zn-TPY-1** only adsorbs a maximum of 0.4 wt % of a H_2 (Figure 6.16).

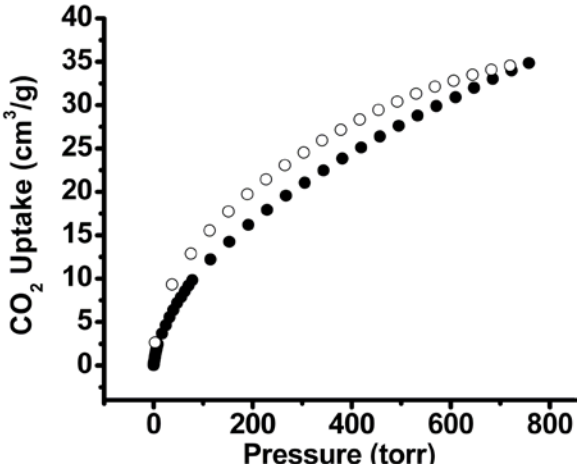

Figure 6.15. CO_2 isotherm for Zn-TPY-1 upon 260 °C activation showing adsorption (filled circles) and desorption (open circles), 273K

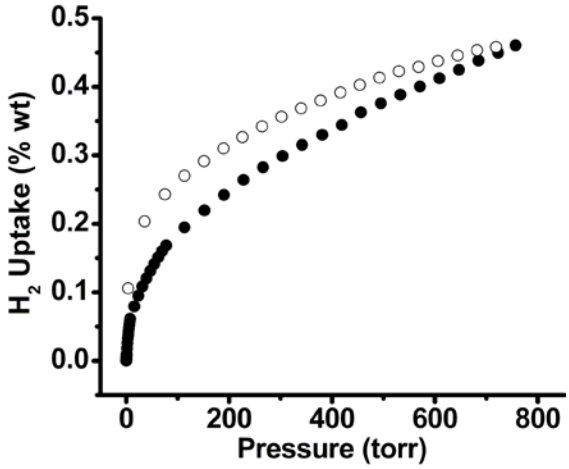

Figure 6.16. H_2 isotherm for Zn-TPY-1 upon 260 °C activation showing adsorption (filled circles) and desorption (open circles), 77K

6.3 CONCLUSION

To the best of our knowledge, we have synthesized the first mesoporous macrocycle demonstrating permanent porosity. **Zn-TPY-1** and **Zn-TPY-2** contain hexameric rings of Zn^{2+}

and a large aromatic ligand that stack together in an a-b-c fashion. This stacking arrangement allows for many π–π interactions, which promote the stability of the structure. Removal of coordinated trifluoroacetate and acetate molecules from Zn^{2+} occurs upon heating at 260 °C leaving open metal sites. The N_2 isotherm shows demonstrates permanent mesoporosity. While these materials do not demonstrate a very large BET surface area, the large 1-D pores could allow for other interesting guest molecules. We demonstrate a new strategy to create permanently porous macrocycles through the incorporation of large aromatic ligands that can participate in many π–π interactions.

6.4 EXPERIMENTAL

6.4.1 Reagents

$Zn(CH_3COO)_2 \bullet 2H_2O$, $Zn(CF_3COO)_2 \bullet xH_2O$, acetic acid, trifluoroacetic acid, NaOH pellets, and DMF were all purchased from Aldrich. Dry acetonitrile (99.9%) was purchased from across. 2-acetylpyridine was purchased from SAFC. Methyl 4-formylbenzoate was purchased from TCI. NH_4OH (29% weight) was purchased from Fisher. All reagents were used as received without further purification.

6.4.2 General procedures

^1H NMR (300 MHz) and ^{13}C NMR (75 MHz) were recorded on a Bruker Avance 300. Fourier transform infrared (FT-IR) spectra were measured on a Nicolet Avatar 360 FT-IR

spectrometer using KBr pellet samples. Absorptions are described as very strong (vs), strong (s), medium (m), weak (w), shoulder (sh), and broad (br) and stretches (st) are labeled symmetric (sym) or asymmetric (as). Data was analyzed using the Omnic Software Package. Mass spectra were obtained with a VG AutoSpec Q.

X-ray powder diffraction patterns were taken using a Bruker AXS D_8 Discover powder diffractometer at 40 kV, 40 mA for Cu Kα, (λ = 1.5406 Å) with a scan speed of 0.20 sec/step and a step size of .02018º. The data were analyzed for d-spacing measurements using the EVA program from the Bruker Powder Analysis Software package. The simulated powder patterns were calculated using PowderCell 2.4. The purity and homogeneity of the bulk products were determined by comparison of the simulated and experimental X-ray powder diffraction patterns. Solvent exchange of the DMF and H_2O guest molecules in **Zn-TPY-1** and **Zn-TPY-2** was performed using anhydrous solvents as follows: 30 min soak in exchange solvent (ES) followed by solvent removal (3X); overnight soak in ES and then solvent removal; 24 h soak in ES and solvent removal; addition of fresh solvent. The elemental microanalysis was performed by the University of Illinois, Department of Chemistry, Microanalytical Laboratory using an Exeter Analytical CE440.

6.4.3 Synthesis of H-TPY

H-TPY was prepared according to a modified literature procedure.[5] NH_4OH (30%, 6 mL) and NaOH (2.92 g, 73 mmol) dissolved in water (5 mL) were added to a solution of Methyl 4-formylbenzoate (6.0 g, 36.6 mmol) and 2-acetylpyridine (8.2 mL, 73 mmol) in ethanol (150 mL). This red solution as stirred open to the atmosphere in a 500 mL round bottom flask equipped with a stir bar for 17 hours to obtain a yellow suspension. Water (300 mL) was added, and the

resulting red solution was transferred to an Erlenmeyer flask (500 mL). The solution was slowly acidified with HNO_3 (2M, aq) to a pH of 4. This blue-gray suspension was then filtered to produce a blue-gray solid. The product was purified by refluxing in ethanol (300 mL) for 1 hour, followed by refluxing in water (200 mL) for 1 hour. A white powder was obtained (3.79 g, 29.3%)

6.4.4 Synthesis of Zn-TPY-1: $Zn_6(C_{22}H_{14}N_3O_2)_6(CF_3COO)_6\bullet(DMF)_7(H_2O)_9$

In a glass vial (20 mL), a solution of (**H-TPY**) (141.2 mg, 0.40 mmol) in DMF (4.0 mL) and a solution of $Zn(CF_3COO)_2 \bullet xH_2O$ (116.6 mg, 0.40 mmol) in DMF (4.0 mL) were combined with 1M $CF_3COOH_{(aq)}$ (300 μL) and H_2O (3.2 mL) to produce a clear solution. The vial was capped and placed in an 85 ºC isotemp oven for 24 hours to produce yellow hexagonal crystals of the product. The crystals were collected, washed with a DMF:H_2O mixture (8:3.2 x 5 mL), and air dried (187 mg, 73 %).

EA Calcd. (%) for $Zn_6(C_{22}H_{14}N_3O_2)_6(CF_3COO)_6\bullet(DMF)_7(H_2O)_9$: C, 51.36; H, 3.94; N, 9.08. Found: C, 51.17; H, 4.08; N, 9.26. EA. Calcd. (%) for the acetonitrile exchange product, $Zn_6(C_{22}H_{14}N_3O_2)_6(CF_3COO)_6\bullet(H_2O)_9$: C, 51.68; H, 3.07; N, 7.53. Found: C, 51.26; H, 2.50; N, 7.68. FT-IR for $Zn_6(C_{22}H_{14}N_3O_2)_6(CH_3COO)_6\bullet(DMF)_7(H_2O)_9$ (KBr 4000-700 cm^{-1}): 3401 (br), 1655 (DMF C=O, m), 1602 (vs), 1560 (m), 1476 (m), 1429 (w), 1386 (vs), 1249 (w), 1162 (w), 1068 (w), 1015 (m), 818 (w), 785 (s), 734 (w), 706 cm^{-1} (w). FT-IR for the acetonitrile exchange product (KBr 4000-700 cm^{-1}): 3408 (br), 1603 (vs), 1559 (m), 1476 (m), 1429 (w), 1385 (vs), 1249 (w), 1169 (w), 1068 (w), 1015 (m), 818 (w), 785 (s), 734 (w), 706 cm^{-1} (w).

6.4.5 Synthesis of Zn-TPY-2: $Zn_6(C_{22}H_{14}N_3O_2)_6(CH_3COO)_6\bullet(DMF)_2(H_2O)_{33}$

In a glass vial (20 mL), a solution of (**H-TPY**) (3.53 mg, 0.01 mmol) in DMF (1.0 mL) and a solution of $Zn(CH_3COO)_2\bullet 2H_2O$ (8.78 mg, 0.04 mmol) in DMF (4.0 mL) were combined with 1M $CH_3COOH_{(aq)}$ (100 μL) and H_2O (2.0 mL) to produce a clear solution. The vial was capped and placed in a 100 ºC isotemp oven for 24 hours to produce yellow hexagonal crystals of the product. The crystals were collected, washed with a DMF:H_2O mixture (5:2 x 5 mL), and air dried (1.6 mg, 26.7 %).

EA Calcd. (%) for $Zn_6(C_{22}H_{14}N_3O_2)_6(CH_3COO)_6\bullet(DMF)_2(H_2O)_{33}$: C, 50.02; H, 5.09; N, 7.78. Found: C, 49.94; H, 4.21; N, 8.27. FT-IR for the as-synthesized material, $Zn_6(C_{22}H_{14}N_3O_2)_6(CH_3COO)_6\bullet(DMF)_2(H_2O)_{33}$ (KBr 4000-700 cm^{-1}): 3401 (br), 1655 (DMF C=O, m), 1602 (vs), 1560 (m), 1476 (m), 1429 (w), 1386 (vs), 1249 (w), 1162 (w), 1068 (w), 1015 (m), 818 (w), 785 (s), 734 (w), 706 cm^{-1} (w). FT-IR for the acetonitrile exchanged product (KBr 4000-700 cm^{-1}): 3408 (br), 1603 (vs), 1559 (m), 1476 (m), 1429 (w), 1385 (vs), 1249 (w), 1169 (w), 1068 (w), 1015 (m), 818 (w), 785 (s), 734 (w), 706 cm^{-1} (w).

6.4.6 Low pressure gas adsorption measurements

Sorption isotherm studies for **Zn-TPY-1** and **Zn-TPY-2** were performed volumetrically as a function of relative pressure by using the Autosorb 1 by Quantachrome. Samples of acetonitrile-exchanged materials were weighed using an AB54-S/FACT (Mettler Toledo) electrogravimetric balance (sensitivity 0.1 mg). 9 mm large bulb cells (from Quantachrome) of a known weight were loaded with ~60 mg of sample for gas sorption experiments. The samples were degassed at 200 °C or 260 °C for 22-24 hours on degassing station until the outgas rate was no more than 3.5

mTorr/min. The degassed sample and sample cell were weighed precisely and then transferred back to the analyzer. The temperature of each sample for N_2 and H_2 adsorption experiments was controlled by a refrigerated bath of either liquid nitrogen (77 K) or liquid argon (87 K). CO_2 isotherms (273 K) were measured in a temperature-controlled water bath. The N_2, CO_2, and H_2 adsorbates were of UHP grade.

6.4.7 Single crystal X-ray diffraction studies

Single crystal XRD data was collected on a Bruker SMART APEX II CCD-based X-ray diffractometer equipped with a normal focus Mo-target X-ray tube (λ = 0.71073Å) operated at 2000 W power (45 kV and 35 mA). The detector was placed at a distance of 6.002 cm from the crystal. 1800 frames were collected with a scan width of 0.3° in omega and phi with an exposure time of 10 s/frame. Crystals were mounted in glass capillaries, and the X-ray intensities were measured at 203K for **Zn-TPY-1** and **Zn-TPY-2**.

6.4.7.1 Single crystal X-ray diffraction studies for Zn-TPY-1

An X-ray crystal structure was determined for $C_{24}H_{14}F_3N_3O_5Zn$, **Zn-TPY-1**, using a single crystal on a Bruker Smart Apex CCD diffractometer with graphite-monochromated MoK_α (λ = 0.71073 Å) radiation. The parameters used during the collection of diffraction data are summarized in Appendix A. The crystal was mounted in a glass loop and placed in a cold N_2 stream (203 K) for data collection.

Unit-cell parameters and systematic absences indicated **Zn-TPY-1** crystallized in trigonal space groups R3 or R-3; centrosymmetric R-3 was chosen based on E-values and the successful solution and refinement of the structure. Unit-cell dimensions were derived from the least-

squares fit of the angular settings of 1850 reflections. Data were corrected for absorption using the Bruker program Sadabs. The structure was solved via direct methods, which located Zn and most of the remaining non-hydrogen atoms. Remaining non-hydrogen atoms were gradually found from several subsequent difference Fourier syntheses. All non-hydrogen atoms were refined anisotropically except for trifluoroacetate C and F atoms. Idealized atom positions were calculated for all hydrogen atoms (*d*-(C_{methyl}-H) = 0.96 Å, d-C_{phenyl}-H)=0.93 Å, *U* = 1.2*Uiso* of attached carbon).

The final Fourier map shows large maximum peak of 2.14 $e^-/Å^{-3}$ which is presumed to be part of unresolvable, disordered solvent. All computer programs used in the data collection and refinements are contained in the Bruker program packages SMART (vers. 5.625), SAINT (vers. 6.22), and SHELXTL (vers. 6.14) and Platon.

6.4.7.2 Single crystal X-ray diffraction studies for Zn-TPY-2

An X-ray crystal structure was determined for $C_{24}H_{17}N_3O_5Zn$, **Zn-TPY-2**, using a single crystal on a Bruker Smart Apex CCD diffractometer with graphite-monochromated MoK_α (λ = 0.71073 Å) radiation. The parameters used during the collection of diffraction data are summarized in Appendix A. The crystal was mounted in a glass loop and placed in a cold N_2 stream (203 K) for data collection.

Unit-cell parameters and systematic absences indicated **Zn-TPY-2** crystallized in trigonal space groups R3 or R-3; centrosymmetric R-3 was chosen based on E-values and the successful solution and refinement of the structure. Unit-cell dimensions were derived from the least-squares fit of the angular settings of 6979 reflections. Data were corrected for absorption using the Bruker program Sadabs. The structure was solved via direct methods, which located Zn and most of the remaining non-hydrogen atoms. Remaining non-hydrogen atoms were gradually

found from several subsequent difference Fourier syntheses. All non-hydrogen atoms were refined anisotropically. Idealized atom positions were calculated for all hydrogen atoms (*d*-(C_{methyl}-H) = 0.96 Å, d-C_{phenyl}-H)=0.93 Å, *U* = 1.2*Uiso* of attached carbon).

The final Fourier map shows a large maximum peak of 2.07 $e^{-}/Å^{-3}$ which is presumed to be part of unresolvable, disordered solvent. All computer programs used in the data collection and refinements are contained in the Bruker program packages SMART (vers. 5.625), SAINT (vers. 6.22), and SHELXTL (vers. 6.14) and Platon.

6.5 REFERENCES

(1) Dewal, M. B.; Lufaso, M. W.; Hughes, A. D.; Samuel, S. A.; Pellechia, P.; Shimizu, L. S. *Chem. Mater.* **2006**, *18*, 4855.
(2) Lim, S.; Kim, H.; Selvapalam, N.; Kim, K. J.; Cho, S.; Seo, G.; Kim, K. *Angew. Chem. Int. Ed.* **2008**, *47*, 3352.
(3) Dobrza≈Ñska, L.; Lloyd, G. O.; Raubenheimer, H. G.; Barbour, L. J. *J. Am. Chem. Soc.* **2005**, *127*, 13134.
(4) Chatterjee, B.; Noveron, J. C.; Resendiz, M. J. E.; Liu, J.; Yamamoto, T.; Parker, D.; Cinke, M.; Nguyen, C. V.; Arif, A. M.; Stang, P. J. *J. Am. Chem. Soc.* **2004**, *126*, 10645.
(5) Constable, E. C.; Dunphy, E. L.; Housecroft, C. E.; Neuburger, M.; Schaffner, S.; Schaper, F.; Batten, S. R. *Dalton T.* **2007**, 4323.
(6) Bae, Y.-S.; Farha, O. K.; Hupp, J. T.; Snurr, R. Q. *J. Mater. Chem.* **2009**, *19*, 2131.
(7) Dincă, M.; Long, J. *Angew. Chem. Int. Ed.* **2008**, *47*, 6766.

APPENDIX A

CRYSTALLOGRAPHIC DATA

Table AA1. Crystal data and structure refinement for Yb-PVDC-1.

Identification code	**Yb-PVDC-1**	
Empirical formula	C39 H30 O10 Yb	
Formula weight	831.67	
Temperature	253(2) K	
Wavelength	0.71073 Å	
Crystal system	Orthorhombic	
Space group	F d d d	
Unit cell dimensions	a = 16.247(6) Å	α = 90°.
	b = 48.939(19) Å	β = 90°.
	c = 80.84(3) Å	γ = 90°.
Volume	64280(43) $Å^3$	
Z	32	
Density (calculated)	0.688 Mg/m^3	
Absorption coefficient	1.189 mm^{-1}	
F(000)	13248	
Crystal size	0.32 x 0.23 x 0.21 mm^3	
Theta range for data collection	3.54 to 23.25°.	
Index ranges	-17<=h<=18, -54<=k<=54, -89<=l<=87	
Reflections collected	95076	
Independent reflections	11507 [R(int) = 0.1522]	
Completeness to theta = 23.25°	99.5 %	
Absorption correction	Semi-empirical from equivalents	
Max. and min. transmission	0.7883 and 0.7021	
Refinement method	Full-matrix least-squares on F^2	
Data / restraints / parameters	11507 / 20 / 399	
Goodness-of-fit on F^2	0.811	
Final R indices [I>2sigma(I)]	R1 = 0.0525, wR2 = 0.1110	
R indices (all data)	R1 = 0.1550, wR2 = 0.1362	
Largest diff. peak and hole	0.531 and -0.258 $e.Å^{-3}$	

Table AA2. Atomic coordinates (x 10^4) and equivalent isotropic displacement parameters ($Å^2$ x 10^3) for Yb-PVDC-1. U(eq) is defined as one third of the trace of the orthogonalized U^{ij} tensor.

	x	y	z	U(eq)
Yb(1)	-1250	8750	6303(1)	88(1)
Yb(2)	1250	9097(1)	6250	110(1)
O(1)	1473(4)	8745(1)	6086(1)	120(2)
O(2)	2601(3)	8517(1)	6135(1)	104(2)
O(3)	-448(4)	6765(1)	3957(1)	138(2)
O(4)	709(4)	6526(1)	3986(1)	115(2)
O(5)	2364(9)	7269(3)	5260(1)	371(8)
O(6)	-255(11)	7780(4)	4900(2)	391(11)
O(7)	-1232(5)	9045(1)	6088(1)	148(3)
O(8)	43(5)	9060(2)	6117(1)	197(4)
O(9)	1099(11)	9564(3)	5044(2)	287(6)
O(10)	771(6)	9564(2)	6162(1)	312(5)
C(1)	1947(6)	8555(2)	6057(1)	100(3)
C(2)	1746(4)	8365(1)	5920(1)	110(3)
C(3)	1022(4)	8402(1)	5831(1)	147(4)
C(4)	857(4)	8239(2)	5694(1)	169(5)
C(5)	1416(5)	8040(1)	5645(1)	160(4)
C(6)	2140(5)	8002(1)	5734(1)	176(4)
C(7)	2305(4)	8165(2)	5871(1)	145(4)
C(8)	1216(10)	7900(3)	5490(2)	240(7)
C(9)	1492(12)	7776(3)	5403(2)	307(11)
C(10)	1187(8)	7632(2)	5233(1)	257(9)
C(11)	1630(7)	7411(2)	5172(1)	283(10)
C(12)	1432(8)	7302(2)	5018(1)	305(15)
C(13)	791(8)	7412(2)	4926(1)	268(10)
C(14)	349(7)	7633(2)	4988(1)	241(8)
C(15)	547(7)	7743(2)	5141(1)	257(8)
C(16)	563(11)	7294(3)	4754(2)	234(8)
C(17)	886(11)	7107(4)	4695(2)	285(9)
C(18)	560(5)	7035(2)	4517(1)	218(8)
C(19)	-21(5)	7148(2)	4411(1)	262(8)

C(20)	-152(4)	7033(2)	4256(1)	203(6)
C(21)	298(5)	6806(2)	4207(1)	134(3)
C(22)	879(5)	6693(1)	4313(1)	164(4)
C(23)	1010(5)	6808(2)	4468(1)	211(6)
C(24)	184(6)	6690(2)	4036(1)	116(3)
C(25)	-551(9)	9111(2)	6035(1)	129(4)
C(26)	-504(5)	9253(1)	5878(1)	113(3)
C(27)	-1201(4)	9375(2)	5811(1)	153(4)
C(28)	-1154(4)	9508(2)	5659(1)	194(5)
C(29)	-410(5)	9519(2)	5575(1)	187(5)
C(30)	287(4)	9397(2)	5642(1)	235(7)
C(31)	240(4)	9264(2)	5793(1)	197(5)
C(32)	-476(10)	9676(3)	5409(2)	240(8)
C(33)	25(10)	9703(3)	5312(2)	258(8)
C(34)	-129(13)	9889(4)	5154(2)	209(8)
C(35)	-693(13)	10114(4)	5135(2)	283(13)
C(36)	487(12)	9787(4)	5037(2)	209(7)
C(37)	2535(14)	7031(3)	5136(3)	530(20)
C(38)	1681(10)	9531(5)	4891(2)	347(13)
C(39)	-515(16)	8013(4)	5036(3)	450(19)

Table AA3. Bond lengths [Å] and angles [°] for Yb-PVDC-1.

Yb(1)-O(4)#1	2.188(6)
Yb(1)-O(4)#2	2.188(6)
Yb(1)-O(2)#3	2.243(6)
Yb(1)-O(2)#4	2.243(6)
Yb(1)-O(7)	2.265(5)
Yb(1)-O(7)#5	2.265(5)
Yb(1)-O(8)#5	2.996(8)
Yb(1)-O(8)	2.996(8)
Yb(2)-O(1)	2.202(6)
Yb(2)-O(1)#4	2.202(6)
Yb(2)-O(8)	2.244(8)
Yb(2)-O(8)#4	2.244(8)
Yb(2)-O(3)#6	2.274(6)
Yb(2)-O(3)#1	2.274(6)
Yb(2)-O(10)#4	2.516(11)
Yb(2)-O(10)	2.516(10)
O(1)-C(1)	1.230(9)
O(2)-C(1)	1.249(8)
O(2)-Yb(1)#4	2.243(6)
O(3)-C(24)	1.264(9)
O(3)-Yb(2)#7	2.274(6)
O(4)-C(24)	1.238(9)
O(4)-Yb(1)#8	2.188(6)
O(5)-C(37)	1.559(16)
O(5)-C(11)	1.553(13)
O(6)-C(14)	1.404(18)
O(6)-C(39)	1.641(15)
O(7)-C(25)	1.227(11)
O(8)-C(25)	1.198(11)
O(9)-C(36)	1.478(17)
O(9)-C(38)	1.565(15)
C(1)-C(2)	1.487(9)
C(2)-C(3)	1.3900

C(2)-C(7)	1.3900
C(3)-C(4)	1.3900
C(3)-H(3A)	0.9300
C(4)-C(5)	1.3900
C(4)-H(4A)	0.9300
C(5)-C(6)	1.3900
C(5)-C(8)	1.468(12)
C(6)-C(7)	1.3900
C(6)-H(6A)	0.9300
C(7)-H(7A)	0.9300
C(8)-C(9)	1.028(13)
C(8)-H(8A)	0.9300
C(9)-C(10)	1.624(12)
C(9)-H(9A)	0.9300
C(10)-C(11)	1.3900
C(10)-C(15)	1.3900
C(11)-C(12)	1.3900
C(12)-C(13)	1.3900
C(12)-H(12A)	0.9300
C(13)-C(14)	1.3900
C(13)-C(16)	1.549(13)
C(14)-C(15)	1.3900
C(15)-H(15A)	0.9300
C(16)-C(17)	1.162(14)
C(16)-H(16A)	0.9300
C(17)-C(18)	1.567(14)
C(17)-H(17A)	0.9300
C(18)-C(19)	1.3900
C(18)-C(23)	1.3900
C(19)-C(20)	1.3900
C(19)-H(19A)	0.9300
C(20)-C(21)	1.3900
C(20)-H(20A)	0.9300
C(21)-C(22)	1.3900
C(21)-C(24)	1.508(9)
C(22)-C(23)	1.3900

C(22)-H(22A)	0.9300
C(23)-H(23A)	0.9300
C(25)-C(26)	1.449(10)
C(26)-C(27)	1.3900
C(26)-C(31)	1.3900
C(27)-C(28)	1.3900
C(27)-H(27A)	0.9300
C(28)-C(29)	1.3900
C(28)-H(28A)	0.9300
C(29)-C(30)	1.3900
C(29)-C(32)	1.549(11)
C(30)-C(31)	1.3900
C(30)-H(30A)	0.9300
C(31)-H(31A)	0.9300
C(32)-C(33)	1.138(13)
C(32)-H(32A)	0.9300
C(33)-C(34)	1.584(14)
C(33)-H(33A)	0.9300
C(34)-C(35)	1.44(2)
C(34)-C(36)	1.47(2)
C(35)-C(36)#9	1.51(2)
C(35)-H(35A)	0.9300
C(36)-C(35)#9	1.51(2)
C(37)-H(37A)	0.9600
C(37)-H(37B)	0.9600
C(37)-H(37C)	0.9600
C(38)-H(38A)	0.9600
C(38)-H(38B)	0.9600
C(38)-H(38C)	0.9600
C(39)-H(39A)	0.9600
C(39)-H(39B)	0.9600
C(39)-H(39C)	0.9600

O(4)#1-Yb(1)-O(4)#2	94.9(3)
O(4)#1-Yb(1)-O(2)#3	82.50(19)
O(4)#2-Yb(1)-O(2)#3	80.1(2)

O(4)#1-Yb(1)-O(2)#4	80.1(2)
O(4)#2-Yb(1)-O(2)#4	82.50(19)
O(2)#3-Yb(1)-O(2)#4	154.2(2)
O(4)#1-Yb(1)-O(7)	96.9(2)
O(4)#2-Yb(1)-O(7)	156.9(2)
O(2)#3-Yb(1)-O(7)	81.9(2)
O(2)#4-Yb(1)-O(7)	119.0(3)
O(4)#1-Yb(1)-O(7)#5	156.9(2)
O(4)#2-Yb(1)-O(7)#5	96.9(2)
O(2)#3-Yb(1)-O(7)#5	119.0(2)
O(2)#4-Yb(1)-O(7)#5	81.9(2)
O(7)-Yb(1)-O(7)#5	79.3(3)
O(4)#1-Yb(1)-O(8)#5	159.03(19)
O(4)#2-Yb(1)-O(8)#5	75.2(2)
O(2)#3-Yb(1)-O(8)#5	77.62(19)
O(2)#4-Yb(1)-O(8)#5	116.0(2)
O(7)-Yb(1)-O(8)#5	86.9(2)
O(7)#5-Yb(1)-O(8)#5	44.0(2)
O(4)#1-Yb(1)-O(8)	75.2(2)
O(4)#2-Yb(1)-O(8)	159.03(19)
O(2)#3-Yb(1)-O(8)	116.0(2)
O(2)#4-Yb(1)-O(8)	77.62(19)
O(7)-Yb(1)-O(8)	44.0(2)
O(7)#5-Yb(1)-O(8)	86.9(2)
O(8)#5-Yb(1)-O(8)	119.7(3)
O(4)#1-Yb(1)-C(25)	88.4(3)
O(4)#2-Yb(1)-C(25)	176.6(3)
O(2)#3-Yb(1)-C(25)	100.1(3)
O(2)#4-Yb(1)-C(25)	98.3(3)
O(7)-Yb(1)-C(25)	21.3(3)
O(7)#5-Yb(1)-C(25)	80.0(2)
O(8)#5-Yb(1)-C(25)	101.5(3)
O(8)-Yb(1)-C(25)	23.0(2)
O(4)#1-Yb(1)-C(25)#5	176.6(3)
O(4)#2-Yb(1)-C(25)#5	88.4(3)
O(2)#3-Yb(1)-C(25)#5	98.3(3)

O(2)#4-Yb(1)-C(25)#5	100.1(3)
O(7)-Yb(1)-C(25)#5	80.0(2)
O(7)#5-Yb(1)-C(25)#5	21.3(3)
O(8)#5-Yb(1)-C(25)#5	23.0(2)
O(8)-Yb(1)-C(25)#5	101.5(3)
C(25)-Yb(1)-C(25)#5	88.2(5)
O(1)-Yb(2)-O(1)#4	77.2(3)
O(1)-Yb(2)-O(8)	78.0(2)
O(1)#4-Yb(2)-O(8)	94.7(3)
O(1)-Yb(2)-O(8)#4	94.7(3)
O(1)#4-Yb(2)-O(8)#4	78.0(2)
O(8)-Yb(2)-O(8)#4	170.7(4)
O(1)-Yb(2)-O(3)#6	75.4(2)
O(1)#4-Yb(2)-O(3)#6	145.1(2)
O(8)-Yb(2)-O(3)#6	100.3(2)
O(8)#4-Yb(2)-O(3)#6	83.1(2)
O(1)-Yb(2)-O(3)#1	145.1(2)
O(1)#4-Yb(2)-O(3)#1	75.4(2)
O(8)-Yb(2)-O(3)#1	83.1(2)
O(8)#4-Yb(2)-O(3)#1	100.3(2)
O(3)#6-Yb(2)-O(3)#1	137.5(3)
O(1)-Yb(2)-O(10)#4	146.0(3)
O(1)#4-Yb(2)-O(10)#4	126.2(3)
O(8)-Yb(2)-O(10)#4	118.6(3)
O(8)#4-Yb(2)-O(10)#4	70.6(3)
O(3)#6-Yb(2)-O(10)#4	72.6(3)
O(3)#1-Yb(2)-O(10)#4	68.9(3)
O(1)-Yb(2)-O(10)	126.2(3)
O(1)#4-Yb(2)-O(10)	146.0(3)
O(8)-Yb(2)-O(10)	70.6(3)
O(8)#4-Yb(2)-O(10)	118.6(3)
O(3)#6-Yb(2)-O(10)	68.9(3)
O(3)#1-Yb(2)-O(10)	72.6(3)
O(10)#4-Yb(2)-O(10)	49.6(5)
C(1)-O(1)-Yb(2)	144.0(5)
C(1)-O(2)-Yb(1)#4	138.1(6)

C(24)-O(3)-Yb(2)#7	137.0(6)
C(24)-O(4)-Yb(1)#8	153.7(5)
C(37)-O(5)-C(11)	100.3(10)
C(14)-O(6)-C(39)	101.5(14)
C(25)-O(7)-Yb(1)	116.5(7)
C(25)-O(8)-Yb(2)	162.3(9)
C(25)-O(8)-Yb(1)	79.6(7)
Yb(2)-O(8)-Yb(1)	114.4(2)
C(36)-O(9)-C(38)	117.0(15)
O(1)-C(1)-O(2)	123.3(8)
O(1)-C(1)-C(2)	118.7(8)
O(2)-C(1)-C(2)	118.0(9)
C(3)-C(2)-C(7)	120.0
C(3)-C(2)-C(1)	119.3(7)
C(7)-C(2)-C(1)	120.5(7)
C(4)-C(3)-C(2)	120.0
C(4)-C(3)-H(3A)	120.0
C(2)-C(3)-H(3A)	120.0
C(3)-C(4)-C(5)	120.0
C(3)-C(4)-H(4A)	120.0
C(5)-C(4)-H(4A)	120.0
C(4)-C(5)-C(6)	120.0
C(4)-C(5)-C(8)	115.1(9)
C(6)-C(5)-C(8)	124.6(9)
C(7)-C(6)-C(5)	120.0
C(7)-C(6)-H(6A)	120.0
C(5)-C(6)-H(6A)	120.0
C(6)-C(7)-C(2)	120.0
C(6)-C(7)-H(7A)	120.0
C(2)-C(7)-H(7A)	120.0
C(9)-C(8)-C(5)	140(2)
C(9)-C(8)-H(8A)	110.2
C(5)-C(8)-H(8A)	110.2
C(8)-C(9)-C(10)	134(2)
C(8)-C(9)-H(9A)	112.8
C(10)-C(9)-H(9A)	112.8

C(11)-C(10)-C(15)	120.0
C(11)-C(10)-C(9)	118.8(10)
C(15)-C(10)-C(9)	120.8(10)
C(12)-C(11)-C(10)	120.0
C(12)-C(11)-O(5)	114.4(8)
C(10)-C(11)-O(5)	125.6(9)
C(11)-C(12)-C(13)	120.0
C(11)-C(12)-H(12A)	120.0
C(13)-C(12)-H(12A)	120.0
C(14)-C(13)-C(12)	120.0
C(14)-C(13)-C(16)	119.1(10)
C(12)-C(13)-C(16)	120.9(10)
O(6)-C(14)-C(13)	125.4(11)
O(6)-C(14)-C(15)	114.3(11)
C(13)-C(14)-C(15)	120.0
C(14)-C(15)-C(10)	120.0
C(14)-C(15)-H(15A)	120.0
C(10)-C(15)-H(15A)	120.0
C(17)-C(16)-C(13)	124.0(18)
C(17)-C(16)-H(16A)	118.0
C(13)-C(16)-H(16A)	118.0
C(16)-C(17)-C(18)	113.8(17)
C(16)-C(17)-H(17A)	123.1
C(18)-C(17)-H(17A)	123.1
C(19)-C(18)-C(23)	120.0
C(19)-C(18)-C(17)	134.9(9)
C(23)-C(18)-C(17)	105.1(9)
C(18)-C(19)-C(20)	120.0
C(18)-C(19)-H(19A)	120.0
C(20)-C(19)-H(19A)	120.0
C(21)-C(20)-C(19)	120.0
C(21)-C(20)-H(20A)	120.0
C(19)-C(20)-H(20A)	120.0
C(20)-C(21)-C(22)	120.0
C(20)-C(21)-C(24)	119.8(7)
C(22)-C(21)-C(24)	120.1(7)

C(21)-C(22)-C(23)	120.0
C(21)-C(22)-H(22A)	120.0
C(23)-C(22)-H(22A)	120.0
C(22)-C(23)-C(18)	120.0
C(22)-C(23)-H(23A)	120.0
C(18)-C(23)-H(23A)	120.0
O(4)-C(24)-O(3)	125.8(8)
O(4)-C(24)-C(21)	117.1(8)
O(3)-C(24)-C(21)	117.1(9)
O(8)-C(25)-O(7)	118.6(10)
O(8)-C(25)-C(26)	122.9(11)
O(7)-C(25)-C(26)	118.5(11)
C(27)-C(26)-C(31)	120.0
C(27)-C(26)-C(25)	120.2(7)
C(31)-C(26)-C(25)	119.8(7)
C(26)-C(27)-C(28)	120.0
C(26)-C(27)-H(27A)	120.0
C(28)-C(27)-H(27A)	120.0
C(29)-C(28)-C(27)	120.0
C(29)-C(28)-H(28A)	120.0
C(27)-C(28)-H(28A)	120.0
C(28)-C(29)-C(30)	120.0
C(28)-C(29)-C(32)	112.7(8)
C(30)-C(29)-C(32)	127.3(8)
C(31)-C(30)-C(29)	120.0
C(31)-C(30)-H(30A)	120.0
C(29)-C(30)-H(30A)	120.0
C(30)-C(31)-C(26)	120.0
C(30)-C(31)-H(31A)	120.0
C(26)-C(31)-H(31A)	120.0
C(33)-C(32)-C(29)	127.3(16)
C(33)-C(32)-H(32A)	116.4
C(29)-C(32)-H(32A)	116.3
C(32)-C(33)-C(34)	120.5(17)
C(32)-C(33)-H(33A)	119.8
C(34)-C(33)-H(33A)	119.8

C(35)-C(34)-C(36)	128.6(13)
C(35)-C(34)-C(33)	128.8(17)
C(36)-C(34)-C(33)	102.5(17)
C(34)-C(35)-C(36)#9	101.6(19)
C(34)-C(35)-H(35A)	129.2
C(36)#9-C(35)-H(35A)	129.2
C(34)-C(36)-O(9)	133.3(16)
C(34)-C(36)-C(35)#9	129.7(17)
O(9)-C(36)-C(35)#9	97(2)
O(5)-C(37)-H(37A)	109.5
O(5)-C(37)-H(37B)	109.5
H(37A)-C(37)-H(37B)	109.5
O(5)-C(37)-H(37C)	109.5
H(37A)-C(37)-H(37C)	109.5
H(37B)-C(37)-H(37C)	109.5
O(9)-C(38)-H(38A)	109.5
O(9)-C(38)-H(38B)	109.5
H(38A)-C(38)-H(38B)	109.5
O(9)-C(38)-H(38C)	109.5
H(38A)-C(38)-H(38C)	109.5
H(38B)-C(38)-H(38C)	109.5
O(6)-C(39)-H(39A)	109.5
O(6)-C(39)-H(39B)	109.5
H(39A)-C(39)-H(39B)	109.5
O(6)-C(39)-H(39C)	109.5
H(39A)-C(39)-H(39C)	109.5
H(39B)-C(39)-H(39C)	109.5

Symmetry transformations used to generate equivalent atoms:

#1 -x,y+1/4,z+1/4 #2 x-1/4,-y+3/2,z+1/4 #3 x-1/2,-y+7/4,-z+5/4

#4 -x+1/4,y,-z+5/4 #5 -x-1/4,-y+7/4,z #6 x+1/4,y+1/4,-z+1

#7 x-1/4,y-1/4,-z+1 #8 x+1/4,-y+3/2,z-1/4 #9 -x,-y+2,-z+1

Table AA4. Anisotropic displacement parameters ($Å^2$ x 10^3) for Yb-PVDC-1. The anisotropic displacement factor exponent takes the form: $-2\pi^2[h^2 a^{*2} U^{11} + ... + 2 h k a^* b^* U^{12}]$

	U^{11}	U^{22}	U^{33}	U^{23}	U^{13}	U^{12}
Yb(1)	120(1)	100(1)	45(1)	0	0	-2(1)
Yb(2)	151(1)	98(1)	81(1)	0	38(1)	0
O(1)	120(5)	147(5)	93(4)	-36(4)	-3(3)	18(4)
O(2)	122(5)	118(4)	73(3)	-27(3)	-6(3)	11(4)
O(3)	141(5)	141(5)	132(5)	-64(4)	-46(4)	42(4)
O(4)	130(5)	153(5)	60(3)	-27(3)	-9(3)	31(4)
O(5)	520(20)	440(20)	153(8)	-2(11)	-54(11)	-175(18)
O(6)	450(20)	540(30)	182(11)	-10(14)	-89(13)	-140(20)
O(7)	241(8)	141(5)	61(4)	20(3)	34(5)	-10(6)
O(8)	211(8)	323(10)	55(4)	38(5)	-7(4)	142(8)
O(9)	318(15)	333(16)	212(11)	96(11)	-46(11)	-26(12)
O(10)	323(13)	275(11)	338(15)	-6(9)	22(10)	19(9)
C(1)	90(7)	142(9)	67(5)	-31(5)	-18(5)	1(6)
C(2)	129(7)	121(7)	79(6)	-34(5)	4(5)	-5(6)
C(3)	145(9)	211(11)	85(6)	-51(6)	-27(6)	3(7)
C(4)	159(9)	221(12)	127(8)	-91(8)	-33(7)	-12(9)
C(5)	178(12)	188(11)	114(8)	-69(8)	4(8)	-36(9)
C(6)	205(12)	166(10)	156(10)	-82(8)	10(9)	24(9)
C(7)	168(9)	161(9)	105(7)	-78(6)	-29(6)	26(8)
C(8)	290(15)	259(16)	172(12)	-125(11)	106(12)	-112(13)
C(9)	530(30)	252(18)	144(12)	-106(11)	53(15)	-100(19)
C(11)	257(18)	330(30)	260(20)	160(20)	-26(17)	-2(19)
C(12)	460(30)	410(30)	46(7)	-81(11)	12(11)	-280(30)
C(13)	390(20)	320(20)	86(9)	-115(12)	-26(12)	-160(18)
C(14)	360(20)	227(16)	141(13)	-147(13)	-22(12)	3(15)
C(15)	340(20)	265(17)	163(12)	-98(12)	56(14)	-97(17)
C(16)	296(19)	180(14)	226(15)	-84(11)	103(14)	-49(13)
C(17)	300(20)	320(30)	237(18)	-46(17)	76(16)	-39(18)
C(18)	199(13)	345(19)	109(9)	-150(11)	28(8)	-109(13)
C(19)	179(12)	400(20)	207(14)	-213(15)	-17(10)	-33(13)
C(20)	140(9)	288(14)	182(11)	-157(10)	-35(8)	25(10)

C(21)	121(8)	187(10)	95(7)	-81(7)	-13(6)	13(7)
C(22)	194(10)	216(11)	80(6)	-47(7)	-35(6)	-1(8)
C(23)	251(14)	290(16)	91(7)	-58(8)	-25(8)	-54(12)
C(24)	105(8)	154(9)	90(7)	-41(6)	-23(6)	22(7)
C(25)	178(12)	137(9)	73(7)	20(6)	30(7)	42(9)
C(26)	119(7)	151(8)	69(5)	48(5)	13(5)	18(6)
C(27)	142(8)	210(10)	106(7)	67(7)	8(7)	13(8)
C(28)	211(12)	255(13)	115(8)	92(8)	7(8)	8(11)
C(29)	229(13)	243(12)	88(7)	97(8)	-38(8)	-86(11)
C(30)	132(9)	470(20)	101(8)	104(11)	-11(7)	-18(11)
C(31)	140(9)	373(17)	78(7)	74(8)	-6(6)	-21(10)
C(32)	274(17)	309(18)	138(12)	91(12)	-17(11)	-129(15)
C(33)	330(20)	308(18)	135(13)	62(12)	5(12)	-118(17)
C(34)	270(19)	270(20)	90(9)	53(10)	11(11)	-107(16)
C(35)	440(30)	224(17)	188(15)	157(14)	-148(17)	-117(18)
C(36)	212(16)	228(17)	187(16)	98(15)	-49(14)	-15(13)
C(37)	860(60)	151(15)	580(40)	-170(20)	400(40)	0(20)
C(38)	310(20)	520(40)	205(16)	-30(20)	93(16)	60(20)
C(39)	530(30)	260(20)	560(40)	-150(20)	320(30)	0(20)

Table AA5. Hydrogen coordinates (x10^4) and isotropic displacement parameters (Å^2 x 10^3) for Yb-PVDC-1.

	x	y	z	U(eq)
H(3A)	648	8535	5863	177
H(4A)	373	8264	5634	203
H(6A)	2514	7869	5702	211
H(7A)	2789	8140	5931	174
H(8A)	672	7933	5461	288
H(9A)	2039	7738	5428	369
H(12A)	1728	7154	4977	367
H(15A)	251	7891	5182	308
H(16A)	141	7378	4696	281
H(17A)	1300	7008	4747	342
H(19A)	-321	7301	4444	314
H(20A)	-541	7109	4185	244
H(22A)	1179	6540	4281	196
H(23A)	1399	6732	4539	253
H(27A)	-1698	9368	5868	183
H(28A)	-1621	9590	5615	233
H(30A)	784	9404	5585	282
H(31A)	707	9182	5838	237
H(32A)	-981	9757	5386	288
H(33A)	528	9615	5324	310
H(35A)	-1081	10181	5209	339
H(37A)	2986	6923	5176	795
H(37B)	2670	7105	5030	795
H(37C)	2053	6918	5127	795
H(38A)	2051	9382	4909	521
H(38B)	1991	9696	4875	521
H(38C)	1357	9496	4794	521
H(39A)	-939	8127	4991	675
H(39B)	-44	8123	5063	675
H(39C)	-716	7926	5135	675

Table AA6. Crystal data and structure refinement for Yb-PVDC-2.

Identification code	**Yb-PVDC-2**	
Empirical formula	C78 H60 O18 Yb2	
Formula weight	1631.34	
Temperature	298(2) K	
Wavelength	0.71073 Å	
Crystal system	Orthorhombic	
Space group	Pnna	
Unit cell dimensions	a = 16.0798(14) Å	α = 90°.
	b = 22.7096(19) Å	β = 90°.
	c = 38.484(3) Å	γ = 90°.
Volume	14053(2) $Å^3$	
Z	4	
Density (calculated)	0.771 Mg/m^3	
Absorption coefficient	1.358 mm^{-1}	
F(000)	3248	
Crystal size	0.5 x 0.45 x 0.45 mm^3	
Theta range for data collection	3.44 to 28.29°.	
Index ranges	-21<=h<=21, -30<=k<=30, -51<=l<=51	
Reflections collected	123644	
Independent reflections	17435 [R(int) = 0.0580]	
Completeness to theta = 28.29°	99.8 %	
Absorption correction	Semi-empirical from equivalents	
Max. and min. transmission	0.543 and 0.468	
Refinement method	Full-matrix least-squares on F^2	
Data / restraints / parameters	17435 / 1228 / 529	
Goodness-of-fit on F^2	1.028	
Final R indices [I>2sigma(I)]	R1 = 0.0581, wR2 = 0.2103	
R indices (all data)	R1 = 0.1046, wR2 = 0.2528	
Largest diff. peak and hole	2.921 and -0.541 $e.Å^{-3}$	

Table AA7. Atomic coordinates (x 10^4) and equivalent isotropic displacement parameters (Å^2 x 10^3) for Yb-PVDC-2. U(eq) is defined as one third of the trace of the orthogonalized U^{ij} tensor.

	x	y	z	U(eq)
C(1)	1524(5)	756(3)	305(2)	48(2)
C(2A)	1830(20)	1165(11)	583(6)	55(2)
C(3A)	1305(16)	1298(10)	859(7)	68(4)
C(4A)	1581(19)	1660(11)	1127(6)	84(4)
C(5A)	2380(20)	1890(12)	1117(6)	89(3)
C(6A)	2906(17)	1757(13)	841(8)	82(3)
C(7A)	2630(20)	1395(13)	574(6)	66(3)
C(8A)	2877(19)	2251(18)	1377(8)	101(6)
C(9A)	2528(18)	2498(15)	1624(7)	98(6)
C(10A)	2935(15)	2808(13)	1915(5)	109(6)
C(11A)	3776(14)	2930(11)	1958(5)	115(6)
C(12A)	4054(14)	3205(13)	2259(6)	113(6)
C(13A)	3490(16)	3358(14)	2518(5)	107(6)
C(14A)	2649(15)	3236(12)	2475(5)	137(7)
C(15A)	2372(13)	2961(13)	2174(6)	120(7)
O(3A)	4492(18)	2796(16)	1722(7)	173(8)
O(4A)	1900(20)	3335(17)	2704(7)	193(9)
C(16A)	5240(30)	2970(20)	2010(13)	185(12)
C(17A)	1040(20)	3160(30)	2490(12)	212(16)
C(18A)	3810(20)	3670(20)	2835(8)	105(7)
C(19A)	4510(20)	3810(20)	2934(7)	107(7)
C(2B)	1776(12)	1185(6)	580(3)	55(2)
C(3B)	1194(9)	1469(6)	788(4)	68(4)
C(4B)	1455(11)	1847(6)	1050(3)	84(4)
C(5B)	2299(12)	1941(7)	1105(4)	89(3)
C(6B)	2882(10)	1657(8)	897(5)	82(3)
C(7B)	2620(11)	1279(7)	635(4)	66(3)
C(8B)	2506(11)	2298(10)	1426(5)	96(5)
C(9B)	3213(12)	2433(9)	1530(4)	106(5)
C(10B)	3429(11)	2760(7)	1853(3)	106(5)
C(11B)	4271(10)	2820(7)	1927(3)	134(5)

C(12B)	4523(8)	3120(8)	2224(4)	115(5)
C(13B)	3933(9)	3362(7)	2446(3)	102(5)
C(14B)	3091(8)	3302(7)	2372(3)	116(5)
C(15B)	2839(8)	3002(7)	2075(4)	119(5)
O(3B)	4927(14)	2550(10)	1720(5)	183(7)
O(4B)	2471(12)	3542(9)	2588(5)	160(6)
C(16B)	5873(19)	2802(16)	1755(9)	218(12)
C(17B)	1582(18)	3352(17)	2392(8)	234(12)
C(18B)	4155(14)	3567(12)	2803(5)	112(6)
C(19B)	4855(14)	3674(12)	2914(4)	112(6)
C(20)	4960(8)	3959(6)	3268(3)	111(4)
C(21)	5768(9)	4068(7)	3326(3)	132(5)
C(22)	6063(7)	4268(5)	3655(2)	98(3)
C(23)	5495(5)	4338(4)	3921(2)	59(2)
C(24)	4695(6)	4226(5)	3859(2)	81(3)
C(25)	4429(7)	4026(6)	3542(3)	108(4)
C(26)	5815(5)	4535(3)	4268(2)	46(2)
C(27)	6362(4)	5984(3)	4709(2)	44(2)
C(28)	6026(5)	6581(2)	4753(2)	72(2)
C(29)	5522(5)	6716(3)	5035(2)	91(3)
C(30)	5249(5)	7290(3)	5085(2)	122(4)
C(31)	5481(6)	7730(2)	4854(3)	136(5)
C(32)	5985(6)	7595(2)	4571(2)	150(5)
C(33)	6258(5)	7021(3)	4521(2)	124(4)
C(34)	5256(11)	8357(5)	4945(5)	181(6)
C(35)	5505(12)	8826(5)	4828(6)	192(7)
C(36)	5225(13)	9432(5)	4917(5)	195(7)
C(37)	4716(14)	9543(6)	5195(5)	234(10)
C(38)	5464(16)	9888(7)	4715(6)	260(10)
C(39)	6210(20)	10181(13)	4187(10)	393(19)
O(9)	5943(15)	9737(7)	4444(7)	327(10)
O(1)	2035(3)	583(2)	89(1)	53(1)
O(2)	765(3)	609(3)	303(1)	67(2)
O(5)	6560(3)	4672(2)	4301(1)	50(1)
O(6)	5284(3)	4545(2)	4513(1)	57(1)
O(7)	6114(3)	5554(2)	4898(1)	46(1)

O(8)	6940(3)	5901(2)	4495(1)	58(1)
Yb(1)	7500	5000	4674(1)	29(1)
Yb(2)	5000	5000	5000	32(1)

Table AA8. Bond lengths [Å] and angles [°] for Yb-PVDC-2.

C(1)-O(1)	1.232(8)
C(1)-O(2)	1.264(9)
C(1)-C(2B)	1.497(9)
C(1)-C(2A)	1.501(13)
C(2A)-C(3A)	1.3900
C(2A)-C(7A)	1.3900
C(3A)-C(4A)	1.3900
C(3A)-H(3AA)	0.9300
C(4A)-C(5A)	1.3900
C(4A)-H(4AA)	0.9300
C(5A)-C(6A)	1.3900
C(5A)-C(8A)	1.518(16)
C(6A)-C(7A)	1.3900
C(6A)-H(6AA)	0.9300
C(7A)-H(7AA)	0.9300
C(8A)-C(9A)	1.238(18)
C(8A)-H(8A)	0.9300
C(9A)-C(10A)	1.478(15)
C(9A)-H(9AA)	0.9300
C(10A)-C(11A)	1.3900
C(10A)-C(15A)	1.3900
C(11A)-C(12A)	1.3900
C(11A)-O(3A)	1.497(18)
C(12A)-C(13A)	1.3900
C(12A)-H(12A)	0.9300
C(13A)-C(14A)	1.3900
C(13A)-C(18A)	1.498(15)
C(14A)-C(15A)	1.3900
C(14A)-O(4A)	1.514(19)
C(15A)-H(15A)	0.9300
O(3A)-C(16A)	1.69(2)
O(4A)-C(17A)	1.65(2)
C(16A)-H(16A)	0.9600

C(16A)-H(16B)	0.9600
C(16A)-H(16C)	0.9600
C(17A)-H(17A)	0.9600
C(17A)-H(17B)	0.9600
C(17A)-H(17C)	0.9600
C(18A)-C(19A)	1.231(18)
C(18A)-H(18A)	0.9300
C(19A)-C(20)	1.514(15)
C(19A)-H(19A)	0.9300
C(2B)-C(3B)	1.3900
C(2B)-C(7B)	1.3900
C(3B)-C(4B)	1.3900
C(3B)-H(3BA)	0.9300
C(4B)-C(5B)	1.3900
C(4B)-H(4BA)	0.9300
C(5B)-C(6B)	1.3900
C(5B)-C(8B)	1.514(12)
C(6B)-C(7B)	1.3900
C(6B)-H(6BA)	0.9300
C(7B)-H(7BA)	0.9300
C(8B)-C(9B)	1.244(15)
C(8B)-H(8BA)	0.9300
C(9B)-C(10B)	1.490(12)
C(9B)-H(9BA)	0.9300
C(10B)-C(11B)	1.3900
C(10B)-C(15B)	1.3900
C(11B)-C(12B)	1.3900
C(11B)-O(3B)	1.457(15)
C(12B)-C(13B)	1.3900
C(12B)-H(12B)	0.9300
C(13B)-C(14B)	1.3900
C(13B)-C(18B)	1.493(13)
C(14B)-C(15B)	1.3900
C(14B)-O(4B)	1.410(14)
C(15B)-H(15B)	0.9300
O(3B)-C(16B)	1.63(2)

O(4B)-C(17B)	1.67(2)
C(16B)-H(16D)	0.9600
C(16B)-H(16E)	0.9600
C(16B)-H(16F)	0.9600
C(17B)-H(17D)	0.9600
C(17B)-H(17E)	0.9600
C(17B)-H(17F)	0.9600
C(18B)-C(19B)	1.228(16)
C(18B)-H(18B)	0.9300
C(19B)-C(20)	1.518(13)
C(19B)-H(19B)	0.9300
C(20)-C(21)	1.341(16)
C(20)-C(25)	1.362(15)
C(21)-C(22)	1.426(12)
C(21)-H(21A)	0.9300
C(22)-C(23)	1.383(11)
C(22)-H(22A)	0.9300
C(23)-C(24)	1.332(11)
C(23)-C(26)	1.498(9)
C(24)-C(25)	1.373(12)
C(24)-H(24A)	0.9300
C(25)-H(25A)	0.9300
C(26)-O(5)	1.244(8)
C(26)-O(6)	1.273(8)
C(27)-O(8)	1.256(8)
C(27)-O(7)	1.280(8)
C(27)-C(28)	1.469(8)
C(27)-Yb(1)	2.891(7)
C(28)-C(29)	1.3900
C(28)-C(33)	1.3900
C(29)-C(30)	1.3900
C(29)-H(29A)	0.9300
C(30)-C(31)	1.3900
C(30)-H(30A)	0.9300
C(31)-C(32)	1.3900
C(31)-C(34)	1.511(12)

C(32)-C(33)	1.3900
C(32)-H(32A)	0.9300
C(33)-H(33A)	0.9300
C(34)-C(35)	1.222(15)
C(34)-H(34A)	0.9300
C(35)-C(36)	1.488(13)
C(35)-H(35A)	0.9300
C(36)-C(38)	1.353(14)
C(36)-C(37)	1.371(14)
C(37)-C(38)#1	1.370(14)
C(37)-H(37A)	0.9300
C(38)-O(9)	1.34(2)
C(38)-C(37)#1	1.370(14)
C(39)-O(9)	1.48(3)
C(39)-H(39A)	0.9600
C(39)-H(39B)	0.9600
C(39)-H(39C)	0.9600
O(1)-Yb(1)#2	2.206(5)
O(2)-Yb(2)#3	2.188(5)
O(5)-Yb(1)	2.215(4)
O(6)-Yb(2)	2.189(5)
O(7)-Yb(2)	2.224(5)
O(7)-Yb(1)	2.700(5)
O(8)-Yb(1)	2.339(5)
Yb(1)-O(1)#4	2.206(5)
Yb(1)-O(1)#5	2.206(5)
Yb(1)-O(5)#6	2.215(5)
Yb(1)-O(8)#6	2.339(5)
Yb(1)-O(7)#6	2.701(5)
Yb(1)-C(27)#6	2.891(7)
Yb(1)-Yb(2)	4.2110(3)
Yb(1)-Yb(2)#6	4.2110(3)
Yb(2)-O(2)#7	2.188(5)
Yb(2)-O(2)#5	2.188(5)
Yb(2)-O(6)#8	2.189(5)
Yb(2)-O(7)#8	2.224(5)

Yb(2)-Yb(1)#8	4.2110(4)

O(1)-C(1)-O(2)	123.8(6)
O(1)-C(1)-C(2B)	120.2(10)
O(2)-C(1)-C(2B)	116.0(9)
O(1)-C(1)-C(2A)	117.3(14)
O(2)-C(1)-C(2A)	118.9(14)
C(3A)-C(2A)-C(7A)	120.0
C(3A)-C(2A)-C(1)	119(2)
C(7A)-C(2A)-C(1)	121(2)
C(4A)-C(3A)-C(2A)	120.0
C(4A)-C(3A)-H(3AA)	120.0
C(2A)-C(3A)-H(3AA)	120.0
C(5A)-C(4A)-C(3A)	120.0
C(5A)-C(4A)-H(4AA)	120.0
C(3A)-C(4A)-H(4AA)	120.0
C(6A)-C(5A)-C(4A)	120.0
C(6A)-C(5A)-C(8A)	108(2)
C(4A)-C(5A)-C(8A)	132(2)
C(7A)-C(6A)-C(5A)	120.0
C(7A)-C(6A)-H(6AA)	120.0
C(5A)-C(6A)-H(6AA)	120.0
C(6A)-C(7A)-C(2A)	120.0
C(6A)-C(7A)-H(7AA)	120.0
C(2A)-C(7A)-H(7AA)	120.0
C(9A)-C(8A)-C(5A)	121(2)
C(9A)-C(8A)-H(8A)	119.6
C(5A)-C(8A)-H(8A)	119.6
C(8A)-C(9A)-C(10A)	127(2)
C(8A)-C(9A)-H(9AA)	116.7
C(10A)-C(9A)-H(9AA)	116.7
C(11A)-C(10A)-C(15A)	120.0
C(11A)-C(10A)-C(9A)	128.0(18)
C(15A)-C(10A)-C(9A)	112.0(18)
C(12A)-C(11A)-C(10A)	120.0
C(12A)-C(11A)-O(3A)	110.4(13)

C(10A)-C(11A)-O(3A)	129.6(13)
C(13A)-C(12A)-C(11A)	120.0
C(13A)-C(12A)-H(12A)	120.0
C(11A)-C(12A)-H(12A)	120.0
C(12A)-C(13A)-C(14A)	120.0
C(12A)-C(13A)-C(18A)	118(2)
C(14A)-C(13A)-C(18A)	122(2)
C(15A)-C(14A)-C(13A)	120.0
C(15A)-C(14A)-O(4A)	107.1(14)
C(13A)-C(14A)-O(4A)	132.9(14)
C(14A)-C(15A)-C(10A)	120.0
C(14A)-C(15A)-H(15A)	120.0
C(10A)-C(15A)-H(15A)	120.0
C(11A)-O(3A)-C(16A)	96(2)
C(14A)-O(4A)-C(17A)	110.0(16)
O(3A)-C(16A)-H(16A)	109.5
O(3A)-C(16A)-H(16B)	109.5
H(16A)-C(16A)-H(16B)	109.5
O(3A)-C(16A)-H(16C)	109.5
H(16A)-C(16A)-H(16C)	109.5
H(16B)-C(16A)-H(16C)	109.5
O(4A)-C(17A)-H(17A)	109.5
O(4A)-C(17A)-H(17B)	109.5
H(17A)-C(17A)-H(17B)	109.5
O(4A)-C(17A)-H(17C)	109.5
H(17A)-C(17A)-H(17C)	109.5
H(17B)-C(17A)-H(17C)	109.5
C(19A)-C(18A)-C(13A)	134(3)
C(19A)-C(18A)-H(18A)	113.1
C(13A)-C(18A)-H(18A)	113.1
C(18A)-C(19A)-C(20)	140(3)
C(18A)-C(19A)-H(19A)	110.2
C(20)-C(19A)-H(19A)	110.2
C(3B)-C(2B)-C(7B)	120.0
C(3B)-C(2B)-C(1)	121.8(12)
C(7B)-C(2B)-C(1)	118.2(12)

C(2B)-C(3B)-C(4B)	120.0
C(2B)-C(3B)-H(3BA)	120.0
C(4B)-C(3B)-H(3BA)	120.0
C(3B)-C(4B)-C(5B)	120.0
C(3B)-C(4B)-H(4BA)	120.0
C(5B)-C(4B)-H(4BA)	120.0
C(6B)-C(5B)-C(4B)	120.0
C(6B)-C(5B)-C(8B)	124.7(14)
C(4B)-C(5B)-C(8B)	114.8(14)
C(7B)-C(6B)-C(5B)	120.0
C(7B)-C(6B)-H(6BA)	120.0
C(5B)-C(6B)-H(6BA)	120.0
C(6B)-C(7B)-C(2B)	120.0
C(6B)-C(7B)-H(7BA)	120.0
C(2B)-C(7B)-H(7BA)	120.0
C(9B)-C(8B)-C(5B)	126.5(17)
C(9B)-C(8B)-H(8BA)	116.7
C(5B)-C(8B)-H(8BA)	116.7
C(8B)-C(9B)-C(10B)	127.2(17)
C(8B)-C(9B)-H(9BA)	116.4
C(10B)-C(9B)-H(9BA)	116.4
C(11B)-C(10B)-C(15B)	120.0
C(11B)-C(10B)-C(9B)	116.5(12)
C(15B)-C(10B)-C(9B)	123.5(12)
C(12B)-C(11B)-C(10B)	120.0
C(12B)-C(11B)-O(3B)	116.4(11)
C(10B)-C(11B)-O(3B)	123.5(11)
C(11B)-C(12B)-C(13B)	120.0
C(11B)-C(12B)-H(12B)	120.0
C(13B)-C(12B)-H(12B)	120.0
C(14B)-C(13B)-C(12B)	120.0
C(14B)-C(13B)-C(18B)	116.8(12)
C(12B)-C(13B)-C(18B)	121.8(12)
C(13B)-C(14B)-C(15B)	120.0
C(13B)-C(14B)-O(4B)	122.1(10)
C(15B)-C(14B)-O(4B)	117.9(10)

C(14B)-C(15B)-C(10B)	120.0
C(14B)-C(15B)-H(15B)	120.0
C(10B)-C(15B)-H(15B)	120.0
C(11B)-O(3B)-C(16B)	118.9(17)
C(14B)-O(4B)-C(17B)	103.8(14)
O(3B)-C(16B)-H(16D)	109.5
O(3B)-C(16B)-H(16E)	109.5
H(16D)-C(16B)-H(16E)	109.5
O(3B)-C(16B)-H(16F)	109.5
H(16D)-C(16B)-H(16F)	109.5
H(16E)-C(16B)-H(16F)	109.5
O(4B)-C(17B)-H(17D)	109.5
O(4B)-C(17B)-H(17E)	109.5
H(17D)-C(17B)-H(17E)	109.5
O(4B)-C(17B)-H(17F)	109.5
H(17D)-C(17B)-H(17F)	109.5
H(17E)-C(17B)-H(17F)	109.5
C(19B)-C(18B)-C(13B)	127.0(17)
C(19B)-C(18B)-H(18B)	116.5
C(13B)-C(18B)-H(18B)	116.5
C(18B)-C(19B)-C(20)	119.9(16)
C(18B)-C(19B)-H(19B)	120.0
C(20)-C(19B)-H(19B)	120.0
C(21)-C(20)-C(25)	117.4(9)
C(21)-C(20)-C(19A)	130.2(19)
C(25)-C(20)-C(19A)	112.3(18)
C(21)-C(20)-C(19B)	109.5(13)
C(25)-C(20)-C(19B)	132.1(13)
C(20)-C(21)-C(22)	121.8(10)
C(20)-C(21)-H(21A)	119.1
C(22)-C(21)-H(21A)	119.1
C(23)-C(22)-C(21)	118.4(10)
C(23)-C(22)-H(22A)	120.8
C(21)-C(22)-H(22A)	120.8
C(24)-C(23)-C(22)	118.9(7)
C(24)-C(23)-C(26)	123.2(7)

C(22)-C(23)-C(26)	117.9(7)
C(23)-C(24)-C(25)	121.6(9)
C(23)-C(24)-H(24A)	119.2
C(25)-C(24)-H(24A)	119.2
C(20)-C(25)-C(24)	121.9(10)
C(20)-C(25)-H(25A)	119.1
C(24)-C(25)-H(25A)	119.1
O(5)-C(26)-O(6)	124.5(6)
O(5)-C(26)-C(23)	119.7(6)
O(6)-C(26)-C(23)	115.7(7)
O(8)-C(27)-O(7)	119.2(6)
O(8)-C(27)-C(28)	119.0(6)
O(7)-C(27)-C(28)	121.6(6)
O(8)-C(27)-Yb(1)	52.1(3)
O(7)-C(27)-Yb(1)	68.6(4)
C(28)-C(27)-Yb(1)	162.0(5)
C(29)-C(28)-C(33)	120.0
C(29)-C(28)-C(27)	120.5(5)
C(33)-C(28)-C(27)	119.4(5)
C(30)-C(29)-C(28)	120.0
C(30)-C(29)-H(29A)	120.0
C(28)-C(29)-H(29A)	120.0
C(29)-C(30)-C(31)	120.0
C(29)-C(30)-H(30A)	120.0
C(31)-C(30)-H(30A)	120.0
C(32)-C(31)-C(30)	120.0
C(32)-C(31)-C(34)	122.0(9)
C(30)-C(31)-C(34)	117.6(9)
C(33)-C(32)-C(31)	120.0
C(33)-C(32)-H(32A)	120.0
C(31)-C(32)-H(32A)	120.0
C(32)-C(33)-C(28)	120.0
C(32)-C(33)-H(33A)	120.0
C(28)-C(33)-H(33A)	120.0
C(35)-C(34)-C(31)	131.0(16)
C(35)-C(34)-H(34A)	114.5

C(31)-C(34)-H(34A)	114.5
C(34)-C(35)-C(36)	128.4(17)
C(34)-C(35)-H(35A)	115.8
C(36)-C(35)-H(35A)	115.8
C(38)-C(36)-C(37)	118.7(9)
C(38)-C(36)-C(35)	119.3(16)
C(37)-C(36)-C(35)	122.0(16)
C(38)#1-C(37)-C(36)	119.8(11)
C(38)#1-C(37)-H(37A)	120.1
C(36)-C(37)-H(37A)	120.1
O(9)-C(38)-C(36)	114.6(17)
O(9)-C(38)-C(37)#1	124.0(18)
C(36)-C(38)-C(37)#1	121.1(12)
O(9)-C(39)-H(39A)	109.5
O(9)-C(39)-H(39B)	109.5
H(39A)-C(39)-H(39B)	109.5
O(9)-C(39)-H(39C)	109.5
H(39A)-C(39)-H(39C)	109.5
H(39B)-C(39)-H(39C)	109.5
C(38)-O(9)-C(39)	121(2)
C(1)-O(1)-Yb(1)#2	154.8(5)
C(1)-O(2)-Yb(2)#3	135.4(5)
C(26)-O(5)-Yb(1)	143.8(4)
C(26)-O(6)-Yb(2)	141.5(5)
C(27)-O(7)-Yb(2)	141.5(4)
C(27)-O(7)-Yb(1)	85.3(4)
Yb(2)-O(7)-Yb(1)	117.21(18)
C(27)-O(8)-Yb(1)	102.9(4)
O(1)#4-Yb(1)-O(1)#5	87.2(3)
O(1)#4-Yb(1)-O(5)#6	92.13(19)
O(1)#5-Yb(1)-O(5)#6	154.56(18)
O(1)#4-Yb(1)-O(5)	154.56(18)
O(1)#5-Yb(1)-O(5)	92.13(19)
O(5)#6-Yb(1)-O(5)	99.1(3)
O(1)#4-Yb(1)-O(8)	79.6(2)
O(1)#5-Yb(1)-O(8)	127.48(19)

O(5)#6-Yb(1)-O(8)	77.15(18)
O(5)-Yb(1)-O(8)	80.77(19)
O(1)#4-Yb(1)-O(8)#6	127.47(19)
O(1)#5-Yb(1)-O(8)#6	79.6(2)
O(5)#6-Yb(1)-O(8)#6	80.77(19)
O(5)-Yb(1)-O(8)#6	77.15(18)
O(8)-Yb(1)-O(8)#6	145.7(3)
O(1)#4-Yb(1)-O(7)	76.63(16)
O(1)#5-Yb(1)-O(7)	76.67(16)
O(5)#6-Yb(1)-O(7)	127.86(16)
O(5)-Yb(1)-O(7)	78.47(16)
O(8)-Yb(1)-O(7)	50.86(16)
O(8)#6-Yb(1)-O(7)	145.02(17)
O(1)#4-Yb(1)-O(7)#6	76.66(16)
O(1)#5-Yb(1)-O(7)#6	76.63(16)
O(5)#6-Yb(1)-O(7)#6	78.47(16)
O(5)-Yb(1)-O(7)#6	127.86(16)
O(8)-Yb(1)-O(7)#6	145.02(17)
O(8)#6-Yb(1)-O(7)#6	50.86(16)
O(7)-Yb(1)-O(7)#6	142.81(19)
O(1)#4-Yb(1)-C(27)	73.54(19)
O(1)#5-Yb(1)-C(27)	102.5(2)
O(5)#6-Yb(1)-C(27)	101.7(2)
O(5)-Yb(1)-C(27)	81.82(19)
O(8)-Yb(1)-C(27)	25.07(18)
O(8)#6-Yb(1)-C(27)	158.94(19)
O(7)-Yb(1)-C(27)	26.19(17)
O(7)#6-Yb(1)-C(27)	150.20(17)
O(1)#4-Yb(1)-C(27)#6	102.5(2)
O(1)#5-Yb(1)-C(27)#6	73.54(19)
O(5)#6-Yb(1)-C(27)#6	81.82(19)
O(5)-Yb(1)-C(27)#6	101.7(2)
O(8)-Yb(1)-C(27)#6	158.94(19)
O(8)#6-Yb(1)-C(27)#6	25.07(18)
O(7)-Yb(1)-C(27)#6	150.19(17)
O(7)#6-Yb(1)-C(27)#6	26.19(17)

C(27)-Yb(1)-C(27)#6	174.7(3)
O(1)#4-Yb(1)-Yb(2)	96.18(13)
O(1)#5-Yb(1)-Yb(2)	57.38(13)
O(5)#6-Yb(1)-Yb(2)	147.67(13)
O(5)-Yb(1)-Yb(2)	62.72(13)
O(8)-Yb(1)-Yb(2)	73.76(13)
O(8)#6-Yb(1)-Yb(2)	117.08(14)
O(7)-Yb(1)-Yb(2)	28.02(10)
O(7)#6-Yb(1)-Yb(2)	133.86(9)
C(27)-Yb(1)-Yb(2)	51.83(15)
C(27)#6-Yb(1)-Yb(2)	126.18(14)
O(1)#4-Yb(1)-Yb(2)#6	57.38(13)
O(1)#5-Yb(1)-Yb(2)#6	96.18(13)
O(5)#6-Yb(1)-Yb(2)#6	62.71(13)
O(5)-Yb(1)-Yb(2)#6	147.66(13)
O(8)-Yb(1)-Yb(2)#6	117.08(14)
O(8)#6-Yb(1)-Yb(2)#6	73.76(13)
O(7)-Yb(1)-Yb(2)#6	133.86(9)
O(7)#6-Yb(1)-Yb(2)#6	28.02(10)
C(27)-Yb(1)-Yb(2)#6	126.18(14)
C(27)#6-Yb(1)-Yb(2)#6	51.83(15)
Yb(2)-Yb(1)-Yb(2)#6	145.352(9)
O(2)#7-Yb(2)-O(2)#5	179.999(2)
O(2)#7-Yb(2)-O(6)#8	92.3(2)
O(2)#5-Yb(2)-O(6)#8	87.7(2)
O(2)#7-Yb(2)-O(6)	87.7(2)
O(2)#5-Yb(2)-O(6)	92.3(2)
O(6)#8-Yb(2)-O(6)	179.998(1)
O(2)#7-Yb(2)-O(7)	90.0(2)
O(2)#5-Yb(2)-O(7)	90.0(2)
O(6)#8-Yb(2)-O(7)	92.97(18)
O(6)-Yb(2)-O(7)	87.03(18)
O(2)#7-Yb(2)-O(7)#8	90.0(2)
O(2)#5-Yb(2)-O(7)#8	90.0(2)
O(6)#8-Yb(2)-O(7)#8	87.04(18)
O(6)-Yb(2)-O(7)#8	92.96(18)

O(7)-Yb(2)-O(7)#8	179.996(1)
O(2)#7-Yb(2)-Yb(1)#8	67.78(15)
O(2)#5-Yb(2)-Yb(1)#8	112.22(15)
O(6)#8-Yb(2)-Yb(1)#8	63.01(14)
O(6)-Yb(2)-Yb(1)#8	116.99(14)
O(7)-Yb(2)-Yb(1)#8	145.23(12)
O(7)#8-Yb(2)-Yb(1)#8	34.78(12)
O(2)#7-Yb(2)-Yb(1)	112.22(15)
O(2)#5-Yb(2)-Yb(1)	67.78(15)
O(6)#8-Yb(2)-Yb(1)	116.99(14)
O(6)-Yb(2)-Yb(1)	63.01(14)
O(7)-Yb(2)-Yb(1)	34.77(12)
O(7)#8-Yb(2)-Yb(1)	145.22(12)
Yb(1)#8-Yb(2)-Yb(1)	180.0

Symmetry transformations used to generate equivalent atoms:

#1 -x+1,-y+2,-z+1 #2 x-1/2,-y+1/2,z-1/2 #3 -x+1/2,y-1/2,-z+1/2

#4 -x+1,y+1/2,z+1/2 #5 x+1/2,-y+1/2,z+1/2 #6 -x+3/2,-y+1,z

#7 -x+1/2,y+1/2,-z+1/2 #8 -x+1,-y+1,-z+1

Table AA9. Anisotropic displacement parameters ($Å^2 x\ 10^3$) for Yb-PVDC-2. The anisotropic displacement factor exponent takes the form: $-2\pi^2[h^2 a^{*2} U^{11} + ... + 2\ h\ k\ a^*\ b^*\ U^{12}]$

	U^{11}	U^{22}	U^{33}	U^{23}	U^{13}	U^{12}
C(1)	58(4)	52(4)	34(3)	-15(3)	-4(3)	-4(3)
C(2A)	60(4)	66(4)	38(3)	-23(3)	-8(3)	-9(4)
C(3A)	78(6)	76(7)	52(6)	-24(5)	-5(5)	3(6)
C(4A)	103(7)	84(8)	65(6)	-40(6)	-3(5)	5(6)
C(5A)	104(6)	95(6)	68(5)	-45(4)	-22(4)	-9(5)
C(6A)	85(5)	88(7)	71(6)	-29(5)	-23(5)	-20(5)
C(7A)	76(5)	73(7)	49(6)	-19(5)	-13(4)	-11(5)
C(8A)	108(12)	111(11)	84(10)	-41(9)	-19(10)	-8(10)
C(9A)	109(12)	103(11)	82(10)	-39(9)	-22(10)	-11(11)
C(10A)	126(11)	114(11)	88(10)	-38(9)	-37(10)	-8(11)
C(11A)	131(10)	127(10)	87(9)	-47(9)	-17(9)	-1(10)
C(12A)	135(11)	118(10)	87(10)	-44(9)	-23(9)	-7(10)
C(13A)	120(10)	114(10)	86(10)	-37(9)	-20(9)	-14(10)
C(14A)	147(10)	149(12)	116(11)	-35(10)	-11(10)	-12(11)
C(15A)	136(12)	125(12)	99(11)	-27(10)	-17(10)	-19(11)
O(3A)	199(15)	195(16)	125(13)	-71(14)	-8(13)	16(15)
O(4A)	201(16)	218(18)	159(16)	-43(16)	39(14)	-18(17)
C(16A)	164(15)	203(18)	188(18)	-11(15)	-21(14)	-13(15)
C(17A)	192(18)	230(20)	220(20)	-4(17)	15(16)	-26(17)
C(18A)	110(12)	117(12)	88(11)	-30(10)	-20(10)	-5(11)
C(19A)	114(12)	128(13)	78(10)	-41(10)	-33(10)	-4(11)
C(2B)	60(4)	66(4)	38(3)	-23(3)	-8(3)	-9(4)
C(3B)	78(6)	76(7)	52(6)	-24(5)	-5(5)	3(6)
C(4B)	103(7)	84(8)	65(6)	-40(6)	-3(5)	5(6)
C(5B)	104(6)	95(6)	68(5)	-45(4)	-22(4)	-9(5)
C(6B)	85(5)	88(7)	71(6)	-29(5)	-23(5)	-20(5)
C(7B)	76(5)	73(7)	49(6)	-19(5)	-13(4)	-11(5)
C(8B)	108(10)	104(9)	76(8)	-54(7)	-13(8)	-4(9)
C(9B)	114(10)	116(10)	86(9)	-42(8)	-21(8)	-23(9)
C(10B)	120(9)	115(9)	83(8)	-45(7)	-26(8)	-9(9)
C(11B)	155(10)	156(10)	89(9)	-59(8)	-6(9)	-2(9)

C(12B)	145(10)	127(10)	73(8)	-44(8)	-8(8)	1(10)
C(13B)	120(9)	114(9)	72(8)	-43(7)	-31(7)	-16(8)
C(14B)	133(9)	127(9)	88(8)	-46(7)	-29(8)	-19(9)
C(15B)	130(9)	128(10)	100(9)	-35(8)	-36(8)	-15(9)
O(3B)	199(13)	211(15)	140(11)	-87(11)	32(12)	37(12)
O(4B)	174(12)	179(13)	127(11)	-84(10)	-7(9)	-40(10)
C(16B)	200(15)	251(19)	203(18)	-33(15)	4(15)	20(15)
C(17B)	185(15)	261(19)	256(19)	23(16)	-31(15)	-26(15)
C(18B)	121(11)	129(10)	85(8)	-42(8)	-30(8)	-13(10)
C(19B)	122(12)	140(12)	72(8)	-42(8)	-33(8)	-6(10)
C(20)	116(8)	158(9)	60(6)	-45(6)	-23(6)	-23(7)
C(21)	134(9)	219(12)	44(5)	-59(7)	5(6)	-31(9)
C(22)	86(6)	164(10)	44(5)	-49(6)	3(4)	-20(7)
C(23)	65(5)	75(5)	38(4)	-27(4)	-8(3)	0(4)
C(24)	64(5)	120(8)	61(5)	-33(5)	-12(4)	-10(5)
C(25)	80(7)	163(10)	80(7)	-40(7)	-27(5)	-21(7)
C(26)	59(4)	50(4)	29(3)	-11(3)	-8(3)	7(3)
C(27)	47(4)	30(3)	55(4)	3(3)	-7(3)	6(3)
C(28)	87(6)	31(4)	96(6)	3(4)	14(5)	16(4)
C(29)	109(8)	46(5)	120(8)	-9(5)	37(6)	11(5)
C(30)	121(9)	66(7)	180(11)	-15(7)	46(8)	26(7)
C(31)	142(10)	52(6)	215(13)	2(7)	28(9)	35(7)
C(32)	187(12)	55(6)	208(13)	55(8)	55(10)	34(7)
C(33)	163(11)	46(5)	163(10)	28(6)	57(9)	7(6)
C(34)	177(13)	64(7)	302(17)	-20(9)	5(13)	39(9)
C(35)	203(15)	54(7)	321(17)	0(10)	28(14)	31(9)
C(36)	228(16)	49(7)	308(18)	-13(9)	50(14)	47(9)
C(37)	280(20)	66(9)	350(20)	-9(12)	77(18)	33(12)
C(38)	320(20)	76(9)	390(20)	-19(12)	135(18)	54(13)
C(39)	550(50)	160(20)	470(40)	50(20)	190(40)	-50(30)
O(9)	420(20)	107(10)	450(20)	14(13)	178(19)	50(13)
O(1)	54(3)	62(3)	44(3)	-23(2)	3(2)	-5(3)
O(2)	54(3)	86(4)	61(3)	-30(3)	2(3)	-19(3)
O(5)	52(3)	65(3)	34(2)	-12(2)	-13(2)	4(3)
O(6)	69(3)	67(3)	36(3)	-15(2)	0(2)	-4(3)
O(7)	55(3)	36(2)	47(3)	1(2)	-4(2)	-4(2)

O(8)	69(4)	46(3)	60(3)	10(2)	12(3)	10(3)
Yb(1)	36(1)	27(1)	24(1)	0	0	2(1)
Yb(2)	34(1)	33(1)	30(1)	-2(1)	-2(1)	4(1)

Table AA10. Hydrogen coordinates (x 10^4) and isotropic displacement parameters ($Å^2$ x 10^3) for Yb-PVDC-2

	x	y	z	U(eq)
H(3AA)	769	1144	866	82
H(4AA)	1230	1749	1311	100
H(6AA)	3442	1911	835	98
H(7AA)	2980	1306	389	79
H(8A)	3450	2288	1350	121
H(9AA)	1950	2488	1626	117
H(12A)	4616	3286	2287	136
H(15A)	1809	2880	2146	144
H(16A)	5779	2886	1911	277
H(16B)	5172	2744	2218	277
H(16C)	5211	3383	2065	277
H(17A)	564	3241	2633	318
H(17B)	1052	2754	2429	318
H(17C)	1005	3397	2282	318
H(18A)	3391	3766	2991	126
H(19A)	4866	3847	2746	128
H(3BA)	629	1407	751	82
H(4BA)	1065	2037	1189	100
H(6BA)	3447	1720	934	98
H(7BA)	3010	1089	496	79
H(8BA)	2059	2429	1558	115
H(9BA)	3656	2317	1390	127
H(12B)	5086	3160	2273	138
H(15B)	2276	2962	2026	143
H(16D)	6246	2554	1626	327
H(16E)	6034	2805	1995	327
H(16F)	5897	3195	1664	327
H(17D)	1120	3492	2527	351
H(17E)	1553	2931	2373	351
H(17F)	1564	3523	2164	351
H(18B)	3716	3619	2957	134

H(19B)	5320	3580	2782	134
H(21A)	6146	4011	3146	159
H(22A)	6624	4349	3689	118
H(24A)	4309	4285	4035	98
H(25A)	3870	3933	3512	129
H(29A)	5367	6422	5190	110
H(30A)	4912	7381	5274	147
H(32A)	6141	7889	4416	180
H(33A)	6595	6931	4332	149
H(34A)	4861	8393	5120	217
H(35A)	5923	8800	4662	231
H(37A)	4494	9232	5323	351
H(39A)	6577	9999	4020	589
H(39B)	6505	10493	4303	589
H(39C)	5737	10339	4069	589

Table AA11. Torsion angles [°] for Yb-PVDC-2.

O(1)-C(1)-C(2A)-C(3A)	-170.4(12)
O(2)-C(1)-C(2A)-C(3A)	10(2)
C(2B)-C(1)-C(2A)-C(3A)	49(27)
O(1)-C(1)-C(2A)-C(7A)	7(2)
O(2)-C(1)-C(2A)-C(7A)	-172.3(13)
C(2B)-C(1)-C(2A)-C(7A)	-133(29)
C(7A)-C(2A)-C(3A)-C(4A)	0.0
C(1)-C(2A)-C(3A)-C(4A)	178(2)
C(2A)-C(3A)-C(4A)-C(5A)	0.0
C(3A)-C(4A)-C(5A)-C(6A)	0.0
C(3A)-C(4A)-C(5A)-C(8A)	-175(4)
C(4A)-C(5A)-C(6A)-C(7A)	0.0
C(8A)-C(5A)-C(6A)-C(7A)	176(3)
C(5A)-C(6A)-C(7A)-C(2A)	0.0
C(3A)-C(2A)-C(7A)-C(6A)	0.0
C(1)-C(2A)-C(7A)-C(6A)	-178(2)
C(6A)-C(5A)-C(8A)-C(9A)	170(4)
C(4A)-C(5A)-C(8A)-C(9A)	-15(6)
C(5A)-C(8A)-C(9A)-C(10A)	173(4)
C(8A)-C(9A)-C(10A)-C(11A)	6(6)
C(8A)-C(9A)-C(10A)-C(15A)	-171(4)
C(15A)-C(10A)-C(11A)-C(12A)	0.0
C(9A)-C(10A)-C(11A)-C(12A)	-177(3)
C(15A)-C(10A)-C(11A)-O(3A)	178(2)
C(9A)-C(10A)-C(11A)-O(3A)	1(4)
C(10A)-C(11A)-C(12A)-C(13A)	0.0
O(3A)-C(11A)-C(12A)-C(13A)	-178.7(18)
C(11A)-C(12A)-C(13A)-C(14A)	0.0
C(11A)-C(12A)-C(13A)-C(18A)	-179(3)
C(12A)-C(13A)-C(14A)-C(15A)	0.0
C(18A)-C(13A)-C(14A)-C(15A)	179(4)
C(12A)-C(13A)-C(14A)-O(4A)	179(2)
C(18A)-C(13A)-C(14A)-O(4A)	-2(4)

C(13A)-C(14A)-C(15A)-C(10A)	0.0
O(4A)-C(14A)-C(15A)-C(10A)	-179.2(18)
C(11A)-C(10A)-C(15A)-C(14A)	0.0
C(9A)-C(10A)-C(15A)-C(14A)	178(3)
C(12A)-C(11A)-O(3A)-C(16A)	9(3)
C(10A)-C(11A)-O(3A)-C(16A)	-170(3)
C(15A)-C(14A)-O(4A)-C(17A)	-7(3)
C(13A)-C(14A)-O(4A)-C(17A)	174(3)
C(12A)-C(13A)-C(18A)-C(19A)	-2(7)
C(14A)-C(13A)-C(18A)-C(19A)	179(5)
C(13A)-C(18A)-C(19A)-C(20)	-157(5)
O(1)-C(1)-C(2B)-C(3B)	168.4(8)
O(2)-C(1)-C(2B)-C(3B)	-8.9(14)
C(2A)-C(1)-C(2B)-C(3B)	-151(29)
O(1)-C(1)-C(2B)-C(7B)	-14.2(13)
O(2)-C(1)-C(2B)-C(7B)	168.5(8)
C(2A)-C(1)-C(2B)-C(7B)	26(28)
C(7B)-C(2B)-C(3B)-C(4B)	0.0
C(1)-C(2B)-C(3B)-C(4B)	177.4(14)
C(2B)-C(3B)-C(4B)-C(5B)	0.0
C(3B)-C(4B)-C(5B)-C(6B)	0.0
C(3B)-C(4B)-C(5B)-C(8B)	-172.5(18)
C(4B)-C(5B)-C(6B)-C(7B)	0.0
C(8B)-C(5B)-C(6B)-C(7B)	171.7(19)
C(5B)-C(6B)-C(7B)-C(2B)	0.0
C(3B)-C(2B)-C(7B)-C(6B)	0.0
C(1)-C(2B)-C(7B)-C(6B)	-177.5(14)
C(6B)-C(5B)-C(8B)-C(9B)	7(3)
C(4B)-C(5B)-C(8B)-C(9B)	179(2)
C(5B)-C(8B)-C(9B)-C(10B)	-177(2)
C(8B)-C(9B)-C(10B)-C(11B)	175(2)
C(8B)-C(9B)-C(10B)-C(15B)	-5(3)
C(15B)-C(10B)-C(11B)-C(12B)	0.0
C(9B)-C(10B)-C(11B)-C(12B)	179.9(17)
C(15B)-C(10B)-C(11B)-O(3B)	176.1(16)
C(9B)-C(10B)-C(11B)-O(3B)	-4.0(19)

C(10B)-C(11B)-C(12B)-C(13B)	0.0
O(3B)-C(11B)-C(12B)-C(13B)	-176.4(14)
C(11B)-C(12B)-C(13B)-C(14B)	0.0
C(11B)-C(12B)-C(13B)-C(18B)	166.0(19)
C(12B)-C(13B)-C(14B)-C(15B)	0.0
C(18B)-C(13B)-C(14B)-C(15B)	-166.7(18)
C(12B)-C(13B)-C(14B)-O(4B)	-179.6(16)
C(18B)-C(13B)-C(14B)-O(4B)	14(2)
C(13B)-C(14B)-C(15B)-C(10B)	0.0
O(4B)-C(14B)-C(15B)-C(10B)	179.6(15)
C(11B)-C(10B)-C(15B)-C(14B)	0.0
C(9B)-C(10B)-C(15B)-C(14B)	-179.9(18)
C(12B)-C(11B)-O(3B)-C(16B)	-22(3)
C(10B)-C(11B)-O(3B)-C(16B)	162(2)
C(13B)-C(14B)-O(4B)-C(17B)	-179.7(17)
C(15B)-C(14B)-O(4B)-C(17B)	1(2)
C(14B)-C(13B)-C(18B)-C(19B)	-176(3)
C(12B)-C(13B)-C(18B)-C(19B)	17(4)
C(13B)-C(18B)-C(19B)-C(20)	172(2)
C(18A)-C(19A)-C(20)-C(21)	174(5)
C(18A)-C(19A)-C(20)-C(25)	-12(7)
C(18A)-C(19A)-C(20)-C(19B)	136(11)
C(18B)-C(19B)-C(20)-C(21)	-176(2)
C(18B)-C(19B)-C(20)-C(25)	16(4)
C(18B)-C(19B)-C(20)-C(19A)	-26(5)
C(25)-C(20)-C(21)-C(22)	-2(2)
C(19A)-C(20)-C(21)-C(22)	172(3)
C(19B)-C(20)-C(21)-C(22)	-172.2(16)
C(20)-C(21)-C(22)-C(23)	1(2)
C(21)-C(22)-C(23)-C(24)	-1.1(17)
C(21)-C(22)-C(23)-C(26)	178.6(11)
C(22)-C(23)-C(24)-C(25)	2.0(17)
C(26)-C(23)-C(24)-C(25)	-177.5(10)
C(21)-C(20)-C(25)-C(24)	3(2)
C(19A)-C(20)-C(25)-C(24)	-172(2)
C(19B)-C(20)-C(25)-C(24)	170.4(18)

C(23)-C(24)-C(25)-C(20)	-3(2)
C(24)-C(23)-C(26)-O(5)	-174.8(9)
C(22)-C(23)-C(26)-O(5)	5.6(12)
C(24)-C(23)-C(26)-O(6)	5.5(12)
C(22)-C(23)-C(26)-O(6)	-174.1(9)
O(8)-C(27)-C(28)-C(29)	-166.0(6)
O(7)-C(27)-C(28)-C(29)	9.9(10)
Yb(1)-C(27)-C(28)-C(29)	-110.6(15)
O(8)-C(27)-C(28)-C(33)	10.0(9)
O(7)-C(27)-C(28)-C(33)	-174.1(6)
Yb(1)-C(27)-C(28)-C(33)	65.5(18)
C(33)-C(28)-C(29)-C(30)	0.0
C(27)-C(28)-C(29)-C(30)	176.0(8)
C(28)-C(29)-C(30)-C(31)	0.0
C(29)-C(30)-C(31)-C(32)	0.0
C(29)-C(30)-C(31)-C(34)	-172.6(11)
C(30)-C(31)-C(32)-C(33)	0.0
C(34)-C(31)-C(32)-C(33)	172.3(12)
C(31)-C(32)-C(33)-C(28)	0.0
C(29)-C(28)-C(33)-C(32)	0.0
C(27)-C(28)-C(33)-C(32)	-176.1(8)
C(32)-C(31)-C(34)-C(35)	-8(3)
C(30)-C(31)-C(34)-C(35)	165(2)
C(31)-C(34)-C(35)-C(36)	176.5(18)
C(34)-C(35)-C(36)-C(38)	-168(3)
C(34)-C(35)-C(36)-C(37)	11(4)
C(38)-C(36)-C(37)-C(38)#1	-7(5)
C(35)-C(36)-C(37)-C(38)#1	174(2)
C(37)-C(36)-C(38)-O(9)	-178.3(18)
C(35)-C(36)-C(38)-O(9)	0(4)
C(37)-C(36)-C(38)-C(37)#1	7(5)
C(35)-C(36)-C(38)-C(37)#1	-174(2)
C(36)-C(38)-O(9)-C(39)	176(2)
C(37)#1-C(38)-O(9)-C(39)	-9(5)
O(2)-C(1)-O(1)-Yb(1)#2	-16.8(18)
C(2B)-C(1)-O(1)-Yb(1)#2	166.2(11)

C(2A)-C(1)-O(1)-Yb(1)#2	163.5(15)
O(1)-C(1)-O(2)-Yb(2)#3	5.7(13)
C(2B)-C(1)-O(2)-Yb(2)#3	-177.1(8)
C(2A)-C(1)-O(2)-Yb(2)#3	-174.5(14)
O(6)-C(26)-O(5)-Yb(1)	-1.9(14)
C(23)-C(26)-O(5)-Yb(1)	178.4(6)
O(5)-C(26)-O(6)-Yb(2)	29.0(13)
C(23)-C(26)-O(6)-Yb(2)	-151.3(6)
O(8)-C(27)-O(7)-Yb(2)	-116.7(7)
C(28)-C(27)-O(7)-Yb(2)	67.4(10)
Yb(1)-C(27)-O(7)-Yb(2)	-129.2(7)
O(8)-C(27)-O(7)-Yb(1)	12.5(6)
C(28)-C(27)-O(7)-Yb(1)	-163.4(7)
O(7)-C(27)-O(8)-Yb(1)	-14.8(7)
C(28)-C(27)-O(8)-Yb(1)	161.2(6)
C(26)-O(5)-Yb(1)-O(1)#4	-45.2(11)
C(26)-O(5)-Yb(1)-O(1)#5	42.7(9)
C(26)-O(5)-Yb(1)-O(5)#6	-160.2(9)
C(26)-O(5)-Yb(1)-O(8)	-85.0(9)
C(26)-O(5)-Yb(1)-O(8)#6	121.5(9)
C(26)-O(5)-Yb(1)-O(7)	-33.2(8)
C(26)-O(5)-Yb(1)-O(7)#6	117.4(8)
C(26)-O(5)-Yb(1)-C(27)	-59.6(8)
C(26)-O(5)-Yb(1)-C(27)#6	116.3(8)
C(26)-O(5)-Yb(1)-Yb(2)	-8.5(8)
C(26)-O(5)-Yb(1)-Yb(2)#6	147.8(7)
C(27)-O(8)-Yb(1)-O(1)#4	-73.4(5)
C(27)-O(8)-Yb(1)-O(1)#5	4.8(5)
C(27)-O(8)-Yb(1)-O(5)#6	-168.0(5)
C(27)-O(8)-Yb(1)-O(5)	90.4(5)
C(27)-O(8)-Yb(1)-O(8)#6	140.8(5)
C(27)-O(8)-Yb(1)-O(7)	7.8(4)
C(27)-O(8)-Yb(1)-O(7)#6	-121.1(4)
C(27)-O(8)-Yb(1)-C(27)#6	-171.0(5)
C(27)-O(8)-Yb(1)-Yb(2)	26.3(4)
C(27)-O(8)-Yb(1)-Yb(2)#6	-118.1(4)

C(27)-O(7)-Yb(1)-O(1)#4	79.8(4)
Yb(2)-O(7)-Yb(1)-O(1)#4	-133.0(2)
C(27)-O(7)-Yb(1)-O(1)#5	170.1(4)
Yb(2)-O(7)-Yb(1)-O(1)#5	-42.8(2)
C(27)-O(7)-Yb(1)-O(5)#6	-2.3(4)
Yb(2)-O(7)-Yb(1)-O(5)#6	144.8(2)
C(27)-O(7)-Yb(1)-O(5)	-94.9(4)
Yb(2)-O(7)-Yb(1)-O(5)	52.2(2)
C(27)-O(7)-Yb(1)-O(8)	-7.5(4)
Yb(2)-O(7)-Yb(1)-O(8)	139.6(3)
C(27)-O(7)-Yb(1)-O(8)#6	-141.5(4)
Yb(2)-O(7)-Yb(1)-O(8)#6	5.7(4)
C(27)-O(7)-Yb(1)-O(7)#6	125.0(4)
Yb(2)-O(7)-Yb(1)-O(7)#6	-87.90(18)
Yb(2)-O(7)-Yb(1)-C(27)	147.1(5)
C(27)-O(7)-Yb(1)-C(27)#6	171.6(4)
Yb(2)-O(7)-Yb(1)-C(27)#6	-41.2(4)
C(27)-O(7)-Yb(1)-Yb(2)	-147.1(5)
C(27)-O(7)-Yb(1)-Yb(2)#6	84.3(4)
Yb(2)-O(7)-Yb(1)-Yb(2)#6	-128.52(14)
O(8)-C(27)-Yb(1)-O(1)#4	100.7(5)
O(7)-C(27)-Yb(1)-O(1)#4	-93.1(4)
C(28)-C(27)-Yb(1)-O(1)#4	34.8(16)
O(8)-C(27)-Yb(1)-O(1)#5	-176.1(4)
O(7)-C(27)-Yb(1)-O(1)#5	-9.9(4)
C(28)-C(27)-Yb(1)-O(1)#5	118.0(16)
O(8)-C(27)-Yb(1)-O(5)#6	11.9(5)
O(7)-C(27)-Yb(1)-O(5)#6	178.1(4)
C(28)-C(27)-Yb(1)-O(5)#6	-53.9(16)
O(8)-C(27)-Yb(1)-O(5)	-85.7(5)
O(7)-C(27)-Yb(1)-O(5)	80.5(4)
C(28)-C(27)-Yb(1)-O(5)	-151.6(16)
O(7)-C(27)-Yb(1)-O(8)	166.2(7)
C(28)-C(27)-Yb(1)-O(8)	-65.9(16)
O(8)-C(27)-Yb(1)-O(8)#6	-82.7(9)
O(7)-C(27)-Yb(1)-O(8)#6	83.5(7)

C(28)-C(27)-Yb(1)-O(8)#6	-148.6(14)
O(8)-C(27)-Yb(1)-O(7)	-166.2(7)
C(28)-C(27)-Yb(1)-O(7)	127.9(18)
O(8)-C(27)-Yb(1)-O(7)#6	99.1(5)
O(7)-C(27)-Yb(1)-O(7)#6	-94.7(6)
C(28)-C(27)-Yb(1)-O(7)#6	33.2(18)
O(8)-C(27)-Yb(1)-Yb(2)	-147.3(5)
O(7)-C(27)-Yb(1)-Yb(2)	18.9(3)
C(28)-C(27)-Yb(1)-Yb(2)	146.9(17)
O(8)-C(27)-Yb(1)-Yb(2)#6	76.6(5)
O(7)-C(27)-Yb(1)-Yb(2)#6	-117.3(3)
C(28)-C(27)-Yb(1)-Yb(2)#6	10.7(17)
C(26)-O(6)-Yb(2)-O(2)#7	92.4(8)
C(26)-O(6)-Yb(2)-O(2)#5	-87.6(8)
C(26)-O(6)-Yb(2)-O(7)	2.2(8)
C(26)-O(6)-Yb(2)-O(7)#8	-177.8(8)
C(26)-O(6)-Yb(2)-Yb(1)#8	155.9(7)
C(26)-O(6)-Yb(2)-Yb(1)	-24.1(7)
C(27)-O(7)-Yb(2)-O(2)#7	-11.7(7)
Yb(1)-O(7)-Yb(2)-O(2)#7	-131.5(2)
C(27)-O(7)-Yb(2)-O(2)#5	168.3(7)
Yb(1)-O(7)-Yb(2)-O(2)#5	48.5(2)
C(27)-O(7)-Yb(2)-O(6)#8	-104.0(7)
Yb(1)-O(7)-Yb(2)-O(6)#8	136.2(2)
C(27)-O(7)-Yb(2)-O(6)	76.0(7)
Yb(1)-O(7)-Yb(2)-O(6)	-43.8(2)
C(27)-O(7)-Yb(2)-Yb(1)#8	-60.2(8)
Yb(1)-O(7)-Yb(2)-Yb(1)#8	180.0
C(27)-O(7)-Yb(2)-Yb(1)	119.8(8)
O(1)#4-Yb(1)-Yb(2)-O(2)#7	99.7(2)
O(1)#5-Yb(1)-Yb(2)-O(2)#7	-177.6(2)
O(5)#6-Yb(1)-Yb(2)-O(2)#7	-4.2(3)
O(5)-Yb(1)-Yb(2)-O(2)#7	-65.3(2)
O(8)-Yb(1)-Yb(2)-O(2)#7	22.5(2)
O(8)#6-Yb(1)-Yb(2)-O(2)#7	-122.3(2)
O(7)-Yb(1)-Yb(2)-O(2)#7	54.1(3)

O(7)#6-Yb(1)-Yb(2)-O(2)#7	177.2(2)
C(27)-Yb(1)-Yb(2)-O(2)#7	36.3(3)
C(27)#6-Yb(1)-Yb(2)-O(2)#7	-149.9(3)
Yb(2)#6-Yb(1)-Yb(2)-O(2)#7	136.89(18)
O(1)#4-Yb(1)-Yb(2)-O(2)#5	-80.3(2)
O(1)#5-Yb(1)-Yb(2)-O(2)#5	2.4(2)
O(5)#6-Yb(1)-Yb(2)-O(2)#5	175.8(3)
O(5)-Yb(1)-Yb(2)-O(2)#5	114.7(2)
O(8)-Yb(1)-Yb(2)-O(2)#5	-157.5(2)
O(8)#6-Yb(1)-Yb(2)-O(2)#5	57.7(2)
O(7)-Yb(1)-Yb(2)-O(2)#5	-125.9(3)
O(7)#6-Yb(1)-Yb(2)-O(2)#5	-2.8(2)
C(27)-Yb(1)-Yb(2)-O(2)#5	-143.7(3)
C(27)#6-Yb(1)-Yb(2)-O(2)#5	30.1(3)
Yb(2)#6-Yb(1)-Yb(2)-O(2)#5	-43.11(18)
O(1)#4-Yb(1)-Yb(2)-O(6)#8	-5.1(2)
O(1)#5-Yb(1)-Yb(2)-O(6)#8	77.5(2)
O(5)#6-Yb(1)-Yb(2)-O(6)#8	-109.1(3)
O(5)-Yb(1)-Yb(2)-O(6)#8	-170.2(2)
O(8)-Yb(1)-Yb(2)-O(6)#8	-82.4(2)
O(8)#6-Yb(1)-Yb(2)-O(6)#8	132.8(2)
O(7)-Yb(1)-Yb(2)-O(6)#8	-50.8(3)
O(7)#6-Yb(1)-Yb(2)-O(6)#8	72.3(2)
C(27)-Yb(1)-Yb(2)-O(6)#8	-68.6(2)
C(27)#6-Yb(1)-Yb(2)-O(6)#8	105.2(2)
Yb(2)#6-Yb(1)-Yb(2)-O(6)#8	32.01(16)
O(1)#4-Yb(1)-Yb(2)-O(6)	174.9(2)
O(1)#5-Yb(1)-Yb(2)-O(6)	-102.5(2)
O(5)#6-Yb(1)-Yb(2)-O(6)	70.9(3)
O(5)-Yb(1)-Yb(2)-O(6)	9.8(2)
O(8)-Yb(1)-Yb(2)-O(6)	97.6(2)
O(8)#6-Yb(1)-Yb(2)-O(6)	-47.2(2)
O(7)-Yb(1)-Yb(2)-O(6)	129.2(3)
O(7)#6-Yb(1)-Yb(2)-O(6)	-107.7(2)
C(27)-Yb(1)-Yb(2)-O(6)	111.4(2)
C(27)#6-Yb(1)-Yb(2)-O(6)	-74.8(2)

Yb(2)#6-Yb(1)-Yb(2)-O(6)	-147.99(16)
O(1)#4-Yb(1)-Yb(2)-O(7)	45.7(2)
O(1)#5-Yb(1)-Yb(2)-O(7)	128.3(3)
O(5)#6-Yb(1)-Yb(2)-O(7)	-58.3(3)
O(5)-Yb(1)-Yb(2)-O(7)	-119.4(3)
O(8)-Yb(1)-Yb(2)-O(7)	-31.5(2)
O(8)#6-Yb(1)-Yb(2)-O(7)	-176.4(3)
O(7)#6-Yb(1)-Yb(2)-O(7)	123.1(3)
C(27)-Yb(1)-Yb(2)-O(7)	-17.7(3)
C(27)#6-Yb(1)-Yb(2)-O(7)	156.1(3)
Yb(2)#6-Yb(1)-Yb(2)-O(7)	82.8(2)
O(1)#4-Yb(1)-Yb(2)-O(7)#8	-134.3(2)
O(1)#5-Yb(1)-Yb(2)-O(7)#8	-51.7(3)
O(5)#6-Yb(1)-Yb(2)-O(7)#8	121.7(3)
O(5)-Yb(1)-Yb(2)-O(7)#8	60.6(3)
O(8)-Yb(1)-Yb(2)-O(7)#8	148.5(2)
O(8)#6-Yb(1)-Yb(2)-O(7)#8	3.6(3)
O(7)-Yb(1)-Yb(2)-O(7)#8	180.0
O(7)#6-Yb(1)-Yb(2)-O(7)#8	-56.9(3)
C(27)-Yb(1)-Yb(2)-O(7)#8	162.3(3)
C(27)#6-Yb(1)-Yb(2)-O(7)#8	-23.9(3)
Yb(2)#6-Yb(1)-Yb(2)-O(7)#8	-97.2(2)

Symmetry transformations used to generate equivalent atoms:

#1 -x+1,-y+2,-z+1 #2 x-1/2,-y+1/2,z-1/2 #3 -x+1/2,y-1/2,-z+1/2

#4 -x+1,y+1/2,z+1/2 #5 x+1/2,-y+1/2,z+1/2 #6 -x+3/2,-y+1,z

#7 -x+1/2,y+1/2,-z+1/2 #8 -x+1,-y+1,-z+1

Table AA12. Crystal data and structure refinement for Ho-PVDC-3.

Identification code	**Ho-PVDC-3**	
Empirical formula	C45 H43 Ho N2 O12	
Formula weight	968.74	
Temperature	203(2) K	
Wavelength	0.71073 Å	
Crystal system	Triclinic	
Space group	P1	
Unit cell dimensions	a = 9.202(3) Å	α = 78.019(7)°.
	b = 10.702(4) Å	β = 87.845(6)°.
	c = 21.866(8) Å	γ = 79.438(7)°.
Volume	2070.8(13) $Å^3$	
Z	2	
Density (calculated)	1.554 Mg/m^3	
Absorption coefficient	1.977 mm^{-1}	
F(000)	980	
Crystal size	0.32 x 0.22 x 0.20 mm^3	
Theta range for data collection	1.90 to 25.00°.	
Index ranges	-10<=h<=10, -12<=k<=12, -25<=l<=25	
Reflections collected	15348	
Independent reflections	7245 [R(int) = 0.0808]	
Completeness to theta = 25.00°	99.4 %	
Absorption correction	Multi-scan (Sadabs)	
Max. and min. transmission	0.6932 and 0.5702	
Refinement method	Full-matrix least-squares on F^2	
Data / restraints / parameters	7245 / 0 / 537	
Goodness-of-fit on F^2	2.219	
Final R indices [I>2sigma(I)]	R1 = 0.1340, wR2 = 0.3241	
R indices (all data)	R1 = 0.1472, wR2 = 0.3283	
Extinction coefficient	0.0046(15)	
Largest diff. peak and hole	10.267 and -3.453 $e.Å^{-3}$	

Table AA13. Atomic coordinates (x 10^4) and equivalent isotropic displacement parameters ($Å^2$ x 10^3) for Ho-PVDC-3. U(eq) is defined as one third of the trace of the orthogonalized U^{ij} tensor.

	x	y	z	U(eq)
Ho	12831(1)	9680(1)	-39(1)	19(1)
O(1)	11534(16)	8877(15)	859(8)	49(4)
C(1)	10180(20)	9170(20)	1028(11)	37(5)
N(1)	12280(20)	5520(20)	159(11)	57(6)
O(2)	9159(14)	9863(15)	694(7)	39(3)
C(2)	9840(20)	8625(18)	1718(8)	28(4)
N(2)	9460(30)	2800(20)	2132(13)	68(7)
C(3)	8530(20)	9210(20)	1977(10)	38(5)
O(3)	9014(17)	6041(16)	6098(7)	47(4)
O(4)	4737(19)	7079(18)	4260(7)	58(5)
C(4)	8220(20)	8780(20)	2598(9)	36(5)
O(5)	3438(14)	1507(14)	9278(5)	31(3)
C(5)	9140(20)	7760(20)	2957(9)	38(5)
O(6)	5460(14)	2090(13)	9569(5)	30(3)
C(6)	10480(20)	7210(20)	2699(10)	37(5)
O(7)	14065(15)	10394(14)	656(6)	34(3)
C(7)	10800(20)	7670(20)	2077(9)	37(5)
O(8)	16015(14)	11146(13)	917(7)	35(3)
C(8)	8850(20)	7270(20)	3626(10)	41(5)
O(9)	8180(20)	10370(20)	3977(10)	84(6)
C(9)	7510(30)	7380(20)	3876(11)	43(5)
O(10)	11914(17)	7689(15)	-137(8)	47(4)
C(10)	7170(30)	6970(20)	4522(9)	38(5)
C(11)	5730(30)	6820(20)	4737(11)	44(5)
O(11)	10960(30)	2630(20)	1273(10)	90(7)
O(12)	11185(14)	11608(12)	221(7)	38(4)
C(12)	5390(30)	6467(19)	5362(11)	45(6)
C(13)	6530(20)	6165(18)	5829(10)	35(5)
C(14)	7940(20)	6328(19)	5637(10)	38(5)
C(15)	8270(30)	6700(20)	4997(11)	46(6)
C(16)	3240(30)	6970(20)	4434(11)	48(6)

C(17)	10470(30)	6240(20)	5916(11)	48(6)
C(18)	6210(30)	5693(18)	6492(10)	38(5)
C(19)	5010(30)	5250(20)	6717(10)	41(5)
C(20)	4800(20)	4650(20)	7384(9)	38(5)
C(21)	3650(30)	3970(20)	7526(10)	45(6)
C(22)	3460(30)	3230(20)	8126(11)	49(6)
C(23)	4440(20)	3185(17)	8582(9)	28(4)
C(24)	5540(20)	3900(20)	8461(10)	42(5)
C(25)	5710(30)	4660(20)	7856(11)	44(5)
C(26)	4401(19)	2200(20)	9179(10)	34(5)
C(27)	14800(20)	10795(17)	1048(8)	27(4)
C(28)	14180(20)	10754(18)	1689(9)	31(4)
C(29)	13230(20)	9960(20)	1923(10)	39(5)
C(30)	12650(30)	9920(20)	2535(11)	50(6)
C(31)	13070(20)	10690(20)	2889(9)	35(5)
C(32)	14060(30)	11480(20)	2665(10)	43(6)
C(33)	14630(30)	11520(20)	2064(10)	39(5)
C(34)	12440(30)	10640(20)	3553(10)	44(6)
C(35)	11210(20)	10230(20)	3763(10)	41(5)
C(36)	10610(30)	10125(18)	4392(10)	38(5)
C(37)	9160(20)	10120(20)	4496(10)	40(5)
C(38)	8450(30)	10020(20)	5078(12)	48(6)
C(40)	6520(40)	10440(40)	4160(30)	150(20)
C(41)	12640(20)	6600(20)	-97(13)	49(6)
C(42)	13100(30)	4260(30)	116(17)	76(9)
C(43)	10940(40)	5590(30)	637(15)	78(9)
C(44)	9820(40)	2350(30)	1615(17)	80(9)
C(45)	8260(30)	2430(30)	2530(17)	80(10)
C(46)	10290(40)	3670(40)	2328(19)	99(13)

Table AA14. Bond lengths [Å] and angles [°] for Ho-PVDC-3.

Ho-O(10)	2.481(15)
Ho-O(2)#1	2.284(14)
Ho-O(7)	2.261(13)
Ho-O(6)#2	2.310(13)
Ho-O(1)	2.350(14)
Ho-O(5)#3	2.343(13)
Ho-O(8)#4	2.408(14)
Ho-O(12)	2.481(12)
O(1)-C(1)	1.29(2)
C(1)-O(2)	1.24(3)
C(1)-C(2)	1.54(3)
N(1)-C(41)	1.27(3)
N(1)-C(42)	1.44(3)
N(1)-C(43)	1.58(4)
O(2)-Ho#1	2.284(14)
C(2)-C(7)	1.35(3)
C(2)-C(3)	1.41(3)
N(2)-C(44)	1.33(4)
N(2)-C(45)	1.44(4)
N(2)-C(46)	1.45(4)
C(3)-C(4)	1.38(3)
C(3)-H(3A)	0.9400
O(3)-C(14)	1.39(3)
O(3)-C(17)	1.43(3)
O(4)-C(11)	1.36(3)
O(4)-C(16)	1.43(3)
C(4)-C(5)	1.37(3)
C(4)-H(4A)	0.9400
O(5)-C(26)	1.24(2)
O(5)-Ho#5	2.343(13)
C(5)-C(6)	1.41(3)
C(5)-C(8)	1.48(3)
O(6)-C(26)	1.29(2)

O(6)-Ho#2	2.310(13)
C(6)-C(7)	1.39(3)
C(6)-H(6A)	0.9400
O(7)-C(27)	1.30(2)
C(7)-H(7A)	0.9400
O(8)-C(27)	1.25(2)
O(8)-Ho#4	2.408(14)
C(8)-C(9)	1.33(3)
C(8)-H(8A)	0.9400
O(9)-C(37)	1.43(3)
O(9)-C(40)	1.55(4)
C(9)-C(10)	1.43(3)
C(9)-H(9A)	0.9400
O(10)-C(41)	1.22(2)
C(10)-C(11)	1.41(3)
C(10)-C(15)	1.43(3)
C(11)-C(12)	1.38(3)
O(11)-C(44)	1.31(4)
C(12)-C(13)	1.43(3)
C(12)-H(12A)	0.9400
C(13)-C(14)	1.38(3)
C(13)-C(18)	1.47(3)
C(14)-C(15)	1.41(3)
C(15)-H(15A)	0.9400
C(16)-H(16A)	0.9700
C(16)-H(16B)	0.9700
C(16)-H(16C)	0.9700
C(17)-H(17A)	0.9700
C(17)-H(17B)	0.9700
C(17)-H(17C)	0.9700
C(18)-C(19)	1.32(3)
C(18)-H(18A)	0.9400
C(19)-C(20)	1.49(3)
C(19)-H(19A)	0.9400
C(20)-C(21)	1.38(3)
C(20)-C(25)	1.36(3)

C(21)-C(22)	1.41(3)
C(21)-H(21A)	0.9400
C(22)-C(23)	1.36(3)
C(22)-H(22A)	0.9400
C(23)-C(24)	1.37(3)
C(23)-C(26)	1.50(3)
C(24)-C(25)	1.42(3)
C(24)-H(24A)	0.9400
C(25)-H(25A)	0.9400
C(27)-C(28)	1.49(2)
C(28)-C(29)	1.34(3)
C(28)-C(33)	1.40(3)
C(29)-C(30)	1.42(3)
C(29)-H(29A)	0.9400
C(30)-C(31)	1.35(3)
C(30)-H(30A)	0.9400
C(31)-C(32)	1.36(3)
C(31)-C(34)	1.53(3)
C(32)-C(33)	1.39(3)
C(32)-H(32A)	0.9400
C(33)-H(33A)	0.9400
C(34)-C(35)	1.32(3)
C(34)-H(34A)	0.9400
C(35)-C(36)	1.45(3)
C(35)-H(35A)	0.9400
C(36)-C(37)	1.34(3)
C(36)-C(38)#6	1.44(3)
C(37)-C(38)	1.40(3)
C(38)-C(36)#6	1.44(3)
C(38)-H(38A)	0.9400
C(40)-H(40A)	0.9700
C(40)-H(40B)	0.9700
C(40)-H(40C)	0.9700
C(42)-H(42A)	0.9700
C(42)-H(42B)	0.9700
C(42)-H(42C)	0.9700

C(43)-H(43A)	0.9700
C(43)-H(43B)	0.9700
C(43)-H(43C)	0.9700
C(44)-H(44A)	0.9400
C(45)-H(45A)	0.9700
C(45)-H(45B)	0.9700
C(45)-H(45C)	0.9700
C(46)-H(46A)	0.9700
C(46)-H(46B)	0.9700
C(46)-H(46C)	0.9700

O(10)-Ho-O(2)#1	68.0(5)
O(10)-Ho-O(7)	139.0(5)
O(2)#1-Ho-O(7)	145.8(5)
O(10)-Ho-O(6)#2	72.2(5)
O(2)#1-Ho-O(6)#2	139.1(5)
O(7)-Ho-O(6)#2	74.2(5)
O(10)-Ho-O(1)	68.5(5)
O(2)#1-Ho-O(1)	95.1(5)
O(7)-Ho-O(1)	82.6(5)
O(6)#2-Ho-O(1)	78.8(5)
O(10)-Ho-O(5)#3	136.6(5)
O(2)#1-Ho-O(5)#3	81.4(5)
O(7)-Ho-O(5)#3	82.4(5)
O(6)#2-Ho-O(5)#3	124.3(4)
O(1)-Ho-O(5)#3	147.1(5)
O(10)-Ho-O(8)#4	69.8(5)
O(2)#1-Ho-O(8)#4	80.5(5)
O(7)-Ho-O(8)#4	123.8(5)
O(6)#2-Ho-O(8)#4	77.1(4)
O(1)-Ho-O(8)#4	136.5(5)
O(5)#3-Ho-O(8)#4	75.5(5)
O(10)-Ho-O(12)	122.6(5)
O(2)#1-Ho-O(12)	73.3(5)
O(7)-Ho-O(12)	73.2(5)
O(6)#2-Ho-O(12)	140.0(5)

O(1)-Ho-O(12)	74.6(5)
O(5)#3-Ho-O(12)	73.0(5)
O(8)#4-Ho-O(12)	141.4(5)
C(1)-O(1)-Ho	131.9(15)
O(2)-C(1)-O(1)	126(2)
O(2)-C(1)-C(2)	118.4(17)
O(1)-C(1)-C(2)	115.4(19)
C(41)-N(1)-C(42)	125(2)
C(41)-N(1)-C(43)	116(2)
C(42)-N(1)-C(43)	118(2)
C(1)-O(2)-Ho#1	156.9(14)
C(7)-C(2)-C(3)	120.4(18)
C(7)-C(2)-C(1)	121.8(17)
C(3)-C(2)-C(1)	117.7(18)
C(44)-N(2)-C(45)	123(3)
C(44)-N(2)-C(46)	120(3)
C(45)-N(2)-C(46)	117(3)
C(4)-C(3)-C(2)	120(2)
C(4)-C(3)-H(3A)	120.2
C(2)-C(3)-H(3A)	120.2
C(14)-O(3)-C(17)	118.2(17)
C(11)-O(4)-C(16)	116.5(18)
C(5)-C(4)-C(3)	120.4(18)
C(5)-C(4)-H(4A)	119.8
C(3)-C(4)-H(4A)	119.8
C(26)-O(5)-Ho#5	142.0(13)
C(4)-C(5)-C(6)	119.8(18)
C(4)-C(5)-C(8)	122.4(19)
C(6)-C(5)-C(8)	118(2)
C(26)-O(6)-Ho#2	131.7(13)
C(7)-C(6)-C(5)	119(2)
C(7)-C(6)-H(6A)	120.4
C(5)-C(6)-H(6A)	120.4
C(27)-O(7)-Ho	178.7(12)
C(2)-C(7)-C(6)	120.6(18)
C(2)-C(7)-H(7A)	119.7

C(6)-C(7)-H(7A)	119.7
C(27)-O(8)-Ho#4	111.6(11)
C(9)-C(8)-C(5)	123(2)
C(9)-C(8)-H(8A)	118.3
C(5)-C(8)-H(8A)	118.3
C(37)-O(9)-C(40)	114(3)
C(8)-C(9)-C(10)	126(2)
C(8)-C(9)-H(9A)	117.1
C(10)-C(9)-H(9A)	117.1
C(41)-O(10)-Ho	126.9(14)
C(11)-C(10)-C(15)	115.4(19)
C(11)-C(10)-C(9)	123(2)
C(15)-C(10)-C(9)	122(2)
O(4)-C(11)-C(12)	125(2)
O(4)-C(11)-C(10)	112.3(19)
C(12)-C(11)-C(10)	123(2)
C(11)-C(12)-C(13)	121(2)
C(11)-C(12)-H(12A)	119.7
C(13)-C(12)-H(12A)	119.7
C(14)-C(13)-C(12)	117.8(19)
C(14)-C(13)-C(18)	121(2)
C(12)-C(13)-C(18)	121.6(19)
C(13)-C(14)-O(3)	116.9(19)
C(13)-C(14)-C(15)	121(2)
O(3)-C(14)-C(15)	122(2)
C(14)-C(15)-C(10)	122(2)
C(14)-C(15)-H(15A)	119.0
C(10)-C(15)-H(15A)	119.0
O(4)-C(16)-H(16A)	109.5
O(4)-C(16)-H(16B)	109.5
H(16A)-C(16)-H(16B)	109.5
O(4)-C(16)-H(16C)	109.5
H(16A)-C(16)-H(16C)	109.5
H(16B)-C(16)-H(16C)	109.5
O(3)-C(17)-H(17A)	109.5
O(3)-C(17)-H(17B)	109.5

H(17A)-C(17)-H(17B)	109.5
O(3)-C(17)-H(17C)	109.5
H(17A)-C(17)-H(17C)	109.5
H(17B)-C(17)-H(17C)	109.5
C(19)-C(18)-C(13)	126(2)
C(19)-C(18)-H(18A)	116.9
C(13)-C(18)-H(18A)	116.9
C(18)-C(19)-C(20)	125(2)
C(18)-C(19)-H(19A)	117.6
C(20)-C(19)-H(19A)	117.6
C(21)-C(20)-C(25)	118.1(19)
C(21)-C(20)-C(19)	118(2)
C(25)-C(20)-C(19)	124(2)
C(20)-C(21)-C(22)	122(2)
C(20)-C(21)-H(21A)	118.9
C(22)-C(21)-H(21A)	118.9
C(23)-C(22)-C(21)	119(2)
C(23)-C(22)-H(22A)	120.5
C(21)-C(22)-H(22A)	120.5
C(22)-C(23)-C(24)	119.7(19)
C(22)-C(23)-C(26)	118.2(18)
C(24)-C(23)-C(26)	121.6(18)
C(23)-C(24)-C(25)	121(2)
C(23)-C(24)-H(24A)	119.6
C(25)-C(24)-H(24A)	119.6
C(20)-C(25)-C(24)	119.8(19)
C(20)-C(25)-H(25A)	120.1
C(24)-C(25)-H(25A)	120.1
O(5)-C(26)-O(6)	122.5(19)
O(5)-C(26)-C(23)	121.8(17)
O(6)-C(26)-C(23)	115.7(16)
O(8)-C(27)-O(7)	122.8(16)
O(8)-C(27)-C(28)	119.8(17)
O(7)-C(27)-C(28)	117.3(17)
C(29)-C(28)-C(33)	119.2(19)
C(29)-C(28)-C(27)	121.2(18)

C(33)-C(28)-C(27)	119.6(18)
C(28)-C(29)-C(30)	121(2)
C(28)-C(29)-H(29A)	119.4
C(30)-C(29)-H(29A)	119.4
C(31)-C(30)-C(29)	119.2(19)
C(31)-C(30)-H(30A)	120.4
C(29)-C(30)-H(30A)	120.4
C(30)-C(31)-C(32)	120.3(18)
C(30)-C(31)-C(34)	119.1(19)
C(32)-C(31)-C(34)	121(2)
C(31)-C(32)-C(33)	120.7(19)
C(31)-C(32)-H(32A)	119.6
C(33)-C(32)-H(32A)	119.6
C(28)-C(33)-C(32)	119.4(19)
C(28)-C(33)-H(33A)	120.3
C(32)-C(33)-H(33A)	120.3
C(35)-C(34)-C(31)	126(2)
C(35)-C(34)-H(34A)	117.0
C(31)-C(34)-H(34A)	117.0
C(34)-C(35)-C(36)	128(2)
C(34)-C(35)-H(35A)	116.2
C(36)-C(35)-H(35A)	116.2
C(37)-C(36)-C(38)#6	118.0(19)
C(37)-C(36)-C(35)	121(2)
C(38)#6-C(36)-C(35)	121(2)
C(36)-C(37)-C(38)	126(2)
C(36)-C(37)-O(9)	119(2)
C(38)-C(37)-O(9)	114(2)
C(37)-C(38)-C(36)#6	116(2)
C(37)-C(38)-H(38A)	122.1
C(36)#6-C(38)-H(38A)	122.1
O(9)-C(40)-H(40A)	109.5
O(9)-C(40)-H(40B)	109.5
H(40A)-C(40)-H(40B)	109.5
O(9)-C(40)-H(40C)	109.5
H(40A)-C(40)-H(40C)	109.5

H(40B)-C(40)-H(40C)	109.5
N(1)-C(41)-O(10)	128(2)
N(1)-C(42)-H(42A)	109.5
N(1)-C(42)-H(42B)	109.5
H(42A)-C(42)-H(42B)	109.5
N(1)-C(42)-H(42C)	109.5
H(42A)-C(42)-H(42C)	109.5
H(42B)-C(42)-H(42C)	109.5
N(1)-C(43)-H(43A)	109.5
N(1)-C(43)-H(43B)	109.5
H(43A)-C(43)-H(43B)	109.5
N(1)-C(43)-H(43C)	109.5
H(43A)-C(43)-H(43C)	109.5
H(43B)-C(43)-H(43C)	109.5
O(11)-C(44)-N(2)	122(3)
O(11)-C(44)-H(44A)	118.8
N(2)-C(44)-H(44A)	118.8
N(2)-C(45)-H(45A)	109.5
N(2)-C(45)-H(45B)	109.5
H(45A)-C(45)-H(45B)	109.5
N(2)-C(45)-H(45C)	109.5
H(45A)-C(45)-H(45C)	109.5
H(45B)-C(45)-H(45C)	109.5
N(2)-C(46)-H(46A)	109.5
N(2)-C(46)-H(46B)	109.5
H(46A)-C(46)-H(46B)	109.5
N(2)-C(46)-H(46C)	109.5
H(46A)-C(46)-H(46C)	109.5
H(46B)-C(46)-H(46C)	109.5

Symmetry transformations used to generate equivalent atoms:

#1 -x+2,-y+2,-z #2 -x+2,-y+1,-z+1 #3 x+1,y+1,z-1

#4 -x+3,-y+2,-z #5 x-1,y-1,z+1 #6 -x+2,-y+2,-z+1

Table AA15. Anisotropic displacement parameters ($Å^2$x 10^3) for Ho-PVDC-3. The anisotropic displacement factor exponent takes the form: $-2\pi^2[h^2 a^{*2} U^{11} + ... + 2 h k a^* b^* U^{12}]$.

	U^{11}	U^{22}	U^{33}	U^{23}	U^{13}	U^{12}
Ho	16(1)	25(1)	15(1)	-5(1)	0(1)	-1(1)
O(1)	39(9)	57(10)	46(10)	-2(8)	16(7)	-10(7)
C(1)	34(11)	42(12)	45(14)	-27(10)	5(10)	-12(9)
N(1)	35(11)	70(15)	71(16)	-14(12)	-2(10)	-23(10)
O(2)	26(7)	59(9)	27(8)	6(7)	3(6)	-11(7)
C(2)	36(10)	38(10)	12(9)	-3(8)	8(8)	-20(9)
N(2)	72(16)	60(14)	81(19)	-31(13)	7(13)	-14(12)
C(3)	35(11)	42(11)	34(12)	-6(9)	16(9)	-8(9)
O(3)	52(9)	59(10)	34(9)	-14(7)	1(7)	-14(8)
O(4)	60(11)	87(13)	21(9)	-10(8)	-2(7)	-3(9)
C(4)	43(12)	43(12)	16(10)	-4(9)	11(9)	1(9)
O(5)	32(7)	57(9)	6(6)	-5(6)	2(5)	-16(6)
C(5)	60(14)	50(12)	4(9)	-2(8)	9(9)	-15(11)
O(6)	41(8)	43(8)	6(6)	2(5)	3(5)	-11(6)
C(6)	36(11)	44(12)	29(12)	-7(9)	4(9)	-5(9)
O(7)	46(8)	53(9)	14(7)	-14(6)	5(6)	-27(7)
C(7)	43(12)	50(12)	20(11)	-16(9)	12(9)	-10(10)
O(8)	25(7)	43(8)	34(8)	-4(6)	-5(6)	-1(6)
C(8)	49(13)	54(13)	28(12)	-24(10)	5(10)	-10(11)
O(9)	91(16)	111(18)	47(13)	-15(12)	2(11)	-10(13)
C(9)	50(13)	44(12)	36(13)	-9(10)	7(10)	-10(10)
C(10)	59(14)	40(11)	20(11)	-13(9)	7(9)	-13(10)
C(11)	67(15)	30(11)	36(13)	-10(9)	7(11)	-9(10)
O(11)	150(20)	65(13)	54(14)	-22(11)	18(14)	-13(14)
O(12)	35(8)	22(6)	62(10)	-23(7)	16(7)	-3(6)
C(12)	57(14)	31(11)	42(14)	-10(10)	21(11)	1(10)
C(13)	49(13)	26(10)	30(12)	-4(8)	-3(9)	-7(9)
C(14)	48(13)	31(10)	34(12)	-6(9)	-2(10)	-5(9)
C(15)	57(14)	52(14)	33(13)	-12(11)	14(11)	-20(11)
C(16)	58(15)	42(13)	42(14)	-13(11)	-15(11)	1(11)
C(17)	58(15)	64(15)	27(13)	-17(11)	2(10)	-22(12)

C(18)	61(14)	30(10)	22(11)	-9(8)	14(10)	-3(10)
C(19)	64(15)	37(11)	22(11)	-7(9)	5(10)	-10(10)
C(20)	58(14)	36(11)	20(11)	-3(9)	11(10)	-14(10)
C(21)	61(14)	64(15)	14(11)	0(10)	-9(9)	-30(12)
C(22)	53(14)	65(15)	38(14)	-15(12)	12(11)	-31(12)
C(23)	31(10)	25(9)	24(10)	2(8)	4(8)	-5(8)
C(24)	45(12)	44(12)	33(13)	5(10)	-18(10)	-4(10)
C(25)	56(14)	41(12)	36(13)	4(10)	5(10)	-26(11)
C(26)	13(9)	46(12)	42(13)	-10(10)	-9(8)	-4(8)
C(27)	45(12)	26(9)	5(9)	-4(7)	1(8)	5(8)
C(28)	38(11)	31(10)	20(10)	-3(8)	-2(8)	0(8)
C(29)	46(12)	54(13)	29(12)	-23(10)	10(9)	-23(11)
C(30)	68(16)	61(15)	25(12)	-4(11)	15(11)	-36(13)
C(31)	44(12)	43(11)	12(10)	2(8)	9(8)	-2(9)
C(32)	69(15)	50(13)	24(12)	-22(10)	8(10)	-29(12)
C(33)	58(14)	39(11)	24(11)	-8(9)	2(10)	-18(10)
C(34)	74(16)	41(12)	17(11)	-9(9)	17(10)	-11(11)
C(35)	45(12)	40(12)	33(12)	-5(9)	14(10)	-2(10)
C(36)	61(14)	24(10)	29(12)	-10(8)	17(10)	-6(9)
C(37)	53(14)	46(12)	23(11)	-13(9)	-6(9)	-8(10)
C(38)	47(13)	35(12)	58(16)	-7(11)	10(11)	0(10)
C(40)	60(20)	90(30)	310(70)	-60(40)	-70(30)	-6(19)
C(41)	35(12)	27(11)	90(20)	-21(12)	-9(12)	-7(9)
C(42)	61(18)	49(15)	120(30)	-21(17)	0(18)	0(14)
C(43)	100(20)	65(19)	70(20)	-13(16)	-1(18)	-22(17)
C(44)	100(20)	70(20)	80(20)	-26(18)	10(20)	-20(18)
C(45)	80(20)	54(17)	110(30)	-26(18)	10(20)	-11(16)
C(46)	70(20)	110(30)	140(40)	-70(30)	10(20)	-30(20)

Table AA16. Hydrogen coordinates (x 10^4) and isotropic displacement parameters ($Å^2$ x 10^3) for Ho-PVDC-3.

	x	y	z	U(eq)
H(3A)	7883	9887	1729	45
H(4A)	7357	9178	2776	43
H(6A)	11136	6532	2946	44
H(7A)	11687	7306	1903	44
H(8A)	9663	6864	3888	50
H(9A)	6707	7755	3604	52
H(12A)	4409	6424	5482	54
H(15A)	9250	6776	4880	55
H(16A)	2630	7180	4061	72
H(16B)	2870	7572	4705	72
H(16C)	3202	6092	4653	72
H(17A)	11106	6010	6282	71
H(17B)	10445	7151	5725	71
H(17C)	10857	5708	5619	71
H(18A)	6926	5713	6783	45
H(19A)	4243	5310	6436	49
H(21A)	2965	4010	7211	54
H(22A)	2669	2780	8210	59
H(24A)	6196	3894	8783	51
H(25A)	6455	5170	7781	53
H(29A)	12948	9428	1675	47
H(30A)	11989	9359	2693	59
H(32A)	14359	11991	2919	52
H(33A)	15313	12069	1911	47
H(34A)	12981	10929	3835	53
H(35A)	10661	9968	3473	49
H(38A)	7429	10048	5119	58
H(40A)	5923	10609	3788	223
H(40B)	6223	11139	4388	223
H(40C)	6381	9626	4427	223
H(42A)	13885	4366	-190	115
H(42B)	12447	3751	-12	115

H(42C)	13527	3830	520	115
H(43A)	10476	6486	614	117
H(43B)	11305	5211	1058	117
H(43C)	10223	5106	531	117
H(44A)	9246	1805	1491	96
H(45A)	7776	1858	2350	120
H(45B)	7545	3202	2568	120
H(45C)	8638	1987	2941	120
H(46A)	11058	3857	2022	149
H(46B)	10743	3270	2731	149
H(46C)	9636	4477	2360	149

Table AA17. Crystal data and structure refinement for Tb-PVDC-3.

Identification code	**Tb-PVDC-3**	
Empirical formula	C45 H42 N2 O12 Tb	
Formula weight	961.73	
Temperature	203(2) K	
Wavelength	0.71073 Å	
Crystal system	Triclinic	
Space group	P-1	
Unit cell dimensions	a = 9.1655(18) Å	α = 78.12(3)°.
	b = 10.667(2) Å	β = 87.89(3)°.
	c = 21.774(4) Å	γ = 79.41(3)°.
Volume	2047.8(7) $Å^3$	
Z	2	
Density (calculated)	1.560 Mg/m^3	
Absorption coefficient	1.794 mm^{-1}	
F(000)	974	
Crystal size	0.28 x 0.18 x 0.12 mm^3	
Theta range for data collection	1.91 to 25.00°.	
Index ranges	-10<=h<=10, -12<=k<=12, -25<=l<=25	
Reflections collected	15496	
Independent reflections	7168 [R(int) = 0.0780]	
Completeness to theta = 25.00°	99.6 %	
Absorption correction	Sadabs	
Max. and min. transmission	0.8135 and 0.6335	
Refinement method	Full-matrix least-squares on F^2	
Data / restraints / parameters	7168 / 8 / 486	
Goodness-of-fit on F^2	2.460	
Final R indices [I>2sigma(I)]	R1 = 0.1584, wR2 = 0.3892	
R indices (all data)	R1 = 0.1728, wR2 = 0.3934	
Largest diff. peak and hole	8.991 and -6.439 $e.Å^{-3}$	

Table AA18. Atomic coordinates (x 10^4) and equivalent isotropic displacement parameters ($Å^2$ x 10^3) for Tb-PVDC-3. U(eq) is defined as one third of the trace of the orthogonalized U^{ij} tensor.

	x	y	z	U(eq)
Tb	2154(1)	5335(1)	5033(1)	20(1)
O(1)	1570(20)	3486(18)	5763(8)	44(4)
C(1)	620(30)	2770(30)	5808(13)	47(7)
C(2)	540(30)	1830(20)	6437(11)	36(6)
O(2)	-380(20)	2839(17)	5450(8)	44(4)
O(3)	-4040(20)	-1060(20)	8910(9)	64(6)
C(3)	-530(30)	1080(30)	6540(12)	51(7)
O(4)	220(30)	-2120(30)	10728(9)	84(9)
C(4)	-690(40)	350(30)	7134(12)	49(7)
O(5)	-6470(20)	-3890(20)	14155(10)	59(5)
C(5)	190(40)	330(30)	7635(10)	46(7)
O(6)	-4140(20)	-4940(20)	14293(8)	54(5)
C(6)	1340(40)	1010(30)	7491(12)	65(10)
C(7)	1550(30)	1780(30)	6888(11)	46(7)
O(7)	-1030(20)	3850(20)	4068(8)	46(5)
O(8)	890(20)	4609(18)	4338(8)	48(5)
C(8)	-30(40)	-240(30)	8285(12)	52(7)
C(9)	-1260(40)	-710(30)	8514(13)	50(7)
O(9)	6810(40)	4570(30)	1019(11)	105(10)
C(10)	-1550(40)	-1140(30)	9177(15)	57(8)
O(10)	2245(16)	6982(14)	4951(7)	27(3)
O(11)	3820(20)	3360(19)	4758(9)	50(5)
C(11)	-2970(40)	-1340(30)	9361(11)	49(7)
C(12)	-3290(40)	-1710(30)	10004(13)	58(8)
C(13)	-2190(30)	-1980(30)	10461(10)	46(7)
C(14)	-770(30)	-1830(30)	10267(14)	51(7)
C(15)	-460(30)	-1500(30)	9655(11)	44(7)
C(16)	-2550(40)	-2370(30)	11108(14)	57(8)
C(17)	-3890(40)	-2250(30)	11361(12)	58(8)
C(18)	-4210(30)	-2770(30)	12038(11)	49(7)
C(19)	-5510(30)	-2170(30)	12303(12)	47(7)

C(20)	-5810(30)	-2640(30)	12904(11)	48(7)
C(21)	-4900(30)	-3590(20)	13296(10)	32(5)
C(22)	-3560(30)	-4200(30)	13004(15)	57(8)
C(23)	-3230(30)	-3760(30)	12405(10)	45(7)
C(24)	-5200(30)	-4130(30)	13946(12)	48(7)
C(25)	-5520(40)	-1270(30)	9068(13)	66(9)
C(26)	1730(40)	-1970(30)	10587(15)	67(9)
C(27)	140(30)	4210(30)	3944(10)	40(7)
C(28)	830(30)	4250(20)	3309(12)	36(6)
C(29)	390(30)	3480(30)	2931(12)	50(8)
C(30)	950(40)	3540(30)	2338(14)	63(10)
C(31)	1990(40)	4340(30)	2093(10)	52(8)
C(32)	2390(40)	5020(30)	2496(15)	65(9)
C(33)	1760(30)	5030(30)	3067(12)	47(7)
C(34)	2610(40)	4350(30)	1444(12)	53(8)
C(35)	3810(30)	4760(30)	1247(12)	62(9)
C(36)	4420(30)	4860(20)	618(11)	43(7)
C(37)	5900(40)	4860(30)	490(12)	49(7)
C(38)	6530(40)	4950(30)	-96(13)	54(8)
C(39)	8560(50)	4620(50)	750(30)	160(30)
N(1)	2750(40)	9190(30)	4878(16)	98(11)
C(40)	1900(60)	10560(50)	4910(30)	170(30)
C(41)	3980(60)	9360(50)	4420(20)	150(20)
C(42)	3050(20)	7440(20)	5126(10)	30(5)
N(2)	5620(40)	2260(30)	2849(16)	86(10)
O(12)	3830(40)	2370(40)	3704(17)	127(13)
C(43)	6760(60)	2550(60)	2330(30)	220(40)
C(44)	4770(50)	1320(40)	2701(18)	93(14)
C(45)	4940(50)	2500(40)	3603(19)	150(30)

Table AA19. Bond lengths [Å] and angles [°] for Tb-PVDC-3.

Tb-O(10)	1.746(14)
Tb-O(8)	2.272(17)
Tb-O(6)#1	2.306(18)
Tb-O(5)#2	2.34(2)
Tb-O(2)#3	2.381(18)
Tb-O(1)	2.395(19)
Tb-O(7)#3	2.424(17)
Tb-O(11)	2.528(19)
Tb-C(42)	2.57(2)
O(1)-C(1)	1.25(3)
C(1)-O(2)	1.21(3)
C(1)-C(2)	1.53(3)
C(2)-C(7)	1.36(4)
C(2)-C(3)	1.36(4)
O(2)-Tb#3	2.381(18)
O(3)-C(11)	1.36(3)
O(3)-C(25)	1.43(4)
C(3)-C(4)	1.38(4)
C(3)-H(3A)	0.9400
O(4)-C(14)	1.32(4)
O(4)-C(26)	1.44(4)
C(4)-C(5)	1.37(4)
C(4)-H(4A)	0.9400
O(5)-C(24)	1.24(3)
O(5)-Tb#4	2.34(2)
C(5)-C(6)	1.38(4)
C(5)-C(8)	1.44(3)
O(6)-C(24)	1.31(4)
O(6)-Tb#1	2.306(18)
C(6)-C(7)	1.42(4)
C(6)-H(6A)	0.9400
C(7)-H(7A)	0.9400
O(7)-C(27)	1.21(3)
O(7)-Tb#3	2.424(17)

O(8)-C(27)	1.30(3)
C(8)-C(9)	1.35(4)
C(8)-H(8A)	0.9400
C(9)-C(10)	1.45(4)
C(9)-H(9A)	0.9400
O(9)-C(37)	1.39(4)
O(9)-C(39)	1.69(6)
C(10)-C(11)	1.39(4)
C(10)-C(15)	1.42(4)
O(10)-C(42)	1.07(2)
C(11)-C(12)	1.41(4)
C(12)-C(13)	1.39(4)
C(12)-H(12A)	0.9400
C(13)-C(14)	1.38(4)
C(13)-C(16)	1.43(4)
C(14)-C(15)	1.34(4)
C(15)-H(15A)	0.9400
C(16)-C(17)	1.32(4)
C(16)-H(16A)	0.9400
C(17)-C(18)	1.50(4)
C(17)-H(17A)	0.9400
C(18)-C(23)	1.38(4)
C(18)-C(19)	1.41(4)
C(19)-C(20)	1.34(3)
C(19)-H(19A)	0.9400
C(20)-C(21)	1.35(4)
C(20)-H(20A)	0.9400
C(21)-C(24)	1.45(3)
C(21)-C(22)	1.47(4)
C(22)-C(23)	1.34(4)
C(22)-H(22A)	0.9400
C(23)-H(23A)	0.9400
C(25)-H(25A)	0.9700
C(25)-H(25B)	0.9700
C(25)-H(25C)	0.9700
C(26)-H(26A)	0.9700

C(26)-H(26B)	0.9700
C(26)-H(26C)	0.9700
C(27)-C(28)	1.49(3)
C(28)-C(33)	1.32(4)
C(28)-C(29)	1.39(3)
C(29)-C(30)	1.36(3)
C(29)-H(29A)	0.9400
C(30)-C(31)	1.42(4)
C(30)-H(30A)	0.9400
C(31)-C(32)	1.35(4)
C(31)-C(34)	1.50(3)
C(32)-C(33)	1.35(4)
C(32)-H(32A)	0.9400
C(33)-H(33A)	0.9400
C(34)-C(35)	1.29(4)
C(34)-H(34A)	0.9400
C(35)-C(36)	1.45(3)
C(35)-H(35A)	0.9400
C(36)-C(37)	1.37(4)
C(36)-C(38)#5	1.42(4)
C(37)-C(38)	1.37(4)
C(38)-C(36)#5	1.42(4)
C(39)-H(39A)	0.9700
C(39)-H(39B)	0.9700
C(39)-H(39C)	0.9700
N(1)-C(41)	1.49(4)
N(1)-C(40)	1.54(5)
N(1)-C(42)	1.81(4)
C(40)-H(40A)	0.9700
C(40)-H(40B)	0.9700
C(40)-H(40C)	0.9700
C(41)-H(41A)	0.9700
C(41)-H(41B)	0.9700
C(41)-H(41C)	0.9700
N(2)-C(44)	1.46(4)
N(2)-C(43)	1.53(5)

N(2)-C(45)	1.79(4)
O(12)-C(45)	1.05(3)
C(43)-H(43A)	0.9700
C(43)-H(43B)	0.9700
C(43)-H(43C)	0.9700
C(44)-H(44A)	0.9700
C(44)-H(44B)	0.9700
C(44)-H(44C)	0.9700
C(45)-H(45A)	0.9400

O(10)-Tb-O(8)	121.8(7)
O(10)-Tb-O(6)#1	86.3(7)
O(8)-Tb-O(6)#1	147.8(8)
O(10)-Tb-O(5)#2	67.2(7)
O(8)-Tb-O(5)#2	84.7(7)
O(6)#1-Tb-O(5)#2	93.3(7)
O(10)-Tb-O(2)#3	52.5(6)
O(8)-Tb-O(2)#3	74.1(7)
O(6)#1-Tb-O(2)#3	137.4(7)
O(5)#2-Tb-O(2)#3	80.9(7)
O(10)-Tb-O(1)	143.0(6)
O(8)-Tb-O(1)	84.2(6)
O(6)#1-Tb-O(1)	80.3(6)
O(5)#2-Tb-O(1)	147.4(7)
O(2)#3-Tb-O(1)	124.8(6)
O(10)-Tb-O(7)#3	69.8(7)
O(8)-Tb-O(7)#3	124.2(7)
O(6)#1-Tb-O(7)#3	78.0(7)
O(5)#2-Tb-O(7)#3	136.6(7)
O(2)#3-Tb-O(7)#3	78.0(6)
O(1)-Tb-O(7)#3	73.7(6)
O(10)-Tb-O(11)	135.7(7)
O(8)-Tb-O(11)	72.8(7)
O(6)#1-Tb-O(11)	75.8(7)
O(5)#2-Tb-O(11)	73.7(7)
O(2)#3-Tb-O(11)	139.6(6)

O(1)-Tb-O(11)	73.7(6)
O(7)#3-Tb-O(11)	140.9(6)
O(10)-Tb-C(42)	18.6(7)
O(8)-Tb-C(42)	138.4(7)
O(6)#1-Tb-C(42)	67.8(7)
O(5)#2-Tb-C(42)	68.0(7)
O(2)#3-Tb-C(42)	71.0(6)
O(1)-Tb-C(42)	135.0(6)
O(7)#3-Tb-C(42)	69.4(7)
O(11)-Tb-C(42)	124.2(7)
C(1)-O(1)-Tb	136.6(17)
O(2)-C(1)-O(1)	128(2)
O(2)-C(1)-C(2)	114(2)
O(1)-C(1)-C(2)	117(2)
C(7)-C(2)-C(3)	121(2)
C(7)-C(2)-C(1)	118(2)
C(3)-C(2)-C(1)	120(2)
C(1)-O(2)-Tb#3	130.3(18)
C(11)-O(3)-C(25)	121(2)
C(2)-C(3)-C(4)	119(3)
C(2)-C(3)-H(3A)	120.5
C(4)-C(3)-H(3A)	120.5
C(14)-O(4)-C(26)	119(2)
C(5)-C(4)-C(3)	124(3)
C(5)-C(4)-H(4A)	118.2
C(3)-C(4)-H(4A)	118.2
C(24)-O(5)-Tb#4	138(2)
C(4)-C(5)-C(6)	115(2)
C(4)-C(5)-C(8)	127(3)
C(6)-C(5)-C(8)	118(3)
C(24)-O(6)-Tb#1	151.1(19)
C(5)-C(6)-C(7)	124(2)
C(5)-C(6)-H(6A)	118.1
C(7)-C(6)-H(6A)	118.1
C(2)-C(7)-C(6)	117(2)
C(2)-C(7)-H(7A)	121.6

C(6)-C(7)-H(7A)	121.6
C(27)-O(7)-Tb#3	110.1(15)
C(27)-O(8)-Tb	178.5(18)
C(9)-C(8)-C(5)	125(3)
C(9)-C(8)-H(8A)	117.7
C(5)-C(8)-H(8A)	117.7
C(8)-C(9)-C(10)	125(3)
C(8)-C(9)-H(9A)	117.7
C(10)-C(9)-H(9A)	117.7
C(37)-O(9)-C(39)	106(3)
C(11)-C(10)-C(15)	116(3)
C(11)-C(10)-C(9)	119(3)
C(15)-C(10)-C(9)	125(3)
C(42)-O(10)-Tb	130.1(16)
O(3)-C(11)-C(10)	118(2)
O(3)-C(11)-C(12)	122(3)
C(10)-C(11)-C(12)	120(3)
C(13)-C(12)-C(11)	122(3)
C(13)-C(12)-H(12A)	119.2
C(11)-C(12)-H(12A)	119.2
C(12)-C(13)-C(14)	118(2)
C(12)-C(13)-C(16)	120(3)
C(14)-C(13)-C(16)	122(3)
C(15)-C(14)-O(4)	125(3)
C(15)-C(14)-C(13)	121(3)
O(4)-C(14)-C(13)	114(3)
C(14)-C(15)-C(10)	123(3)
C(14)-C(15)-H(15A)	118.3
C(10)-C(15)-H(15A)	118.3
C(17)-C(16)-C(13)	127(3)
C(17)-C(16)-H(16A)	116.5
C(13)-C(16)-H(16A)	116.5
C(16)-C(17)-C(18)	124(3)
C(16)-C(17)-H(17A)	117.9
C(18)-C(17)-H(17A)	117.9
C(23)-C(18)-C(19)	120(2)

C(23)-C(18)-C(17)	122(2)
C(19)-C(18)-C(17)	117(3)
C(20)-C(19)-C(18)	118(3)
C(20)-C(19)-H(19A)	120.9
C(18)-C(19)-H(19A)	120.9
C(19)-C(20)-C(21)	125(3)
C(19)-C(20)-H(20A)	117.6
C(21)-C(20)-H(20A)	117.6
C(20)-C(21)-C(24)	127(2)
C(20)-C(21)-C(22)	115(2)
C(24)-C(21)-C(22)	118(2)
C(23)-C(22)-C(21)	121(3)
C(23)-C(22)-H(22A)	119.4
C(21)-C(22)-H(22A)	119.4
C(22)-C(23)-C(18)	120(3)
C(22)-C(23)-H(23A)	120.1
C(18)-C(23)-H(23A)	120.1
O(5)-C(24)-O(6)	121(2)
O(5)-C(24)-C(21)	119(3)
O(6)-C(24)-C(21)	120(2)
O(3)-C(25)-H(25A)	109.5
O(3)-C(25)-H(25B)	109.5
H(25A)-C(25)-H(25B)	109.5
O(3)-C(25)-H(25C)	109.5
H(25A)-C(25)-H(25C)	109.5
H(25B)-C(25)-H(25C)	109.5
O(4)-C(26)-H(26A)	109.5
O(4)-C(26)-H(26B)	109.5
H(26A)-C(26)-H(26B)	109.5
O(4)-C(26)-H(26C)	109.5
H(26A)-C(26)-H(26C)	109.5
H(26B)-C(26)-H(26C)	109.5
O(7)-C(27)-O(8)	124(2)
O(7)-C(27)-C(28)	121(2)
O(8)-C(27)-C(28)	115(2)
C(33)-C(28)-C(29)	118(2)

C(33)-C(28)-C(27)	124(2)
C(29)-C(28)-C(27)	118(2)
C(30)-C(29)-C(28)	119(3)
C(30)-C(29)-H(29A)	120.3
C(28)-C(29)-H(29A)	120.3
C(29)-C(30)-C(31)	122(2)
C(29)-C(30)-H(30A)	118.8
C(31)-C(30)-H(30A)	118.8
C(32)-C(31)-C(30)	114(2)
C(32)-C(31)-C(34)	125(3)
C(30)-C(31)-C(34)	121(3)
C(31)-C(32)-C(33)	123(3)
C(31)-C(32)-H(32A)	118.5
C(33)-C(32)-H(32A)	118.5
C(28)-C(33)-C(32)	123(3)
C(28)-C(33)-H(33A)	118.6
C(32)-C(33)-H(33A)	118.6
C(35)-C(34)-C(31)	124(3)
C(35)-C(34)-H(34A)	117.8
C(31)-C(34)-H(34A)	117.8
C(34)-C(35)-C(36)	127(3)
C(34)-C(35)-H(35A)	116.5
C(36)-C(35)-H(35A)	116.5
C(37)-C(36)-C(38)#5	117(2)
C(37)-C(36)-C(35)	123(3)
C(38)#5-C(36)-C(35)	120(3)
C(38)-C(37)-C(36)	125(3)
C(38)-C(37)-O(9)	120(3)
C(36)-C(37)-O(9)	114(3)
C(37)-C(38)-C(36)#5	118(3)
O(9)-C(39)-H(39A)	109.5
O(9)-C(39)-H(39B)	109.5
H(39A)-C(39)-H(39B)	109.5
O(9)-C(39)-H(39C)	109.5
H(39A)-C(39)-H(39C)	109.5
H(39B)-C(39)-H(39C)	109.5

C(41)-N(1)-C(40)	107(3)
C(41)-N(1)-C(42)	101(2)
C(40)-N(1)-C(42)	152(3)
N(1)-C(40)-H(40A)	109.4
N(1)-C(40)-H(40B)	109.5
H(40A)-C(40)-H(40B)	109.5
N(1)-C(40)-H(40C)	109.5
H(40A)-C(40)-H(40C)	109.5
H(40B)-C(40)-H(40C)	109.5
N(1)-C(41)-H(41A)	109.5
N(1)-C(41)-H(41B)	109.5
H(41A)-C(41)-H(41B)	109.5
N(1)-C(41)-H(41C)	109.5
H(41A)-C(41)-H(41C)	109.5
H(41B)-C(41)-H(41C)	109.5
O(10)-C(42)-N(1)	114(2)
O(10)-C(42)-Tb	31.3(11)
N(1)-C(42)-Tb	145.5(16)
C(44)-N(2)-C(43)	110(3)
C(44)-N(2)-C(45)	104(2)
C(43)-N(2)-C(45)	146(3)
N(2)-C(43)-H(43A)	109.4
N(2)-C(43)-H(43B)	109.5
H(43A)-C(43)-H(43B)	109.5
N(2)-C(43)-H(43C)	109.5
H(43A)-C(43)-H(43C)	109.5
H(43B)-C(43)-H(43C)	109.5
N(2)-C(44)-H(44A)	109.5
N(2)-C(44)-H(44B)	109.5
H(44A)-C(44)-H(44B)	109.5
N(2)-C(44)-H(44C)	109.5
H(44A)-C(44)-H(44C)	109.5
H(44B)-C(44)-H(44C)	109.5
O(12)-C(45)-N(2)	116(3)
O(12)-C(45)-H(45A)	122.0
N(2)-C(45)-H(45A)	122.0

Symmetry transformations used to generate equivalent atoms:

#1 -x,-y,-z+2 #2 x+1,y+1,z-1 #3 -x,-y+1,-z+1

#4 x-1,y-1,z+1 #5 -x+1,-y+1,-z

Table AA20. Anisotropic displacement parameters ($Å^2$ x 10^3) for Tb-PVDC-3. The anisotropic displacement factor exponent takes the form: $-2\pi^2[h^2 a^{*2} U^{11} + ... + 2 h k a^* b^* U^{12}]$

	U^{11}	U^{22}	U^{33}	U^{23}	U^{13}	U^{12}
Tb	15(1)	29(1)	15(1)	-1(1)	4(1)	-3(1)
C(1)	28(14)	53(17)	45(16)	36(13)	-6(11)	-21(12)
C(2)	43(15)	38(14)	22(12)	3(10)	5(10)	-6(12)
O(3)	55(14)	87(16)	38(11)	4(11)	-9(10)	-1(12)
C(3)	59(19)	65(19)	26(14)	3(13)	6(13)	-16(15)
O(4)	68(16)	140(20)	24(10)	-8(12)	9(10)	24(16)
C(4)	70(20)	40(16)	32(14)	7(12)	2(13)	-9(14)
C(5)	80(20)	50(16)	5(10)	0(10)	7(11)	-16(15)
O(6)	50(12)	82(15)	26(9)	11(9)	-7(9)	-23(11)
C(6)	80(20)	90(30)	19(13)	22(14)	-28(14)	-40(20)
C(7)	56(18)	59(18)	24(13)	2(12)	20(12)	-26(14)
O(7)	31(10)	74(14)	33(10)	-9(9)	10(8)	-11(9)
O(8)	64(13)	52(11)	37(10)	-20(9)	4(9)	-25(10)
C(8)	70(20)	55(18)	27(14)	-1(13)	12(14)	-12(16)
C(9)	70(20)	38(16)	40(15)	-3(12)	9(14)	-6(14)
O(9)	130(30)	130(30)	39(14)	6(15)	6(15)	10(20)
C(10)	60(20)	45(17)	59(19)	-4(15)	25(16)	-3(15)
C(11)	80(20)	46(16)	20(13)	6(11)	-4(13)	-12(15)
C(12)	70(20)	70(20)	33(15)	-10(14)	23(15)	-20(17)
C(13)	80(20)	55(17)	10(11)	-12(11)	16(12)	-16(15)
C(14)	56(19)	33(15)	59(19)	-3(13)	5(15)	0(13)
C(15)	45(16)	49(16)	29(14)	-3(12)	12(12)	5(13)
C(16)	60(20)	52(18)	52(18)	-7(14)	19(16)	-9(15)
C(17)	70(20)	80(20)	24(14)	-10(14)	15(14)	0(17)
C(18)	49(17)	80(20)	15(12)	-6(13)	11(11)	-7(15)
C(19)	52(17)	55(17)	33(14)	-10(13)	22(13)	-11(14)
C(20)	62(19)	64(19)	19(12)	-5(12)	7(12)	-15(15)
C(21)	42(14)	38(14)	12(10)	10(9)	-1(10)	-13(11)
C(22)	50(18)	45(17)	70(20)	3(15)	34(16)	-16(14)
C(23)	51(17)	65(18)	10(11)	2(11)	6(11)	2(14)
C(24)	45(17)	80(20)	26(13)	-19(14)	24(12)	-32(16)

C(25)	100(30)	80(20)	21(14)	8(14)	2(15)	-30(20)
C(26)	100(30)	51(19)	48(19)	4(15)	-12(18)	-22(19)
C(27)	65(19)	44(15)	6(10)	-5(10)	8(11)	4(13)
C(29)	70(20)	55(18)	34(14)	-15(13)	32(14)	-32(15)
C(30)	80(20)	80(20)	46(17)	-46(17)	38(16)	-50(20)
C(31)	80(20)	70(20)	5(11)	-7(12)	17(12)	-16(16)
C(32)	80(20)	70(20)	51(19)	-1(16)	31(17)	-28(18)
C(33)	46(16)	67(19)	29(14)	-16(13)	-5(12)	-9(14)
C(34)	70(20)	53(18)	26(14)	6(12)	10(14)	-13(16)
C(35)	50(18)	100(30)	20(13)	19(14)	21(13)	1(17)
C(36)	70(20)	33(14)	26(13)	-9(11)	17(12)	-4(13)
C(37)	70(20)	42(16)	32(14)	-5(12)	-12(14)	-6(14)
C(38)	70(20)	62(19)	31(14)	-18(14)	29(14)	-5(16)
C(39)	60(30)	130(50)	290(90)	-70(50)	-70(40)	10(30)
N(2)	80(20)	70(20)	110(30)	-20(20)	20(20)	-18(18)
C(43)	110(50)	100(40)	440(130)	0(60)	50(70)	-60(40)
C(44)	90(30)	130(40)	70(30)	-40(30)	20(20)	-40(30)
C(45)	170(60)	70(30)	230(70)	-90(40)	-110(50)	30(40)

Table AA21. Hydrogen coordinates (x 10^4) and isotropic displacement parameters ($Å^2$ x 10^3) for Tb-PVDC-3.

	x	y	z	U(eq)
H(3A)	-1158	1055	6211	61
H(4A)	-1428	-170	7199	59
H(6A)	2024	971	7810	79
H(7A)	2354	2225	6806	56
H(8A)	742	-301	8568	63
H(9A)	-1973	-748	8225	61
H(12A)	-4269	-1782	10128	70
H(15A)	542	-1505	9537	53
H(16A)	-1752	-2762	11382	68
H(17A)	-4697	-1804	11101	70
H(19A)	-6144	-1457	12064	56
H(20A)	-6725	-2281	13065	58
H(22A)	-2932	-4916	13242	69
H(23A)	-2332	-4124	12234	54
H(25A)	-6118	-1062	8689	98
H(25B)	-5952	-705	9351	98
H(25C)	-5501	-2168	9271	98
H(26A)	2294	-2173	10973	100
H(26B)	1749	-1077	10377	100
H(26C)	2155	-2554	10315	100
H(29A)	-283	2918	3082	60
H(30A)	629	3031	2083	75
H(32A)	3142	5517	2376	78
H(33A)	1996	5610	3303	56
H(34A)	2084	4040	1163	64
H(35A)	4358	5020	1542	75
H(39A)	9228	4465	1108	241
H(39B)	8597	5474	495	241
H(39C)	8858	3959	507	241
H(40A)	1129	10497	5221	249
H(40B)	1462	10975	4501	249

H(40C)	2587	11074	5016	249
H(41A)	4576	8512	4409	219
H(41B)	4587	9910	4549	219
H(41C)	3567	9755	4008	219
H(43A)	7347	3138	2438	331
H(43B)	6244	2945	1936	331
H(43C)	7403	1741	2285	331
H(44A)	3986	1212	3007	140
H(44B)	5424	493	2712	140
H(44C)	4340	1646	2286	140
H(45A)	5528	2723	3892	185

Table AA22. Crystal data and structure refinement for Nd-PVDC-3.

Identification code	**Nd-PVDC-3**	
Empirical formula	C45 H44 N2 Nd O12	
Formula weight	949.06	
Temperature	203(2) K	
Wavelength	0.71073 Å	
Crystal system	Triclinic	
Space group	P-1	
Unit cell dimensions	a = 9.258(2) Å	α = 78.623(5)°.
	b = 10.765(3) Å	β = 88.322(5)°.
	c = 21.866(6) Å	γ = 79.430(5)°.
Volume	2100.1(9) $Å^3$	
Z	2	
Density (calculated)	1.501 Mg/m^3	
Absorption coefficient	1.302 mm^{-1}	
F(000)	968	
Crystal size	0.31 x 0.06 x 0.02 mm^3	
Theta range for data collection	1.90 to 25.00°.	
Index ranges	-10<=h<=11, -12<=k<=12, -25<=l<=25	
Reflections collected	16116	
Independent reflections	7366 [R(int) = 0.0682]	
Completeness to theta = 25.00°	99.8 %	
Absorption correction	Sadabs	
Max. and min. transmission	0.9744 and 0.6883	
Refinement method	Full-matrix least-squares on F^2	
Data / restraints / parameters	7366 / 0 / 541	
Goodness-of-fit on F^2	1.133	
Final R indices [I>2sigma(I)]	R1 = 0.0676, wR2 = 0.1590	
R indices (all data)	R1 = 0.0939, wR2 = 0.1663	
Largest diff. peak and hole	4.338 and -1.611 $e.Å^{-3}$	

Table AA23. Atomic coordinates (x 10^4) and equivalent isotropic displacement parameters ($Å^2$ x 10^3) for Nd-PVDC-3. U(eq) is defined as one third of the trace of the orthogonalized U^{ij} tensor.

	x	y	z	U(eq)
Nd	12875(1)	9650(1)	-57(1)	19(1)
O(1)	11547(6)	8848(5)	889(3)	28(1)
C(1)	10252(9)	9143(7)	1061(3)	20(2)
N(1)	12252(10)	5503(8)	185(4)	56(2)
O(2)	9240(6)	9839(6)	708(2)	29(1)
C(2)	9871(8)	8650(7)	1723(3)	20(2)
N(2)	9423(12)	2865(10)	2114(5)	70(3)
C(3)	8593(9)	9211(8)	1992(4)	28(2)
O(3)	9017(8)	6031(7)	6106(3)	46(2)
O(4)	4752(8)	7106(7)	4261(3)	53(2)
C(4)	8259(9)	8801(8)	2604(4)	29(2)
O(5)	3319(6)	1642(5)	9223(3)	28(1)
C(5)	9210(10)	7762(8)	2983(4)	31(2)
O(6)	5353(6)	2188(5)	9546(2)	25(1)
C(6)	10478(10)	7209(9)	2715(4)	34(2)
O(7)	14263(6)	10401(5)	667(2)	26(1)
C(7)	10815(9)	7650(8)	2097(4)	29(2)
O(8)	16059(6)	11239(5)	982(2)	29(1)
C(8)	8871(11)	7262(8)	3631(4)	36(2)
O(9)	8171(11)	10394(9)	3983(4)	80(3)
C(9)	7539(11)	7394(9)	3893(4)	40(2)
O(10)	11870(6)	7638(6)	-146(3)	34(1)
C(10)	7206(11)	6973(8)	4543(4)	35(2)
C(11)	5762(11)	6842(8)	4730(4)	37(2)
O(11)	10986(12)	2631(9)	1293(5)	92(3)
O(12)	11258(6)	11612(5)	242(3)	28(1)
C(12)	5464(11)	6457(8)	5354(4)	35(2)
C(13)	6548(10)	6183(7)	5822(4)	33(2)
C(14)	7984(10)	6319(8)	5634(4)	34(2)
C(15)	8278(11)	6715(8)	5015(4)	37(2)
C(16)	3266(11)	7017(10)	4413(5)	48(3)

C(17)	10482(11)	6210(10)	5935(5)	49(3)
C(18)	6247(11)	5694(8)	6482(4)	35(2)
C(19)	5053(11)	5220(9)	6702(4)	38(2)
C(20)	4809(10)	4636(8)	7350(4)	30(2)
C(21)	3637(11)	3982(10)	7474(4)	44(3)
C(22)	3459(10)	3255(9)	8069(4)	40(2)
C(23)	4424(9)	3192(8)	8540(4)	26(2)
C(24)	5523(9)	3916(8)	8429(4)	30(2)
C(25)	5704(9)	4640(8)	7845(4)	31(2)
C(26)	4346(9)	2264(7)	9157(4)	23(2)
C(27)	14869(8)	10845(7)	1078(4)	21(2)
C(28)	14177(9)	10807(8)	1709(3)	25(2)
C(29)	13227(10)	9977(9)	1931(4)	35(2)
C(30)	12655(11)	9938(10)	2526(4)	45(3)
C(31)	13022(10)	10700(9)	2923(4)	37(2)
C(32)	13987(11)	11531(9)	2684(4)	39(2)
C(33)	14570(10)	11588(9)	2097(4)	34(2)
C(34)	12389(12)	10671(9)	3552(4)	42(2)
C(35)	11188(12)	10239(8)	3755(4)	41(2)
C(36)	10606(11)	10134(8)	4396(4)	39(2)
C(37)	9100(11)	10163(8)	4495(4)	36(2)
C(38)	8486(11)	10025(8)	5084(4)	38(2)
C(40)	6517(14)	10474(14)	4138(9)	120(7)
C(41)	12535(12)	6577(11)	-113(6)	56(3)
C(42)	13080(14)	4247(11)	206(8)	102(6)
C(43)	10954(16)	5583(13)	627(7)	87(4)
C(44)	9877(16)	2379(12)	1602(6)	74(4)
C(45)	8218(16)	2454(15)	2502(9)	111(6)
C(46)	10255(15)	3681(15)	2338(7)	90(5)

Table AA24. Bond lengths [Å] and angles [°] for Nd-PVDC-3.

Nd-O(2)#1	2.370(5)
Nd-O(7)	2.413(5)
Nd-O(6)#2	2.429(5)
Nd-O(1)	2.464(5)
Nd-O(5)#3	2.489(5)
Nd-O(8)#4	2.506(5)
Nd-O(12)	2.541(5)
Nd-O(10)	2.552(6)
Nd-O(7)#4	2.928(5)
Nd-C(27)#4	3.069(8)
O(1)-C(1)	1.250(9)
C(1)-O(2)	1.262(9)
C(1)-C(2)	1.495(10)
N(1)-C(41)	1.277(13)
N(1)-C(42)	1.420(14)
N(1)-C(43)	1.521(15)
O(2)-Nd#1	2.370(5)
C(2)-C(7)	1.393(11)
C(2)-C(3)	1.396(11)
N(2)-C(44)	1.351(15)
N(2)-C(46)	1.430(15)
N(2)-C(45)	1.461(16)
C(3)-C(4)	1.369(11)
C(3)-H(3A)	0.9400
O(3)-C(14)	1.378(11)
O(3)-C(17)	1.433(11)
O(4)-C(11)	1.361(11)
O(4)-C(16)	1.422(12)
C(4)-C(5)	1.425(12)
C(4)-H(4A)	0.9400
O(5)-C(26)	1.249(9)
O(5)-Nd#5	2.489(5)
C(5)-C(6)	1.385(12)
C(5)-C(8)	1.460(11)

O(6)-C(26)	1.262(9)
O(6)-Nd#2	2.429(5)
C(6)-C(7)	1.387(11)
C(6)-H(6A)	0.9400
O(7)-C(27)	1.283(9)
O(7)-Nd#4	2.928(5)
C(7)-H(7A)	0.9400
O(8)-C(27)	1.249(9)
O(8)-Nd#4	2.506(5)
C(8)-C(9)	1.340(13)
C(8)-H(8A)	0.9400
O(9)-C(37)	1.386(12)
O(9)-C(40)	1.549(16)
C(9)-C(10)	1.447(12)
C(9)-H(9A)	0.9400
O(10)-C(41)	1.184(12)
C(10)-C(15)	1.405(13)
C(10)-C(11)	1.410(13)
C(11)-C(12)	1.381(12)
O(11)-C(44)	1.255(14)
C(12)-C(13)	1.404(13)
C(12)-H(12A)	0.9400
C(13)-C(14)	1.405(13)
C(13)-C(18)	1.472(11)
C(14)-C(15)	1.370(11)
C(15)-H(15A)	0.9400
C(16)-H(16A)	0.9700
C(16)-H(16B)	0.9700
C(16)-H(16C)	0.9700
C(17)-H(17A)	0.9700
C(17)-H(17B)	0.9700
C(17)-H(17C)	0.9700
C(18)-C(19)	1.340(13)
C(18)-H(18A)	0.9400
C(19)-C(20)	1.461(11)
C(19)-H(19A)	0.9400

C(20)-C(25)	1.384(12)
C(20)-C(21)	1.390(13)
C(21)-C(22)	1.403(12)
C(21)-H(21A)	0.9400
C(22)-C(23)	1.368(12)
C(22)-H(22A)	0.9400
C(23)-C(24)	1.379(11)
C(23)-C(26)	1.520(11)
C(24)-C(25)	1.382(11)
C(24)-H(24A)	0.9400
C(25)-H(25A)	0.9400
C(27)-C(28)	1.499(10)
C(27)-Nd#4	3.069(8)
C(28)-C(29)	1.378(11)
C(28)-C(33)	1.404(12)
C(29)-C(30)	1.385(12)
C(29)-H(29A)	0.9400
C(30)-C(31)	1.394(13)
C(30)-H(30A)	0.9400
C(31)-C(32)	1.397(12)
C(31)-C(34)	1.476(11)
C(32)-C(33)	1.373(11)
C(32)-H(32A)	0.9400
C(33)-H(33A)	0.9400
C(34)-C(35)	1.315(13)
C(34)-H(34A)	0.9400
C(35)-C(36)	1.476(12)
C(35)-H(35A)	0.9400
C(36)-C(37)	1.401(13)
C(36)-C(38)#6	1.399(13)
C(37)-C(38)	1.383(12)
C(38)-C(36)#6	1.399(13)
C(38)-H(38A)	0.9400
C(40)-H(40A)	0.9700
C(40)-H(40B)	0.9700
C(40)-H(40C)	0.9700

C(41)-H(41)	0.9400
C(42)-H(42A)	0.9700
C(42)-H(42B)	0.9700
C(42)-H(42C)	0.9700
C(43)-H(43A)	0.9700
C(43)-H(43B)	0.9700
C(43)-H(43C)	0.9700
C(44)-H(44A)	0.9400
C(45)-H(45A)	0.9700
C(45)-H(45B)	0.9700
C(45)-H(45C)	0.9700
C(46)-H(46A)	0.9700
C(46)-H(46B)	0.9700
C(46)-H(46C)	0.9700

O(2)#1-Nd-O(7)	145.01(19)
O(2)#1-Nd-O(6)#2	140.9(2)
O(7)-Nd-O(6)#2	72.80(18)
O(2)#1-Nd-O(1)	94.16(18)
O(7)-Nd-O(1)	83.30(18)
O(6)#2-Nd-O(1)	77.92(17)
O(2)#1-Nd-O(5)#3	78.44(18)
O(7)-Nd-O(5)#3	83.16(18)
O(6)#2-Nd-O(5)#3	129.01(17)
O(1)-Nd-O(5)#3	143.59(18)
O(2)#1-Nd-O(8)#4	80.46(18)
O(7)-Nd-O(8)#4	124.69(18)
O(6)#2-Nd-O(8)#4	79.39(18)
O(1)-Nd-O(8)#4	135.74(18)
O(5)#3-Nd-O(8)#4	78.70(18)
O(2)#1-Nd-O(12)	73.04(19)
O(7)-Nd-O(12)	72.78(18)
O(6)#2-Nd-O(12)	137.26(18)
O(1)-Nd-O(12)	73.63(17)
O(5)#3-Nd-O(12)	70.10(17)
O(8)#4-Nd-O(12)	142.24(18)

O(2)#1-Nd-O(10)	68.41(19)
O(7)-Nd-O(10)	139.19(19)
O(6)#2-Nd-O(10)	73.21(19)
O(1)-Nd-O(10)	68.04(19)
O(5)#3-Nd-O(10)	136.70(19)
O(8)#4-Nd-O(10)	69.23(18)
O(12)-Nd-O(10)	122.09(18)
O(2)#1-Nd-O(7)#4	117.43(16)
O(7)-Nd-O(7)#4	78.00(18)
O(6)#2-Nd-O(7)#4	69.27(16)
O(1)-Nd-O(7)#4	145.75(16)
O(5)#3-Nd-O(7)#4	61.99(16)
O(8)#4-Nd-O(7)#4	47.37(16)
O(12)-Nd-O(7)#4	125.95(16)
O(10)-Nd-O(7)#4	109.85(17)
O(2)#1-Nd-C(27)#4	96.77(19)
O(7)-Nd-C(27)#4	102.56(19)
O(6)#2-Nd-C(27)#4	76.16(18)
O(1)-Nd-C(27)#4	150.24(19)
O(5)#3-Nd-C(27)#4	66.01(19)
O(8)#4-Nd-C(27)#4	23.20(19)
O(12)-Nd-C(27)#4	136.09(18)
O(10)-Nd-C(27)#4	90.5(2)
O(7)#4-Nd-C(27)#4	24.57(17)
C(1)-O(1)-Nd	132.4(5)
O(1)-C(1)-O(2)	123.6(7)
O(1)-C(1)-C(2)	118.5(7)
O(2)-C(1)-C(2)	117.8(7)
C(41)-N(1)-C(42)	128.3(11)
C(41)-N(1)-C(43)	116.1(9)
C(42)-N(1)-C(43)	115.2(10)
C(1)-O(2)-Nd#1	157.9(5)
C(7)-C(2)-C(3)	118.0(7)
C(7)-C(2)-C(1)	120.8(7)
C(3)-C(2)-C(1)	121.1(7)
C(44)-N(2)-C(46)	119.6(11)

C(44)-N(2)-C(45)	122.3(12)
C(46)-N(2)-C(45)	117.6(11)
C(4)-C(3)-C(2)	121.7(8)
C(4)-C(3)-H(3A)	119.1
C(2)-C(3)-H(3A)	119.1
C(14)-O(3)-C(17)	117.2(7)
C(11)-O(4)-C(16)	118.8(7)
C(3)-C(4)-C(5)	120.2(8)
C(3)-C(4)-H(4A)	119.9
C(5)-C(4)-H(4A)	119.9
C(26)-O(5)-Nd#5	134.2(5)
C(6)-C(5)-C(4)	117.9(7)
C(6)-C(5)-C(8)	120.0(8)
C(4)-C(5)-C(8)	122.1(8)
C(26)-O(6)-Nd#2	130.7(5)
C(5)-C(6)-C(7)	121.3(8)
C(5)-C(6)-H(6A)	119.4
C(7)-C(6)-H(6A)	119.4
C(27)-O(7)-Nd	173.8(5)
C(27)-O(7)-Nd#4	83.9(4)
Nd-O(7)-Nd#4	102.00(18)
C(6)-C(7)-C(2)	120.9(8)
C(6)-C(7)-H(7A)	119.6
C(2)-C(7)-H(7A)	119.6
C(27)-O(8)-Nd#4	104.6(5)
C(9)-C(8)-C(5)	126.2(9)
C(9)-C(8)-H(8A)	116.9
C(5)-C(8)-H(8A)	116.9
C(37)-O(9)-C(40)	115.2(10)
C(8)-C(9)-C(10)	126.6(9)
C(8)-C(9)-H(9A)	116.7
C(10)-C(9)-H(9A)	116.7
C(41)-O(10)-Nd	127.7(6)
C(15)-C(10)-C(11)	117.1(8)
C(15)-C(10)-C(9)	122.2(9)
C(11)-C(10)-C(9)	120.7(9)

O(4)-C(11)-C(12)	124.8(9)
O(4)-C(11)-C(10)	115.4(8)
C(12)-C(11)-C(10)	119.8(9)
C(11)-C(12)-C(13)	122.7(9)
C(11)-C(12)-H(12A)	118.6
C(13)-C(12)-H(12A)	118.6
C(14)-C(13)-C(12)	117.4(7)
C(14)-C(13)-C(18)	120.0(8)
C(12)-C(13)-C(18)	122.6(8)
C(15)-C(14)-O(3)	124.5(9)
C(15)-C(14)-C(13)	120.0(9)
O(3)-C(14)-C(13)	115.5(7)
C(14)-C(15)-C(10)	123.1(9)
C(14)-C(15)-H(15A)	118.4
C(10)-C(15)-H(15A)	118.4
O(4)-C(16)-H(16A)	109.5
O(4)-C(16)-H(16B)	109.5
H(16A)-C(16)-H(16B)	109.5
O(4)-C(16)-H(16C)	109.5
H(16A)-C(16)-H(16C)	109.5
H(16B)-C(16)-H(16C)	109.5
O(3)-C(17)-H(17A)	109.5
O(3)-C(17)-H(17B)	109.5
H(17A)-C(17)-H(17B)	109.5
O(3)-C(17)-H(17C)	109.5
H(17A)-C(17)-H(17C)	109.5
H(17B)-C(17)-H(17C)	109.5
C(19)-C(18)-C(13)	126.0(9)
C(19)-C(18)-H(18A)	117.0
C(13)-C(18)-H(18A)	117.0
C(18)-C(19)-C(20)	126.0(9)
C(18)-C(19)-H(19A)	117.0
C(20)-C(19)-H(19A)	117.0
C(25)-C(20)-C(21)	117.7(7)
C(25)-C(20)-C(19)	124.4(8)
C(21)-C(20)-C(19)	117.8(8)

C(20)-C(21)-C(22)	120.7(8)
C(20)-C(21)-H(21A)	119.7
C(22)-C(21)-H(21A)	119.7
C(23)-C(22)-C(21)	120.4(8)
C(23)-C(22)-H(22A)	119.8
C(21)-C(22)-H(22A)	119.8
C(22)-C(23)-C(24)	118.8(7)
C(22)-C(23)-C(26)	120.0(8)
C(24)-C(23)-C(26)	121.0(7)
C(23)-C(24)-C(25)	121.1(8)
C(23)-C(24)-H(24A)	119.4
C(25)-C(24)-H(24A)	119.4
C(20)-C(25)-C(24)	120.9(8)
C(20)-C(25)-H(25A)	119.6
C(24)-C(25)-H(25A)	119.6
O(5)-C(26)-O(6)	126.7(7)
O(5)-C(26)-C(23)	117.4(7)
O(6)-C(26)-C(23)	115.9(7)
O(8)-C(27)-O(7)	122.1(7)
O(8)-C(27)-C(28)	119.0(7)
O(7)-C(27)-C(28)	118.8(7)
O(8)-C(27)-Nd#4	52.2(4)
O(7)-C(27)-Nd#4	71.5(4)
C(28)-C(27)-Nd#4	160.9(5)
C(29)-C(28)-C(33)	119.1(7)
C(29)-C(28)-C(27)	121.9(7)
C(33)-C(28)-C(27)	119.0(7)
C(28)-C(29)-C(30)	120.0(8)
C(28)-C(29)-H(29A)	120.0
C(30)-C(29)-H(29A)	120.0
C(31)-C(30)-C(29)	122.4(9)
C(31)-C(30)-H(30A)	118.8
C(29)-C(30)-H(30A)	118.8
C(30)-C(31)-C(32)	116.2(8)
C(30)-C(31)-C(34)	122.2(8)
C(32)-C(31)-C(34)	121.6(8)

C(33)-C(32)-C(31)	122.5(8)
C(33)-C(32)-H(32A)	118.7
C(31)-C(32)-H(32A)	118.7
C(32)-C(33)-C(28)	119.8(8)
C(32)-C(33)-H(33A)	120.1
C(28)-C(33)-H(33A)	120.1
C(35)-C(34)-C(31)	126.4(9)
C(35)-C(34)-H(34A)	116.8
C(31)-C(34)-H(34A)	116.8
C(34)-C(35)-C(36)	126.4(10)
C(34)-C(35)-H(35A)	116.8
C(36)-C(35)-H(35A)	116.8
C(37)-C(36)-C(38)#6	118.1(8)
C(37)-C(36)-C(35)	119.6(9)
C(38)#6-C(36)-C(35)	122.3(9)
O(9)-C(37)-C(38)	118.3(9)
O(9)-C(37)-C(36)	118.9(8)
C(38)-C(37)-C(36)	122.7(9)
C(37)-C(38)-C(36)#6	119.2(9)
C(37)-C(38)-H(38A)	120.4
C(36)#6-C(38)-H(38A)	120.4
O(9)-C(40)-H(40A)	109.5
O(9)-C(40)-H(40B)	109.5
H(40A)-C(40)-H(40B)	109.5
O(9)-C(40)-H(40C)	109.5
H(40A)-C(40)-H(40C)	109.5
H(40B)-C(40)-H(40C)	109.5
O(10)-C(41)-N(1)	130.3(11)
O(10)-C(41)-H(41)	114.9
N(1)-C(41)-H(41)	114.9
N(1)-C(42)-H(42A)	109.5
N(1)-C(42)-H(42B)	109.5
H(42A)-C(42)-H(42B)	109.5
N(1)-C(42)-H(42C)	109.5
H(42A)-C(42)-H(42C)	109.5
H(42B)-C(42)-H(42C)	109.5

N(1)-C(43)-H(43A)	109.5
N(1)-C(43)-H(43B)	109.5
H(43A)-C(43)-H(43B)	109.5
N(1)-C(43)-H(43C)	109.5
H(43A)-C(43)-H(43C)	109.5
H(43B)-C(43)-H(43C)	109.5
O(11)-C(44)-N(2)	123.6(13)
O(11)-C(44)-H(44A)	118.2
N(2)-C(44)-H(44A)	118.2
N(2)-C(45)-H(45A)	109.5
N(2)-C(45)-H(45B)	109.5
H(45A)-C(45)-H(45B)	109.5
N(2)-C(45)-H(45C)	109.5
H(45A)-C(45)-H(45C)	109.5
H(45B)-C(45)-H(45C)	109.5
N(2)-C(46)-H(46A)	109.5
N(2)-C(46)-H(46B)	109.5
H(46A)-C(46)-H(46B)	109.5
N(2)-C(46)-H(46C)	109.5
H(46A)-C(46)-H(46C)	109.5
H(46B)-C(46)-H(46C)	109.5

Symmetry transformations used to generate equivalent atoms:

#1 -x+2,-y+2,-z #2 -x+2,-y+1,-z+1 #3 x+1,y+1,z-1

#4 -x+3,-y+2,-z #5 x-1,y-1,z+1 #6 -x+2,-y+2,-z+1

Table AA25. Anisotropic displacement parameters ($Å^2$ x 10^3) for Nd-PVDC-3. The anisotropic displacement factor exponent takes the form: $-2\pi^2[h^2 a^{*2} U^{11} + ... + 2 h k a^* b^* U^{12}]$.

	U^{11}	U^{22}	U^{33}	U^{23}	U^{13}	U^{12}
Nd	22(1)	16(1)	18(1)	-1(1)	8(1)	-2(1)
O(1)	24(3)	23(3)	34(3)	-3(2)	12(3)	1(2)
C(1)	30(5)	13(4)	20(4)	-8(3)	6(4)	-5(3)
N(1)	61(6)	33(5)	78(7)	-15(5)	10(5)	-15(4)
O(2)	28(3)	41(4)	14(3)	3(2)	5(2)	-10(3)
C(2)	24(4)	17(4)	20(4)	-7(3)	8(3)	-4(3)
N(2)	79(7)	52(7)	85(8)	-27(6)	14(6)	-14(5)
C(3)	36(5)	27(5)	17(4)	0(3)	6(4)	1(4)
O(3)	58(4)	48(4)	32(4)	-2(3)	8(3)	-15(3)
O(4)	65(5)	59(5)	29(4)	2(3)	9(4)	-6(4)
C(4)	37(5)	29(5)	21(4)	-9(4)	12(4)	1(4)
O(5)	24(3)	21(3)	33(3)	7(2)	7(3)	-1(2)
C(5)	44(5)	31(5)	19(4)	-5(4)	11(4)	-12(4)
O(6)	32(3)	16(3)	20(3)	5(2)	6(3)	3(2)
C(6)	42(5)	28(5)	27(5)	4(4)	9(4)	-2(4)
O(7)	28(3)	28(3)	22(3)	-5(2)	4(2)	-1(2)
C(7)	36(5)	24(5)	22(4)	-1(3)	12(4)	1(4)
O(8)	31(3)	26(3)	28(3)	-6(2)	11(3)	-4(3)
C(8)	53(6)	26(5)	26(5)	-3(4)	8(4)	-6(4)
O(9)	109(7)	73(6)	61(6)	-20(5)	16(5)	-15(5)
C(9)	61(7)	34(6)	26(5)	-6(4)	17(5)	-10(5)
O(10)	38(3)	20(4)	47(4)	-11(3)	8(3)	-9(3)
C(10)	60(6)	21(5)	23(5)	-1(4)	14(4)	-7(4)
C(11)	60(6)	22(5)	25(5)	0(4)	8(5)	-4(4)
O(11)	118(8)	68(7)	92(7)	-24(5)	20(6)	-19(6)
O(12)	24(3)	19(3)	38(3)	-5(2)	12(3)	-1(2)
C(12)	50(6)	17(5)	36(5)	-7(4)	20(4)	1(4)
C(13)	60(6)	10(4)	24(5)	-2(3)	16(4)	1(4)
C(14)	56(6)	20(5)	22(5)	0(3)	14(4)	-2(4)
C(15)	58(6)	24(5)	29(5)	-8(4)	16(5)	-4(4)
C(16)	64(7)	31(6)	44(6)	-6(4)	4(5)	6(5)

C(17)	58(7)	44(7)	44(6)	-8(5)	11(5)	-6(5)
C(18)	61(6)	20(5)	22(4)	-1(4)	11(4)	-3(4)
C(19)	58(6)	28(5)	26(5)	-4(4)	11(4)	-6(4)
C(20)	43(5)	20(5)	23(4)	1(3)	9(4)	-2(4)
C(21)	59(7)	50(7)	25(5)	2(4)	-4(5)	-20(5)
C(22)	41(5)	44(6)	38(5)	-2(4)	6(5)	-23(5)
C(23)	33(5)	19(4)	23(4)	1(3)	9(4)	0(3)
C(24)	35(5)	28(5)	24(4)	1(4)	4(4)	-5(4)
C(25)	35(5)	27(5)	30(5)	1(4)	12(4)	-13(4)
C(26)	26(4)	15(4)	25(4)	-6(3)	11(4)	7(3)
C(27)	24(4)	13(4)	23(4)	-3(3)	5(3)	3(3)
C(28)	29(4)	28(5)	17(4)	-6(3)	6(3)	-3(4)
C(29)	47(6)	40(6)	25(5)	-19(4)	18(4)	-17(4)
C(30)	58(7)	46(6)	37(6)	-15(5)	20(5)	-25(5)
C(31)	51(6)	34(5)	28(5)	-14(4)	15(4)	-7(4)
C(32)	59(6)	38(6)	26(5)	-20(4)	17(4)	-13(5)
C(33)	41(5)	35(5)	28(5)	-9(4)	12(4)	-11(4)
C(34)	70(7)	33(6)	25(5)	-11(4)	23(5)	-12(5)
C(35)	71(7)	23(5)	26(5)	-8(4)	20(5)	2(5)
C(36)	64(7)	17(5)	31(5)	-3(4)	24(5)	-2(4)
C(37)	58(6)	23(5)	23(5)	-1(4)	4(4)	-6(4)
C(38)	60(6)	22(5)	29(5)	-10(4)	20(5)	3(4)
C(40)	50(8)	69(11)	240(20)	-52(12)	-38(11)	15(7)
C(41)	41(6)	40(7)	93(9)	-17(6)	8(6)	-16(5)
C(42)	76(9)	21(7)	210(18)	-36(8)	31(10)	0(6)
C(43)	108(11)	50(8)	100(11)	-5(7)	35(9)	-21(8)
C(44)	95(10)	55(8)	82(10)	-30(7)	28(8)	-25(7)
C(45)	76(10)	78(11)	189(18)	-52(11)	45(11)	-17(8)
C(46)	90(10)	103(12)	96(11)	-58(10)	21(9)	-26(9)

Table AA26. Hydrogen coordinates (x 10^4) and isotropic displacement parameters (Å^2 x 10^3) for Nd-PVDC-3.

	x	y	z	U(eq)
H(3A)	7944	9887	1747	34
H(4A)	7399	9207	2775	35
H(6A)	11122	6521	2956	41
H(7A)	11693	7269	1929	35
H(8A)	9664	6803	3890	43
H(9A)	6740	7801	3627	48
H(12A)	4496	6375	5471	42
H(15A)	9242	6818	4902	45
H(16A)	2679	7232	4034	72
H(16B)	2893	7613	4685	72
H(16C)	3213	6145	4624	72
H(17A)	11104	5976	6304	74
H(17B)	10471	7107	5746	74
H(17C)	10863	5670	5639	74
H(18A)	6959	5717	6775	42
H(19A)	4302	5267	6414	46
H(21A)	2958	4028	7155	53
H(22A)	2669	2807	8145	48
H(24A)	6159	3917	8756	36
H(25A)	6446	5142	7783	37
H(29A)	12968	9437	1679	42
H(30A)	11995	9377	2666	53
H(32A)	14247	12071	2936	47
H(33A)	15229	12149	1955	40
H(34A)	12894	10993	3835	50
H(35A)	10647	9970	3464	50
H(38A)	7472	10037	5133	46
H(40A)	5955	10633	3754	180
H(40B)	6196	11172	4359	180
H(40C)	6363	9668	4397	180
H(41)	13411	6514	-343	68

H(42A)	13887	4290	-86	153
H(42B)	12453	3696	94	153
H(42C)	13467	3897	625	153
H(43A)	10462	6473	584	131
H(43B)	11301	5259	1053	131
H(43C)	10271	5068	526	131
H(44A)	9332	1823	1471	89
H(45A)	7735	1920	2296	167
H(45B)	7516	3205	2564	167
H(45C)	8604	1963	2902	167
H(46A)	11017	3882	2040	136
H(46B)	10702	3244	2737	136
H(46C)	9610	4473	2388	136

Table AA27. Crystal data and structure refinement for Er-PVDC-3.

Identification code	**Er-PVDC-3**	
Empirical formula	C42 H36 Er N O12	
Formula weight	913.98	
Temperature	293(2) K	
Wavelength	0.71073 Å	
Crystal system	Triclinic	
Space group	P -1	
Unit cell dimensions	a = 8.942(4) Å	α = 78.278(9)°.
	b = 10.817(6) Å	β = 87.967(9)°.
	c = 21.818(11) Å	γ = 78.977(10)°.
Volume	2028.2(18) $Å^3$	
Z	2	
Density (calculated)	1.497 Mg/m^3	
Absorption coefficient	2.131 mm^{-1}	
F(000)	918	
Crystal size	.22 x .07 x .08 mm^3	
Theta range for data collection	1.91 to 23.00°.	
Index ranges	-9<=h<=9, -11<=k<=11, -23<=l<=23	
Reflections collected	13125	
Independent reflections	5633 [R(int) = 0.0918]	
Completeness to theta = 23.00°	100.0 %	
Absorption correction	Semi-empirical from equivalents	
Max. and min. transmission	.85 and .63	
Refinement method	Full-matrix least-squares on F^2	
Data / restraints / parameters	5633 / 602 / 440	
Goodness-of-fit on F^2	2.073	
Final R indices [I>2sigma(I)]	R1 = 0.1637, wR2 = 0.3489	
R indices (all data)	R1 = 0.2384, wR2 = 0.3714	
Largest diff. peak and hole	3.557 and -2.958 $e.Å^{-3}$	

Table AA28. Atomic coordinates (x 10^4) and equivalent isotropic displacement parameters ($Å^2$ x 10^3) for Er-PVDC-3. U(eq) is defined as one third of the trace of the orthogonalized U^{ij} tensor.

	x	y	z	U(eq)
Er	12915(1)	4564(2)	-34(1)	95(1)
N	9160(40)	7960(30)	2135(19)	162(14)
O(1)	11440(20)	3950(17)	811(8)	100(5)
C(1)	10050(30)	4320(30)	991(10)	71(6)
C(2)	9820(30)	3720(20)	1691(9)	61(5)
O(2)	9040(20)	5022(19)	677(7)	87(5)
O(3)	9079(15)	1053(14)	6089(6)	60(4)
C(3)	10790(30)	2680(20)	2025(10)	66(5)
O(4)	4653(14)	2109(14)	4242(6)	59(4)
C(4)	10490(20)	2230(20)	2652(10)	54(5)
C(5)	9150(20)	2883(18)	2925(9)	43(4)
C(6)	8220(20)	3894(19)	2595(9)	57(6)
O(6)	3290(20)	-3438(18)	9239(8)	95(5)
C(7)	8490(30)	4340(20)	1960(9)	65(6)
O(7)	14200(30)	5380(20)	625(7)	114(7)
C(8)	8900(20)	2289(18)	3602(8)	43(5)
O(8)	15937(18)	6288(16)	894(7)	78(5)
O(9)	8066(19)	5355(19)	3989(8)	95(5)
C(9)	7520(20)	2433(18)	3873(8)	44(5)
C(10)	7210(20)	1965(18)	4532(8)	40(4)
O(10)	11440(20)	6402(19)	221(9)	110(6)
C(11)	8300(20)	1779(17)	4983(8)	47(5)
O(11)	10580(90)	9080(70)	2090(20)	330(30)
C(12)	7980(20)	1352(19)	5619(8)	48(4)
O(12)	11960(20)	2450(20)	-71(9)	135(8)
C(13)	6510(20)	1199(17)	5811(8)	38(4)
C(14)	5420(20)	1416(17)	5356(8)	45(4)
C(15)	5720(20)	1829(19)	4736(9)	48(5)
C(16)	10590(20)	1250(20)	5908(9)	58(6)
C(17)	3190(20)	1940(20)	4411(9)	53(5)
C(18)	6210(20)	712(17)	6459(8)	45(4)

C(19)	5020(20)	250(20)	6689(9)	57(5)
C(20)	4780(20)	-410(20)	7357(8)	48(4)
C(21)	3560(30)	-980(20)	7484(9)	74(6)
C(22)	3370(30)	-1750(30)	8075(9)	80(6)
C(23)	4310(30)	-1780(30)	8536(9)	71(6)
C(24)	5530(20)	-1090(20)	8420(9)	66(5)
C(25)	5700(20)	-390(20)	7842(8)	50(4)
C(27)	14830(30)	5770(20)	1022(11)	65(6)
C(28)	14140(20)	5860(20)	1657(9)	62(5)
C(29)	13210(30)	5020(30)	1901(10)	93(7)
C(30)	12570(30)	4970(30)	2514(10)	91(7)
C(31)	13000(20)	5730(20)	2869(9)	64(5)
C(32)	13930(20)	6547(19)	2622(9)	53(5)
C(33)	14490(20)	6570(20)	2026(9)	62(5)
C(34)	12380(20)	5670(20)	3528(9)	59(5)
C(35)	11170(20)	5255(19)	3749(9)	54(5)
C(36)	10580(20)	5146(19)	4399(9)	51(4)
C(37)	11570(20)	4959(19)	4910(9)	53(5)
C(38)	9060(20)	5180(20)	4500(9)	55(5)
C(39)	6350(30)	5470(30)	4140(17)	123(11)
C(41)	8590(80)	8200(60)	1480(30)	310(30)
C(42)	8220(50)	7360(50)	2800(30)	240(30)
C(43)	10240(150)	8600(130)	2520(50)	400(40)
O(5)	5390(20)	-2890(17)	9540(8)	91(5)
C(26)	4330(30)	-2790(30)	9174(13)	94(8)

Table AA29. Bond lengths [Å] and angles [°] for Er-PVDC-3.

Er-O(2)#1	2.200(19)
Er-O(5)#2	2.237(18)
Er-O(7)	2.280(19)
Er-O(1)	2.290(14)
Er-O(10)	2.32(2)
Er-O(8)#3	2.374(16)
Er-O(6)#4	2.480(18)
Er-O(12)	2.60(2)
Er-O(7)#3	2.85(2)
Er-C(27)#3	2.93(2)
N-C(43)	1.62(13)
N-C(41)	1.49(5)
N-C(42)	1.72(6)
O(1)-C(1)	1.30(3)
C(1)-O(2)	1.20(3)
C(1)-C(2)	1.56(3)
C(2)-C(3)	1.37(3)
C(2)-C(7)	1.42(3)
O(2)-Er#1	2.200(19)
O(3)-C(12)	1.39(2)
O(3)-C(16)	1.43(2)
C(3)-C(4)	1.39(3)
C(3)-H(3A)	0.9300
O(4)-C(17)	1.38(2)
O(4)-C(15)	1.41(2)
C(4)-C(5)	1.44(2)
C(4)-H(4A)	0.9300
C(5)-C(6)	1.34(3)
C(5)-C(8)	1.51(2)
C(6)-C(7)	1.40(2)
C(6)-H(6A)	0.9300
O(6)-C(26)	1.26(3)
O(6)-Er#5	2.480(18)

C(7)-H(7A)	0.9300
O(7)-C(27)	1.23(3)
O(7)-Er#3	2.85(2)
C(8)-C(9)	1.35(2)
C(8)-H(8A)	0.9300
O(8)-C(27)	1.22(2)
O(8)-Er#3	2.374(16)
O(9)-C(38)	1.41(2)
O(9)-C(39)	1.54(3)
C(9)-C(10)	1.46(2)
C(9)-H(9A)	0.9300
C(10)-C(11)	1.37(2)
C(10)-C(15)	1.41(2)
C(11)-C(12)	1.41(2)
C(11)-H(11A)	0.9300
O(11)-C(43)	1.04(15)
C(12)-C(13)	1.40(2)
C(13)-C(14)	1.37(2)
C(13)-C(18)	1.44(2)
C(14)-C(15)	1.37(2)
C(14)-H(14A)	0.9300
C(16)-H(16A)	0.9600
C(16)-H(16B)	0.9600
C(16)-H(16C)	0.9600
C(17)-H(17A)	0.9600
C(17)-H(17B)	0.9600
C(17)-H(17C)	0.9600
C(18)-C(19)	1.30(3)
C(18)-H(18A)	0.9300
C(19)-C(20)	1.52(3)
C(19)-H(19A)	0.9300
C(20)-C(21)	1.35(3)
C(20)-C(25)	1.37(3)
C(21)-C(22)	1.41(3)
C(21)-H(21A)	0.9300
C(22)-C(23)	1.32(3)

C(22)-H(22A)	0.9300
C(23)-C(24)	1.42(3)
C(23)-C(26)	1.59(3)
C(24)-C(25)	1.35(3)
C(24)-H(24A)	0.9300
C(25)-H(25A)	0.9300
C(27)-C(28)	1.51(3)
C(27)-Er#3	2.93(2)
C(28)-C(33)	1.30(3)
C(28)-C(29)	1.37(3)
C(29)-C(30)	1.43(3)
C(29)-H(29A)	0.9300
C(30)-C(31)	1.35(3)
C(30)-H(30A)	0.9300
C(31)-C(32)	1.35(3)
C(31)-C(34)	1.51(2)
C(32)-C(33)	1.37(2)
C(32)-H(32A)	0.9300
C(33)-H(33A)	0.9300
C(34)-C(35)	1.29(3)
C(34)-H(34A)	0.9300
C(35)-C(36)	1.49(2)
C(35)-H(35A)	0.9300
C(36)-C(38)	1.36(3)
C(36)-C(37)	1.40(3)
C(37)-C(38)#6	1.38(3)
C(38)-C(37)#6	1.38(3)
C(39)-H(39A)	0.9600
C(39)-H(39B)	0.9600
C(39)-H(39C)	0.9600
C(41)-H(41A)	0.9600
C(41)-H(41B)	0.9600
C(41)-H(41C)	0.9600
C(42)-H(42A)	0.9600
C(42)-H(42B)	0.9600
C(42)-H(42C)	0.9600

C(43)-H(43A)	0.9300
O(5)-C(26)	1.23(3)
O(5)-Er#2	2.237(18)

O(2)#1-Er-O(5)#2	139.8(7)
O(2)#1-Er-O(7)	144.7(8)
O(5)#2-Er-O(7)	74.9(7)
O(2)#1-Er-O(1)	91.8(6)
O(5)#2-Er-O(1)	82.4(7)
O(7)-Er-O(1)	86.6(6)
O(2)#1-Er-O(10)	76.9(7)
O(5)#2-Er-O(10)	136.3(7)
O(7)-Er-O(10)	69.2(8)
O(1)-Er-O(10)	71.7(7)
O(2)#1-Er-O(8)#3	79.1(6)
O(5)#2-Er-O(8)#3	79.1(6)
O(7)-Er-O(8)#3	123.6(6)
O(1)-Er-O(8)#3	138.0(6)
O(10)-Er-O(8)#3	142.3(6)
O(2)#1-Er-O(6)#4	76.9(6)
O(5)#2-Er-O(6)#4	130.7(6)
O(7)-Er-O(6)#4	81.3(6)
O(1)-Er-O(6)#4	138.8(6)
O(10)-Er-O(6)#4	67.2(6)
O(8)#3-Er-O(6)#4	79.3(6)
O(2)#1-Er-O(12)	70.0(7)
O(5)#2-Er-O(12)	71.1(7)
O(7)-Er-O(12)	139.3(7)
O(1)-Er-O(12)	67.5(6)
O(10)-Er-O(12)	125.5(7)
O(8)#3-Er-O(12)	70.8(6)
O(6)#4-Er-O(12)	138.6(6)
O(2)#1-Er-O(7)#3	115.0(5)
O(5)#2-Er-O(7)#3	71.2(6)
O(7)-Er-O(7)#3	76.8(6)
O(1)-Er-O(7)#3	151.6(7)

O(10)-Er-O(7)#3	121.4(6)
O(8)#3-Er-O(7)#3	47.4(5)
O(6)#4-Er-O(7)#3	61.6(6)
O(12)-Er-O(7)#3	111.6(6)
O(2)#1-Er-C(27)#3	93.7(6)
O(5)#2-Er-C(27)#3	79.0(6)
O(7)-Er-C(27)#3	101.4(7)
O(1)-Er-C(27)#3	157.0(6)
O(10)-Er-C(27)#3	131.3(7)
O(8)#3-Er-C(27)#3	23.8(5)
O(6)#4-Er-C(27)#3	64.2(6)
O(12)-Er-C(27)#3	93.5(6)
O(7)#3-Er-C(27)#3	24.6(5)
C(43)-N-C(41)	136(6)
C(43)-N-C(42)	94(5)
C(41)-N-C(42)	126(4)
C(1)-O(1)-Er	136.3(18)
O(2)-C(1)-O(1)	127(2)
O(2)-C(1)-C(2)	122(2)
O(1)-C(1)-C(2)	111(3)
C(3)-C(2)-C(7)	122.2(18)
C(3)-C(2)-C(1)	124(2)
C(7)-C(2)-C(1)	114(2)
C(1)-O(2)-Er#1	153.4(19)
C(12)-O(3)-C(16)	117.0(14)
C(2)-C(3)-C(4)	119.2(19)
C(2)-C(3)-H(3A)	120.4
C(4)-C(3)-H(3A)	120.4
C(17)-O(4)-C(15)	116.1(14)
C(3)-C(4)-C(5)	118(2)
C(3)-C(4)-H(4A)	120.9
C(5)-C(4)-H(4A)	120.8
C(6)-C(5)-C(4)	121.9(18)
C(6)-C(5)-C(8)	124.4(16)
C(4)-C(5)-C(8)	113.7(18)
C(5)-C(6)-C(7)	120.6(18)

C(5)-C(6)-H(6A)	119.7
C(7)-C(6)-H(6A)	119.7
C(26)-O(6)-Er#5	133.3(18)
C(6)-C(7)-C(2)	118(2)
C(6)-C(7)-H(7A)	121.1
C(2)-C(7)-H(7A)	121.1
C(27)-O(7)-Er	174.5(15)
C(27)-O(7)-Er#3	81.3(15)
Er-O(7)-Er#3	103.2(6)
C(9)-C(8)-C(5)	122.5(18)
C(9)-C(8)-H(8A)	118.8
C(5)-C(8)-H(8A)	118.8
C(27)-O(8)-Er#3	104.4(15)
C(38)-O(9)-C(39)	116.7(19)
C(8)-C(9)-C(10)	125.3(18)
C(8)-C(9)-H(9A)	117.3
C(10)-C(9)-H(9A)	117.3
C(11)-C(10)-C(15)	117.3(17)
C(11)-C(10)-C(9)	121.6(16)
C(15)-C(10)-C(9)	120.7(17)
C(10)-C(11)-C(12)	121.2(18)
C(10)-C(11)-H(11A)	119.4
C(12)-C(11)-H(11A)	119.4
O(3)-C(12)-C(13)	115.9(16)
O(3)-C(12)-C(11)	123.5(17)
C(13)-C(12)-C(11)	120.6(18)
C(14)-C(13)-C(12)	117.6(16)
C(14)-C(13)-C(18)	121.6(16)
C(12)-C(13)-C(18)	120.5(17)
C(15)-C(14)-C(13)	121.8(17)
C(15)-C(14)-H(14A)	119.1
C(13)-C(14)-H(14A)	119.1
C(14)-C(15)-C(10)	121.1(18)
C(14)-C(15)-O(4)	125.3(17)
C(10)-C(15)-O(4)	113.5(16)
O(3)-C(16)-H(16A)	109.5

O(3)-C(16)-H(16B)	109.5
H(16A)-C(16)-H(16B)	109.5
O(3)-C(16)-H(16C)	109.5
H(16A)-C(16)-H(16C)	109.5
H(16B)-C(16)-H(16C)	109.5
O(4)-C(17)-H(17A)	109.5
O(4)-C(17)-H(17B)	109.5
H(17A)-C(17)-H(17B)	109.5
O(4)-C(17)-H(17C)	109.5
H(17A)-C(17)-H(17C)	109.5
H(17B)-C(17)-H(17C)	109.5
C(19)-C(18)-C(13)	128(2)
C(19)-C(18)-H(18A)	116.2
C(13)-C(18)-H(18A)	116.2
C(18)-C(19)-C(20)	128(2)
C(18)-C(19)-H(19A)	116.2
C(20)-C(19)-H(19A)	116.2
C(21)-C(20)-C(25)	118.6(18)
C(21)-C(20)-C(19)	118.6(19)
C(25)-C(20)-C(19)	122.7(18)
C(20)-C(21)-C(22)	121(2)
C(20)-C(21)-H(21A)	119.3
C(22)-C(21)-H(21A)	119.4
C(23)-C(22)-C(21)	119(2)
C(23)-C(22)-H(22A)	120.5
C(21)-C(22)-H(22A)	120.5
C(22)-C(23)-C(24)	120(2)
C(22)-C(23)-C(26)	121(2)
C(24)-C(23)-C(26)	118(2)
C(25)-C(24)-C(23)	120(2)
C(25)-C(24)-H(24A)	120.2
C(23)-C(24)-H(24A)	120.2
C(24)-C(25)-C(20)	121(2)
C(24)-C(25)-H(25A)	119.6
C(20)-C(25)-H(25A)	119.6
O(8)-C(27)-O(7)	122(2)

O(8)-C(27)-C(28)	115(2)
O(7)-C(27)-C(28)	123(2)
O(8)-C(27)-Er#3	51.8(12)
O(7)-C(27)-Er#3	74.1(14)
C(28)-C(27)-Er#3	161.2(16)
C(33)-C(28)-C(29)	116.1(19)
C(33)-C(28)-C(27)	126(2)
C(29)-C(28)-C(27)	117(2)
C(28)-C(29)-C(30)	122(2)
C(28)-C(29)-H(29A)	118.9
C(30)-C(29)-H(29A)	118.9
C(31)-C(30)-C(29)	118(2)
C(31)-C(30)-H(30A)	121.2
C(29)-C(30)-H(30A)	121.2
C(30)-C(31)-C(32)	119.1(19)
C(30)-C(31)-C(34)	119.0(19)
C(32)-C(31)-C(34)	122(2)
C(31)-C(32)-C(33)	120(2)
C(31)-C(32)-H(32A)	119.8
C(33)-C(32)-H(32A)	119.8
C(28)-C(33)-C(32)	124(2)
C(28)-C(33)-H(33A)	117.9
C(32)-C(33)-H(33A)	117.9
C(35)-C(34)-C(31)	127(2)
C(35)-C(34)-H(34A)	116.5
C(31)-C(34)-H(34A)	116.5
C(34)-C(35)-C(36)	128(2)
C(34)-C(35)-H(35A)	116.2
C(36)-C(35)-H(35A)	116.2
C(38)-C(36)-C(37)	119.8(17)
C(38)-C(36)-C(35)	118.9(19)
C(37)-C(36)-C(35)	121.3(18)
C(38)#6-C(37)-C(36)	117.4(19)
C(36)-C(38)-C(37)#6	123(2)
C(36)-C(38)-O(9)	120.0(18)
C(37)#6-C(38)-O(9)	117.1(19)

O(9)-C(39)-H(39A)	109.5
O(9)-C(39)-H(39B)	109.5
H(39A)-C(39)-H(39B)	109.5
O(9)-C(39)-H(39C)	109.5
H(39A)-C(39)-H(39C)	109.5
H(39B)-C(39)-H(39C)	109.5
N-C(41)-H(41A)	109.7
N-C(41)-H(41B)	109.2
H(41A)-C(41)-H(41B)	109.5
N-C(41)-H(41C)	109.5
H(41A)-C(41)-H(41C)	109.5
H(41B)-C(41)-H(41C)	109.5
N-C(42)-H(42A)	109.6
N-C(42)-H(42B)	109.3
H(42A)-C(42)-H(42B)	109.5
N-C(42)-H(42C)	109.5
H(42A)-C(42)-H(42C)	109.5
H(42B)-C(42)-H(42C)	109.5
O(11)-C(43)-N	88(10)
O(11)-C(43)-H(43A)	136.3
N-C(43)-H(43A)	135.3
C(26)-O(5)-Er#2	133.3(19)
O(5)-C(26)-O(6)	127(3)
O(5)-C(26)-C(23)	117(2)
O(6)-C(26)-C(23)	116(2)

Symmetry transformations used to generate equivalent atoms:

#1 -x+2,-y+1,-z #2 -x+2,-y,-z+1 #3 -x+3,-y+1,-z

#4 x+1,y+1,z-1 #5 x-1,y-1,z+1 #6 -x+2,-y+1,-z+1

Table AA30. Anisotropic displacement parameters ($Å^2$ x 10^3) for Er-PVDC-3. The anisotropic displacement factor exponent takes the form: $-2\pi^2[h^2 a^{*2} U^{11} + ... + 2 h k a^* b^* U^{12}]$.

	U^{11}	U^{22}	U^{33}	U^{23}	U^{13}	U^{12}
Er	87(1)	154(2)	54(1)	-39(1)	49(1)	-39(1)
N	160(30)	110(30)	220(30)	-60(20)	-100(30)	30(20)
O(1)	129(12)	108(13)	85(11)	-55(10)	71(9)	-50(10)
C(1)	107(13)	88(15)	38(9)	-36(8)	39(8)	-53(11)
C(2)	89(13)	47(12)	53(8)	-14(7)	42(8)	-25(8)
O(2)	134(13)	109(15)	32(8)	-17(8)	17(8)	-59(10)
O(3)	58(9)	77(10)	46(7)	-15(7)	3(6)	-14(8)
C(3)	68(12)	52(13)	80(10)	-21(9)	41(9)	-18(8)
O(4)	44(8)	78(10)	46(7)	0(7)	2(6)	-4(7)
C(4)	49(10)	48(12)	65(9)	-21(8)	17(9)	-3(8)
C(5)	45(10)	27(10)	53(9)	-7(7)	14(7)	-2(7)
C(6)	73(12)	32(11)	51(9)	4(8)	33(9)	12(8)
C(7)	83(13)	48(12)	50(9)	7(8)	35(9)	-2(9)
O(7)	194(18)	131(15)	32(7)	-3(9)	23(10)	-85(14)
O(9)	79(9)	126(14)	74(10)	-23(10)	-3(8)	-1(11)
C(11)	49(11)	34(11)	48(7)	0(9)	13(8)	1(9)
O(11)	360(50)	370(60)	280(50)	-190(50)	-100(50)	10(40)
C(12)	52(9)	47(11)	40(8)	-13(9)	4(6)	8(9)
O(12)	129(17)	180(20)	113(15)	-60(15)	44(13)	-54(16)
C(14)	49(9)	44(12)	40(7)	-16(9)	17(7)	1(9)
C(18)	48(10)	31(11)	44(8)	-6(8)	8(7)	19(8)
C(19)	59(11)	55(13)	43(8)	2(9)	7(8)	7(10)
C(20)	48(10)	55(12)	38(7)	-16(8)	8(7)	-1(9)
C(21)	82(13)	112(17)	38(8)	-13(10)	8(9)	-44(12)
C(22)	84(14)	127(18)	34(9)	-9(10)	11(9)	-42(13)
C(23)	74(12)	110(15)	32(8)	-13(10)	18(8)	-31(11)
C(24)	59(12)	94(16)	38(8)	3(10)	9(8)	-14(10)
C(25)	48(11)	54(12)	40(7)	-2(9)	6(7)	-2(9)
C(28)	70(12)	74(14)	35(9)	-5(8)	29(9)	-7(10)
C(29)	120(17)	126(18)	56(11)	-43(12)	42(11)	-63(13)
C(30)	115(16)	128(18)	58(11)	-42(11)	45(11)	-79(13)

C(31)	72(12)	84(14)	47(9)	-28(9)	30(8)	-33(10)
C(32)	61(12)	49(12)	47(9)	-12(9)	24(8)	-8(9)
C(33)	75(13)	53(13)	54(10)	-14(9)	39(10)	-8(10)
C(34)	70(12)	58(13)	47(9)	-12(9)	28(9)	-11(10)
C(35)	66(12)	49(12)	42(8)	-4(10)	18(8)	-8(10)
C(36)	68(9)	48(11)	40(8)	-15(9)	18(6)	-16(10)
C(37)	66(11)	45(13)	47(9)	-19(10)	10(8)	7(11)
C(38)	63(8)	52(12)	46(10)	-5(10)	10(6)	-7(11)
C(39)	63(10)	120(20)	190(30)	-40(20)	-21(14)	-5(18)
C(41)	500(80)	310(60)	220(50)	-90(40)	20(50)	-330(60)
C(42)	150(40)	150(40)	420(70)	-20(50)	-30(50)	-60(30)
C(43)	380(60)	430(70)	370(70)	-130(60)	-60(60)	-10(50)

Table AA31. Hydrogen coordinates (x 10^4) and isotropic displacement parameters (Å^2 x 10^3) for Er-PVDC-3.

	x	y	z	U(eq)
H(3A)	11639	2273	1833	79
H(4A)	11128	1533	2889	65
H(6A)	7385	4308	2789	69
H(7A)	7821	5014	1722	78
H(8A)	9737	1806	3839	52
H(9A)	6690	2866	3619	52
H(11A)	9267	1938	4867	56
H(14A)	4444	1279	5472	54
H(16A)	11233	1019	6271	87
H(16B)	10554	2132	5717	87
H(16C)	10979	715	5614	87
H(17A)	2560	2147	4044	79
H(17B)	2788	2490	4695	79
H(17C)	3213	1059	4611	79
H(18A)	6945	727	6746	54
H(19A)	4222	345	6411	68
H(21A)	2827	-869	7175	89
H(22A)	2607	-2236	8140	96
H(24A)	6201	-1121	8740	79
H(25A)	6452	106	7773	60
H(29A)	12988	4460	1660	111
H(30A)	11888	4430	2663	109
H(32A)	14201	7098	2858	64
H(33A)	15150	7128	1878	74
H(34A)	12944	5952	3804	71
H(35A)	10593	4998	3467	65
H(39A)	5793	5560	3762	185
H(39B)	6015	6204	4326	185
H(39C)	6191	4707	4428	185
H(41A)	9283	8604	1199	459
H(41B)	7602	8750	1444	459

H(41C)	8507	7396	1372	459
H(42A)	8826	7309	3159	363
H(42B)	8066	6512	2777	363
H(42C)	7256	7909	2824	363
H(43A)	10456	8549	2934	476

Table AA32. Crystal data and structure refinement for Yb-PVDC-3.

Identification code	**Yb-PVDC-3**	
Empirical formula	C42 H30 N O12 Yb	
Formula weight	913.71	
Temperature	203(2) K	
Wavelength	0.71073 Å	
Crystal system	Triclinic	
Space group	P -1	
Unit cell dimensions	a = 8.811(2) Å	α = 77.152(5)°.
	b = 10.951(3) Å	β = 87.703(5)°.
	c = 21.944(5) Å	γ = 78.251(6)°.
Volume	2021.1(9) $Å^3$	
Z	2	
Density (calculated)	1.501 Mg/m^3	
Absorption coefficient	2.376 mm^{-1}	
F(000)	910	
Crystal size	0.30 x 0.13 x 0.08 mm^3	
Theta range for data collection	1.90 to 23.33°.	
Index ranges	-9<=h<=9, -12<=k<=12, -24<=l<=24	
Reflections collected	13440	
Independent reflections	5809 [R(int) = 0.0731]	
Completeness to theta = 23.33°	99.5 %	
Absorption correction	Multi-scan (Sadabs)	
Max. and min. transmission	0.8327 and 0.5359	
Refinement method	Full-matrix least-squares on F^2	
Data / restraints / parameters	5809 / 0 / 465	
Goodness-of-fit on F^2	1.665	
Final R indices [I>2sigma(I)]	R1 = 0.1363, wR2 = 0.2787	
R indices (all data)	R1 = 0.2227, wR2 = 0.3002	
Largest diff. peak and hole	2.291 and -1.213 $e.Å^{-3}$	

Table AA33. Atomic coordinates (x 10^4) and isotropic displacement parameters ($Å^2$ x 10^3) for Yb-PVDC-3. U(eq) is defined as one third of the trace of the orthogonalized U^{ij} tensor.

	x	y	z	U(eq)
Yb	2874(2)	4653(5)	4952(1)	86(2)
Yb'	2772(3)	3652(8)	4892(1)	94(2)
O(1)	1357(18)	3770(18)	5778(5)	145(7)
C(1)	80(30)	4220(20)	5970(7)	84(7)
C(2)	-160(20)	3730(20)	6685(8)	78(6)
O(2)	-881(18)	5069(16)	5673(5)	108(6)
O(3)	-5327(12)	2151(10)	9232(4)	65(3)
C(3)	-1370(20)	4369(17)	6957(7)	76(5)
O(4)	-872(11)	1070(10)	11079(4)	59(3)
C(4)	-1660(20)	3893(15)	7592(6)	62(5)
C(5)	-749(18)	2784(14)	7924(6)	44(4)
O(5)	-6950(20)	-3190(30)	14269(6)	251(15)
C(6)	493(19)	2162(16)	7638(7)	67(5)
O(6)	-4638(15)	-2822(12)	14565(6)	99(4)
C(7)	770(20)	2680(20)	7016(8)	83(6)
O(7)	5710(40)	4587(16)	4333(10)	232(14)
C(8)	-1058(19)	2289(14)	8592(6)	62(4)
O(8)	3950(20)	3680(30)	4073(8)	300(20)
C(9)	-2428(18)	2461(13)	8853(6)	52(4)
O(9)	12025(17)	4628(13)	990(6)	114(5)
C(10)	-2738(18)	2054(13)	9534(6)	47(4)
O(10)	1900(70)	6070(50)	5205(9)	560(50)
C(11)	-4276(18)	1907(13)	9700(6)	51(4)
O(11)	2010(30)	2080(40)	4980(8)	289(17)
C(12)	-4544(16)	1458(13)	10349(6)	45(4)
C(13)	-3433(17)	1166(12)	10786(6)	45(4)
C(14)	-1946(17)	1359(13)	10598(6)	49(4)
C(15)	-1634(17)	1742(12)	9984(6)	47(4)
C(16)	-3730(17)	680(13)	11456(6)	53(4)
C(17)	-4963(17)	151(13)	11665(6)	59(4)
C(18)	-5229(19)	-399(15)	12344(6)	58(4)

C(19)	-6400(20)	-1105(18)	12464(8)	86(6)
C(20)	-6610(20)	-1773(17)	13069(7)	77(5)
C(21)	-5680(20)	-1752(19)	13538(6)	81(6)
C(22)	-4540(20)	-1029(18)	13415(7)	80(6)
C(23)	-4352(19)	-345(16)	12824(6)	70(5)
C(24)	-5820(30)	-2640(20)	14196(11)	119(8)
C(25)	-6873(15)	2021(15)	9381(7)	60(4)
C(26)	675(17)	1191(16)	10915(7)	69(5)
C(27)	4880(30)	4030(30)	3992(13)	120(9)
C(28)	5760(30)	4060(20)	3293(10)	108(9)
C(29)	6700(30)	4970(30)	3122(8)	162(12)
C(30)	7320(30)	5020(20)	2506(9)	116(8)
C(31)	7052(18)	4292(17)	2122(7)	59(4)
C(32)	6140(20)	3482(17)	2345(7)	78(5)
C(33)	5490(20)	3320(20)	2910(9)	93(7)
C(34)	7790(20)	4393(18)	1514(7)	92(7)
C(35)	8790(30)	4754(17)	1263(8)	112(9)
C(36)	9380(20)	4846(13)	588(6)	59(5)
C(37)	10919(19)	4797(15)	485(7)	59(4)
C(38)	8413(19)	5042(15)	93(8)	65(4)
C(39)	13692(16)	4563(18)	833(9)	89(6)
O(12)	9190(40)	670(30)	3067(16)	279(13)
N	10900(30)	1930(20)	2883(12)	160(8)
C(40)	11470(60)	1480(50)	3500(20)	300(20)
C(41)	11790(30)	2570(30)	2275(14)	164(11)
C(42)	10010(40)	1280(40)	2660(16)	185(13)

Table AA34. Bond lengths [Å] and angles [°] for Yb-PVDC-3.

Yb-Yb'	1.154(4)
Yb-O(10)	1.80(6)
Yb-O(2)#1	2.202(15)
Yb-O(6)#2	2.341(14)
Yb-O(1)	2.359(12)
Yb-O(7)#3	2.42(3)
Yb-O(8)	2.47(3)
Yb-O(5)#4	2.53(2)
Yb-O(7)	2.79(3)
Yb-C(27)	2.80(3)
Yb-O(11)	3.06(4)
Yb-Yb#3	3.993(7)
Yb'-O(11)	1.94(4)
Yb'-O(6)#2	2.005(14)
Yb'-O(8)	2.039(16)
Yb'-O(2)#1	2.172(17)
Yb'-O(1)	2.281(13)
Yb'-C(27)	2.68(3)
Yb'-O(10)	2.83(5)
Yb'-O(7)	3.08(3)
O(1)-C(1)	1.23(2)
C(1)-O(2)	1.21(2)
C(1)-C(2)	1.56(2)
C(2)-C(7)	1.34(2)
C(2)-C(3)	1.35(2)
O(2)-Yb'#1	2.172(17)
O(2)-Yb#1	2.202(15)
O(3)-C(11)	1.355(17)
O(3)-C(25)	1.416(16)
C(3)-C(4)	1.406(19)
C(3)-H(3A)	0.9400
O(4)-C(14)	1.385(16)
O(4)-C(26)	1.421(17)
C(4)-C(5)	1.380(19)

C(4)-H(4A)	0.9400
C(5)-C(6)	1.374(19)
C(5)-C(8)	1.481(18)
O(5)-C(24)	1.25(2)
O(5)-Yb#5	2.53(2)
C(6)-C(7)	1.39(2)
C(6)-H(6A)	0.9400
O(6)-C(24)	1.30(2)
O(6)-Yb'#2	2.005(14)
O(6)-Yb#2	2.341(14)
C(7)-H(7A)	0.9400
O(7)-C(27)	1.38(3)
O(7)-Yb#3	2.42(3)
C(8)-C(9)	1.312(19)
C(8)-H(8A)	0.9400
O(8)-C(27)	0.96(4)
C(9)-C(10)	1.491(17)
C(9)-H(9A)	0.9400
O(9)-C(37)	1.460(19)
O(9)-C(39)	1.486(19)
C(10)-C(15)	1.353(18)
C(10)-C(11)	1.421(19)
C(11)-C(12)	1.426(17)
C(12)-C(13)	1.340(17)
C(12)-H(12A)	0.9400
C(13)-C(14)	1.401(19)
C(13)-C(16)	1.480(17)
C(14)-C(15)	1.353(17)
C(15)-H(15A)	0.9400
C(16)-C(17)	1.350(19)
C(16)-H(16A)	0.9400
C(17)-C(18)	1.506(18)
C(17)-H(17A)	0.9400
C(18)-C(23)	1.351(19)
C(18)-C(19)	1.40(2)
C(19)-C(20)	1.39(2)

C(19)-H(19A)	0.9400
C(20)-C(21)	1.35(2)
C(20)-H(20A)	0.9400
C(21)-C(22)	1.38(2)
C(21)-C(24)	1.57(3)
C(22)-C(23)	1.368(19)
C(22)-H(22A)	0.9400
C(23)-H(23A)	0.9400
C(24)-H(24A)	0.9900
C(25)-H(25A)	0.9700
C(25)-H(25B)	0.9700
C(25)-H(25C)	0.9700
C(26)-H(26A)	0.9700
C(26)-H(26B)	0.9700
C(26)-H(26C)	0.9700
C(27)-C(28)	1.69(3)
C(28)-C(33)	1.34(3)
C(28)-C(29)	1.40(3)
C(29)-C(30)	1.43(2)
C(29)-H(29A)	0.9400
C(30)-C(31)	1.34(2)
C(30)-H(30A)	0.9400
C(31)-C(32)	1.32(2)
C(31)-C(34)	1.45(2)
C(32)-C(33)	1.34(2)
C(32)-H(32A)	0.9400
C(33)-H(33A)	0.9400
C(34)-C(35)	1.12(2)
C(34)-H(34A)	0.9400
C(35)-C(36)	1.54(2)
C(35)-H(35A)	0.9400
C(36)-C(38)	1.36(2)
C(36)-C(37)	1.36(2)
C(37)-C(38)#6	1.37(2)
C(38)-C(37)#6	1.37(2)
C(39)-H(39A)	0.9700

C(39)-H(39B)	0.9700
C(39)-H(39C)	0.9700
O(12)-C(42)	1.28(4)
N-C(42)	1.33(3)
N-C(40)	1.41(5)
N-C(41)	1.62(3)

Yb'-Yb-O(10)	145.1(11)
Yb'-Yb-O(2)#1	73.3(5)
O(10)-Yb-O(2)#1	87.2(15)
Yb'-Yb-O(6)#2	58.9(4)
O(10)-Yb-O(6)#2	133.4(12)
O(2)#1-Yb-O(6)#2	132.1(6)
Yb'-Yb-O(1)	71.9(5)
O(10)-Yb-O(1)	78.9(8)
O(2)#1-Yb-O(1)	87.9(5)
O(6)#2-Yb-O(1)	79.1(5)
Yb'-Yb-O(7)#3	134.0(5)
O(10)-Yb-O(7)#3	63.5(14)
O(2)#1-Yb-O(7)#3	150.4(8)
O(6)#2-Yb-O(7)#3	76.4(6)
O(1)-Yb-O(7)#3	91.0(5)
Yb'-Yb-O(8)	54.8(7)
O(10)-Yb-O(8)	147.5(10)
O(2)#1-Yb-O(8)	75.4(6)
O(6)#2-Yb-O(8)	76.2(5)
O(1)-Yb-O(8)	126.6(9)
O(7)#3-Yb-O(8)	126.9(8)
Yb'-Yb-O(5)#4	138.4(5)
O(10)-Yb-O(5)#4	61.7(8)
O(2)#1-Yb-O(5)#4	80.3(5)
O(6)#2-Yb-O(5)#4	136.0(6)
O(1)-Yb-O(5)#4	139.1(8)
O(7)#3-Yb-O(5)#4	81.4(5)
O(8)-Yb-O(5)#4	88.1(8)
Yb'-Yb-O(7)	93.6(5)

O(10)-Yb-O(7)	121.0(10)
O(2)#1-Yb-O(7)	113.8(7)
O(6)#2-Yb-O(7)	70.7(6)
O(1)-Yb-O(7)	149.8(7)
O(7)#3-Yb-O(7)	80.2(6)
O(8)-Yb-O(7)	47.9(8)
O(5)#4-Yb-O(7)	68.4(7)
Yb'-Yb-C(27)	71.8(6)
O(10)-Yb-C(27)	138.0(9)
O(2)#1-Yb-C(27)	89.5(7)
O(6)#2-Yb-C(27)	75.4(6)
O(1)-Yb-C(27)	142.8(8)
O(7)#3-Yb-C(27)	108.6(8)
O(8)-Yb-C(27)	19.8(9)
O(5)#4-Yb-C(27)	76.5(8)
O(7)-Yb-C(27)	28.5(7)
Yb'-Yb-O(11)	12.2(4)
O(10)-Yb-O(11)	133.3(10)
O(2)#1-Yb-O(11)	70.4(6)
O(6)#2-Yb-O(11)	63.0(6)
O(1)-Yb-O(11)	60.4(6)
O(7)#3-Yb-O(11)	133.2(6)
O(8)-Yb-O(11)	66.2(8)
O(5)#4-Yb-O(11)	144.7(6)
O(7)-Yb-O(11)	105.6(6)
C(27)-Yb-O(11)	83.8(7)
Yb'-Yb-Yb#3	117.7(2)
O(10)-Yb-Yb#3	95.1(13)
O(2)#1-Yb-Yb#3	144.0(3)
O(6)#2-Yb-Yb#3	68.1(3)
O(1)-Yb-Yb#3	127.9(4)
O(7)#3-Yb-Yb#3	43.5(6)
O(8)-Yb-Yb#3	84.1(7)
O(5)#4-Yb-Yb#3	69.6(4)
O(7)-Yb-Yb#3	36.7(6)
C(27)-Yb-Yb#3	65.1(6)

O(11)-Yb-Yb#3	127.1(5)
Yb-Yb'-O(11)	160.6(6)
Yb-Yb'-O(6)#2	91.6(5)
O(11)-Yb'-O(6)#2	94.0(9)
Yb-Yb'-O(8)	97.7(11)
O(11)-Yb'-O(8)	100.3(12)
O(6)#2-Yb'-O(8)	94.7(6)
Yb-Yb'-O(2)#1	76.1(5)
O(11)-Yb'-O(2)#1	98.1(9)
O(6)#2-Yb'-O(2)#1	167.7(7)
O(8)-Yb'-O(2)#1	85.8(6)
Yb-Yb'-O(1)	79.4(5)
O(11)-Yb'-O(1)	82.2(7)
O(6)#2-Yb'-O(1)	88.3(5)
O(8)-Yb'-O(1)	175.9(9)
O(2)#1-Yb'-O(1)	90.6(6)
Yb-Yb'-C(27)	84.0(7)
O(11)-Yb'-C(27)	115.1(9)
O(6)#2-Yb'-C(27)	83.8(7)
O(8)-Yb'-C(27)	17.8(12)
O(2)#1-Yb'-C(27)	93.5(7)
O(1)-Yb'-C(27)	161.4(9)
Yb-Yb'-O(10)	21.4(9)
O(11)-Yb'-O(10)	139.6(10)
O(6)#2-Yb'-O(10)	102.8(11)
O(8)-Yb'-O(10)	114.3(11)
O(2)#1-Yb'-O(10)	66.0(11)
O(1)-Yb'-O(10)	62.2(7)
C(27)-Yb'-O(10)	103.2(9)
Yb-Yb'-O(7)	64.5(4)
O(11)-Yb'-O(7)	134.6(8)
O(6)#2-Yb'-O(7)	68.3(7)
O(8)-Yb'-O(7)	44.2(10)
O(2)#1-Yb'-O(7)	104.5(6)
O(1)-Yb'-O(7)	135.3(7)
C(27)-Yb'-O(7)	26.4(6)

O(10)-Yb'-O(7)	85.7(9)
C(1)-O(1)-Yb'	143.2(14)
C(1)-O(1)-Yb	130.5(15)
Yb'-O(1)-Yb	28.74(18)
O(2)-C(1)-O(1)	125.6(16)
O(2)-C(1)-C(2)	120(2)
O(1)-C(1)-C(2)	114(2)
C(7)-C(2)-C(3)	120.8(16)
C(7)-C(2)-C(1)	121.8(19)
C(3)-C(2)-C(1)	117(2)
C(1)-O(2)-Yb'#1	170.6(15)
C(1)-O(2)-Yb#1	140.1(15)
Yb'#1-O(2)-Yb#1	30.6(2)
C(11)-O(3)-C(25)	119.2(10)
C(2)-C(3)-C(4)	118.2(18)
C(2)-C(3)-H(3A)	120.9
C(4)-C(3)-H(3A)	120.9
C(14)-O(4)-C(26)	117.4(10)
C(5)-C(4)-C(3)	120.9(15)
C(5)-C(4)-H(4A)	119.5
C(3)-C(4)-H(4A)	119.5
C(6)-C(5)-C(4)	119.7(12)
C(6)-C(5)-C(8)	119.6(14)
C(4)-C(5)-C(8)	120.7(13)
C(24)-O(5)-Yb#5	128.2(18)
C(5)-C(6)-C(7)	117.9(17)
C(5)-C(6)-H(6A)	121.1
C(7)-C(6)-H(6A)	121.1
C(24)-O(6)-Yb'#2	162.3(15)
C(24)-O(6)-Yb#2	132.8(14)
Yb'#2-O(6)-Yb#2	29.5(2)
C(2)-C(7)-C(6)	122.4(16)
C(2)-C(7)-H(7A)	118.8
C(6)-C(7)-H(7A)	118.8
C(27)-O(7)-Yb#3	172.7(16)
C(27)-O(7)-Yb	76.3(18)

Yb#3-O(7)-Yb	99.8(6)
C(27)-O(7)-Yb'	60.1(16)
Yb#3-O(7)-Yb'	114.4(6)
Yb-O(7)-Yb'	21.9(2)
C(9)-C(8)-C(5)	124.7(15)
C(9)-C(8)-H(8A)	117.7
C(5)-C(8)-H(8A)	117.7
C(27)-O(8)-Yb'	122(3)
C(27)-O(8)-Yb	100(3)
Yb'-O(8)-Yb	27.5(4)
C(8)-C(9)-C(10)	125.2(14)
C(8)-C(9)-H(9A)	117.4
C(10)-C(9)-H(9A)	117.4
C(37)-O(9)-C(39)	118.7(13)
C(15)-C(10)-C(11)	119.4(12)
C(15)-C(10)-C(9)	124.0(13)
C(11)-C(10)-C(9)	116.4(14)
Yb-O(10)-Yb'	13.5(3)
O(3)-C(11)-C(10)	117.7(11)
O(3)-C(11)-C(12)	126.2(13)
C(10)-C(11)-C(12)	116.0(14)
Yb'-O(11)-Yb	7.2(3)
C(13)-C(12)-C(11)	123.4(13)
C(13)-C(12)-H(12A)	118.3
C(11)-C(12)-H(12A)	118.3
C(12)-C(13)-C(14)	118.1(12)
C(12)-C(13)-C(16)	122.6(13)
C(14)-C(13)-C(16)	119.4(13)
C(15)-C(14)-O(4)	125.1(13)
C(15)-C(14)-C(13)	120.1(14)
O(4)-C(14)-C(13)	114.7(11)
C(10)-C(15)-C(14)	122.8(14)
C(10)-C(15)-H(15A)	118.6
C(14)-C(15)-H(15A)	118.6
C(17)-C(16)-C(13)	123.4(14)
C(17)-C(16)-H(16A)	118.3

C(13)-C(16)-H(16A)	118.3
C(16)-C(17)-C(18)	123.6(15)
C(16)-C(17)-H(17A)	118.2
C(18)-C(17)-H(17A)	118.2
C(23)-C(18)-C(19)	119.0(14)
C(23)-C(18)-C(17)	125.1(15)
C(19)-C(18)-C(17)	115.7(14)
C(20)-C(19)-C(18)	119.6(16)
C(20)-C(19)-H(19A)	120.2
C(18)-C(19)-H(19A)	120.2
C(21)-C(20)-C(19)	120.5(16)
C(21)-C(20)-H(20A)	119.8
C(19)-C(20)-H(20A)	119.8
C(20)-C(21)-C(22)	119.3(13)
C(20)-C(21)-C(24)	119.0(17)
C(22)-C(21)-C(24)	121.5(17)
C(23)-C(22)-C(21)	120.7(16)
C(23)-C(22)-H(22A)	119.7
C(21)-C(22)-H(22A)	119.7
C(18)-C(23)-C(22)	120.8(15)
C(18)-C(23)-H(23A)	119.6
C(22)-C(23)-H(23A)	119.6
O(5)-C(24)-O(6)	129(2)
O(5)-C(24)-C(21)	116(2)
O(6)-C(24)-C(21)	115(2)
O(5)-C(24)-H(24A)	92.3
O(6)-C(24)-H(24A)	92.3
C(21)-C(24)-H(24A)	92.3
O(3)-C(25)-H(25A)	109.5
O(3)-C(25)-H(25B)	109.5
H(25A)-C(25)-H(25B)	109.5
O(3)-C(25)-H(25C)	109.5
H(25A)-C(25)-H(25C)	109.5
H(25B)-C(25)-H(25C)	109.5
O(4)-C(26)-H(26A)	109.5
O(4)-C(26)-H(26B)	109.5

H(26A)-C(26)-H(26B)	109.5
O(4)-C(26)-H(26C)	109.5
H(26A)-C(26)-H(26C)	109.5
H(26B)-C(26)-H(26C)	109.5
O(8)-C(27)-O(7)	134(4)
O(8)-C(27)-C(28)	119(3)
O(7)-C(27)-C(28)	107(2)
O(8)-C(27)-Yb'	40(2)
O(7)-C(27)-Yb'	93.5(16)
C(28)-C(27)-Yb'	159(2)
O(8)-C(27)-Yb	60(3)
O(7)-C(27)-Yb	75.2(16)
C(28)-C(27)-Yb	163.3(16)
Yb'-C(27)-Yb	24.2(3)
C(33)-C(28)-C(29)	122.6(17)
C(33)-C(28)-C(27)	122(2)
C(29)-C(28)-C(27)	115(2)
C(28)-C(29)-C(30)	112.7(19)
C(28)-C(29)-H(29A)	123.7
C(30)-C(29)-H(29A)	123.7
C(31)-C(30)-C(29)	125.0(19)
C(31)-C(30)-H(30A)	117.5
C(29)-C(30)-H(30A)	117.5
C(32)-C(31)-C(30)	115.5(16)
C(32)-C(31)-C(34)	124.2(17)
C(30)-C(31)-C(34)	120.2(18)
C(31)-C(32)-C(33)	126.2(18)
C(31)-C(32)-H(32A)	116.9
C(33)-C(32)-H(32A)	116.9
C(32)-C(33)-C(28)	118.0(19)
C(32)-C(33)-H(33A)	121.0
C(28)-C(33)-H(33A)	121.0
C(35)-C(34)-C(31)	139(2)
C(35)-C(34)-H(34A)	110.3
C(31)-C(34)-H(34A)	110.3
C(34)-C(35)-C(36)	133(3)

C(34)-C(35)-H(35A)	113.6
C(36)-C(35)-H(35A)	113.6
C(38)-C(36)-C(37)	119.2(13)
C(38)-C(36)-C(35)	122.7(16)
C(37)-C(36)-C(35)	118.0(17)
C(36)-C(37)-C(38)#6	124.5(15)
C(36)-C(37)-O(9)	122.6(15)
C(38)#6-C(37)-O(9)	112.9(15)
C(36)-C(38)-C(37)#6	116.3(14)
O(9)-C(39)-H(39A)	109.5
O(9)-C(39)-H(39B)	109.5
H(39A)-C(39)-H(39B)	109.5
O(9)-C(39)-H(39C)	109.5
H(39A)-C(39)-H(39C)	109.5
H(39B)-C(39)-H(39C)	109.5
C(42)-N-C(40)	119(3)
C(42)-N-C(41)	104(3)
C(40)-N-C(41)	127(3)
O(12)-C(42)-N	115(4)

Symmetry transformations used to generate equivalent atoms:

#1 -x,-y+1,-z+1 #2 -x,-y,-z+2 #3 -x+1,-y+1,-z+1

#4 x+1,y+1,z-1 #5 x-1,y-1,z+1 #6 -x+2,-y+1,-z

Table AA35. Anisotropic displacement parameters ($Å^2$ x 10^3) for Yb-PVDC-3. The anisotropic displacement factor exponent takes the form: $-2\pi^2[h^2 a^{*2} U^{11} + ... + 2 h k a^* b^* U^{12}]$.

	U^{11}	U^{22}	U^{33}	U^{23}	U^{13}	U^{12}
Yb	88(1)	130(4)	44(1)	-19(1)	41(1)	-41(1)
Yb'	104(2)	151(6)	34(1)	-6(2)	37(1)	-64(2)
O(1)	117(11)	270(20)	49(7)	-14(10)	48(8)	-86(13)
C(1)	93(15)	160(20)	29(9)	-15(12)	31(11)	-97(16)
C(2)	84(14)	124(18)	46(10)	-35(12)	33(11)	-61(14)
O(2)	118(12)	175(16)	29(6)	25(8)	0(7)	-77(11)
O(3)	59(7)	91(9)	33(5)	5(5)	-2(5)	-9(6)
C(3)	109(15)	93(14)	32(8)	-10(9)	6(10)	-44(12)
O(4)	58(7)	88(8)	34(5)	-9(5)	9(5)	-28(6)
C(4)	91(12)	48(10)	40(8)	-9(8)	30(9)	-5(10)
C(5)	72(10)	38(10)	30(7)	-13(7)	8(8)	-22(9)
O(5)	205(19)	520(40)	58(8)	57(15)	-8(10)	-280(30)
C(6)	77(11)	73(12)	51(9)	-18(9)	29(9)	-22(10)
C(7)	64(12)	150(20)	48(11)	-45(12)	26(10)	-30(14)
O(7)	470(40)	113(14)	117(15)	-10(12)	160(20)	-110(20)
C(8)	77(11)	58(11)	42(8)	-1(8)	14(9)	-2(9)
O(8)	92(12)	520(50)	115(14)	150(20)	73(11)	81(19)
C(9)	62(10)	48(10)	36(8)	3(7)	10(8)	0(8)
O(9)	125(12)	127(12)	93(10)	-39(9)	20(9)	-18(10)
C(10)	62(10)	33(9)	36(8)	3(7)	11(8)	2(8)
O(10)	1140(120)	760(80)	71(14)	-90(30)	110(40)	-850(90)
C(11)	73(11)	39(9)	37(8)	-6(7)	24(8)	-9(9)
O(11)	200(20)	660(60)	87(12)	-180(20)	71(13)	-170(30)
C(12)	48(9)	50(10)	39(8)	-13(7)	15(8)	-11(8)
C(13)	60(10)	36(9)	29(7)	0(7)	10(8)	2(8)
C(14)	64(10)	45(10)	37(8)	-10(7)	16(8)	-9(9)
C(15)	59(10)	29(9)	38(8)	8(7)	14(8)	8(8)
C(16)	59(9)	56(10)	40(8)	-5(7)	10(8)	-6(9)
C(17)	54(9)	50(10)	51(9)	19(8)	20(8)	1(9)
C(18)	69(11)	72(12)	31(8)	-13(8)	5(8)	-10(10)
C(19)	82(12)	115(16)	67(11)	-6(11)	23(10)	-57(13)

C(20)	100(14)	102(14)	35(9)	-3(9)	25(10)	-51(12)
C(21)	103(14)	133(17)	13(7)	-6(9)	19(9)	-53(13)
C(22)	93(13)	130(16)	33(8)	-21(10)	26(9)	-59(13)
C(23)	84(12)	108(15)	34(9)	-24(9)	23(9)	-51(11)
C(25)	43(9)	67(11)	60(10)	-8(8)	0(8)	5(9)
C(26)	68(11)	80(13)	61(10)	-21(9)	0(9)	-10(10)
C(28)	104(16)	103(17)	75(14)	31(13)	68(13)	14(14)
C(29)	270(30)	220(30)	41(11)	-47(14)	67(16)	-150(30)
C(30)	160(20)	140(20)	68(13)	2(13)	38(14)	-94(18)
C(31)	62(10)	82(13)	36(8)	-15(9)	2(8)	-20(10)
C(32)	95(14)	81(14)	55(11)	-10(10)	12(10)	-21(12)
C(33)	103(16)	122(19)	59(12)	-11(12)	23(12)	-51(14)
C(34)	94(14)	107(16)	45(10)	7(10)	44(10)	18(12)
C(35)	160(20)	65(13)	64(12)	22(10)	67(13)	35(13)
C(36)	100(13)	29(9)	38(8)	0(7)	28(9)	-5(9)
C(39)	37(10)	121(17)	109(15)	-24(13)	2(10)	-16(11)

Table AA36. Hydrogen coordinates (x 10^4) and isotropic displacement parameters (Å^2 x 10^3) for Yb-PVDC-3.

	x	y	z	U(eq)
H(3A)	-2009	5112	6729	91
H(4A)	-2486	4336	7793	75
H(6A)	1133	1409	7856	80
H(7A)	1646	2286	6820	100
H(8A)	-213	1817	8847	75
H(9A)	-3282	2875	8591	63
H(12A)	-5553	1362	10476	54
H(15A)	-608	1793	9866	57
H(16A)	-3024	743	11752	64
H(17A)	-5694	125	11370	71
H(19A)	-7048	-1129	12138	103
H(20A)	-7404	-2243	13152	93
H(22A)	-3894	-1007	13740	96
H(23A)	-3601	170	12751	84
H(24A)	-6386	-1923	14371	143
H(25A)	-7482	2235	9000	90
H(25B)	-7312	2592	9651	90
H(25C)	-6883	1146	9594	90
H(26A)	1311	958	11290	104
H(26B)	688	2068	10707	104
H(26C)	1082	629	10636	104
H(29A)	6894	5495	3383	194
H(30A)	7969	5605	2361	139
H(32A)	5927	2969	2081	93
H(33A)	4860	2715	3036	111
H(34A)	7259	4048	1250	111
H(35A)	9396	5063	1515	134
H(39A)	14284	4443	1212	134
H(39B)	13820	5352	550	134
H(39C)	14059	3850	634	134

Table AA37. Crystal data and structure refinement for Zn-TPY-1.

Identification code	**Zn-TPY-1**	
Empirical formula	C24 H14 F3 N3 O5 Zn	
Formula weight	546.75	
Temperature	203(2) K	
Wavelength	0.71073 Å	
Crystal system	Trigonal	
Space group	R -3	
Unit cell dimensions	a = 39.5632(16) Å	α = 90°.
	b = 39.5632(16) Å	β = 90°.
	c = 10.6133(9) Å	γ = 120°.
Volume	14386.8(15) $Å^3$	
Z	18	
Density (calculated)	1.136 Mg/m^3	
Absorption coefficient	0.816 mm^{-1}	
F(000)	4968	
Crystal size	0.25 x 0.22 x 0.14 mm^3	
Theta range for data collection	1.78 to 26.00°.	
Index ranges	-48<=h<=48, -48<=k<=48, -13<=l<=13	
Reflections collected	41547	
Independent reflections	6275 [R(int) = 0.0386]	
Completeness to theta = 26.00°	99.6 %	
Absorption correction	multi-scan	
Max. and min. transmission	.94 and .83	
Refinement method	Full-matrix least-squares on F^2	
Data / restraints / parameters	6275 / 3 / 306	
Goodness-of-fit on F^2	2.780	
Final R indices [I>2sigma(I)]	R1 = 0.0970, wR2 = 0.2933	
R indices (all data)	R1 = 0.1125, wR2 = 0.3007	
Extinction coefficient	0.00010(11)	
Largest diff. peak and hole	2.144 and -0.900 $e.Å^{-3}$	

Table AA38. Atomic coordinates (x 10^4) and equivalent isotropic displacement parameters ($Å^2$ x 10^3) for Zn-TPY-1. U(eq) is defined as one third of the trace of the orthogonalized U^{ij} tensor.

	x	y	z	U(eq)
Zn(1)	7798(1)	782(1)	9118(1)	46(1)
C(1)	7272(2)	823(2)	11270(6)	62(2)
O(1)	9651(1)	4040(1)	8891(4)	61(1)
F(1)	8349(5)	22(5)	10369(15)	295(7)
C(2)	7133(2)	997(2)	12085(6)	66(2)
O(2)	10131(1)	3938(1)	8269(4)	52(1)
F(2)	8384(6)	215(6)	12190(20)	367(10)
C(3)	7346(2)	1385(2)	12220(7)	74(2)
O(3)	8367(2)	779(2)	11052(5)	78(1)
F(3)	7835(5)	-194(5)	11535(14)	282(6)
O(4)	7832(1)	361(1)	10031(4)	66(1)
C(4)	7699(2)	1608(2)	11566(6)	62(2)
C(5)	7810(2)	1408(2)	10763(5)	47(1)
O(5)	8854(2)	3749(2)	7746(9)	144(3)
C(6)	8156(2)	1605(2)	9916(5)	44(1)
C(7)	8428(2)	2009(2)	9927(5)	47(1)
C(8)	8726(1)	2165(2)	9072(5)	43(1)
C(9)	8748(2)	1909(2)	8184(5)	45(1)
C(10)	8478(1)	1516(2)	8254(5)	40(1)
N(11)	7603(1)	1016(1)	10617(4)	49(1)
C(11)	8473(2)	1219(2)	7378(5)	44(1)
N(12)	8195(1)	1372(1)	9095(4)	41(1)
C(12)	8747(2)	1309(2)	6412(6)	55(2)
N(13)	8190(1)	855(1)	7577(5)	50(1)
C(13)	8721(2)	1005(2)	5684(7)	69(2)
C(14)	8430(2)	635(2)	5881(7)	71(2)
C(15)	8167(2)	572(2)	6841(7)	64(2)
C(16)	9374(2)	2732(2)	8482(5)	48(1)
C(17)	9629(2)	3133(2)	8391(5)	47(1)
C(18)	9529(2)	3389(2)	8862(5)	44(1)
C(19)	9179(2)	3254(2)	9477(6)	60(2)

C(20)	8913(2)	2852(2)	9576(6)	56(2)
C(21)	9011(2)	2586(2)	9041(5)	45(1)
C(22)	9787(2)	3821(2)	8677(5)	51(1)
C(23)	8113(2)	451(2)	10774(6)	66(2)
C(24)	8164(6)	160(7)	11160(20)	232(9)

Table AA39. Bond lengths [Å] and angles [°] for Zn-TPY-1.

Zn(1)-O(2)#1	1.968(4)
Zn(1)-O(4)	1.991(4)
Zn(1)-N(12)	2.060(4)
Zn(1)-N(11)	2.168(5)
Zn(1)-N(13)	2.171(5)
C(1)-N(11)	1.334(7)
C(1)-C(2)	1.378(10)
O(1)-C(22)	1.249(7)
F(1)-C(24)	1.391(16)
C(2)-C(3)	1.340(10)
O(2)-C(22)	1.274(7)
O(2)-Zn(1)#2	1.968(4)
F(2)-C(24)	1.345(16)
C(3)-C(4)	1.409(9)
O(3)-C(23)	1.213(8)
F(3)-C(24)	1.412(16)
O(4)-C(23)	1.258(8)
C(4)-C(5)	1.374(8)
C(5)-N(11)	1.352(7)
C(5)-C(6)	1.489(7)
C(6)-N(12)	1.332(7)
C(6)-C(7)	1.413(7)
C(7)-C(8)	1.365(7)
C(8)-C(9)	1.417(7)
C(8)-C(21)	1.472(7)
C(9)-C(10)	1.381(7)
C(10)-N(12)	1.320(6)
C(10)-C(11)	1.490(7)
C(11)-N(13)	1.327(7)
C(11)-C(12)	1.402(8)
C(12)-C(13)	1.391(8)
N(13)-C(15)	1.328(8)
C(13)-C(14)	1.351(9)
C(14)-C(15)	1.385(10)

C(16)-C(21)	1.387(8)
C(16)-C(17)	1.396(7)
C(17)-C(18)	1.354(8)
C(18)-C(19)	1.376(8)
C(18)-C(22)	1.501(8)
C(19)-C(20)	1.405(8)
C(20)-C(21)	1.407(8)
C(23)-C(24)	1.33(2)

O(2)#1-Zn(1)-O(4)	99.44(18)
O(2)#1-Zn(1)-N(12)	131.99(17)
O(4)-Zn(1)-N(12)	128.42(17)
O(2)#1-Zn(1)-N(11)	93.27(16)
O(4)-Zn(1)-N(11)	100.84(19)
N(12)-Zn(1)-N(11)	76.00(17)
O(2)#1-Zn(1)-N(13)	104.70(17)
O(4)-Zn(1)-N(13)	97.68(19)
N(12)-Zn(1)-N(13)	75.68(17)
N(11)-Zn(1)-N(13)	151.64(17)
N(11)-C(1)-C(2)	124.1(6)
C(3)-C(2)-C(1)	117.5(6)
C(22)-O(2)-Zn(1)#2	109.9(4)
C(2)-C(3)-C(4)	121.4(7)
C(23)-O(4)-Zn(1)	119.1(4)
C(5)-C(4)-C(3)	116.7(6)
N(11)-C(5)-C(4)	123.0(5)
N(11)-C(5)-C(6)	113.7(5)
C(4)-C(5)-C(6)	123.1(5)
N(12)-C(6)-C(7)	120.1(5)
N(12)-C(6)-C(5)	115.3(4)
C(7)-C(6)-C(5)	124.6(5)
C(8)-C(7)-C(6)	120.2(5)
C(7)-C(8)-C(9)	117.8(5)
C(7)-C(8)-C(21)	121.8(5)
C(9)-C(8)-C(21)	120.4(5)
C(10)-C(9)-C(8)	118.8(5)

N(12)-C(10)-C(9)	122.2(5)
N(12)-C(10)-C(11)	114.1(4)
C(9)-C(10)-C(11)	123.7(5)
C(1)-N(11)-C(5)	117.2(5)
C(1)-N(11)-Zn(1)	126.4(4)
C(5)-N(11)-Zn(1)	115.6(3)
N(13)-C(11)-C(12)	121.2(5)
N(13)-C(11)-C(10)	115.4(5)
C(12)-C(11)-C(10)	123.4(5)
C(10)-N(12)-C(6)	120.8(4)
C(10)-N(12)-Zn(1)	119.9(3)
C(6)-N(12)-Zn(1)	119.3(3)
C(13)-C(12)-C(11)	118.2(6)
C(15)-N(13)-C(11)	119.0(5)
C(15)-N(13)-Zn(1)	126.1(4)
C(11)-N(13)-Zn(1)	115.0(4)
C(14)-C(13)-C(12)	120.3(6)
C(13)-C(14)-C(15)	117.7(6)
N(13)-C(15)-C(14)	123.6(6)
C(21)-C(16)-C(17)	120.8(5)
C(18)-C(17)-C(16)	120.7(5)
C(17)-C(18)-C(19)	119.9(5)
C(17)-C(18)-C(22)	121.1(5)
C(19)-C(18)-C(22)	119.0(5)
C(18)-C(19)-C(20)	120.9(6)
C(21)-C(20)-C(19)	119.2(5)
C(16)-C(21)-C(20)	118.4(5)
C(16)-C(21)-C(8)	121.9(5)
C(20)-C(21)-C(8)	119.6(5)
O(1)-C(22)-O(2)	124.2(5)
O(1)-C(22)-C(18)	118.8(5)
O(2)-C(22)-C(18)	116.9(5)
O(3)-C(23)-C(24)	116.4(12)
O(3)-C(23)-O(4)	126.8(7)
C(24)-C(23)-O(4)	116.2(12)
C(23)-C(24)-F(2)	118(2)

C(23)-C(24)-F(1)	119.6(18)
F(2)-C(24)-F(1)	97.5(18)
C(23)-C(24)-F(3)	118.8(18)
F(2)-C(24)-F(3)	97.6(17)
F(1)-C(24)-F(3)	100.8(17)

Symmetry transformations used to generate equivalent atoms:

#1 y+1/3,-x+y+2/3,-z+5/3 #2 x-y+1/3,x-1/3,-z+5/3

Table AA40. Anisotropic displacement parameters ($Å^2$ x 10^3) for Zn-TPY-1. The anisotropic displacement factor exponent takes the form: $-2\pi^2[h^2 a^{*2} U^{11} + ... + 2 h k a^* b^* U^{12}]$.

	U^{11}	U^{22}	U^{33}	U^{23}	U^{13}	U^{12}
Zn(1)	35(1)	39(1)	56(1)	-1(1)	-1(1)	11(1)
C(1)	43(3)	58(4)	62(4)	9(3)	6(3)	8(3)
O(1)	71(3)	40(2)	71(3)	-3(2)	12(2)	27(2)
C(2)	45(3)	76(5)	59(4)	6(3)	18(3)	17(3)
O(2)	53(2)	34(2)	60(2)	4(2)	-1(2)	15(2)
C(3)	58(4)	92(6)	75(5)	2(4)	21(3)	39(4)
O(3)	69(3)	76(3)	87(3)	-21(3)	-18(3)	34(3)
O(4)	76(3)	54(2)	67(3)	-4(2)	-22(2)	31(2)
C(4)	53(4)	62(4)	66(4)	-3(3)	15(3)	26(3)
C(5)	36(3)	53(3)	44(3)	-1(2)	3(2)	16(2)
O(5)	128(6)	110(5)	184(8)	-39(5)	-25(6)	52(5)
C(6)	35(3)	44(3)	46(3)	-1(2)	1(2)	15(2)
C(7)	43(3)	46(3)	48(3)	-8(2)	1(2)	20(2)
C(8)	39(3)	40(3)	44(3)	0(2)	4(2)	16(2)
C(9)	37(3)	40(3)	49(3)	-3(2)	3(2)	14(2)
C(10)	34(3)	41(3)	44(3)	-1(2)	0(2)	18(2)
N(11)	40(2)	48(3)	48(3)	3(2)	4(2)	14(2)
C(11)	38(3)	42(3)	48(3)	-8(2)	-2(2)	17(2)
N(12)	35(2)	42(2)	45(2)	-4(2)	-3(2)	18(2)
C(12)	47(3)	56(3)	57(3)	-9(3)	6(3)	21(3)
N(13)	40(2)	41(2)	58(3)	-5(2)	0(2)	12(2)
C(13)	62(4)	63(4)	72(4)	-12(3)	18(3)	24(3)
C(14)	77(5)	64(4)	77(5)	-24(3)	0(4)	39(4)
C(15)	60(4)	45(3)	78(4)	-8(3)	8(3)	20(3)
C(16)	44(3)	38(3)	55(3)	-4(2)	3(2)	15(2)
C(17)	43(3)	39(3)	51(3)	-4(2)	0(2)	15(2)
C(18)	46(3)	39(3)	41(3)	-2(2)	0(2)	15(2)
C(19)	67(4)	45(3)	61(4)	-4(3)	10(3)	22(3)
C(20)	52(3)	42(3)	65(4)	-6(3)	12(3)	18(3)
C(21)	45(3)	38(3)	48(3)	-6(2)	-1(2)	18(2)
C(22)	62(4)	39(3)	44(3)	-2(2)	-3(3)	20(3)

C(23)	87(5)	72(4)	52(4)	-11(3)	-9(3)	51(4)

Table AA41. Hydrogen coordinates (x 10^4) and isotropic displacement parameters (Å^2 x 10^3) for Zn-TPY-1.

	x	y	z	U(eq)
H(1A)	7123	551	11168	75
H(2A)	6899	849	12529	79
H(3A)	7257	1512	12763	89
H(4A)	7852	1879	11672	74
H(7A)	8404	2171	10525	56
H(9A)	8942	2006	7559	53
H(12A)	8943	1568	6261	66
H(13A)	8907	1056	5053	83
H(14A)	8406	427	5384	85
H(15A)	7962	316	6979	77
H(16A)	9450	2558	8160	58
H(17A)	9873	3227	8000	57
H(19A)	9116	3433	9837	72
H(20A)	8674	2761	9995	67

Table AA42. Crystal data and structure refinement for Zn-TPY-2.

Identification code	**Zn-TPY-2**	
Empirical formula	C24 H17 N3 O5 Zn	
Formula weight	492.78	
Temperature	203(2) K	
Wavelength	0.71073 Å	
Crystal system	Rhombohedral	
Space group	R-3	
Unit cell dimensions	a = 39.5398(19) Å	α = 90°.
	b = 39.5398(19) Å	β = 90°.
	c = 10.5602(10) Å	γ = 120°.
Volume	14297.9(17) $Å^3$	
Z	18	
Density (calculated)	1.030 Mg/m^3	
Absorption coefficient	0.802 mm^{-1}	
F(000)	4536	
Crystal size	0.18 x 0.24 x 0.26 mm^3	
Theta range for data collection	1.03 to 28.35°.	
Index ranges	-52<=h<=52, -52<=k<=52, -13<=l<=14	
Reflections collected	48880	
Independent reflections	7903 [R(int) = 0.0699]	
Completeness to theta = 28.35°	99.6 %	
Absorption correction	Multi-scan (Sadabs)	
Refinement method	Full-matrix least-squares on F^2	
Data / restraints / parameters	7903 / 0 / 298	
Goodness-of-fit on F^2	1.874	
Final R indices [I>2sigma(I)]	R1 = 0.0986, wR2 = 0.2839	
R indices (all data)	R1 = 0.1441, wR2 = 0.3045	
Largest diff. peak and hole	2.071 and -0.763 $e.Å^{-3}$	

Table AA43. Atomic coordinates (x 10^4) and equivalent isotropic displacement parameters (Å^2 x 10^3) for Zn-TPY-2. U(eq) is defined as one third of the trace of the orthogonalized U^{ij} tensor.

	x	y	z	U(eq)
Zn	2979(1)	778(1)	4218(1)	50(1)
N(1)	3416(1)	1023(1)	5710(4)	54(1)
C(1)	3557(2)	830(2)	6387(6)	65(2)
O(1)	4412(1)	4043(1)	3782(4)	67(1)
N(2)	3180(1)	1371(1)	4153(4)	46(1)
C(2)	3857(2)	1005(2)	7207(6)	72(2)
O(2)	3824(1)	3938(1)	3200(4)	56(1)
O(3)	2533(1)	353(1)	5126(4)	69(1)
N(3)	2660(1)	842(1)	2673(4)	54(1)
C(3)	4038(2)	1400(2)	7357(7)	75(2)
O(4)	2381(2)	761(2)	6005(5)	92(2)
C(4)	3917(2)	1622(2)	6650(6)	67(2)
C(5)	3600(2)	1413(2)	5828(5)	52(1)
O(5)	4928(2)	3782(2)	2667(7)	123(2)
C(6)	3457(2)	1613(2)	4946(5)	48(1)
C(7)	3588(2)	2005(2)	4942(5)	52(1)
C(8)	3447(2)	2161(1)	4037(5)	48(1)
C(9)	3171(2)	1906(1)	3185(5)	47(1)
C(10)	3039(1)	1512(1)	3268(5)	44(1)
C(11)	2738(1)	1206(1)	2423(5)	47(1)
C(12)	2550(2)	1290(2)	1494(6)	62(2)
C(13)	2278(2)	987(2)	734(7)	78(2)
C(14)	2193(2)	605(2)	983(7)	73(2)
C(15)	2388(2)	548(2)	1964(6)	65(2)
C(16)	3948(2)	2856(2)	4524(6)	63(2)
C(17)	4090(2)	3251(2)	4410(6)	63(2)
C(18)	3883(2)	3394(2)	3797(5)	53(1)
C(19)	3514(2)	3126(1)	3296(5)	54(1)
C(20)	3375(2)	2737(1)	3389(5)	53(1)
C(21)	3591(2)	2585(1)	3983(5)	50(1)
C(22)	4052(2)	3824(2)	3583(5)	53(1)

C(23)	2322(2)	434(2)	5791(6)	71(2)
C(24)	1950(4)	165(5)	6343(14)	216(8)

Table AA44. Bond lengths [Å] and angles [°] for Zn-TPY-2.

Zn-O(3)	1.973(4)
Zn-O(2)#1	1.976(3)
Zn-N(2)	2.067(4)
Zn-N(3)	2.152(4)
Zn-N(1)	2.177(5)
N(1)-C(5)	1.341(6)
N(1)-C(1)	1.352(7)
C(1)-C(2)	1.350(9)
C(1)-H(1A)	0.9400
O(1)-C(22)	1.260(6)
N(2)-C(6)	1.330(6)
N(2)-C(10)	1.343(6)
C(2)-C(3)	1.363(9)
C(2)-H(2A)	0.9400
O(2)-C(22)	1.264(6)
O(2)-Zn#2	1.976(3)
O(3)-C(23)	1.250(8)
N(3)-C(11)	1.340(6)
N(3)-C(15)	1.349(7)
C(3)-C(4)	1.404(8)
C(3)-H(3A)	0.9400
O(4)-C(23)	1.216(8)
C(4)-C(5)	1.404(8)
C(4)-H(4A)	0.9400
C(5)-C(6)	1.502(7)
C(6)-C(7)	1.369(7)
C(7)-C(8)	1.396(7)
C(7)-H(7A)	0.9400
C(8)-C(9)	1.384(7)
C(8)-C(21)	1.476(7)
C(9)-C(10)	1.376(7)
C(9)-H(9A)	0.9400
C(10)-C(11)	1.496(7)

C(11)-C(12)	1.367(7)
C(12)-C(13)	1.396(8)
C(12)-H(12A)	0.9400
C(13)-C(14)	1.397(9)
C(13)-H(13A)	0.9400
C(14)-C(15)	1.376(9)
C(14)-H(14A)	0.9400
C(15)-H(15A)	0.9400
C(16)-C(17)	1.377(8)
C(16)-C(21)	1.396(7)
C(16)-H(16A)	0.9400
C(17)-C(18)	1.366(8)
C(17)-H(17A)	0.9400
C(18)-C(19)	1.407(7)
C(18)-C(22)	1.500(7)
C(19)-C(20)	1.354(7)
C(19)-H(19A)	0.9400
C(20)-C(21)	1.413(7)
C(20)-H(20A)	0.9400
C(23)-C(24)	1.440(14)
C(24)-H(24A)	0.9700
C(24)-H(24B)	0.9700
C(24)-H(24C)	0.9700

O(3)-Zn-O(2)#1	100.73(17)
O(3)-Zn-N(2)	131.04(17)
O(2)#1-Zn-N(2)	128.07(16)
O(3)-Zn-N(3)	98.17(17)
O(2)#1-Zn-N(3)	103.96(15)
N(2)-Zn-N(3)	75.97(16)
O(3)-Zn-N(1)	101.55(18)
O(2)#1-Zn-N(1)	92.47(15)
N(2)-Zn-N(1)	75.50(15)
N(3)-Zn-N(1)	151.44(16)
C(5)-N(1)-C(1)	117.4(5)
C(5)-N(1)-Zn	115.6(3)

C(1)-N(1)-Zn	126.2(4)
C(2)-C(1)-N(1)	123.7(6)
C(2)-C(1)-H(1A)	118.1
N(1)-C(1)-H(1A)	118.1
C(6)-N(2)-C(10)	120.3(4)
C(6)-N(2)-Zn	120.3(3)
C(10)-N(2)-Zn	119.3(3)
C(1)-C(2)-C(3)	119.0(6)
C(1)-C(2)-H(2A)	120.5
C(3)-C(2)-H(2A)	120.5
C(22)-O(2)-Zn#2	111.8(3)
C(23)-O(3)-Zn	118.7(4)
C(11)-N(3)-C(15)	118.2(5)
C(11)-N(3)-Zn	116.2(3)
C(15)-N(3)-Zn	125.5(4)
C(2)-C(3)-C(4)	120.5(6)
C(2)-C(3)-H(3A)	119.7
C(4)-C(3)-H(3A)	119.7
C(3)-C(4)-C(5)	116.3(6)
C(3)-C(4)-H(4A)	121.8
C(5)-C(4)-H(4A)	121.8
N(1)-C(5)-C(4)	123.0(5)
N(1)-C(5)-C(6)	114.6(5)
C(4)-C(5)-C(6)	122.3(5)
N(2)-C(6)-C(7)	121.3(5)
N(2)-C(6)-C(5)	113.9(4)
C(7)-C(6)-C(5)	124.7(5)
C(6)-C(7)-C(8)	119.7(5)
C(6)-C(7)-H(7A)	120.1
C(8)-C(7)-H(7A)	120.1
C(9)-C(8)-C(7)	117.7(4)
C(9)-C(8)-C(21)	121.2(4)
C(7)-C(8)-C(21)	121.0(5)
C(10)-C(9)-C(8)	120.0(4)
C(10)-C(9)-H(9A)	120.0
C(8)-C(9)-H(9A)	120.0

N(2)-C(10)-C(9)	120.8(4)
N(2)-C(10)-C(11)	114.0(4)
C(9)-C(10)-C(11)	125.2(4)
N(3)-C(11)-C(12)	122.8(5)
N(3)-C(11)-C(10)	114.5(4)
C(12)-C(11)-C(10)	122.7(5)
C(11)-C(12)-C(13)	118.8(5)
C(11)-C(12)-H(12A)	120.6
C(13)-C(12)-H(12A)	120.6
C(12)-C(13)-C(14)	119.2(6)
C(12)-C(13)-H(13A)	120.4
C(14)-C(13)-H(13A)	120.4
C(15)-C(14)-C(13)	117.7(5)
C(15)-C(14)-H(14A)	121.1
C(13)-C(14)-H(14A)	121.1
N(3)-C(15)-C(14)	123.2(5)
N(3)-C(15)-H(15A)	118.4
C(14)-C(15)-H(15A)	118.4
C(17)-C(16)-C(21)	121.1(5)
C(17)-C(16)-H(16A)	119.4
C(21)-C(16)-H(16A)	119.4
C(18)-C(17)-C(16)	121.4(5)
C(18)-C(17)-H(17A)	119.3
C(16)-C(17)-H(17A)	119.3
C(17)-C(18)-C(19)	118.4(5)
C(17)-C(18)-C(22)	121.2(5)
C(19)-C(18)-C(22)	120.3(5)
C(20)-C(19)-C(18)	120.5(5)
C(20)-C(19)-H(19A)	119.7
C(18)-C(19)-H(19A)	119.7
C(19)-C(20)-C(21)	121.7(5)
C(19)-C(20)-H(20A)	119.1
C(21)-C(20)-H(20A)	119.1
C(16)-C(21)-C(20)	116.7(5)
C(16)-C(21)-C(8)	121.6(5)
C(20)-C(21)-C(8)	121.7(5)

O(1)-C(22)-O(2)	124.8(5)
O(1)-C(22)-C(18)	117.8(5)
O(2)-C(22)-C(18)	117.4(5)
O(4)-C(23)-O(3)	125.5(7)
O(4)-C(23)-C(24)	107.0(9)
O(3)-C(23)-C(24)	127.2(10)
C(23)-C(24)-H(24A)	109.5
C(23)-C(24)-H(24B)	109.5
H(24A)-C(24)-H(24B)	109.5
C(23)-C(24)-H(24C)	109.5
H(24A)-C(24)-H(24C)	109.5
H(24B)-C(24)-H(24C)	109.5

Symmetry transformations used to generate equivalent atoms:

#1 x-y+1/3,x-1/3,-z+2/3 #2 y+1/3,-x+y+2/3,-z+2/3

Table AA45. Anisotropic displacement parameters ($Å^2$ x 10^3) for Zn-TPY-2. The anisotropic displacement factor exponent takes the form: $-2\pi^2[h^2 a^{*2} U^{11} + ... + 2 h k a^* b^* U^{12}]$.

	U^{11}	U^{22}	U^{33}	U^{23}	U^{13}	U^{12}
Zn	57(1)	41(1)	61(1)	-2(1)	-1(1)	31(1)
N(1)	66(3)	46(2)	58(3)	1(2)	-5(2)	35(2)
C(1)	83(4)	63(4)	65(4)	6(3)	-3(3)	50(3)
O(1)	66(3)	47(2)	75(3)	-7(2)	-15(2)	17(2)
N(2)	50(2)	43(2)	53(2)	-2(2)	-4(2)	29(2)
C(2)	80(4)	88(5)	70(4)	14(3)	-1(3)	59(4)
O(2)	59(2)	37(2)	63(2)	5(2)	9(2)	17(2)
O(3)	70(3)	55(2)	76(3)	2(2)	13(2)	28(2)
N(3)	58(3)	45(2)	66(3)	-6(2)	-8(2)	32(2)
C(3)	75(4)	91(5)	77(4)	0(4)	-14(3)	55(4)
O(4)	90(4)	85(3)	105(4)	-31(3)	-4(3)	48(3)
C(4)	72(4)	67(4)	71(4)	-1(3)	-15(3)	41(3)
C(5)	59(3)	54(3)	57(3)	-4(2)	-6(2)	38(3)
O(5)	101(4)	87(4)	170(6)	-20(4)	-11(4)	38(3)
C(6)	54(3)	51(3)	51(3)	-8(2)	-9(2)	35(2)
C(7)	54(3)	51(3)	52(3)	-3(2)	-6(2)	28(2)
C(8)	53(3)	44(3)	54(3)	-3(2)	-3(2)	30(2)
C(9)	50(3)	44(3)	52(3)	-4(2)	-7(2)	28(2)
C(10)	44(3)	44(3)	51(3)	-4(2)	-2(2)	28(2)
C(11)	49(3)	43(3)	54(3)	-7(2)	-6(2)	27(2)
C(12)	70(4)	50(3)	73(4)	-8(3)	-13(3)	35(3)
C(13)	79(4)	68(4)	91(5)	-13(3)	-37(4)	42(4)
C(14)	73(4)	59(4)	87(5)	-26(3)	-29(3)	32(3)
C(15)	69(4)	42(3)	81(4)	-12(3)	-15(3)	27(3)
C(16)	61(3)	46(3)	80(4)	-9(3)	-24(3)	26(3)
C(17)	69(4)	49(3)	69(4)	-6(3)	-18(3)	28(3)
C(18)	59(3)	44(3)	50(3)	-3(2)	-5(2)	22(2)
C(19)	58(3)	40(3)	65(3)	-2(2)	-7(3)	25(2)
C(20)	55(3)	39(3)	59(3)	-2(2)	-7(2)	19(2)
C(21)	57(3)	42(3)	51(3)	-6(2)	-6(2)	25(2)
C(22)	61(3)	43(3)	51(3)	-2(2)	-2(2)	23(3)

C(23)	68(4)	77(4)	61(4)	-10(3)	2(3)	32(4)
C(24)	122(11)	310(20)	190(14)	20(14)	9(10)	89(13)

Table AA46. Hydrogen coordinates (x 10^4) and isotropic displacement parameters ($Å^2$ x 10^3) for Zn-TPY-2.

	x	y	z	U(eq)
H(1A)	3438	558	6281	78
H(2A)	3942	857	7668	86
H(3A)	4244	1525	7938	90
H(4A)	4042	1895	6722	81
H(7A)	3772	2169	5546	62
H(9A)	3075	2002	2550	56
H(12A)	2602	1547	1370	75
H(13A)	2155	1038	63	93
H(14A)	2008	394	497	88
H(15A)	2329	291	2149	77
H(16A)	4093	2767	4974	75
H(17A)	4334	3427	4761	76
H(19A)	3364	3218	2893	65
H(20A)	3128	2563	3050	64
H(24A)	1851	309	6810	325
H(24B)	1980	-10	6914	325
H(24C)	1767	14	5678	325